A Case Study of Two Autopilot Design Methodologies: Linear Quadratic and H-Infinity for a Tail Controlled Missile

by Mark Anthony Edeburn

Submitted to the
Massachusetts Institute of Technology
Department of Electrical Engineering and Computer Science

in partial fulfillment of the requirements for the:
Master of Science Degree in Electrical Engineering
and
Bachelor of Science Degree in Mechanical Engineering

May 1993

Signature of Author Signature redacted
Department of Electrical Engineering and Computer Science

Certified by Signature redacted
Professor Michael Athans
Professor of Electrical Engineering

Certified by Signature redacted
Dr. F. S. Kramer
Technical Advisor Raytheon Co.

Accepted by Signature redacted
Cambell L. Searle
Chair, Department Committee on Graduate Students

Table of Contents

Section **Page**

Table of Figures

Figure **Page**

Table of Tables

Table **Page**

A Case Study of Two Autopilot Design Methodologies:
Linear Quadratic and H-Infinity
for a Tail Controlled Missile

by Mark Anthony Edeburn

Submitted to the
Massachusetts Institute of Technology
Department of Electrical Engineering and Computer Science

in partial fulfillment of the requirements for:
a Master of Science Degree in Electrical Engineering
and a Bachelor of Science Degree in Mechanical Engineering
May 1993

Abstract

Three different autopilot design techniques have been applied to a tail controlled, coupled missile model. The three techniques are Linear Quadratic, H_∞ and H_2.

The closed loop performances of these three designs have been analyzed using both classical and multivariable techniques at the nominal design point and at a number of different operating points. This analysis involved both the time and the frequency domain performance of the different designs. Particular comparisons involved how the system performance degraded as the operating point changed in altitude, speed, angle of attack and wind angle from the nominal design point.

The results show that all three design techniques result in a controller that satisfy the design specifications. The LQ controller is approximately one fifth the size of the H_∞ and H_2 controllers. As the operating point is changed from the nominal design point, the performance of all three systems degrades. No one design was consistently better than any other. The LQ design showed potentially the greatest sensitivity to perturbations in the design model and the greatest sensitivity to disturbances.

Thesis supervisors:

Professor M. Athans	Professor Electrical Engineering and Computer Science
Dr. F. S. Kramer	Raytheon Co.

Acknowledgments

I would like to thank Raytheon Company for giving me the opportunity to continue my studies at MIT.

I would also like to extend my gratitude to Professor M. Athans and to Dr. F. Kramer for their support and guidance during the course of my studies.

To my friends and family: Thanks for all the help and concern. You gave me more than I can ever repay.

A special thanks to Dr. R. M. Sanner: Thank you for all your help and thanks for entertaining Jen and keeping her from being anymore of a delightful pain than she already is. Without that aid, I could never have completed this thesis.

To Jen: No mere words can suffice, so simply thanks.

And finally to Dr. F.W. Nesline Jr. Thank you. An engineer could never ask for or have a better mentor or friend.

Chapter 1 Introduction

1.1 Introduction

Recent developments in missile technology has made the interception of tactical ballistic missiles an operational reality for defensive forces. These technical advances were the results of improvements in:

Radar system
Estimation algorithms
Guidance algorithms
Airframes and propulsion systems
Processing speed and storage capability of computational resources

In addition these interceptions require the use of rapidly responding flight control systems. Figure 1-1 shows how relationships between the missile seeker, estimator, guidance algorithms and the flight control system interact to enable the missile to intercept its target.

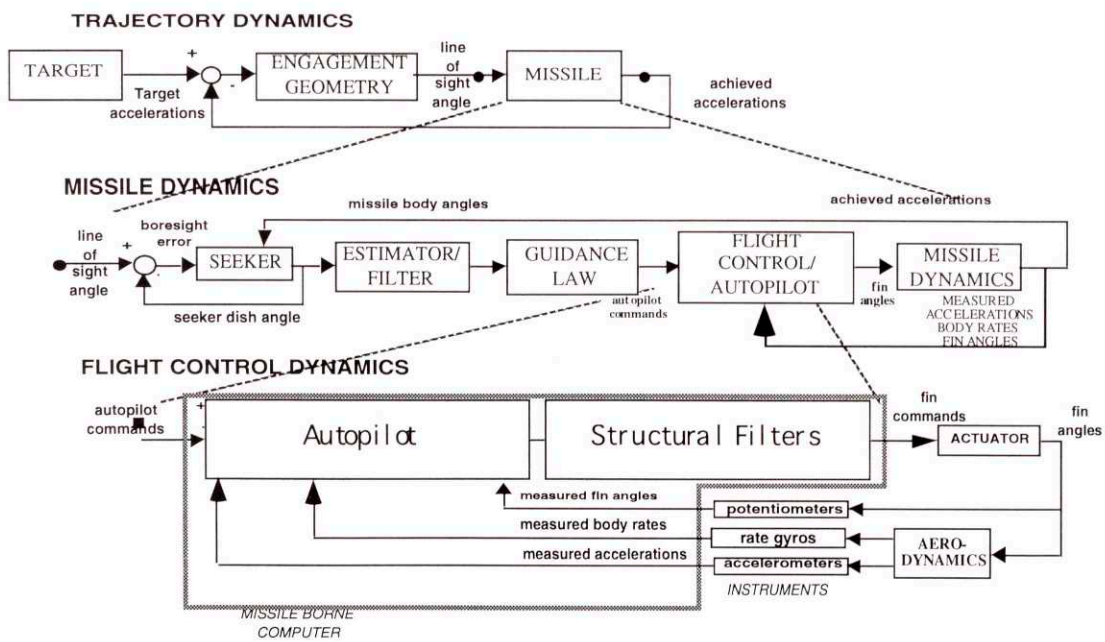

Figure 1-1 Overall Engagement Components

The central component of any flight control system is the autopilot. The basic function of an autopilot is to take commands from the guidance system and determine the correct control actions to force the missile to follow the commands while maintaining stability. The resulting force on the fins (from the airflow around the missile) rotates the missile body to an angle of attack relative to the free stream velocity. This lift force acting on the missile body generates the achieved accelerations.

Autopilots accomplish command following and ensure stability by using a linear combination of predetermined gains with measurements of a portion of the missile's dynamic state. The usual portions of the missile's dynamic state used for an autopilot are accelerations, rotational rates, fin deflections and angles of attack. The gains in the autopilot are often a tabular function of the missile's altitude and speed or of its dynamic pressure.

1.2 Motivation

Recent advances in modern control theory allow the designer unparalleled flexibility in the choice of methods to determine these gain sets. However there has been very little published literature comparing the time domain characteristics of these controllers. The purpose of this thesis is to contrast and compare the designs resulting from two of the modern linear design techniques: Linear Quadratic and H_∞. One additional autopilot design will be completed. This design will be an H_2 design which combines several of the features of the LQ theory with those of the H_∞ theory.

The autopilot designed for this thesis differs from conventional autopilots by having the additional capability of controlling the missile's roll orientation. This control is in the form of command following, allowing for continual commanded changes in the missile's roll orientation.

1.3 Background

As shown in Figure 1-2 the missile autopilot converts commands into fin deflection commands. There are two basic autopilot configurations that are currently in wide use. They are: bank to turn (BTT) and skid to turn (STT). [1],[2],[3],[4] The bank to turn autopilots originally evolved from aircraft and are primarily used on asymmetric airframes with a preferred flight orientation. In a BTT maneuver, the missile rolls around the velocity vector, then accelerates along the plane of the velocity vector and the body axis. The skid to turn systems are used most often on symmetric airframes. [5],[6],[7] In a STT maneuver, the missile maneuvers without first rotating around the velocity vector. These maneuvers are typically faster than a BTT maneuver, but they do not control the roll angle of the missile. [8],[9],[10]

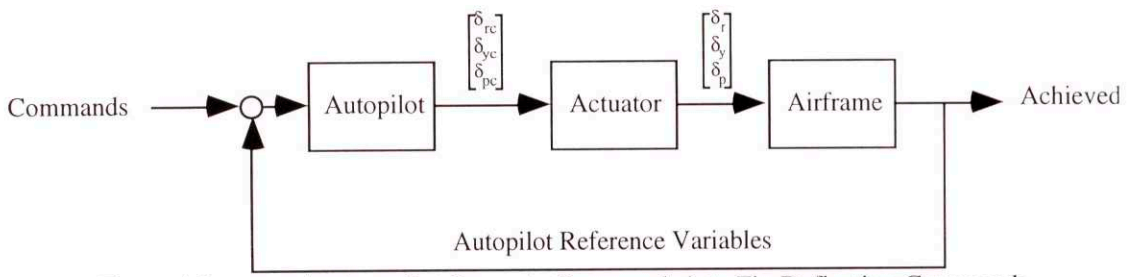

Figure 1-2 An Autopilot Converts Commands into Fin Deflection Commands

The most common type of autopilot for an anti-aircraft or a tactical ballistic missile defense system is a skid to turn, command following autopilot. Those are the type of autopilots designed and evaluated in this thesis.

In a missile autopilot there are three independent control directions which are used to . satisfy the performance requirements. These are roll, yaw and pitch. The roll control is concerned chiefly with the rotational dynamics of missile. The pitch and yaw controls relate primarily to the lateral dynamics of the airframe.

Traditional classical autopilot design techniques require the use of three independent controllers to provide the system's performance. The controller for the roll dynamics has historically been designed to be the fastest, with the lateral controllers being somewhat slower. The roll controller is required to be fastest in order to prevent the induced roll motion from coupling back into the lateral dynamic responses. Required stability margins dictate how fast the roll controller can be, and this in turn dictates the acceptable bandwidth of the lateral controllers. However this three independent controller system approach has proven to be too slow to accommodate the fast response times and robustness required of current missile autopilot designs. [11],[12]

Modern control theory techniques have shown that multivariable control techniques offer better performance and posses better stability margins and disturbance rejection properties than classical controller techniques. In a multivariable design, the three missile channels (roll, yaw, and pitch) are coupled. This coupling allows greater flexibility in meeting the performance and stability goals than is possible with classical techniques. These performance improvements are attainable with individual loop crossover frequencies comparable to that of a classical design. [13]

Several types of modern multivariable control theory have evolved. Three will be used in this thesis. The first of these is the Linear Quadratic (LQ) theory using full state feedback developed in the 1960's. The second is H_2 control developed in the early 1980's as LQ control theory with frequency dependent performance weights. The third is H_∞ control theory developed in the latter half of the 1980's. [14],[15],[16],[17],[18],[19] The purpose of this thesis is to contrast and compare these types of control theory for missile autopilot design.

Analysis contained in similar work to date has largely been restricted to planar design cases. [13],[20],[1],[2] These preliminary designs have not been conducted on the full cross-coupled models representative of those actually needed for the design of missile autopilots. In addition the current design of tail controlled missiles do not have explicit roll angle control incorporated into their autopilot architecture's and do not have the capability of simultaneously following a roll angle command and a combination of lateral acceleration commands. The proposed autopilot design effort will attempt to satisfy these goals and to demonstrate the performance differences resulting from these different design techniques.

The basic design consideration for the autopilots is the speed of response to commands while maintaining stable operation. Stability in the face of variations from the nominal design values is also a requirement in order to ensure the system's operational capability in the face of uncertainties in available information or design models.

H_∞ theory attempts to minimize the peak value of a weighted sensitivity function across all frequencies. H_2 theory attempts to minimize the squared area under the weighted sensitivity function. By limiting this peak value or total area, the H_∞ and H_2 theory result in more robustness to parameter variations and improved disturbance rejection properties than the LQ design methodology. However these improvements are at the expense of a much higher order, more complex compensator. An additional difference between the H_∞ and H_2 theories and Liner Quadratic theory is that H_∞ and H_2 are frequency based design techniques while the LQ theory is time domain based. [21],[22],[23],[24],[25],[26]

Little analysis to date has compared the time domain performances of an H_∞ controller with that of an LQ.[27]

One important point to remember in evaluating the different designs is that: while there may be perturbation combinations that result in instabilities in the simpler LQ controller, the performance characteristics of the H_∞ or H_2 autopilot may have degraded to such an extent that their responses are unacceptable from the performance perspective. If the time domain performance degrades so much so that the interceptor misses its target then the design is a failure.

Instrumentation has improved to such an extent that good quality instruments are becoming commonplace onboard modern missiles. These instruments give a good estimate of the missile's current operating point thereby alleviating the wide robustness range required in controller design as recently as even 10 years ago. Improvements in onboard computer speed and the quantity of available data storage has provided the means for the rapid interpolation of autopilot gains and the use of gain scheduled controllers. This combination of advancements has to some extent eliminated the requirements for such a wide range of parameter robustness that was required in earlier autopilot designs.

1.4 Contribution of Thesis

The purpose of this thesis is to design autopilots for a non-minimum phase, tail controlled missile using three different modern design techniques. Once the designs are complete, the closed loop time domain performance, and the frequency domain performance will be evaluated. This thesis shows that there is no one technique which is clearly better for the analysis conditions. All three designs fulfill the nominal requirements and all three suffer performance degradations at the perturbed flight conditions. In general the LQ design was more susceptible to changes in the flight condition. The LQ design usually had the best single loop classical Bode gain and phase margins, and had a greater sensitivity to

disturbances. The H_2 design generally had the poorest Bode margins, but did have the least variation in those margins at the different operating points

1.5 Proposed Analysis

The basic task covered in this thesis is the design of three acceleration command following, skid to turn autopilot configurations and a comparison of their closed loop performances.

Each of the three autopilot designs: LQ, H_∞ and H_2 will be synthesized at the same nominal condition. At that flight condition their time domain performances will have the same basic performance characteristics and their Bode crossover frequencies will match. The performance measures used for this verification of the frequency domain characteristics are the classical single loop crossover frequencies of the controller with the loop broken at the plant input. Figure 1-3 shows an example for the yaw channel of one such block diagram. The time domain performance measure is the step response risetime.

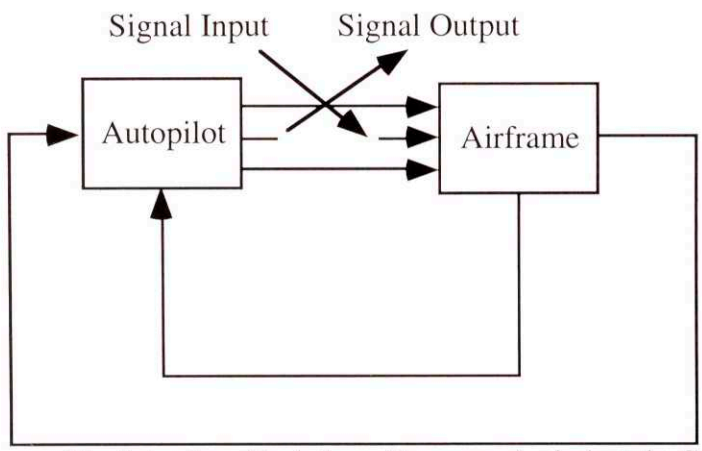

Figure 1-3 The Setup for a Single Loop Frequency Analysis at the Control, With Only One Loop Broken

When this design has been completed, the autopilots will be contrasted. This comparison will involve:

1) Comparison of the time domain and frequency domain performances of the systems using the nominal design plants.

2) Perturbing the nominal plant and again evaluating their performances
   Such perturbations will include:
   a) Using an airframe from a different flight condition (Mach, altitude, angle-of-attack and wind angle, and different combinations of these)

3) Evaluating the impact on computational requirements (floating point operations and required storage)

The design procedure will be a three step process. The first design will be an LQ design. Once this LQ design has been completed, the H_∞ design will be performed. The H_∞ design must fulfill the same performance requirements as the LQ design. Finally the H_2 controller will be designed. This design too will undergo iterations to satisfy the same performance requirements as used in the other designs.

1.6 Thesis Overview

This thesis consists of 12 chapters. Chapter Two contains a general discussion of autopilots and their function. It also covers some of the early decisions that must be made in any autopilot design task. Chapter three contains the derivation of the missile model used in the design phase. Chapter four covers the design specifications for the autopilot designs. Chapters five, six and seven contain the autopilot design for the LQ, H_∞ and H_2 controllers respectively. Chapter eight compares the nominal performance of the autopilots. Chapters nine and ten cover comparisons of the systems' closed loop performance when the design is used at a flight condition other than the design point. In particular chapter nine covers variations in altitude and speed, while chapter ten covers variations in the angle of attack and wind angle. Chapter eleven covers simultaneous variations in the flight condition. Finally chapter twelve summarizes some of the results, extends one earlier comparison and recommends directions for future research.

Chapter 2 Autopilots

2.1 Autopilots and Their Functions

As mentioned in the previous chapter the function of an autopilot is to determine the correct set of control actions that will not only ensure stability but also track the reference commands from guidance. The autopilot must accomplish this function for the duration of the flight, regardless of the missile's flight condition.

During the course of an engagement the missile can cover an extremely wide range of operating environment and flight conditions. The missile starts at rest on the ground (if ground launched) or at an initial speed and altitude (if air launched). From this initial condition the missile's operating environment will change to some different combination of speed and altitude. Engagement speeds may run from subsonic to supersonic speeds greater than Mach 6 and altitudes range from sea level to more than 30 kilometers.

Additionally at launch the missile is flying at a total angle of attack (the angle between the missile's centerline and the missile's velocity vector) of zero and with an undefined wind angle (the angle that the relative wind makes with the number 1 fin, see Figure 2-1). At intercept the angle of attack can be expected to be anything from zero to the airframe's maximum limit, and the wind angle can be anywhere from 0° to 360°. (Certain operational requirements may preclude some combinations of angle of attack and wind angle. For example the angle of attack may be limited to allow for airflow to a RAM jet etc.)

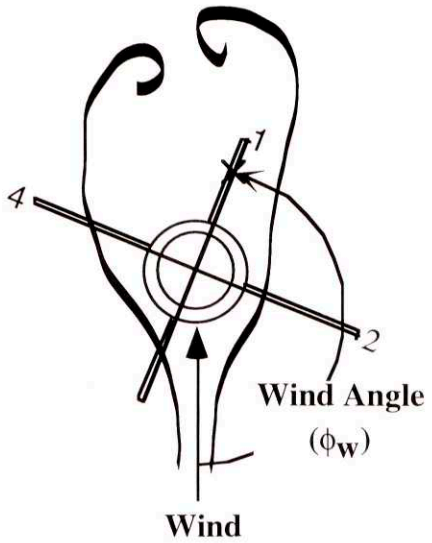

Aft Forward View

Figure 2-1 Definition of Aerodynamic Wind Angle (ϕ_W)

The autopilot must maintain its performance within a specified narrow range despite these wide variations in the flight conditions.

2.1 An Overview of Aerodynamics and It's Effects

During an engagement four crucial parameters (altitude, speed, angle of attack and wind angle) will undergo significant variations. These four parameters are amongst the most influential in determining the aerodynamic characteristics of the missile. However the rate of these changes varies. A typical missile processor runs at several hundred Hertz. On this time scale the rates of change of missile altitude and speed are slow. On the other hand the rates of change of angle of attack and of wind angle are much faster.

The altitude and speed are generally well known in a missile (calculated by onboard instruments or determined on the ground and broadcast to the missile). The angle of attack can be determined from the onboard instruments or based upon estimates using onboard data. The wind angle is determined from estimates and onboard instrument readings.

Typical errors for missile speed and altitude are on the order of 1 - 2 percent, while angle of attack errors of $\pm 5^{\circ}$ can be expected. Wind angle errors of $\pm 30\%$ or more are not unusual.

The nature of angle of attack is such that the smaller the value of the angle of attack, the less variations in it affect the missile's performance. Therefore an error of 3° on a total angle of 3° represents a 100% variation, but because the total actual angle is small, (3°), it's effects are small. The most sensitive design areas for angle of attack variations are in the region of approximately 15°.

Most tail controlled missiles that utilize a skid to turn philosophy are symmetric in either 180° or 90° quadrants. This means that if the missile's wind angle is rotated by either 180° or 90° degrees, the aerodynamic behavior is approximately the same as that at the original condition although the responses of the lateral channels may have been switched for a 90° rotation. Wind angle effects are least noticeable at 45°, 135°, 225°, and 315° angles for a missile possessing 4 quadrant (90°) symmetry. The most sensitive areas for perturbation analysis are between 0° and 45° (45° or to 90°).

The altitude and speed of the missile determine its dynamic pressure as well as several other key aerodynamic properties. The effects of angle of attack and wind angle are twofold. First, they determine several of the important aerodynamic characteristics of the missile and secondly they create the cross-coupling inherent in missiles.

When the missile is flying at a non-zero angle of attack, the body of the missile shields some portion of the missile from the airflow. The larger the angle of attack, the greater the effects of this shading. This shading creates an area of low pressure and an induced roll

moment as shown in Figure 2-2. The wind angle determines which portion of the missile is shielded from the free stream airflow. This shielding and its induced moments result in cross-coupling and a difference in the effectiveness of the control surfaces. Because of the extreme sensitivity of the missile's aerodynamics to this wind angle it is important that any missile autopilot design evaluate these effects. See Figure 2-3.

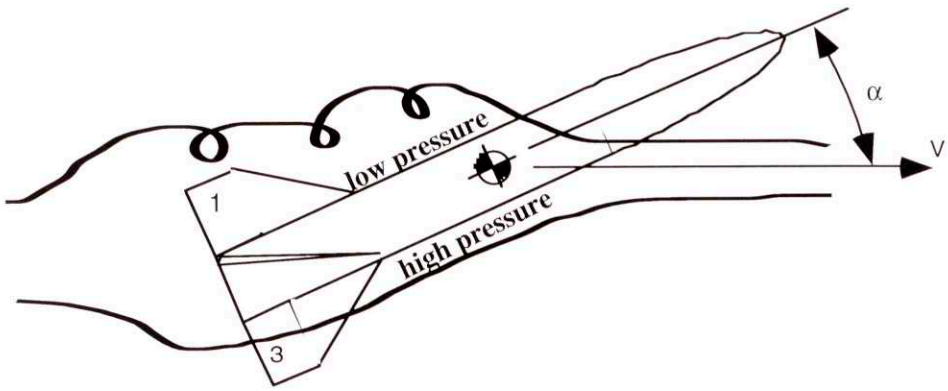

Figure 2-2 An Angle of Attack Results in Aerodynamic Shading

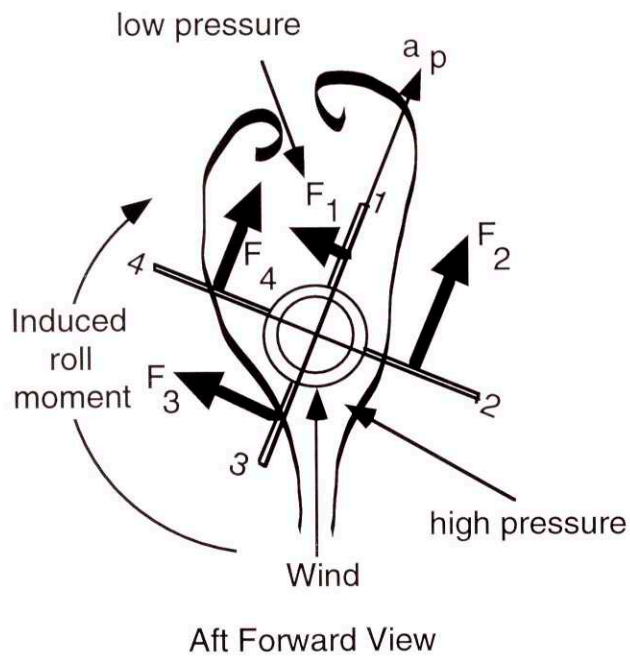

Figure 2-3 A Wind Angle Induces a Roll Moment

2.1 Missile Model Considerations

Of crucial importance to the design of any control system is the plant model. Important decisions involved in the preliminary phases of the design effort involve the tradeoff between model size and model realism. The more realistic the model, the larger and more complex it becomes. The designer must determine what level of fidelity is justified and form his model based upon this analysis. An additional important constraint is computational complexity. A large and complex model requires more time to perform control calculations , and more time to perform the required analyses . As the model size increases, the number of required mathematical operations increases by approximately the square of the number of states in the model.

In order to design a missile autopilot, several decisions must be made. These include:

The type of autopilot.
The expected operational envelope.
The type of gain scheduling (if any).
The quality and type of the available measurements and information.
The size and speed of the autopilot processor.

Only after this information is known can the designer begin the model derivation and development process.

Perhaps the most fundamental question is the type of autopilot. This question covers more than just is choice between a linear and a nonlinear design. It also includes the such choices as between: command following or attitude control, and bank to turn or skid to turn philosophies.

The missile's motion is characterized by a set of nonlinear coupled differential equations. These equations are used to analyze the trajectories followed by the missile in space and determine the missile's speed, altitude, orientation, etc. If a nonlinear autopilot is being designed, then a suitable subset of these nonlinear equations may be used as the design model. If a linear autopilot is being designed then these equations must be linearized about an operating point. The theory necessary to develop a nonlinear autopilot that is capable of tracking acceleration commands has not been developed as of yet for aerodynamically controlled missiles.

The autopilots (controllers) will accept yaw acceleration, pitch acceleration and roll angle commands. The output from the autopilots will be fin deflection commands. These commands will be the inputs to the actuator models of the airframe model. The resultant body motions will be fed back to the autopilot, thereby forming a closed loop system.

Chapter 3 Plant Model Derivation

The model used in a control design must include all of the relevant dynamics of the plant. For this missile design the important components are the missile airframe and the control actuation system (CAS). The dynamics of the sensors (gyros and accelerometers) are high frequency (typically with natural frequencies on the order of at least 700 radians per second) and do not need to be accounted for at this stage of the design.

The basic design plant that will be used for this thesis represents a linearized, generic tail controlled missile. These equations comprise a 9 state model derived from the coupled aerodynamic equations. The inputs to this model are the fin angle commands (roll, yaw and pitch). Its outputs are the two lateral accelerations and the roll angle. Internal state variables are: the roll angle, the two planar angles of attack, the three body rates, and the three fin angles. The model assumes first order actuators to translate the fin commands into fin deflections. The airframe in question is evaluated at a nominal condition of Mach 4.0, medium altitude, 15° angle of attack, and a wind angle of 22.5°.

3.1 Basic Plant Equations

The plant model for this design contains two principal pieces, the airframe and the CAS.

3.1.1 Missile Equations of Motion

As mentioned previously, the missile model is that is used to design the autopilot is of fundamental importance. The missile's operating condition and dynamic motion is characterized by an infinite set of coupled, nonlinear, time varying differential equations. A full treatment on the nonlinear dynamic motion of missiles can be found in reference [29]. In order to design an autopilot, simplifications must be made. This resulting set of differential equations determines the design plant or model.

Several simplifying assumptions are made. First it is assumed that the missile is in burnout. This results in the simplification that the mass properties are constant and the location of the center of gravity (CG) is fixed.

Second it is assumed that the missile possesses four quadrant mass symmetry. This ensures that the cross products of inertia: I_{xy}, I_{xz}, and I_{yz} are identically zero and that the principal lateral moments of inertia I_{yy} and I_{zz} are equal.

The coordinate system to be used for the following derivations is a "3 down" system. Figure 3-1 and Table 3-1 show the axis definitions and summarizes some of the nomenclature.

	Roll Axis	Yaw Axis	Pitch Axis
Angular Rates (rad/sec)	P	Q	R
Incremental Angular Rates (rad/sec)	p	q	r
Angular Displacements (radians)	Θ		
Force (Newtons)	F_x	F_y	F_z
Velocity (m/s)	U	V	W
Incremental Velocity (m/s)	u	v	w
Moments	L	M	N
Fin Deflections (rad)	δ_r	δ_y	δ_p

Table 3-1 Nomenclature for a 3 Down System

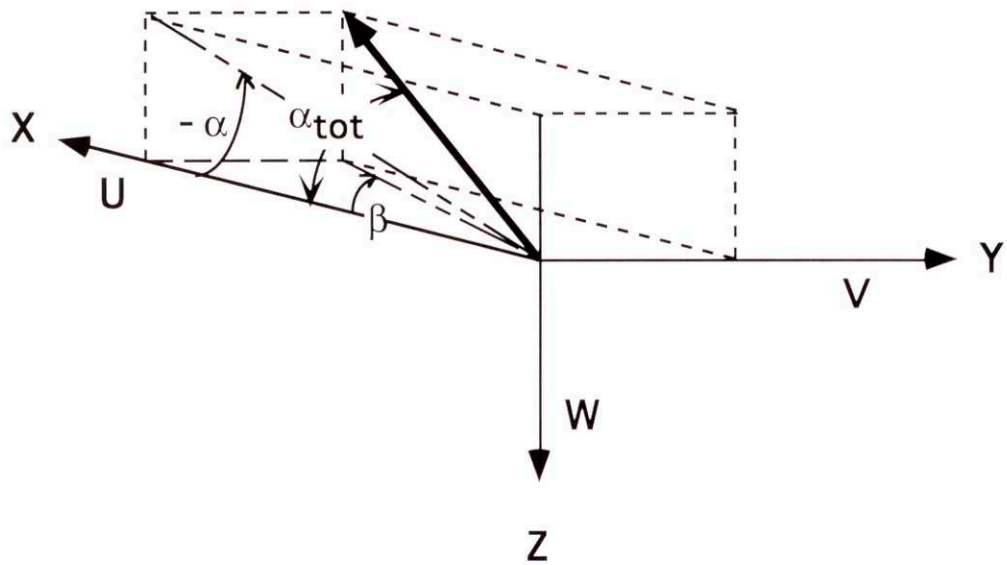

Figure 3-1 The Design System is a 3 Down Coordinate System

Given these simplifications the missile kinematics can be characterized by 6 coupled differential equations. The three equations for the translationial dynamics expressed in vector form as:

$$\vec{F} = \frac{d}{dt}(m\vec{V}) \tag{3.1}$$

When expanded out, and the effects of the missile's rotation included this gives:

$$F_x = m(\dot{U} + QW - RV) \tag{3.2}$$

$$F_y = m(\dot{V} + RU - PW) \tag{3.3}$$

$$F_z = m(\dot{W} + PV - QU) \tag{3.4}$$

The three equations for the rotational dynamics are expressed in vector form as:

$$\vec{M} = \frac{d}{dt}(\vec{H}) \tag{3.5}$$

When expanded out, this results in:

$$L = I_{XX}\,\dot{P} \tag{3.6}$$

$$M = I_{yy}\,\dot{Q} - (I_{yy} - I_{xx})PR \tag{3.7}$$

$$N = I_{yy}\,\dot{R} - (I_{yy} - I_{xx})PQ \tag{3.8}$$

However for autopilot design it is more useful to express these equations using the derivatives of the components of the total angle of attack, i.e. alpha and beta, than the derivatives of the pitch and yaw lateral velocities (V and W).

Accordingly the side slip angle of attack β and the planar angle of attack α can be defined as:

$$\beta = \tan^{-1}\left(\frac{V}{U}\right) \tag{3.9}$$

$$\alpha = \tan^{-1}\left(\frac{W}{U}\right) \tag{3.10}$$

The time derivatives of β and α are:

$$\dot{\beta} = \frac{-V\dot{U} + U\dot{V}}{U^2 + V^2} \tag{3.11}$$

$$\dot{\alpha} = \frac{-W\dot{U} + U\dot{W}}{U^2 + W^2} \tag{3.12}$$

Defining two velocity combinations as,

$$V_\alpha = (U^2 + V^2)^{\frac{1}{2}} \tag{3.13}$$

and

$$V_\beta = (U^2 + W^2)^{\frac{1}{2}} \tag{3.14}$$

multiply equation (3.3) by U and (3.2) by V subtract, and then rewrite equation (3.11) as

$$\begin{aligned}\dot{\beta} = -R + \frac{\frac{F_y}{m}\cos(\beta) - \frac{F_x}{m}\sin(\beta)}{V_\beta} + Q\frac{V_\alpha}{V_\beta}\sin(\alpha)\sin(\beta) \\ + P\frac{V_\alpha}{V_\beta}\sin(\alpha)\cos(\beta)\end{aligned} \tag{3.15}$$

Similarly, multiply equation (3.5) by U, equation (3.3) by W and subtract them. Equation (3.12) may then be rewritten as:

$$\begin{aligned}\dot{\alpha} = Q + \frac{\frac{F_z}{m}\cos(\alpha) - \frac{F_x}{m}\sin(\alpha)}{V_\alpha} - P\frac{V_\beta}{V_\alpha}\sin(\beta)\cos(\alpha) \\ - R\frac{V_\beta}{V_\alpha}\sin(\beta)\sin(\alpha)\end{aligned} \tag{3.16}$$

The equations (3.3), (3.15), (3.16), (3.6), (3.7), and (3.8) are now linearized about a nominal operating point by assuming small perturbations about the nominal. The nominal operating point values are denoted by a subscript O.

Linearizing equations (3.9) and (3.10) about α_O and β_O yields respectively:

$$v = \frac{V_{\beta_o}}{cos(\beta_o)} \Delta\beta + tan(\beta_o)u \tag{3.17}$$

$$w = \frac{V_{\alpha_o}}{\cos(\alpha_o)} \Delta\alpha + \tan(\alpha_o)u \tag{3.18}$$

Where

$$\Delta\alpha \equiv \alpha - \alpha_o \tag{3.19}$$

and

$$\Delta\beta \equiv \beta - \beta_o \tag{3.20}$$

Linearization of the dynamics then gives:

$$\begin{aligned} \dot{u} = {} & \frac{\Delta F_x}{m} - \frac{Q_o V_{\alpha_o}}{\cos(\alpha_o)} \Delta\alpha - [Q_o \tan(\alpha_o) - R_o \tan(\beta_o)]u \\ & + [\frac{R_o V_{\beta_o}}{\cos(\beta_o)}]\Delta\beta - [V_{\alpha_o} \sin(\alpha)]q + [V_{\beta_o} \sin(\beta_o)]r \end{aligned} \tag{3.21}$$

$$\begin{aligned} \Delta\dot{\beta} = {} & -r + \left[\frac{\cos(\beta_o)}{mV_{\beta_o}}\right]\Delta F_y - \left[\frac{\sin(\beta_o)}{mV_{\beta_o}}\right]\Delta F_x \\ & + \left[\frac{V_{\alpha_o}}{V_{\beta_o}} \sin(\alpha_o)\sin(\beta_o)\right]q + \left[\frac{V_{\alpha_o}}{V_{\beta_o}} \sin(\alpha_o)\cos(\beta_o)\right]p \\ & + \left[\frac{V_{\alpha_o}}{V_{\beta_o}} Q_o \frac{\sin(\beta_o)}{\cos(\alpha_o)}\right]\Delta\alpha + [\mu]\Delta\beta + \left[\frac{-\frac{F_{y_o}}{m} + \frac{F_{x_o}}{m}\tan(\beta_o)}{V_{\beta_o}^2}\right]u \end{aligned} \tag{3.22}$$

with

$$\begin{aligned} \mu \equiv {} & \frac{-2\frac{F_{y_o}}{m}\sin(\beta_o) - \frac{F_{x_o}}{m}\{\cos(\beta_o) - \sin(\beta_o)\tan(\beta_o)\}}{V_{\beta_o}} \\ & + \frac{V_{\alpha_o}}{V_{\beta_o}} Q_o \sin(\alpha_o)\{\cos(\beta_o) - \sin(\beta_o)\tan(\beta_o)\} \end{aligned} \tag{3.23}$$

$$\Delta\dot{\alpha} = q + \left[\frac{\cos(\alpha_o)}{mV_{\alpha_o}}\right]\Delta F_z - \left[\frac{\sin(\alpha_o)}{mV_{\alpha_o}}\right]\Delta F_x$$
$$-\left[\frac{V\beta_o}{V_{\alpha_o}}\sin(\beta_o)\sin(\alpha_o)\right]r - \left[\frac{V\beta_o}{V_{\alpha_o}}\sin(\beta_o)\cos(\alpha_o)\right]p \qquad (3.24)$$
$$-\left[\frac{V\beta_o}{V\alpha_o}R_o\frac{\sin(\alpha_o)}{\cos(\beta_o)}\right]\Delta\beta + [\psi]\Delta\alpha + \left[\frac{-\frac{F_{z_o}}{m} + \frac{F_{x_o}}{m}\tan(\alpha_o)}{V_{\alpha_o}^{\ 2}}\right]u$$

with

$$\psi \equiv \frac{-2\frac{F_{z_o}}{m}\sin(\alpha_o) - \frac{F_{x_o}}{m}\{\cos(\alpha_o) - \sin(\alpha_o)\tan(\alpha_o)\}}{V_{\alpha_o}}$$
$$--\frac{V_{\beta_o}}{V_{\alpha_o}}R_o sin(\alpha_o) - F\{cos(\alpha_o) - sin(\alpha_o)tan(\alpha_o)\} \qquad (3.25)$$

$$\dot{p} = \frac{\Delta L}{I_{xx}} \qquad (3.26)$$

$$\dot{q} = \left(1 - \frac{I_{xx}}{I_{yy}}\right)R_o p + \frac{\Delta M}{I_{yy}} \qquad (3.27)$$

$$\dot{r} = -(1 - \frac{I_{xx}}{I_{yy}})Q_o p + \frac{\Delta N}{I_{yy}} \qquad (3.28)$$

Using partial differentiation and incremental analysis the aerodynamic force and moment perturbations are simplified to the following:

$$\Delta F_x = \frac{\partial F_x}{\partial u}\Delta u + \frac{\partial F_x}{\partial \alpha}\Delta\alpha + \frac{\partial F_x}{\partial \beta}\Delta\beta$$
$$+ \frac{\partial F_x}{\partial \delta_r}\Delta\delta_r + \frac{\partial F_x}{\partial \delta_y}\Delta\delta_y + \frac{\partial F_x}{\partial \delta_p}\Delta\delta_p \qquad (3.29)$$

$$\Delta F_y = \frac{\partial F_y}{\partial u}\Delta u + \frac{\partial F_y}{\partial \alpha}\Delta\alpha + \frac{\partial F_y}{\partial \beta}\Delta\beta + \frac{\partial F_y}{\partial \delta_r}\Delta\delta_r + \frac{\partial F_y}{\partial \delta_y}\Delta\delta_y + \frac{\partial F_y}{\partial \delta_p}\Delta\delta_p \tag{3.30}$$

$$\Delta F_z = \frac{\partial F_z}{\partial u}\Delta u + \frac{\partial F_z}{\partial \alpha}\Delta\alpha + \frac{\partial F_z}{\partial \beta}\Delta\beta + \frac{\partial F_z}{\partial \delta_r}\Delta\delta_r + \frac{\partial F_z}{\partial \delta_y}\Delta\delta_y + \frac{\partial F_z}{\partial \delta_p}\Delta\delta_p \tag{3.31}$$

$$\Delta L = \frac{\partial L}{\partial u}\Delta u + \frac{\partial L}{\partial \alpha}\Delta\alpha + \frac{\partial L}{\partial \beta}\Delta\beta + \frac{\partial L}{\partial \delta_r}\Delta\delta_r + \frac{\partial L}{\partial \delta_y}\Delta\delta_y + \frac{\partial L}{\partial \delta_p}\Delta\delta_p \tag{3.32}$$

$$\Delta M = \frac{\partial M}{\partial u}\Delta u + \frac{\partial M}{\partial \alpha}\Delta\alpha + \frac{\partial M}{\partial \beta}\Delta\beta + \frac{\partial M}{\partial \delta_r}\Delta\delta_r + \frac{\partial M}{\partial \delta_y}\Delta\delta_y + \frac{\partial M}{\partial \delta_p}\Delta\delta_p \tag{3.33}$$

$$\Delta N = \frac{\partial N}{\partial u}\Delta u + \frac{\partial N}{\partial \alpha}\Delta\alpha + \frac{\partial N}{\partial \beta}\Delta\beta + \frac{\partial N}{\partial \delta_r}\Delta\delta_r + \frac{\partial N}{\partial \delta_y}\Delta\delta_y + \frac{\partial N}{\partial \delta_p}\Delta\delta_p \tag{3.34}$$

The nominal operating values are found by trimming out the airframe at a specified flight condition. The definition of trim for this analysis is that there are no net moments acting on the vehicle and that the roll rate is zero. In addition the further stipulation is made that the planar angles of attack are constant at trim (i.e. $\dot{\alpha}$ and $\dot{\beta}$ are zero).

The aerodynamic forces and moments are the results of several components. Both the body and the fins generate lift and drag, while the moments on the body are primarily the results of the fins and the aerodynamic shading (see Figures 2-2 and 2-3). To determine the trim level forces the fin deflections are incrementally changed until there are no net moments acting on the airframe.

One final simplification results from the time span that the linearization is desired to be valid for. All time histories of the simulations are for a maximum of 1 second. On this time scale all perturbations and changes of the forward velocity U can be neglected.

This gives a nominal state space model of:

$$\begin{aligned} \dot{x} &= Ax + Bu \\ y &= Cx + Du \end{aligned} \tag{3.35}$$

$$x \in R^n,\ u \in R^m,\ y \in R^p$$

with

$$x \equiv [\Delta\alpha\ \Delta\beta\ P\ Q\ R]^T \tag{3.36}$$

$$u \equiv [\Delta\delta r\ \ \Delta\delta y\ \ \Delta\delta p\ ]^T \tag{3.37}$$

and

$$y \equiv [\eta_y\ \ \eta_p\ \ \alpha\ \ \beta\ \ P\ \ Q\ \ R]^T \tag{3.38}$$

The seven outputs from the plant are the two accelerations (η_y and η_p) the two planar angles of attack (α and β) and the three body rates (P, Q and R). The desired autopilot configuration however is to maintain and follow not only acceleration commands, but a roll angle command also. This requires that the model be augmented with an integral of the roll rate to form the roll angle θ. The final state vector is therefore:

$$x \equiv [\Delta\alpha\ \ \Delta\beta\ \ \theta\ \ P\ \ Q\ \ R]^T \tag{3.39}$$

3.1.2 Actuators

The state equations derived in section 3.1 are a function of perturbations in the three fin angles (δ_r, δ_y and δ_p). The output of the autopilot is fin commands (δ_{rc}, δ_{yc} and δ_{pc}). These fin commands are converted into fin deflections by the actuators. For this portion of the analysis the three required actuators are assumed to be identical and are each modeled by a linear first order transfer function:

$$\delta(s) = \left(\frac{200}{s + 200}\right)\delta_c(s) \tag{3.40}$$

The gain and phase of the actuators are shown in Figure 3-2.

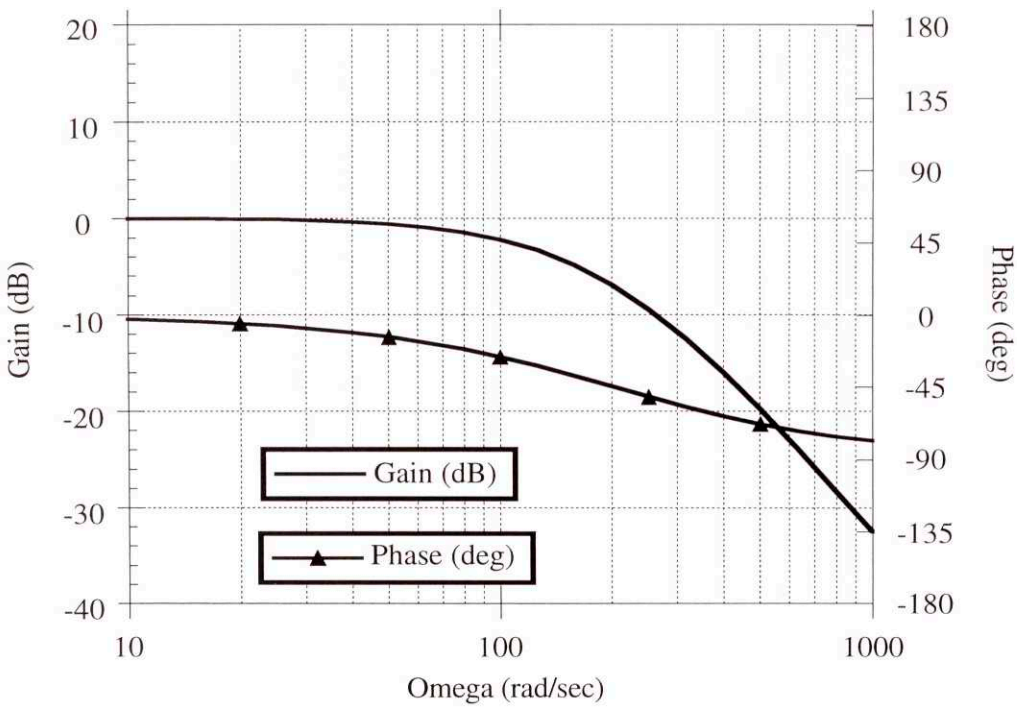

Figure 3-2 Gain and Phase Characteristics of the Actuator Models

3.2 Open Loop Plant Characteristics

For simplicity the Δ in the angles of attack and fin deflections terms are now dropped. It is assumed that when the trim data is generated, initial angles and fin deflections are required. In the time domain analysis resulting deflections and changes are assumed to be perturbations on these trim and initial values.

The chosen operating point for the nominal design model is Mach 4, medium altitude, a wind angle of 22.5° and an angle of attack of 15°. This condition represents a highly cross-coupled flight condition. The open loop airframe poles and zeros are found in Table 3-2 and diagrammed in Figure 3-3. The open loop singular values from the fin angles to the three controlled outputs are shown in Figure 3-4.

There are a total of 9 states in the final open loop plant model. They are:

$$x_{plant} \equiv [\Delta\alpha \; \Delta\beta \; \theta \; P \; Q \; R \; \delta_R \; \delta_Y \; \delta_P]^T \tag{3.41}$$

There are 11 outputs of the basic open loop plant for feedback to the autopilot. They are:

$$y_{plant} \equiv [\eta_y \; \eta_p \; \Delta\alpha \; \Delta\beta \; \theta \; P \; Q \; R \; \delta_R \; \delta_Y \; \delta_P]^T \tag{3.42}$$

The three controlled variables are:

$$y_{controlled} \equiv [\eta_y \; \eta_p \; \theta \;]^T \tag{3.43}$$

The three inputs to the model are:

$$u_{plant} \equiv [\delta_{rc} \; \delta_{yc} \; \delta_{pc} \;^T \tag{3.44}$$

The actual numeric values used for this design can be found in Appendix 1. The accelerations are in m/sec^2. The fin angles, roll angle and rotational rates are in radians and radians per second respectively.

Airframe Poles

Real	Imag	Freq.	Damp
0	0.0	0	
-0.1206	0.0	0.1206	
-0.4913	-7.993	8.008	
-0.4913	7.993	8.008	0.061
-0.4574	-11.45	11.46	
-0.4574	11.45	11.46	0.040
-200	0.0	200	
-200	0.0	200	
-200	0.0	200	

Airframe Zeros

Real	Imag	Freq.	Damp
-35.9	0.0	35.9	
-31.82	0.0	31.82	
31.48	0.0	31.48	
35.69	0.0	35.69	

Table 3-2 Open Loop Airframe Poles and Zeros

As can be seen in Table 3-2 the Nominal system is stable. It contains a pole at the origin from the roll angle (the integral of the roll rate). There are two complex pairs, near the origin that are lightly damped. Table 3-2 also shows the location of the two non-minimum phase zeros. This non-minimum phase is characteristic of tail controlled missile. In a tail controlled missile, the initial fin deflection first generates a force in the opposite direction from the command. This force rotates the missile body, and the resultant body lifting force provides the commanded acceleration.

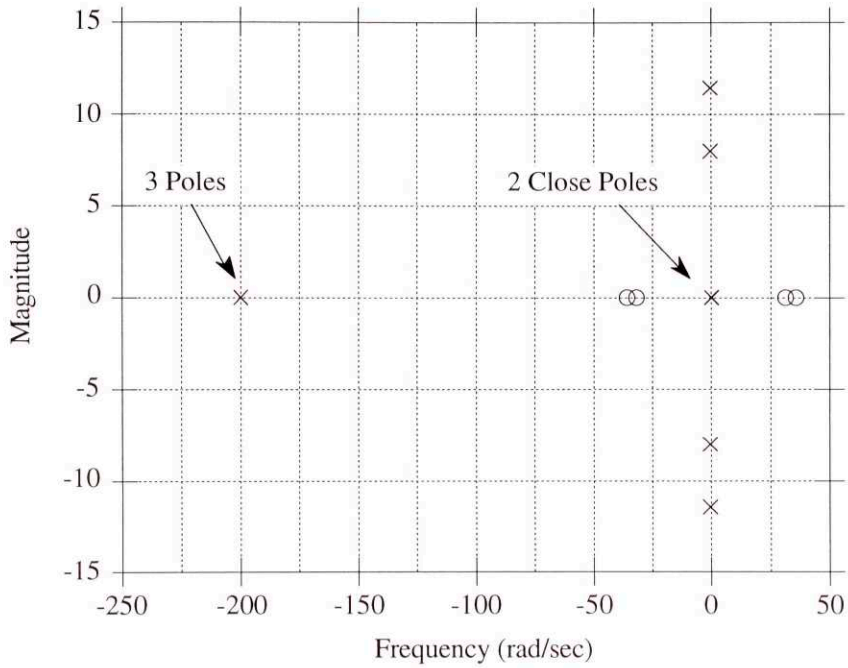

Figure 3-3 Pole/Zero Plot of the Nominal Open Loop Plant

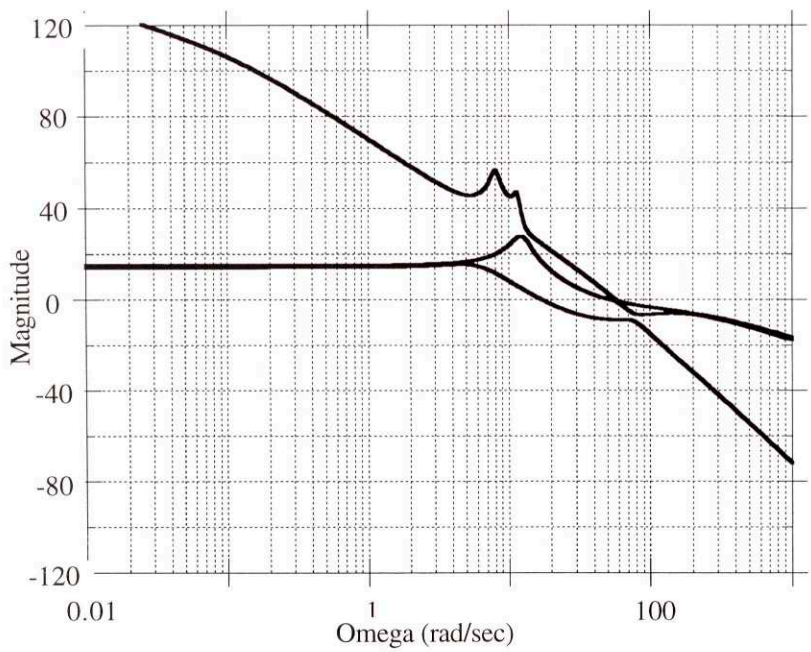

Figure 3-4 Singular Values of Nominal Open Loop Plant from the Three Fin Commands to the Controlled Outputs

Chapter 4 Autopilot Performance Requirements

In order to provide a realistic comparison between the 3 autopilot designs, both time domain and frequency domain constraints are expressed. These constraints involve the required 63% rise times for external commands and the crossover frequencies of the three systems evaluated from a single loop point of view. The time domain constraint specifies the time required for the control output to reach 63% of its specified value as shown in Figure 4-1. In order to limit the autopilot bandwidth, all three autopilots are designed with the same open loop crossover frequencies with the loop broken at the control and the remaining loops closed.

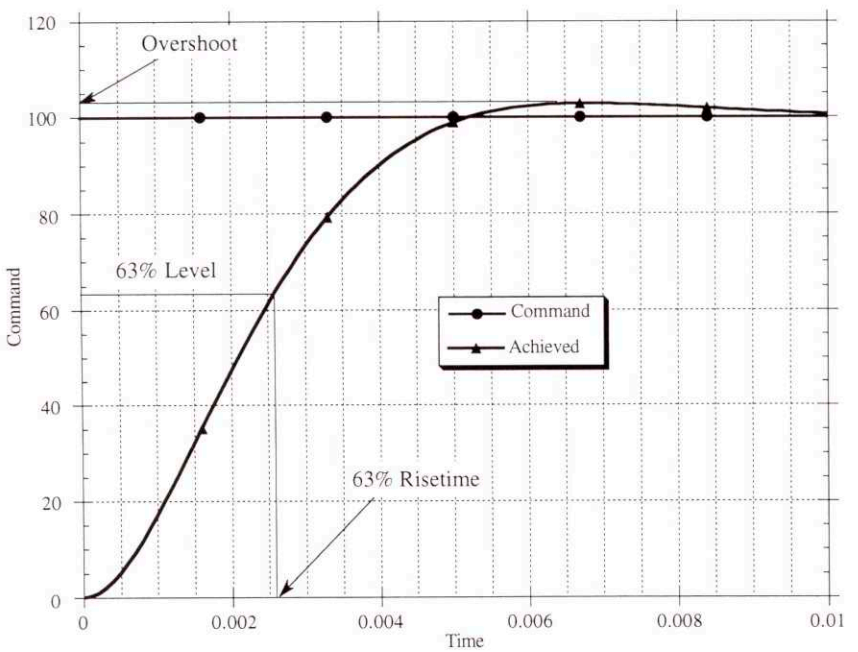

Figure 4-1 Control System Transient Performance Measures

4.1 Time Domain Requirements

The autopilots are to follow external commands (presumably generated by some other subsystem such as an optimal guidance system). The form that these commands take in an operational missile is a series of step commands that are held constant from update to update. The rate of these commands varies from missile to missile and typically cover a range from 1 to 100 Hertz. The magnitude of the command variation from one update to the next depends on the type of guidance law, the time to go until intercept, and the missile's rate of closure with the target.

A typical measure of control system performance is the time required for a variable to attain 63% of its step-commanded value. Another measure of performance is the amount of overshoot a system exhibits to a step input.

The expected responsiveness of an aerodynamically controlled missile is a function of the dynamic pressure and the fin effectiveness. The greater the dynamic pressure and the more effective the fins are, the more responsive the missile is. For the nominal design condition the design goals are a 63% risetime of 0.20 seconds for lateral acceleration commands and 0.10 seconds for the roll channel angle command. It is important not to have too fast a risetime because of the inherent maximum fin rate capabilities in any actuator. Those nonlinear limitations are not modeled.

The total risetime requirement imposed on all the autopilot designs is to have no more than a 0.01 sec root sum squared error. That is; if the individual channel time errors are defined as:

$$\begin{aligned} e_{roll} &\equiv |0.10 - t63_{roll}| \\ e_{yaw} &\equiv |0.10 - t63_{yaw}| \\ e_{pitch} &\equiv |0.10 - t63_{pitch}| \end{aligned} \tag{4.1}$$

then the root sum square error is defined as:

$$Rss\ e_{total} \equiv \sqrt{e_{roll}^2 + e_{yaw}^2 + e_{pitch}^2} \tag{4.2}$$

The requirement is to that the RSS error must be less than 0.01 seconds. The overshoot is desired to be less than 2% in both lateral channels.

4.2 Frequency Domain Requirements

The missile model used in the design stage models the short period, roll and actuator modes. Neglected in this model are instrument dynamics, computational lags, and body bending modes. These high frequency dynamics contribute considerable phase lag as the open loop frequency increases. In addition, as a missile flies through the atmosphere; the buffeting it experiences during its passage through the air, the vibrations introduced by the movements of the fins, and any number of other disturbances will excite the vibrational modes of the missile. These modes cause high frequency accelerations and body rates to be detected by the flight control system instruments. If these parasitic dynamics are not accommodated for in the controller design the closed loop system may go unstable.[28] For this reason the crossover frequencies of the autopilot broken at the control input are constrained to values well below the CAS natural frequency and well below the frequency of the lowest structural modes. Typically the maximum design crossover frequency is 5-10

times smaller than the lowest significant structural mode. If the crossover frequency is too large, these flexible body modes may be detected by the onboard instruments, fed back to the autopilot and amplified by the closed loop flight control system. In order to separate the roll dynamics from the lateral dynamics, the roll channel crossover frequency is typically higher than the lateral crossover frequencies.

For all three designs it will be assumed that there are high frequency flexible body modes at frequencies beginning at 320 rad/second for the lateral channels and 600 rad/second for the torsional channel. These high frequency modes are the reason that the controllers' bandwidth are limited to the specified values. The nominal design the desired crossover frequencies of the lateral channels with the respective loop broken at the input to the control and the remaining loops closed are 30 rad/sec. and the desired value for the roll channel is 60 rad/sec..

Chapter 5 Linear Quadratic Autopilot Design

The goal of this autopilot is to force the airframe to track the pitch and yaw lateral acceleration and roll angle commands. As shown in Figure 5-1 the inputs to a full state controller are the missile states and the reference commands; the outputs are the fin deflection commands.

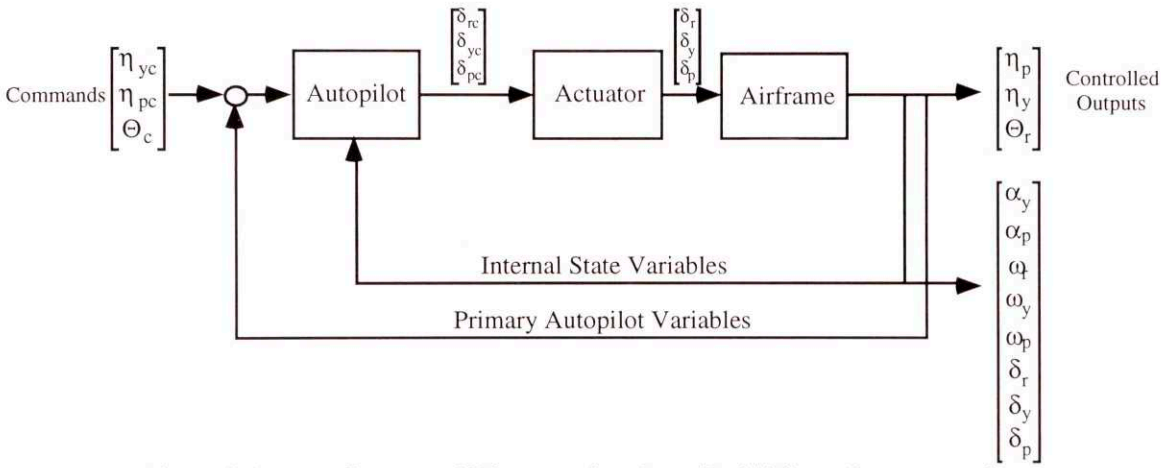

Figure 5-1 Conceptual Diagram of an Autopilot/Airframe Interconnection

The Linear Quadratic autopilot is a full state feedback design. It is to have zero steady state error and must satisfy the performance goals as discussed in Chapter 4.

5.1 Methodology

A Linear Quadratic design is constructed by solving for the solution an algebraic Ricatti equation that results from the standard multivariable control quadratic cost function minimization.

The missile airframe and CAS are modeled by the following linear state space representation.

$$\dot{x} = Ax + Bu$$
$$y = Cx + Du \tag{5.1}$$

$$x \in R^n,\ u \in R^m,\ y \in R^p$$

where x is the state vector, u the control vector and y is the controlled output vector. The LQ full state control law

$$u = F^* x \tag{5.2}$$

that satisfies the performance goals is found using an optimal full state gain matrix. The optimal full state feedback gain matrix is:

$$F^* = -R^{-1}B^T K \tag{5.3}$$

where K is the solution to the steady state algebraic Ricatti equation:

$$0 = A^T K + KA - KBR^{-1}B^T K + Q \tag{5.4}$$

This Ricatti equation results from the minimization of the linear quadratic performance cost:

$$J = \int_0^\infty (\mathrm{x}^T \mathrm{Q} \mathrm{x} + \rho \mathrm{u}^T \mathrm{R} \mathrm{u}) dt \tag{5.5}$$

where the state weighting matrix Q is positive semi-definite, and the control weight R is positive definite. The time and frequency domain specifications are met by careful adjustment of the Q and R state and control weighting matrices. The scalar parameter ρ determines how much control action is penalized in the final solution.

The final full state solution F* composed of the following elements:

$$F^* = \left[F^{1}_{3x3} \;\vdots\; \begin{matrix} F^{2r}_{1x1} \\ \cdots \\ F^{2l}_{2x2} \end{matrix} \;\vdots\; \begin{matrix} F^{3r}_{1x1} \\ \cdots \\ F^{3l}_{2x2} \end{matrix} \;\vdots\; F^{4}_{3x3} \right]$$

The individual gain blocks (F^1, F^{2r}, F^{2l}, etc.) multiply states of the airframe. The subscripts on each block denote the dimension of that block. The interconnections of these blocks and what signals are fed to each set can be seen in Figure 5-3.

5.2 Design Plant

As discussed in Chapter 4 the time domain goals for the autopilot design is to have a 63% rise time of 0.20 seconds for both the yaw and the pitch channels and a 63% rise of 0.10 seconds for the roll channel. The frequency domain requirement is to have a crossover frequency of 30 radians per second for the yaw and pitch channels and a crossover frequency of 60 radians per second for the roll channel.

One additional unique requirement for the LQ autopilot design is to have zero steady state error. See Figure 4-1. This is accomplished by putting integral compensation on the errors between the commands and the attained signals. The effect of this block of integrator is to independently force the errors to zero. See Figure 5-2.

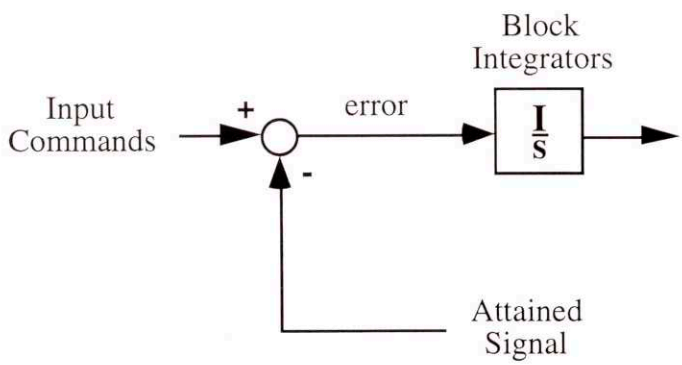

Figure 5-2 Block Integrators Assure Zero Steady State Tracking Error

This augmentation however must be done to the design plant that is used by the LQ algorithms. In order to avoid the nonlinear effects of the too rapid fin deflections, a strictly integral type of controller will be used. Experience has shown that a strictly integral controller (I) results in smoother performance characteristics in the time domain than does a proportional + integral controller (PI) for the acceleration channels. Therefore to obtain a strictly I type controller for the lateral channels, the states for the accelerations must not be included in the design model. However their integrals must be included. The resulting states for the design model are:

$$x_{LQ\ design\ plant} \equiv \left[\int \eta_y \int \eta_p \int \theta\ \alpha\ \beta\ \theta\ P\ Q\ R\ \delta_R\ \delta_Y\ \delta_P \right]^T \tag{5.6}$$

There are several ways to accomplish this state reorganization. The easiest conceptually is to recognize that the first two outputs from the nominal plant model are the accelerations. If these are added to the A matrix, then these states will represent the integrals of the accelerations.

$$A_{LQ\ design\ plant} \equiv \begin{bmatrix} 0 & C_{Nominal\ plant} \\ 0 & A_{Nominal\ plant} \end{bmatrix} \tag{5.7}$$

$$B_{LQ\ design\ plant} \equiv \begin{bmatrix} D_{Nominal\ plant} \\ B_{Nominal\ plant} \end{bmatrix} \tag{5.8}$$

$$C_{LQ\ design\ plant} \equiv [I] \tag{5.9}$$

$$D_{LQ\ design\ plant} \equiv [0] \tag{5.10}$$

The addition of the integral of roll angle will provide the final needed state for the LQ design model. The actual numeric values used for this design can be found in Appendix 2.

The architecture of such a full state controller is shown in Figure 5-3.

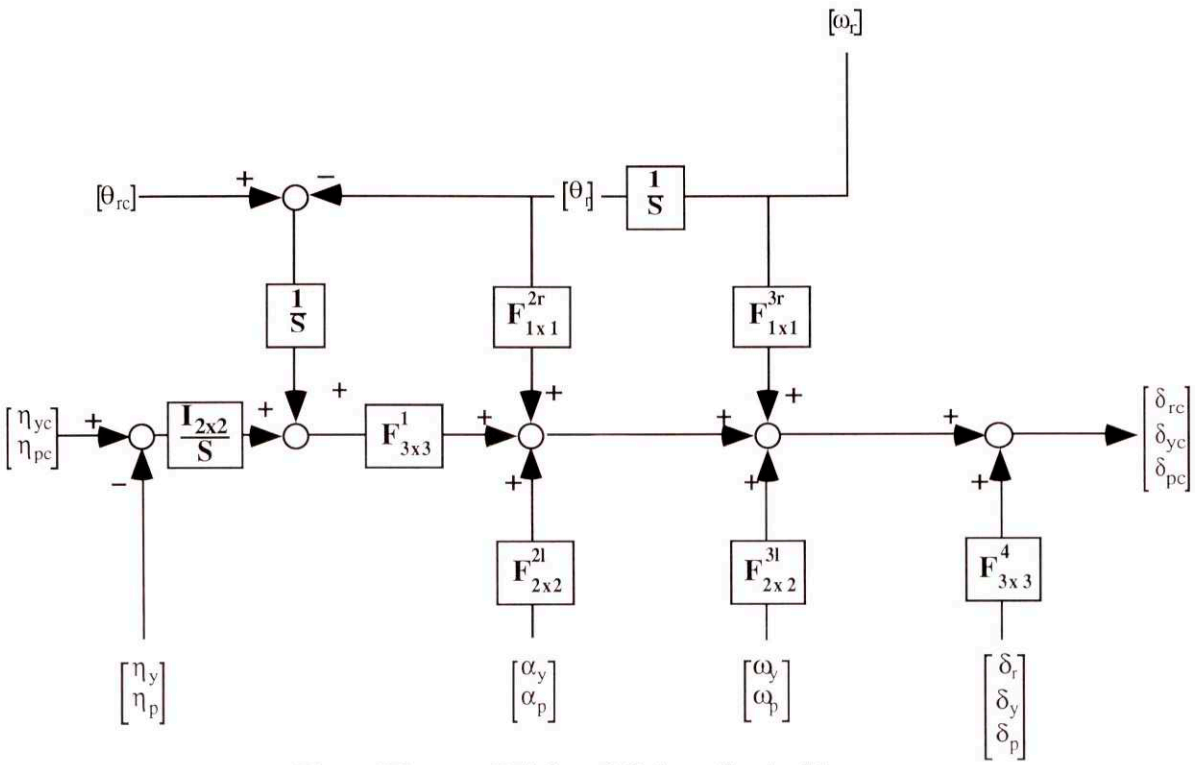

Figure 5-3 Full State LQ Autopilot Architecture

5.3 Design Process

The performance of an LQ autopilot is determined by the Q and R matrices of equation (5.4). The task of determining the elements of the Q and R matrices required to satisfy the design specifications however is a complex process requiring numerous iterations. The total number of elements in the Q matrix is the square of the number of the states. For the proposed design this results in 144 elements. In general the size of the R matrix is much smaller than the Q matrix. The R matrix has a total number of elements equal to the square of the number of controls or in this case 9. However these matrices must be positive semi-definite and positive definite respectively. This limits the total free elements of the Q matrix to 78 and a total of 6 for the R matrix.

In order to efficiently design the autopilot, several key assumptions were made:

1) The principal assumption was that the Q matrix did not need to fully populated.
2) The assumption was made that the channels performance could be determined independently at first to arrive at a preliminary design and then the final tuning could be performed.
3) The control weighting factor ρ was embedded in the R matrix.
4) The R matrix was assumed to have a diagonal shape.

Once these assumptions were made the Q and R matrices were adjusted by a two pass nonlinear optimization process. See Figure 5-4. The first or outer level of optimization was done on the Q matrix. The elements of the Q matrix under analysis were changed, a new Q matrix was formed and then the R matrix optimization was conducted. The R matrix was used to control the crossover frequencies of the single loops broken at the control, and when the frequency domain requirements were fulfilled, the time domain response was checked. Based on the results of the time domain analysis, the Q matrix was modified and the process repeated. This optimization was performed separately for each channel.

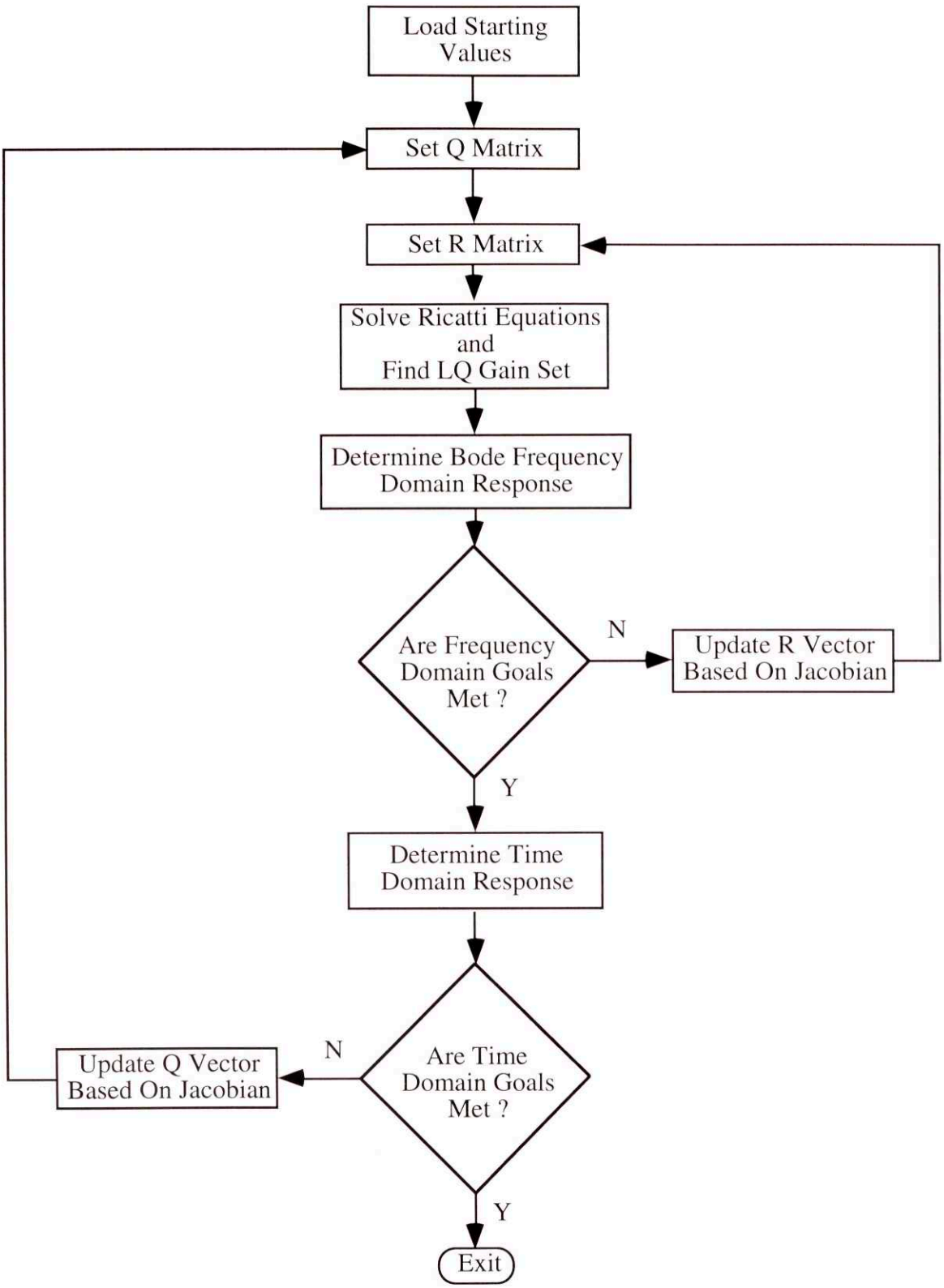

Figure 5-4 The LQ Weighting Matrices are Found by Trials and by Optimization

When preliminary values had been determined for each channel, the optimization process was again performed with the results of the first iteration used as the starting point for the second iteration. The final Q and R matrices from this iteration were then used to generate the full state LQ autopilot gains. This final controller design is in no way a unique design, and different choices of weighting parameters could result in a controller which would satisfy all the performance requirements but have different performance characteristics..

5.4 Nominal Performance

The final values for the Q and R matrices for the LQ Autopilot are shown in Tables 5-1 and 5-2. The LQ autopilot poles are shown in Table 5-3.

$\int\eta_y$	$\int\eta_p$	$\int\theta$	α	β	θ	ω_r	ω_y	ω_p	δ_r	δ_y	δ_p	
22398	0	0	0	0	0	0	149	0	0	0	0	$\int\eta_y$
0	9503	0	0	0	0	0	0	97	0	0	0	$\int\eta_p$
0	0	899	0	0	0	0	0	0	0	0	0	$\int\theta$
0	0	0	2498	0	0	0	0	0	0	0	0	α
0	0	0	0	823	0	0	0	0	0	0	0	β
0	0	0	0	0	6302	0	0	0	0	0	0	θ
0	0	0	0	0	0	17	0	0	0	0	0	ω_r
149	0	0	0	0	0	0	1	0	0	0	0	ω_y
0	97	0	0	0	0	0	0	1	0	0	0	ω_p
0	0	0	0	0	0	0	0	0	1.00E-10	0	0	δ_r
0	0	0	0	0	0	0	0	0	0	1.00E-10	0	δ_y
0	0	0	0	0	0	0	0	0	0	0	1.00E-10	δ_p

Table 5-1 LQ Autopilot State Weighting Matrix Q

δr	δy	δp	
9196	0	0	δr
0	1740	0	δy
0	0	789	δp

Table 5-2 LQ Autopilot Control Weighting Matrix R

	Real	Imag	Freq.	Damp
1	0.0	0.0	0.0	
2	0.0	0.0	0.0	
3	0.0	0.0	0.0	

Table 5-3 LQ Autopilot Poles

The closed loop performance of the system is summarized in Tables 5-4 and 5-5. The risetime requirement is satisfied exactly, and the single loop bode crossover frequencies are within the total allowed error. The overshoot in the roll channel is larger than was desired and showed a very slow decay rate.

	Yaw	Pitch	Roll
Crossover Frequency (rad/sec)	30.7	30.2	59.9
63% Rise time (sec)	0.20	0.20	0.10
Overshoot (%)	2.2	0.0	5.5

Table 5-4 LQ Autopilot Nominal Performance Results

	Gain Margin (dB)	Phase Margin (deg)
Roll	∞	106
Yaw	∞	73
Pitch	∞	93

Table 5-5 LQ Autopilot Nominal Bode Stability Margins

The time domain responses to steps are shown in Figures 5-6 through 5-11. As shown in Figure 5-11 the roll channel has good 63% risetime performance but a slow settling time. The is particularly noticeable in the acceleration step response (Figures 5-7 and 5-9). The

Bode plots of the individual yaw, pitch and roll channels are shown in Figures 5-12 through 5-13. For these plots, the loop was broken at the plant input and the remaining feedback loops were closed. See Figure 2-2. As defined in Figure 5-5 there are three distinct places where signals can enter the system. They are the normal commands, the perturbations to the plant which are modeled as disturbances at the plant input and disturbances which are reflected at the plant output. From these three inputs, four types of transfer functions can be evaluated. They are the:

Loop Transfer
Sensitivity
Perturbation to Control
Complementary Sensitivity

These transfer functions show respectively: the open loop transfer function from the commands to the controlled outputs; the sensitivity of the closed loop system to disturbances at the plant output, the transfer function from perturbations at the plant input to the controlled output, and the closed loop transfer function from the commands to the output. The derivation for these transfer functions is shown in Appendix 8.

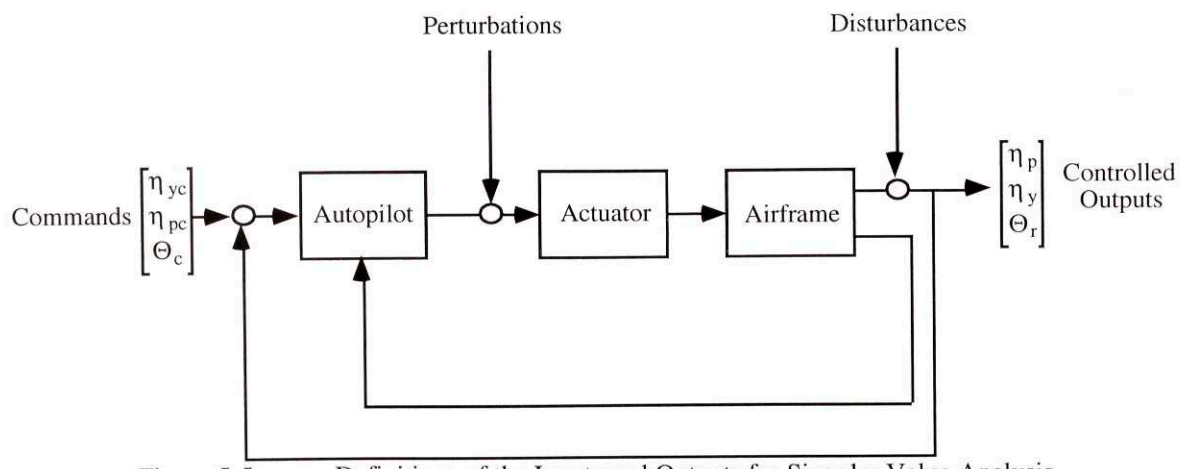

Figure 5-5 Definitions of the Inputs and Outputs for Singular Value Analysis

Figure 5-15 shows the loop gain of the LQ autopilot. Figure 5-16 shows the sensitivity to disturbances of the LQ design. As can be seen in Figure 5-17 the LQ design can amplify perturbations that occur with a frequency of approximately 1 to 60 Hertz, depending upon their direction. The singular values from the commands to the controlled outputs are shown in Figure 5-18.

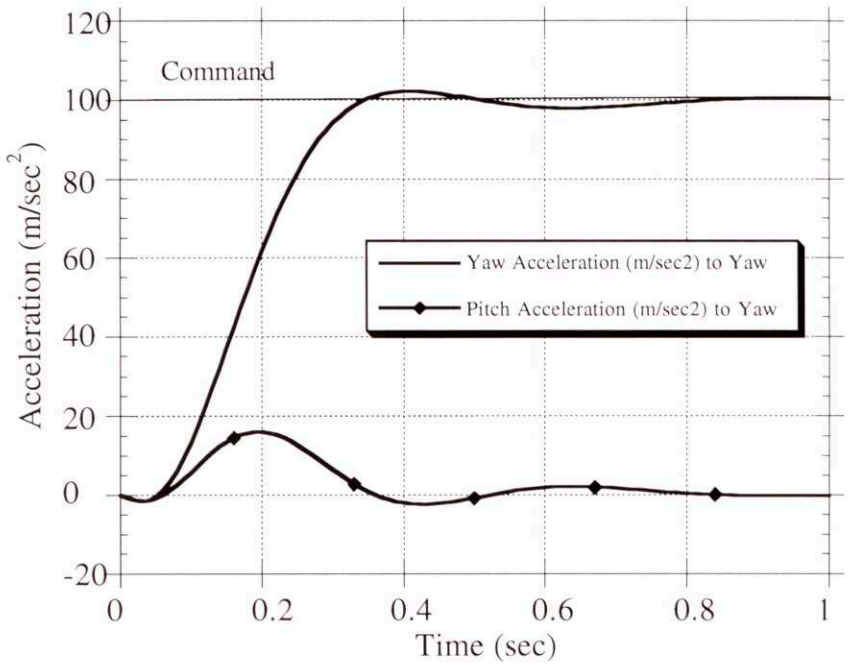

Figure 5-6 LQ Autopilot Acceleration Responses Due to a Yaw Step Command

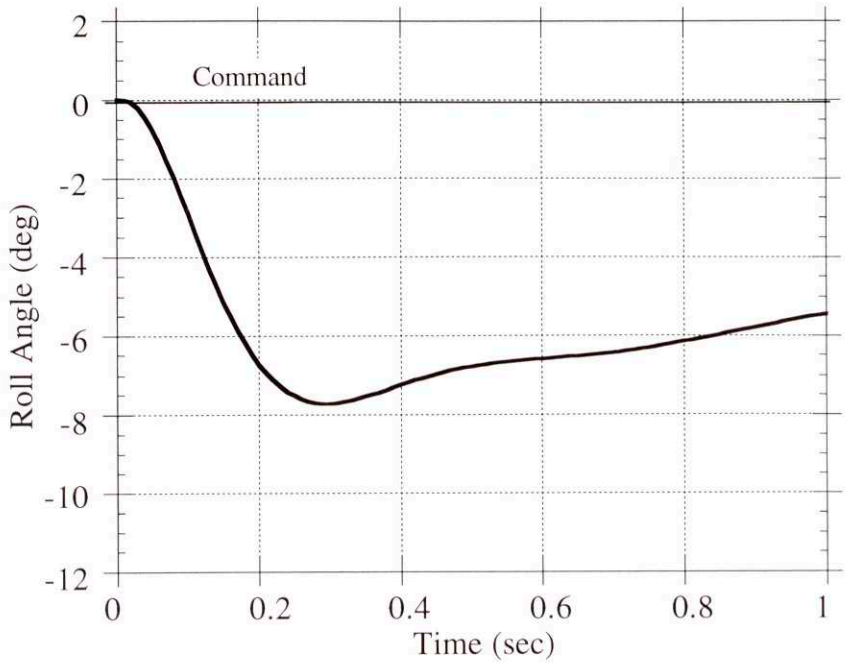

Figure 5-7 LQ Autopilot Roll Angle Response Due to a Yaw Step Command

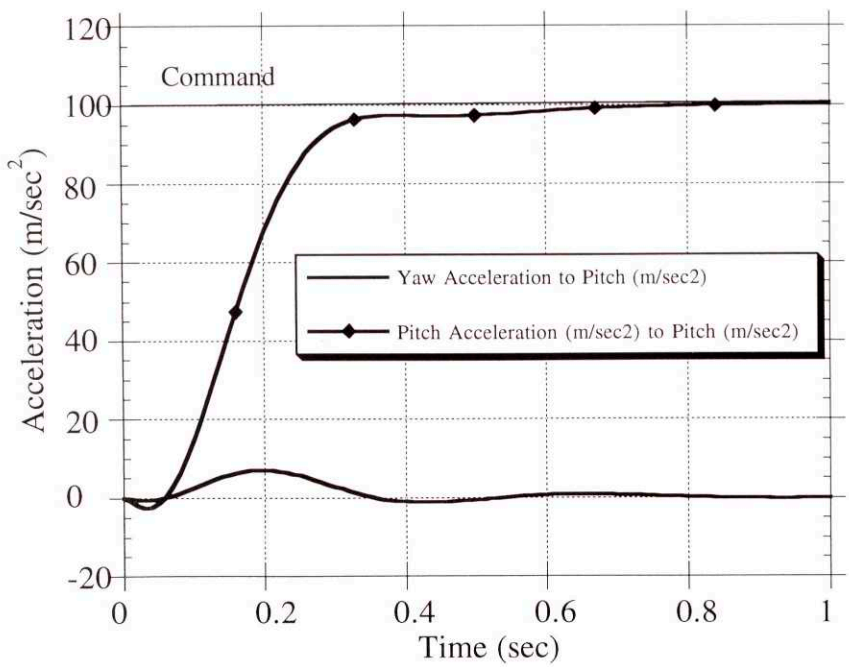

Figure 5-8 LQ Autopilot Acceleration Responses Due to a Pitch Step Command

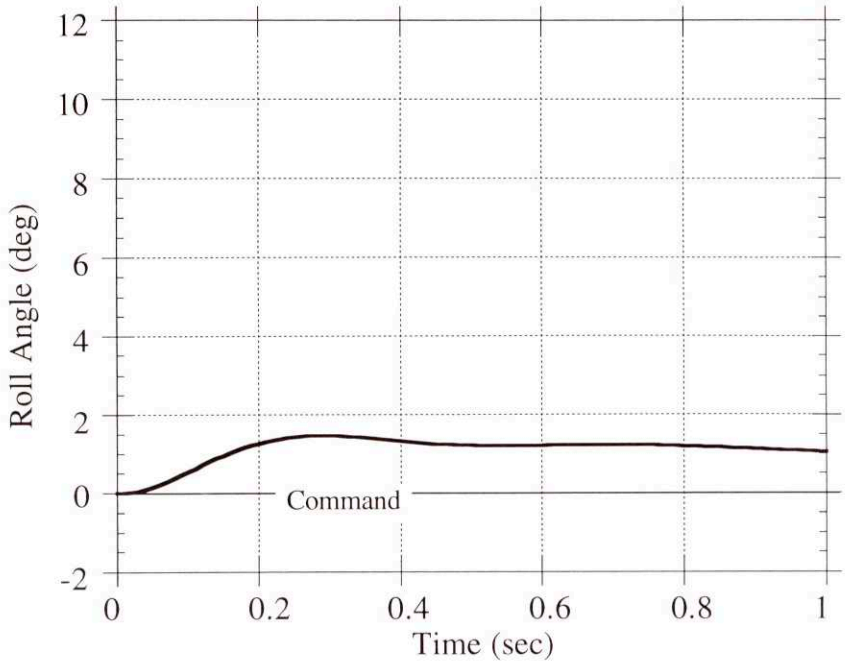

Figure 5-9 LQ Autopilot Roll Angle Response Due to a Pitch Step Command

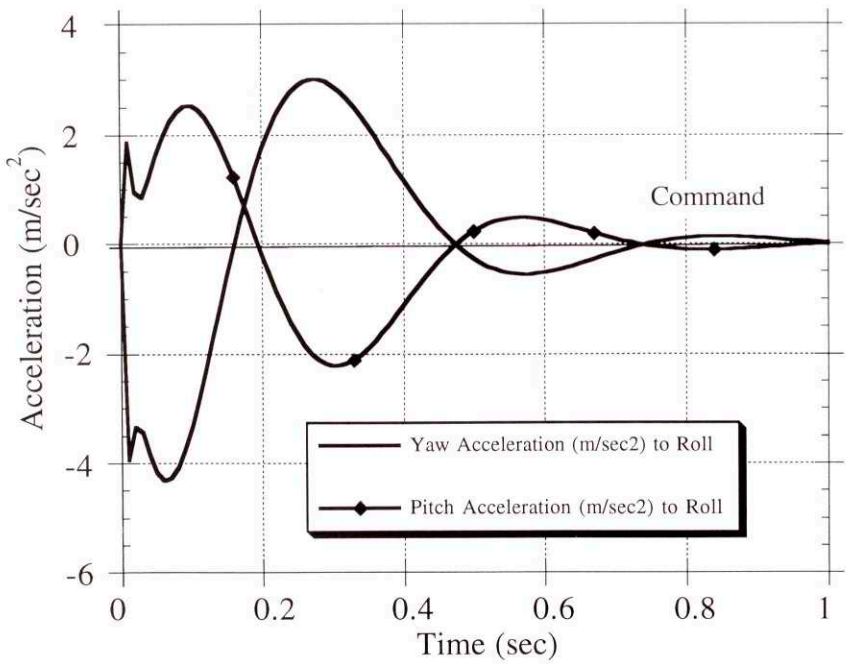

Figure 5-10 LQ Autopilot Acceleration Responses Due to a Roll Angle Step Command

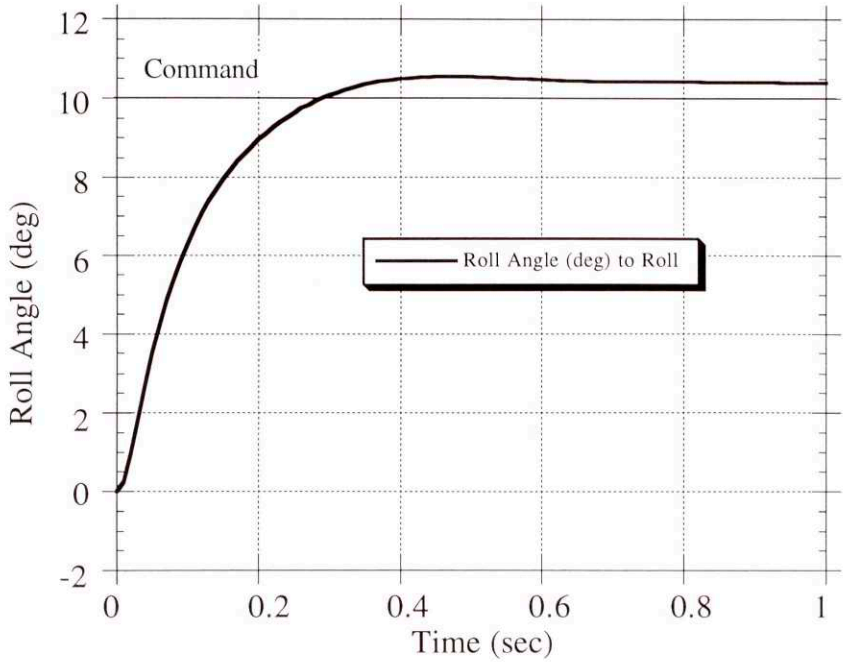

Figure 5-11 LQ Autopilot Roll Angle Response Due to a Roll Angle Step Command

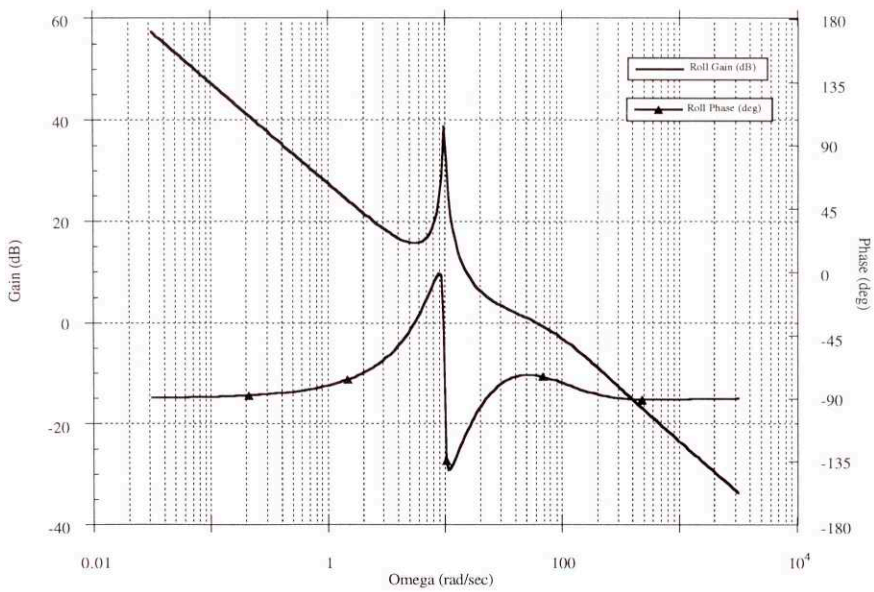

Figure 5-12 LQ Autopilot Roll Channel Bode Plot with the Roll Loop Broken at the Airframe Input

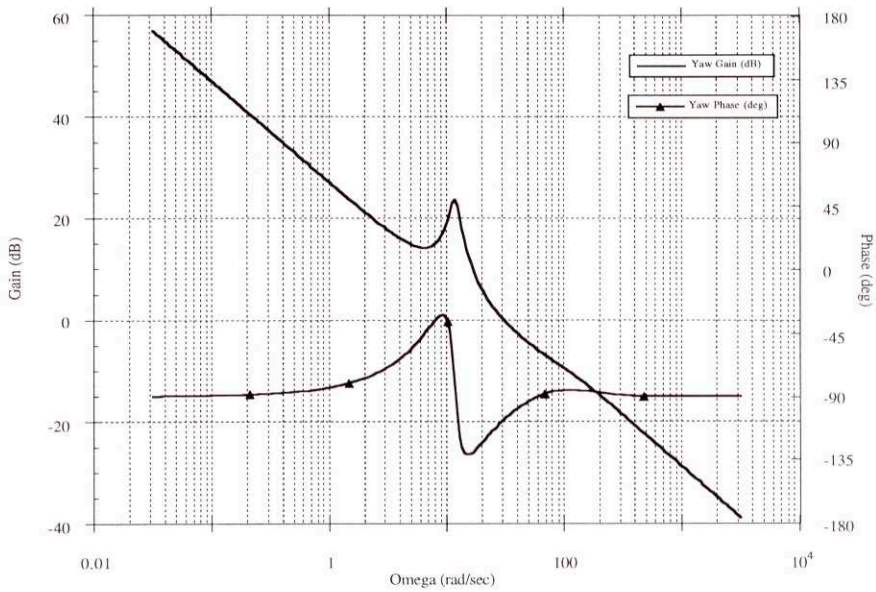

Figure 5-13 LQ Autopilot Yaw Channel Bode Plot with the Yaw Loop Broken at the Airframe Input

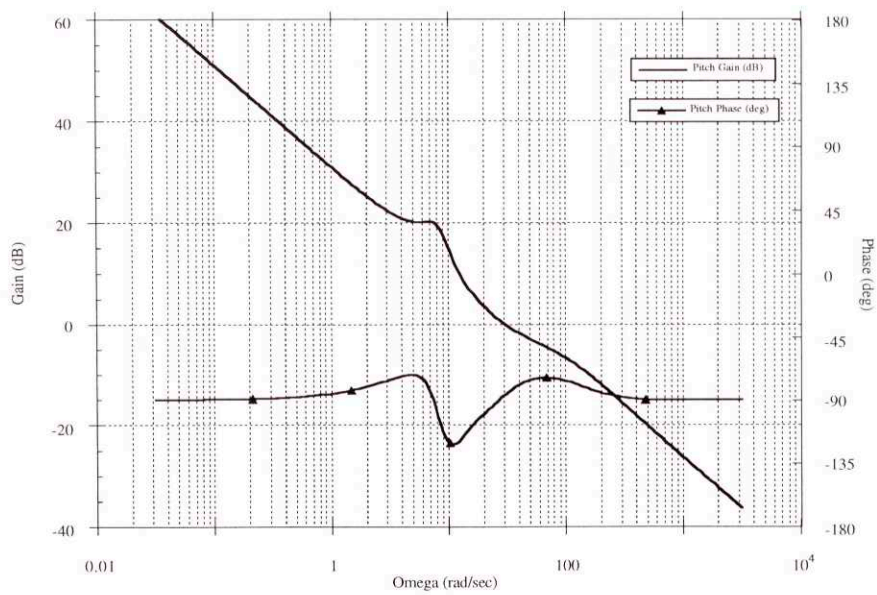

Figure 5-14 LQ Autopilot Pitch Channel Bode Plot with the Pitch Loop Broken at the Airframe Input

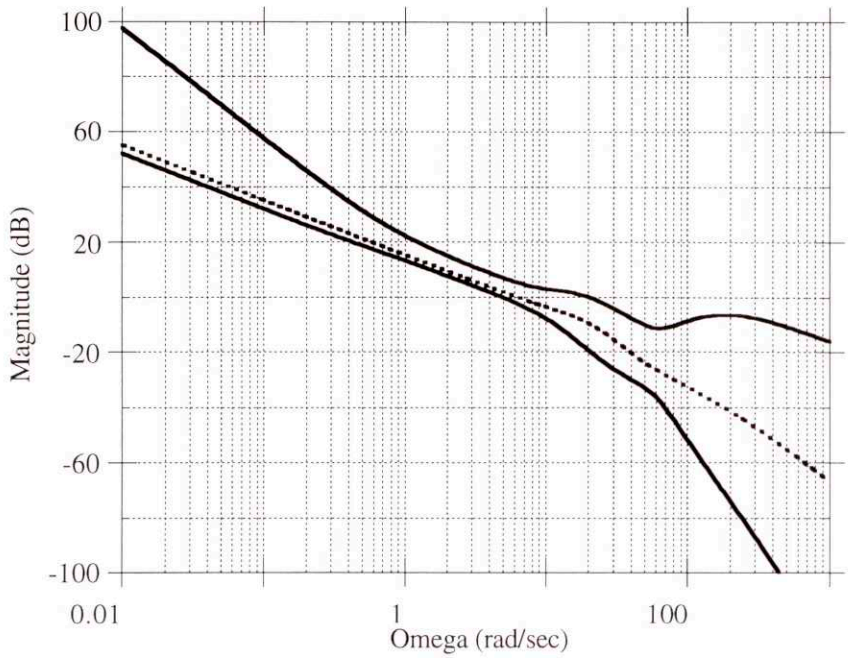

Figure 5-15 LQ Autopilot Loop Transfer Function

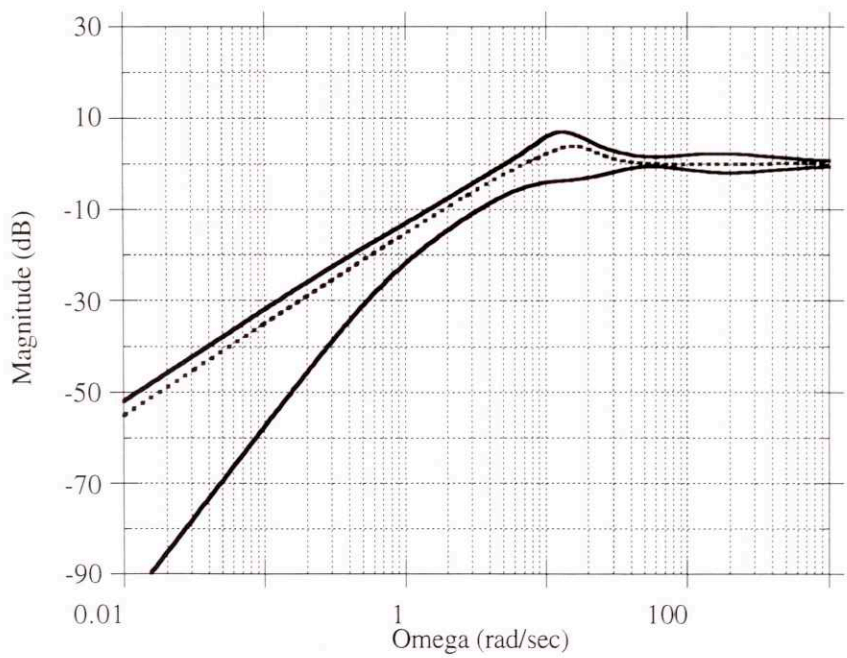

Figure 5-16 LQ Autopilot Singular Values Disturbances to The Controlled Outputs

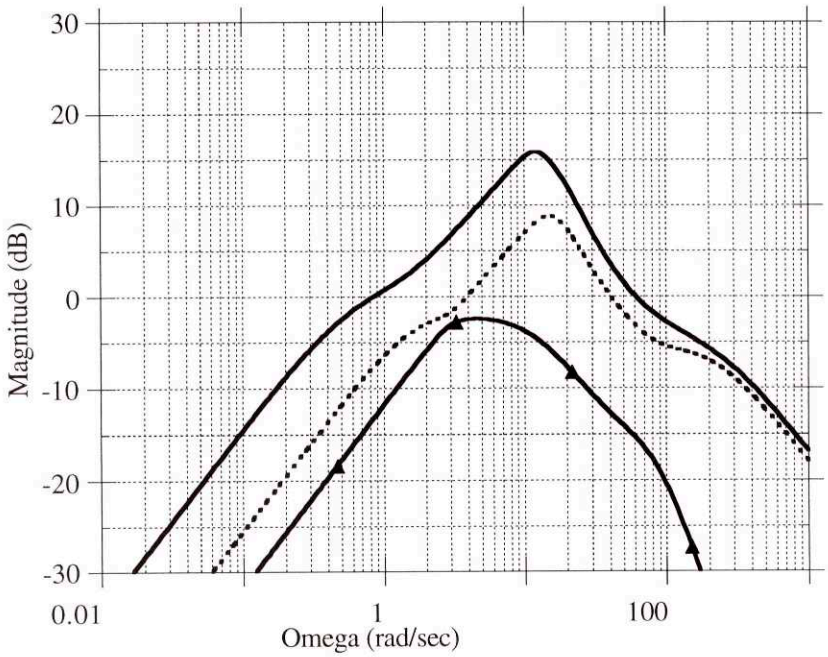

Figure 5-17 LQ Autopilot Singular Values Perturbations to The Controlled Outputs

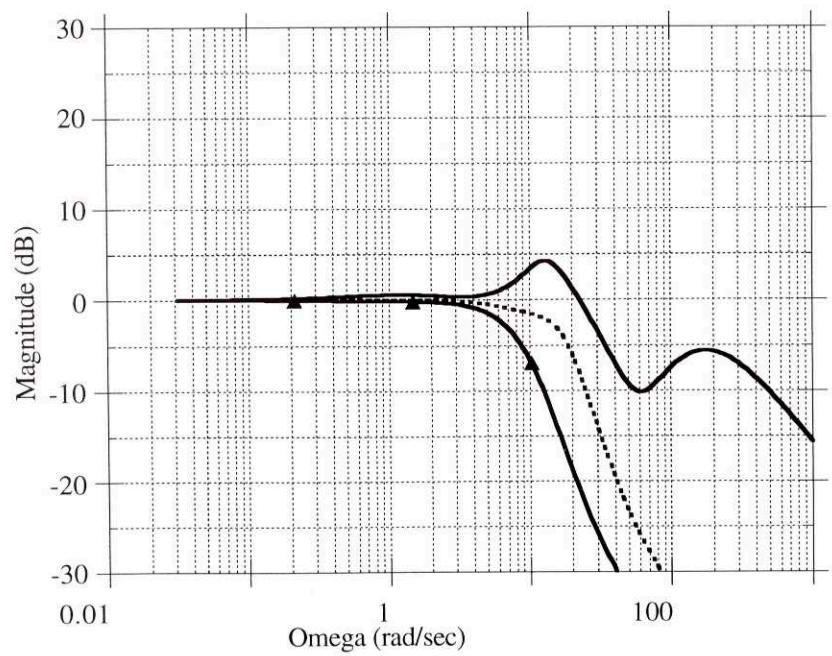

Figure 5-18 LQ Autopilot Singular Values Autopilot Commands to The Controlled Outputs

Chapter 6 H_∞ Autopilot Design

In contrast to the relatively simple structure of the LQ autopilot from Chapter 5, an H_∞ or an H_2 autopilot is much more complex. The number of states of an H_∞ or H_2 autopilot is equal to the number of the states in the design model plus the number of states in the frequency weighting filters. As shown in Figure 6-1 the reason for this relatively large number of states is that these types of autopilots contain a sub-optimal filter to enhance the disturbance rejection properties and robustness to parameter variations of the autopilot.

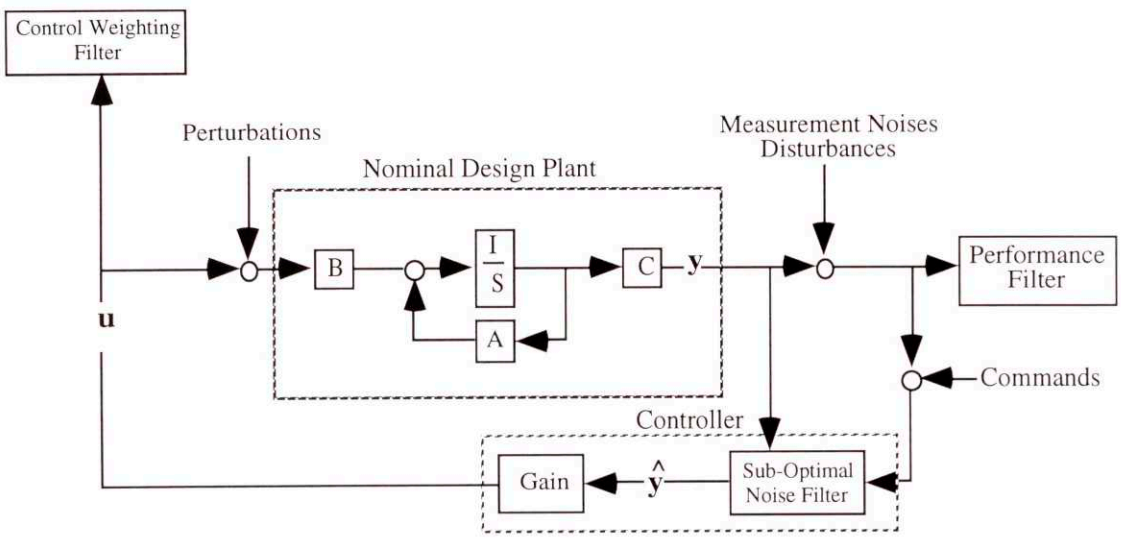

Figure 6-1 H_∞ and H_2 Autopilot/Airframe Interconnection

The design goal for the H_∞ and H_2 autopilots are the same as those for the LQ autopilot that were originally discussed in Chapter 4. To reiterate those goal were:

0.20 second 63% rise times for the yaw and pitch channels
0.10 second 63% rise times for the roll channel
30 radians per second crossover frequencies for the yaw and pitch channels
60 radians per second crossover frequency for the roll channel

As usual it is desired to limit the amount of overshoot and to have as little steady state error as possible. The requirement for zero steady state error in the lateral channels that was

imposed on the LQ design is relaxed for this design because of the additional difficulty imposed by the integrator dynamics near the origin

6.1 H_∞ Control Law Synthesis

The H_2 and H_∞ control algorithms used in this thesis implement full output feedback controllers based on the interconnection model shown in Figure 6-2. [21],[23]

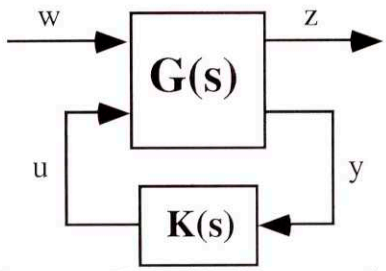

Figure 6-2 H_∞ and H_2 Interconnection Model

The vector w contains the exogenous inputs, the vector z is the controlled output, the vector y is the internal states available for feedback, and the u is the control vector for the plant. The state space equations for the augmented system are:

$$\begin{aligned} \dot{x}(t) &= Ax(t) + B_1 w(t) + B_2 u(t) \\ z(t) &= C_1 x(t) + D_{11} w(t) + D_{12} u(t) \\ y(t) &= C_2 x(t) + D_{21} w(t) + D_{22} u(t) \end{aligned} \tag{6.1}$$

The generalized plant model G(s) is defined as:

$$G(s) = \left[\begin{array}{c|cc} A & B_1 & B_2 \\ \hline C_1 & D_{11} & D_{12} \\ C_2 & D_{21} & D_{22} \end{array}\right] \tag{6.2}$$

This generalized plant includes not only the nominal design plant as derived in Chapter 3 but any performance weighting functions that are used in the design process.

An H_∞ controller minimizes the infinity norm of the generalized plant G(s). The infinity norm is defined as:

$$\|G\|_\infty = \sup_{\omega} \sigma_{max}[G(j\omega)] \tag{6.3}$$

The minimizing solution involves two Hamiltonian matrices:

$$H_2 = \begin{bmatrix} A & \gamma^{-2}B_1B_1^T - B_2B_2^T \\ -C_1^TC_1 & -A^T \end{bmatrix} \tag{6.4}$$

$$J_2 = \begin{bmatrix} A^T & \gamma^{-2}C_1^TC_1 - C_2^TC_2 \\ -B_1B_1^T & -A \end{bmatrix} \tag{6.5}$$

These Hamiltonians expand into the following Ricatti equations:

$$0 = A^TX + XA + X(\gamma^{-2}B_1B_1^T - B_2B_2^T)X + C_1^TC_1 \tag{6.6}$$

$$0 = AY + YA^T + Y(\gamma^{-2}C_1^TC_1 - C_2^TC_2)Y + B_1B_1^T \tag{6.7}$$

If the following terms are defined:

$$\begin{aligned} F_\infty &= -B_2^TX, \quad L_\infty = -YC_2^T \\ Z_\infty &= (I - \gamma^{-2}YX)^{-1} \end{aligned} \tag{6.8}$$

$$\hat{A}_\infty = A + \gamma^{-2}B_1B_1^TX + B_2F_\infty + Z_\infty L_\infty C_2 \tag{6.9}$$

then a controller which satisfies the constraint is:

$$K(s) = \begin{bmatrix} \hat{A}_2 & -Z_\infty L_2 \\ F_2 & 0 \end{bmatrix} \tag{6.10}$$

The equations documented in the previous sections were evaluated using routines commercially available. The inputs to these routines are a design plant and a minimum gamma to evaluate. The algorithm then search for the minimum attainable γ in the specified range.

6.2 Design Plant

The airframe design plant for both H_∞ and H_2 autopilots are the same. The airframe states are those in the basic plant. They are:

$$x_{H_\infty \text{ and } H_2 \text{ design plant}} \equiv [\Delta\alpha \; \Delta\beta \; \theta \; P \; Q \; R \; \delta_R \; \delta_Y \; \delta_P]^T \tag{6.11}$$

There are 11 outputs for the design plant. They are:

$$y_{H_\infty \text{ and } H_2 \text{ design plant}} \equiv [\eta_y \; \eta_p \; \Delta\alpha \; \Delta\beta \; \theta \; P \; Q \; R \; \delta_R \; \delta_Y \; \delta_P]^T \tag{6.12}$$

In addition, the design algorithms acknowledge the potential for plant perturbations at the input and disturbances at the output as shown in Figure 6-3.

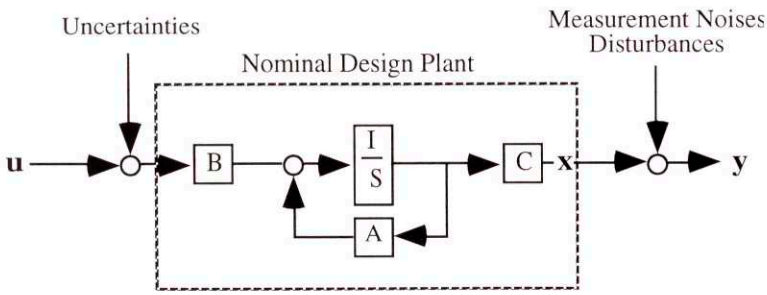

Figure 6-3 H_∞ and H_2 Autopilot/Airframe Interconnection

The type of uncertainties that are reflected at the input are usually multiplicative in nature. This means that the airframe has been scaled by some unknown possibly frequency dependent quantity. That is:

$$G(s)_{Actual} = (I + \Delta)G(s)_{Nominal} \tag{6.13}$$

Theses types of errors are associated with the plant model and typically result from poor model derivations, hardware problems, and inexact knowledge of the local operating point.

The types of errors that are modeled by the disturbances are usually additive in nature. They are readily envisioned as noises on instruments, exogenous disturbances such as wind, etc..

The performance filters discussed in the following section are augmented to the airframe to form the final state space design model. This final model has 15 states and 17 inputs. The inputs are the three commands, the three perturbations and the 11 measurement noises. The state space A, B, C, and D matrices are shown in Appendix 3.

6.3 Design Process

The performance of an H_∞ controller is determined indirectly by the weighting filters that are used in the design process. These filters can be made frequency dependent thereby offering the designer great flexibility in the design process. There are two basic types of filters that are used to control the bandwidth of the controller and regulate its performance. These two filters are the control weighting filter and the performance weighting filter respectively.

The control weighting filter is used to control the bandwidth of the system, the higher the penalty at a given frequency the more that frequency component will be penalized. This

penalty has the effect reducing the level of activity at the frequency in the final solution. It is used to regulate the control activity also. Generally the magnitude of the penalty increases as the frequency increases. This is to reflect the growing uncertainty in most models as the frequency increases and the desire to have less high frequency control activity. (The effects of unmodeled dynamics, low order design models, etc. are most prevalent at the higher frequencies.)

The performance weighting filter is used for the controller's closed loop performance. At low frequencies this filter has an effect on the steady state error. The crossover of this filter indirectly controls the rise time of the autopilot.

The actual design process requires numerous iterations of the filter structure. These iterations result from a comparison of the resultant closed loop system's performance in both the time and frequency domains and the performance specifications.

6.3.a H_∞ Filters

The control weighting filter for the H_∞ autopilot was designed with the idea of limiting high frequency control action, but allowing low frequency actions and particularly allowing for steady state fin deflections. This steady state allowance is to account for the steady state fin deflections required to satisfy step input requirements. There are three 1^{st} order filters for the H_∞ design. One filter each for the roll, yaw and pitch channels. The final filters used for the autopilot design are:

$$G(s)_{Roll\ Control} = \frac{20s}{s + 350} \tag{6.14}$$

$$G(s)_{Yaw\ Control} = \frac{20s}{s + 550} \tag{6.15}$$

$$G(s)_{Pitch\ Control} = \frac{20s}{s + 350} \tag{6.16}$$

Their respective frequency responses can be found in Figures 6-4 and 6-5.

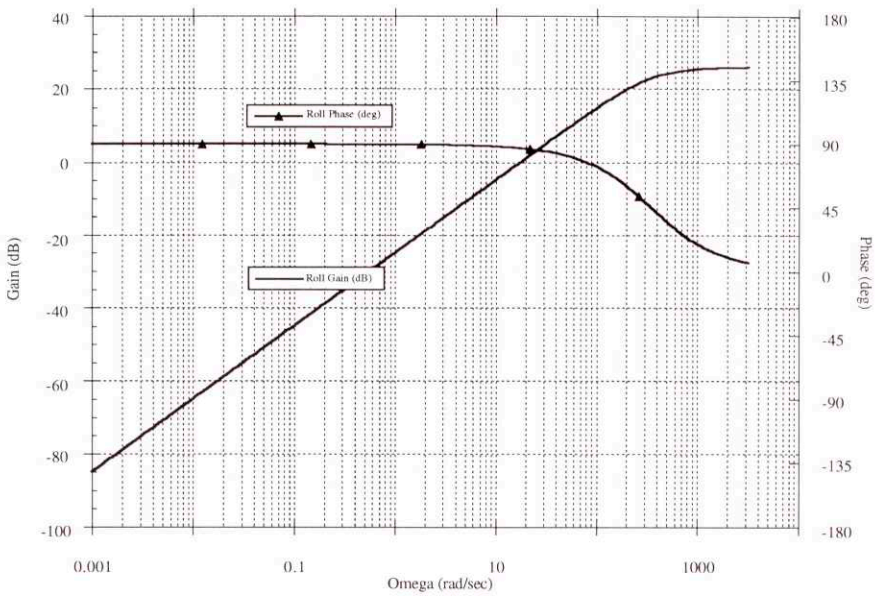

Figure 6-4 H_∞ Autopilot Roll Channel Control Weighting Filter

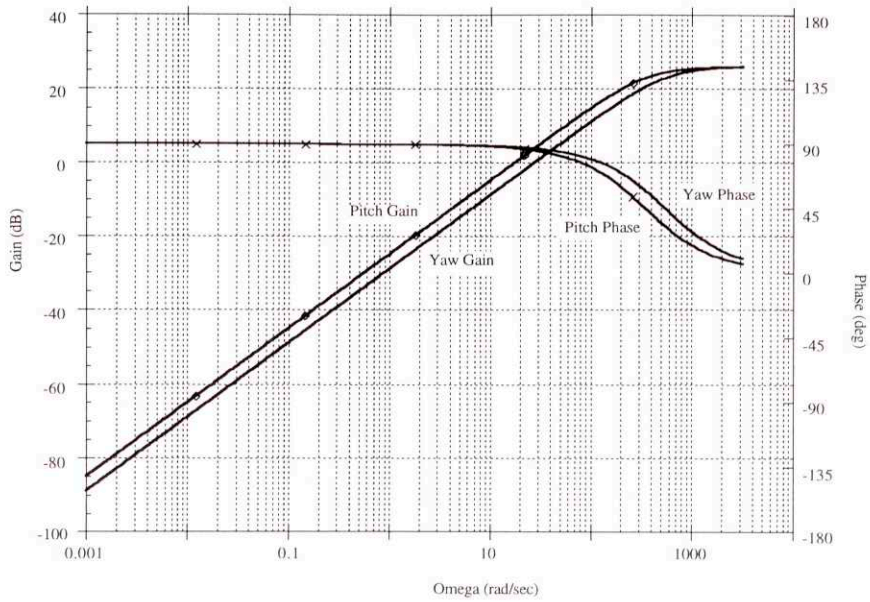

Figure 6-5 H_∞ Autopilot Lateral Channel Control Weighting Filter

There are also three first order performance filters used in the H_∞ design. One each for the roll, yaw and pitch channel. The inputs to these filters are the roll angle θ, and the two lateral accelerations η_y and η_p. The performance weighting filters used are as follows:

$$G(s)_{Roll\ Performance} = \frac{0.5(s + 35)}{s + 1.4} \tag{6.17}$$

$$G(s)_{Yaw\ Performance} = \frac{0.5(s + 3.5)}{s + 0.035} \tag{6.18}$$

$$G(s)_{Pitch\ Performance} = \frac{0.5(s + 3.5)}{s + 0.035} \tag{6.19}$$

Their respective frequency responses can be found in Figures 6-6 and 6-7.

The values of the A, B, C and D matrices after the augmentation of the filters can be found in Appendix 4.

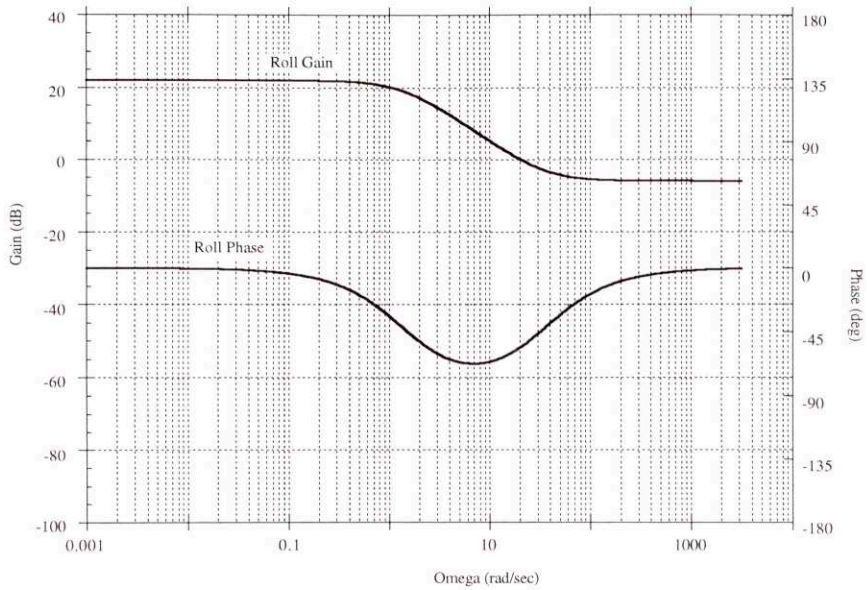

Figure 6-6 H_∞ Autopilot Roll Channel Performance Filter

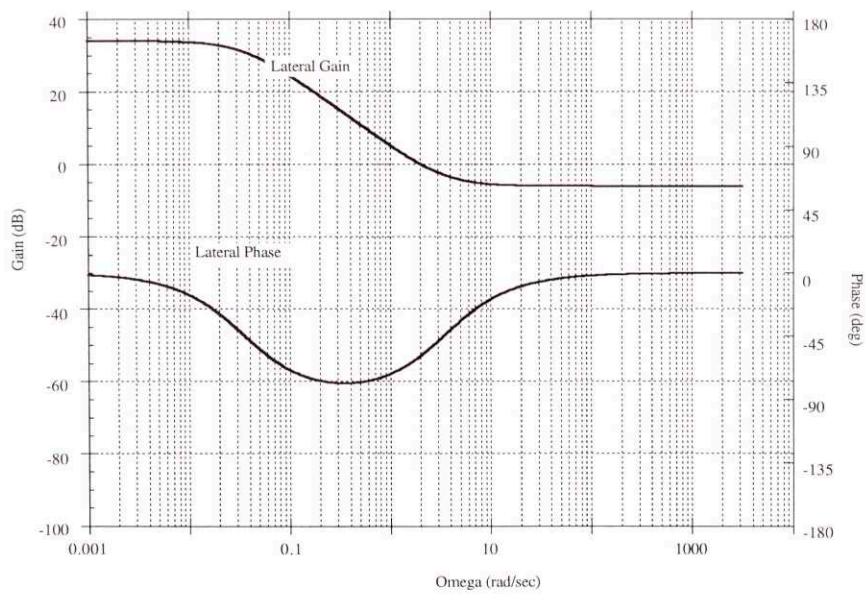

Figure 6-7 H_∞ Autopilot Lateral Channel Performance Filter

6.4 Nominal Performance

The final H_∞ autopilot has 15 states. The minimum achievable gamma for this condition using these filters is 3.6719. The H_∞ autopilot poles are shown in Table 6-1. The actual values of the A, B, C matrices for the compensator are shown in Appendix 5.

Real	Imag	Freq.	Damp
-0.035	0.0	0.035	
-0.035	0.0	0.035	
-0.9805	0.0	0.9805	
-1.4	0.0	1.4	
-8.999	0.0	8.999	
-10.56	0.0	10.56	
-53.59	-29.49	61.17	
-53.59	29.49	61.17	0.8761
-76.01	-37.34	84.68	
-76.01	37.34	84.68	0.8975
-291.1	0.0	291.1	
-303.9	0.0	303.9	
-515.9	-386.4	644.6	
-515.9	386.4	644.6	0.8004
-11290	0.0	11290	

Table 6-1 H_∞ Autopilot Poles

The closed loop performance of the system is summarized in Tables 6-2 and 6-3. The risetime requirement is satisfied exactly for the lateral channels, and is slightly too fast in the roll channel. The single loop bode crossover frequencies are within the total allowed error. The roll and pitch channels exhibit a steady state undershoot, while the yaw channel exhibits a slight overshoot. This steady state error is a direct consequence of the design decision not to augment the design plant with integrators. As long as this steady state error is small, it will not affect the missile's performance.

	Yaw	Pitch	Roll
Crossover Frequency (rad/sec)	29.6	30.1	60.2
63% Rise time (sec)	0.20	0.20	0.097
Overshoot (%)	0.77	-0.71	-1.4

Table 6-2 H_∞ Autopilot Nominal Performance Results

	Gain Margin (dB)	Phase Margin (deg)
Roll	∞	74
Yaw	∞	50
Pitch	-19,∞	46

Table 6-3 H_∞ Autopilot Nominal Bode Stability Margins

The Time domain responses to steps are shown in Figures 6-9 through 6-14. The Bode plots of the individual yaw, pitch and roll channels are shown in Figures 6-15 through 6-17. For these plots, the loop was broken at the plant input and the remaining feedback loops were closed. See Figure 2-2. As defined in Figure 6-8 there are three distinct places where signals can enter the system. They are the normal commands, the perturbations to the plant which are modeled as disturbances at the plant input and disturbances which are reflected at the plant output.

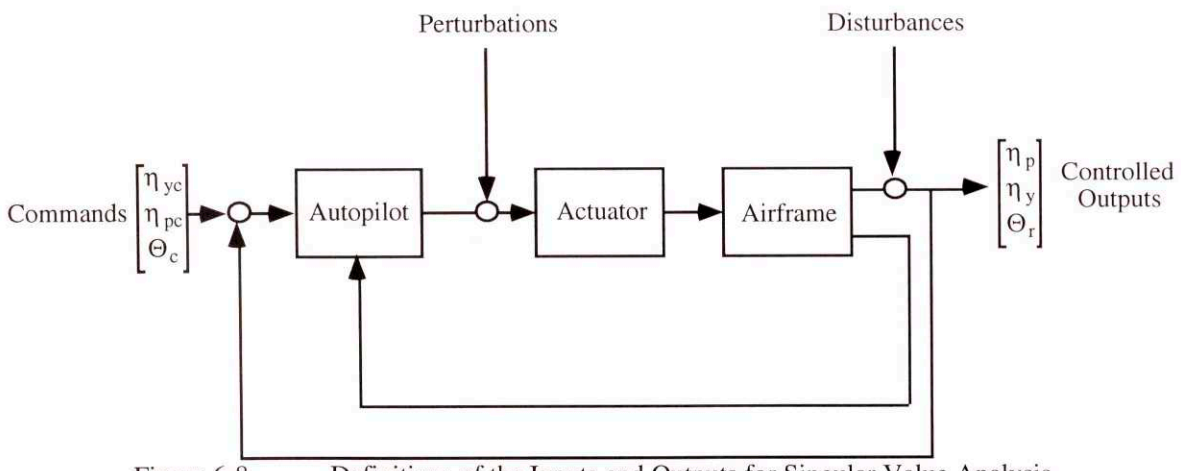

Figure 6-8 Definitions of the Inputs and Outputs for Singular Value Analysis

From these three inputs, four transfer functions may be derived. These are the loop transfer function (Figure 6-18), the sensitivity transfer function (Figure 6-19), the perturbation to the controlled output transfer function (Figure 6-20), and the complementary sensitivity function (Figure 6-21)

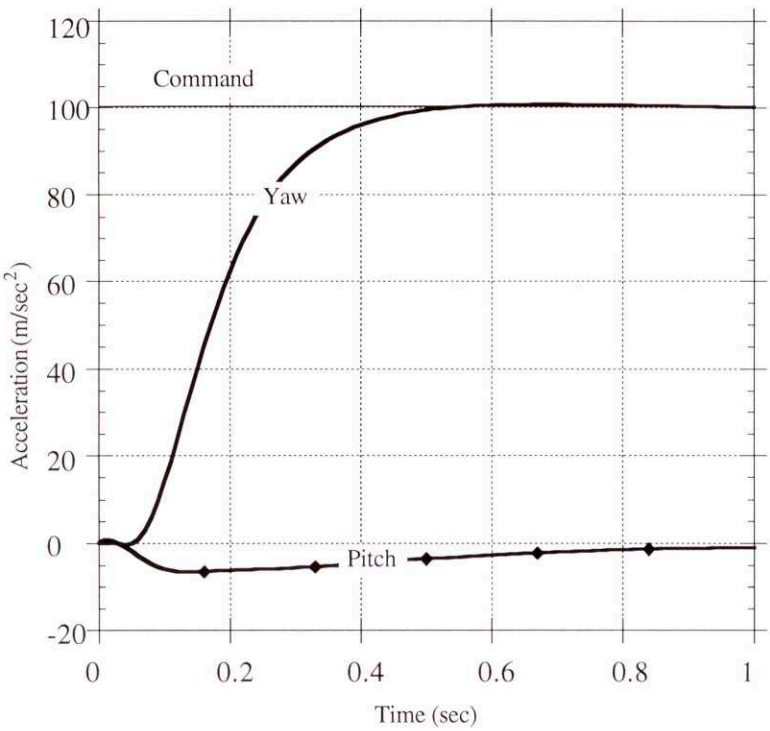

Figure 6-9 H∞ Autopilot Acceleration Responses Due to a Yaw Step Command

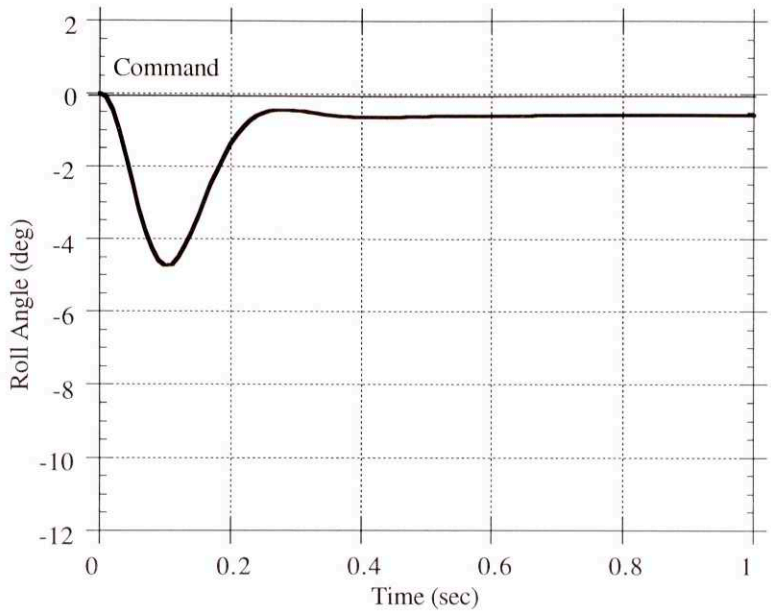

Figure 6-10 H_∞ Autopilot Roll Angle Response Due to a Yaw Step Command

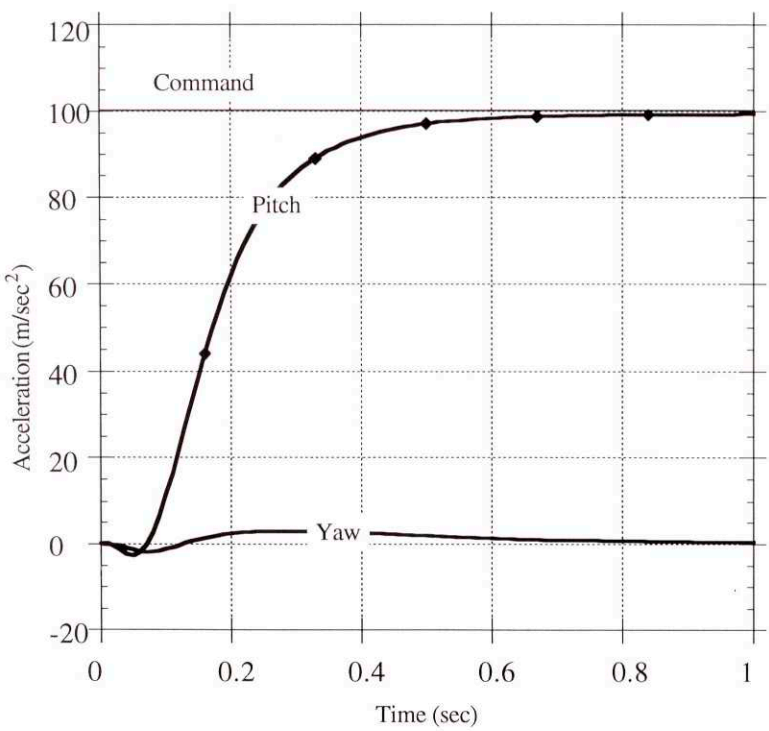

Figure 6-11 H_∞ Autopilot Acceleration Responses Due to a Pitch Step Command

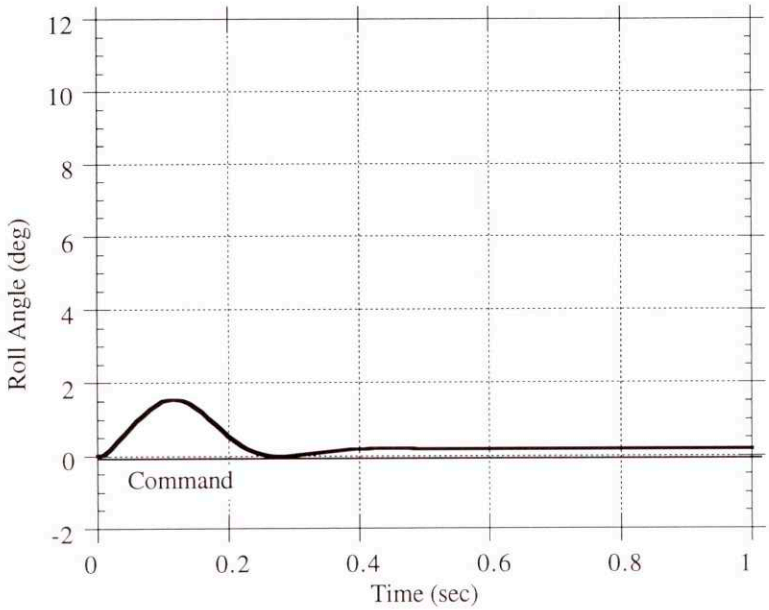

Figure 6-12 H_∞ Autopilot Roll Angle Response Due to a Pitch Step Command

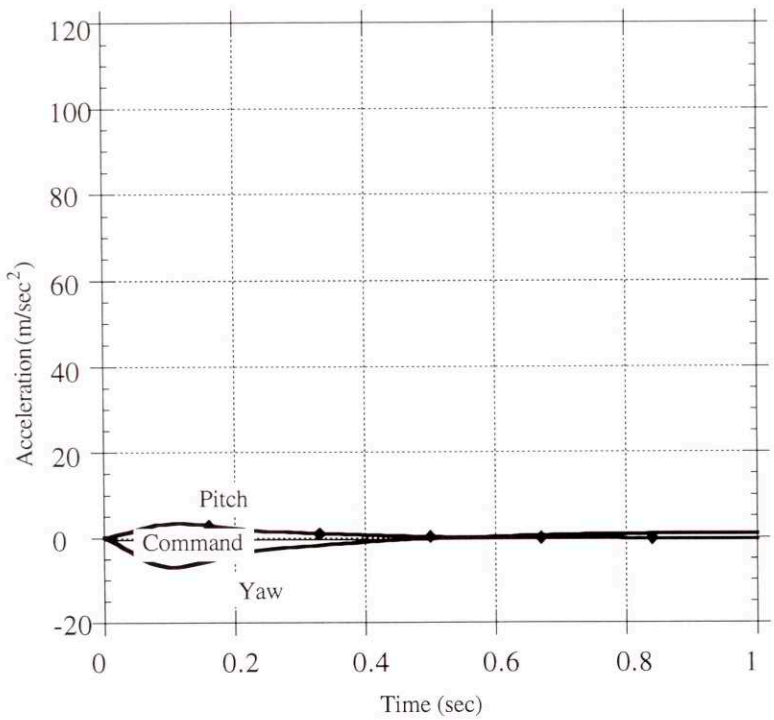

Figure 6-13 H_∞ Autopilot Acceleration Responses Due to a Roll Step Command

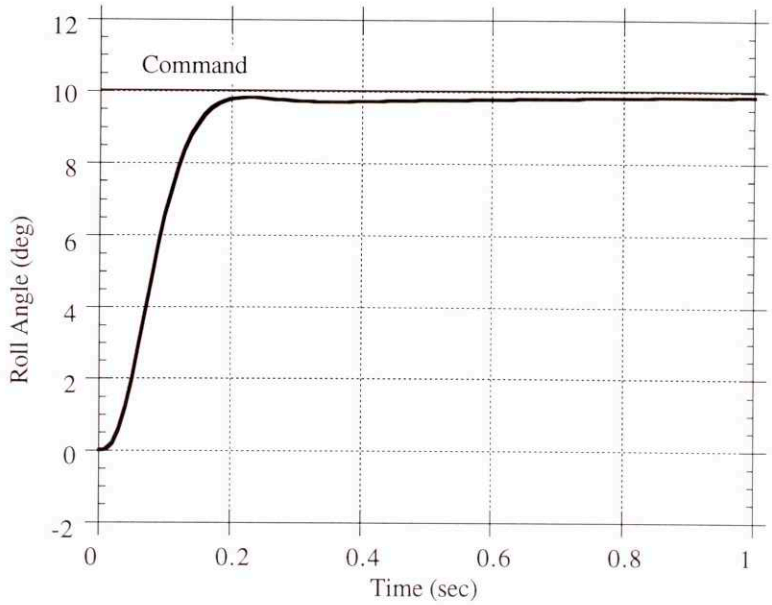

Figure 6-14 H_∞ Autopilot Roll Angle Response Due to a Roll Step Command

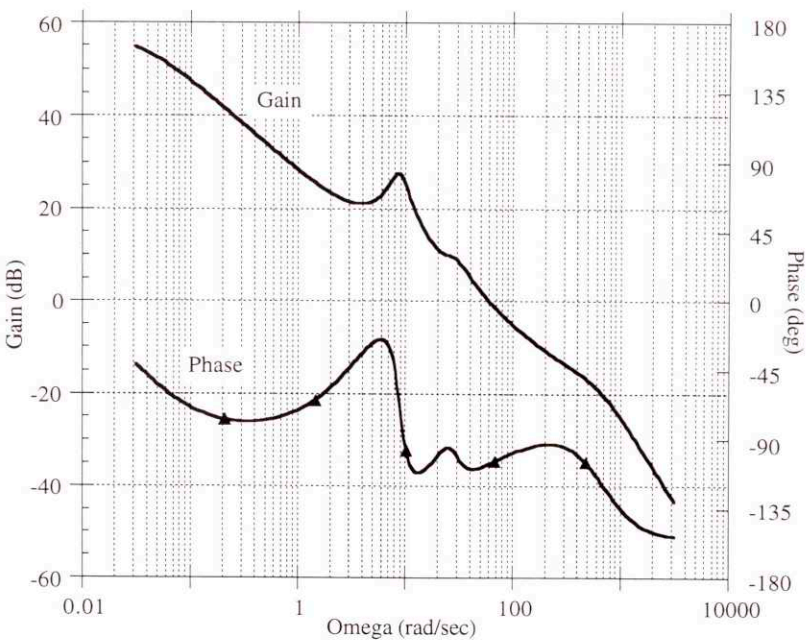

Figure 6-15 H_∞ Autopilot Roll Channel Bode Plot

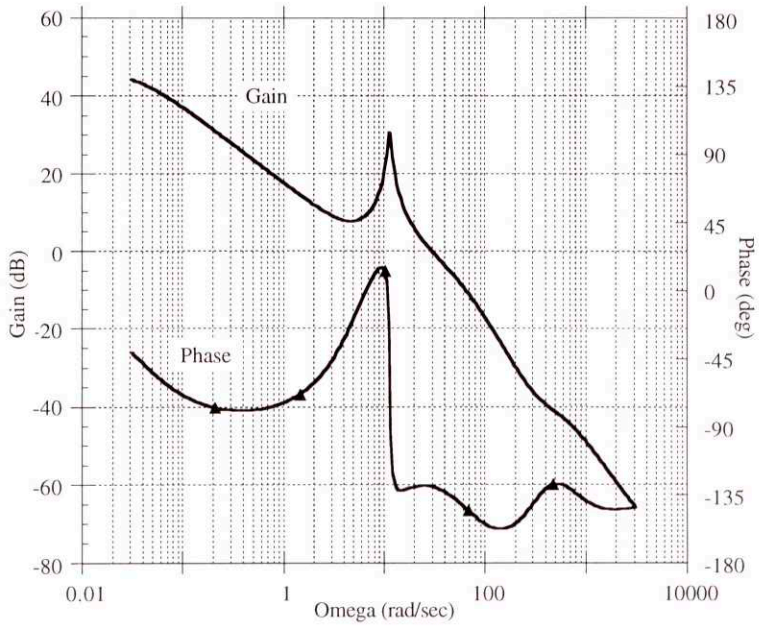

Figure 6-16 H_∞ Autopilot Yaw Channel Bode Plot

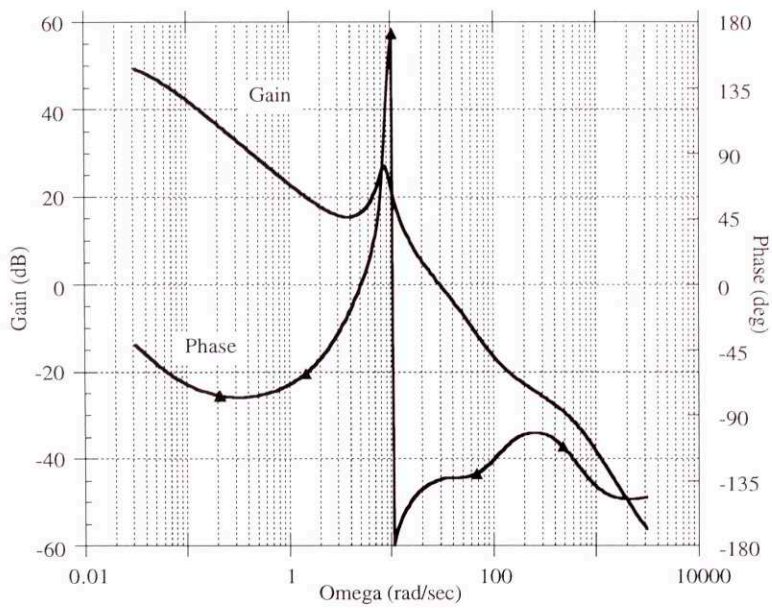

Figure 6-17 H_∞ Autopilot Pitch Channel Bode Plot

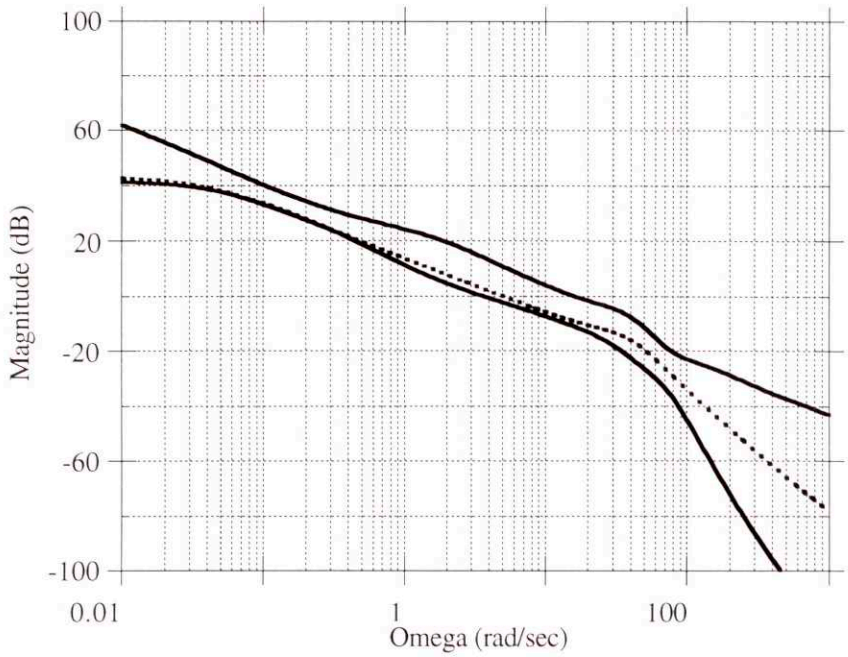

Figure 6-18 H_∞ Autopilot Loop Transfer Function

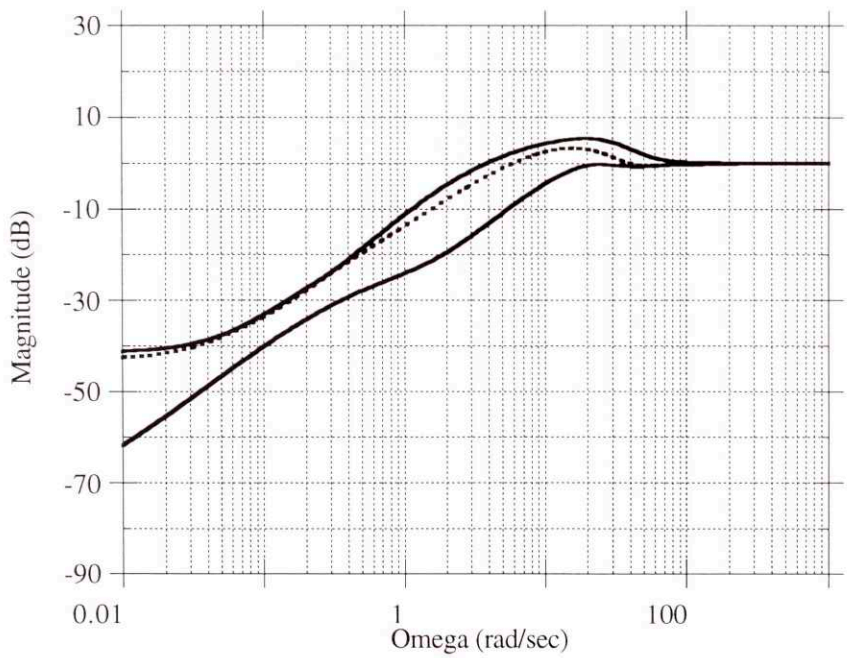

Figure 6-19 H_∞ Autopilot Singular Values Disturbances to Achieved

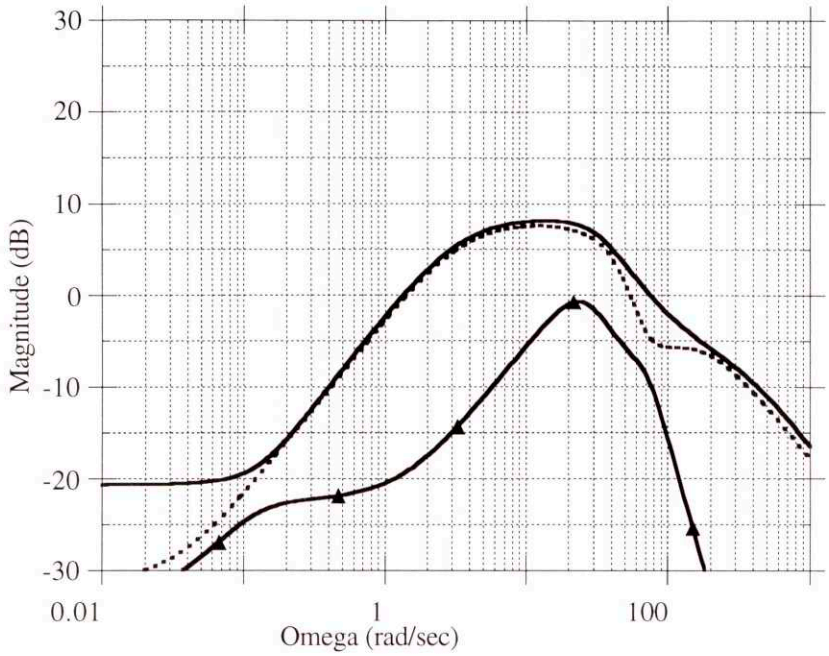

Figure 6-20 H_∞ Autopilot Singular Values Perturbations to Achieved

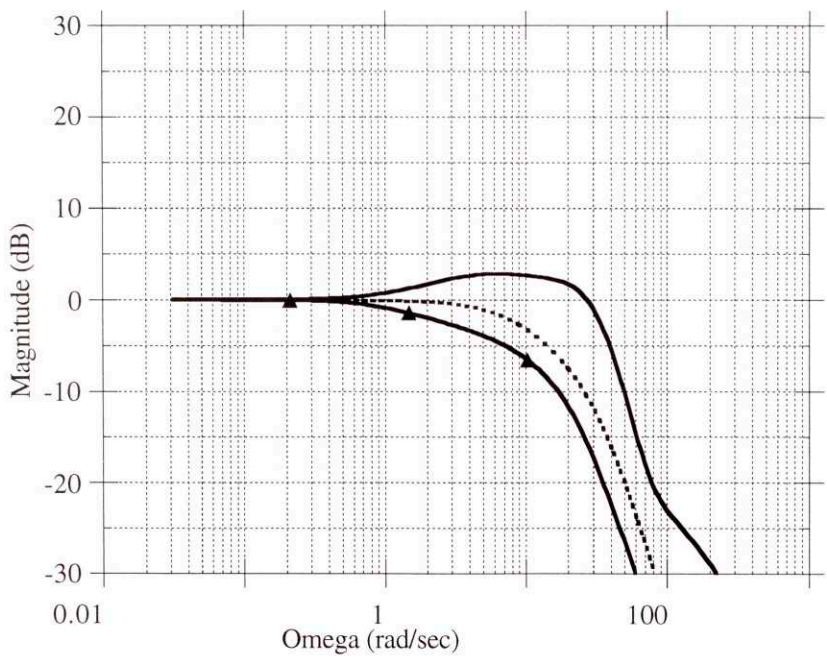

Figure 6-21 H_∞ Autopilot Singular Values Commanded to Achieved

Chapter 7 H_2 Autopilot Design

Like the H_∞ theory used in the previous chapter, H_2 control theory results in a controller with the same number of states as the augmented design model. The reason for this relatively large number of states is that these types of autopilots contain a sub-optimal filter to enhance the disturbance rejection properties and robustness to parameter variations of the autopilot.

The design goals for the H_2 autopilots are the same as those for the LQ autopilot that were originally discussed in Chapter 5. To reiterate those goals were:

0.20 second 63% rise times for the yaw and pitch channels
0.10 second 63% rise times for the roll channel
30 radians per second crossover frequencies for the yaw and pitch channels
60 radians per second crossover frequency for the roll channel

As usual it is desired to limit the amount of overshoot and to have as little steady state error as possible. The requirement for zero steady state error in the lateral channels that was imposed on the LQ design is relaxed for this design because of the additional difficulty imposed by the integrator dynamics near the origin

7.1 H_2 Control Law Synthesis

The H_2 control algorithms used in this thesis implement full output feedback controllers based on the interconnection model shown in Figure 7-1. [21],[23]

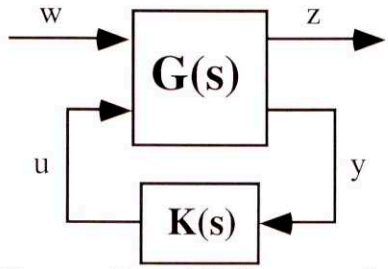

Figure 7-1 H_∞ and H_2 Interconnection Model

The vector w contains the exogenous inputs, the vector z is the controlled output, the vector y is the internal states available for feedback, and the u is the control vector for the plant. The state space equations for the augmented system are:

$$\begin{aligned} \dot{x}(t) &= Ax(t) + B_1 w(t) + B_2 u(t) \\ z(t) &= C_1 x(t) + D_{11} w(t) + D_{12} u(t) \\ y(t) &= C_2 x(t) + D_{21} w(t) + D_{22} u(t) \end{aligned} \tag{7.1}$$

The generalized plant model G(s) is defined as:

$$G(s) = \left[\begin{array}{c|cc} A & B_1 & B_2 \\ \hline C_1 & D_{11} & D_{12} \\ C_2 & D_{21} & D_{22} \end{array}\right] \tag{7.2}$$

This generalized plant includes not only the nominal design plant as derived in Chapter 3 but any performance weighting functions that are used in the design process.

An H_2 controller minimizes the two norm of the generalized plant G(s). The two norm is defined as:

$$\| G \|_2 = \left(\frac{1}{2\pi} \int_{-\infty}^{\infty} trace[G(j\omega)^* G(j\omega)] dw \right)^{1/2} \tag{7.3}$$

The minimizing solution involves two Hamiltonian matrices:

$$H_2 = \begin{bmatrix} A & -B_2 B_2{}^T \\ -C_1{}^T C_1 & -A^T \end{bmatrix} \tag{7.4}$$

$$J_2 = \begin{bmatrix} A^T & -C_2{}^T C_2 \\ -B_1 B_1{}^T & -A \end{bmatrix} \tag{7.5}$$

These Hamiltonians expand into the following Ricatti equations:

$$0 = A^{TX} + XA + X(-B_2 B_2{}^T)X + C_1{}^T C_1 \tag{7.6}$$

$$0 = AY + YA^T + Y(-C_2{}^T C_2)Y + B_1 B_1{}^T \tag{7.7}$$

Define

$$F_2 = -B_2{}^{TX}, \quad L_2 = -Y_2 C_2{}^T \tag{7.8}$$

$$\hat{A}_2 = A + B_2 F_2 + L_2 C_2 \tag{7.9}$$

Then the optimal controller is:

$$K(s) = \begin{bmatrix} \hat{A}_2 & -L_2 \\ F_2 & 0 \end{bmatrix} \tag{7.10}$$

As can be seen by comparing these equations with those from Chapter 6, if the parameter γ is set to large value, the resulting controller from an H_∞ design algorithm will serve as an H_2 controller.

These control methodologies result in systems with the same number of states and very similar performance and robustness properties. For a given application an H_∞ controller will have the smallest peak singular value while a H_2 controller will have the minimum total area under the peak singular value curve.

7.2 Design Plant

The design plant airframes for both H_∞ and H_2 autopilots are the same. The airframe states are those in the basic plant. They are:

$$x_{H_\infty \text{ and } H_2 \text{ design plant}} \equiv \left[\Delta\alpha \; \Delta\beta \; \theta \; P \; Q \; R \; \delta_R \; \delta_Y \; \delta_P\right]^T \tag{7.11}$$

There are 11 outputs for the design plant. They are:

$$y_{H_\infty \text{ and } H_2 \text{ design plant}} \equiv \left[\eta_y \; \eta_p \; \Delta\alpha \; \Delta\beta \; \theta \; P \; Q \; R \; \delta_R \; \delta_Y \; \delta_P\right]^T \tag{7.12}$$

The performance filters discussed in the following section are augmented to form the final state space design model. This final model has 15 states and 17 inputs. The inputs are the three commands, the three perturbations and the 11 measurement noises. The state space A, B, C, and D matrices are shown in Appendix 6.

7.3 Design Process

As in the H_∞ design the performance of an H_2 controller is adjusted by its weighting filters. These filters can be made frequency dependent thereby offering the designer great flexibility in the design process. There are two basic types of filters that are used to control the bandwidth of the controller and regulate its performance. These two filters are the control weighting filter and the performance weighting filter respectively.

Despite the similar structure of the H_∞ and H_2 controllers and the similar function of the performance weighting filters the same filters that were used for an H_∞ design do not yield

equivalent performance when used to design an H_2 controller. If the filters used for the H_∞ autopilot design from Section 6.3 are used for an H_2 design both the time domain and frequency domain properties change. The time domain properties and Bode crossover frequencies of such a controller are summarized in Table 7-1.

	Yaw	Pitch	Roll
Crossover Frequency (rad/sec)	24.4	25.8	46.1
63% Rise time (sec)	0.24	0.25	0.11
Overshoot (%)	-0.50	-1.7	-1.7

Table 7-1 H_2 Autopilot Nominal Performance Results Using H_∞ Filters

This performance does not satisfy the performance criteria required of the design and therefore the H_2 design requires modifications to the filters used for its design.

As in the H_∞ design the control weighting filters are used to control the bandwidth of the system, the higher the penalty the more that frequency will be penalized. It is used to regulate the control activity also. Generally the magnitude of the penalty increases as the frequency increases.

The performance weighting filter is used for the controller's closed loop performance. At low frequencies this filter has an effect on the steady state error. The crossover of this filter controls the rise time of the autopilot.

The actual design process requires the iteration of the filter structure depending upon the resulting closed loop system's performance in both the time and frequency domains.

7.3.a H_2 Filters

The control weighting filters for the H_2 autopilot were designed with the idea of limiting high frequency control action, but allowing low frequency actions and particularly allowing for steady state fin deflections. This steady state allowance is to account for the steady state fin deflections required to satisfy step input requirements. There are three 1st order filters for the H_2 design. One filter each for the roll, yaw and pitch channels. The final filters used for the autopilot design are:

$$G(s)_{Roll\ Control} = \frac{15s}{s + 725} \tag{7.13}$$

$$G(s)_{Yaw\ Control} = \frac{15s}{s + 875} \tag{7.14}$$

$$G(s)_{Pitch\ Control} = \frac{15s}{s + 625} \tag{7.15}$$

Their respective frequency responses can be found in Figures 7-2 and 7-3. These final values were chosen based on an iterative search method. A controller was designed and its closed loop Bode bandwidth was examined. If the system had too low of a crossover frequency, the filter pole was increased in frequency, if the crossover was too high, the bandwidth of the filter was decreased. The H_2 controller performance required that there be less penalty applied to the controls over a wider frequency range than did the H_∞ design.

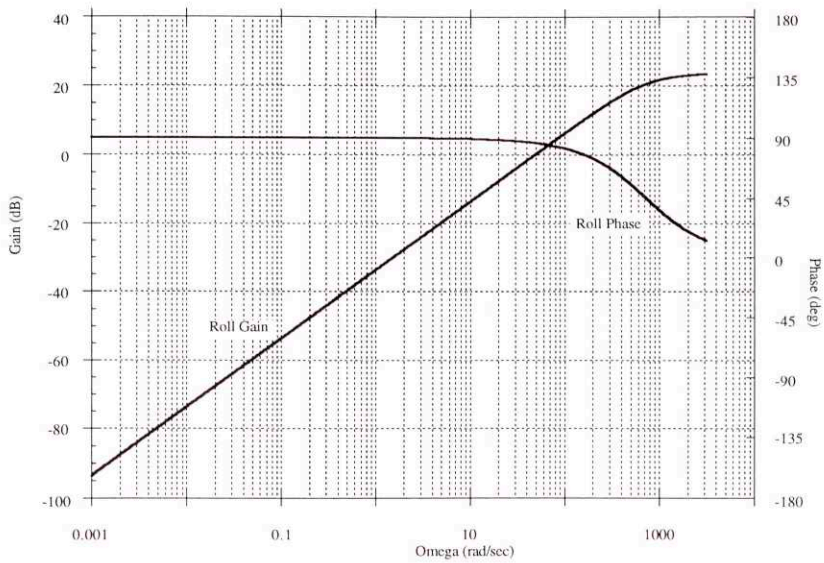

Figure 7-2 H_2 Autopilot Roll Channel Control Weighting Filter

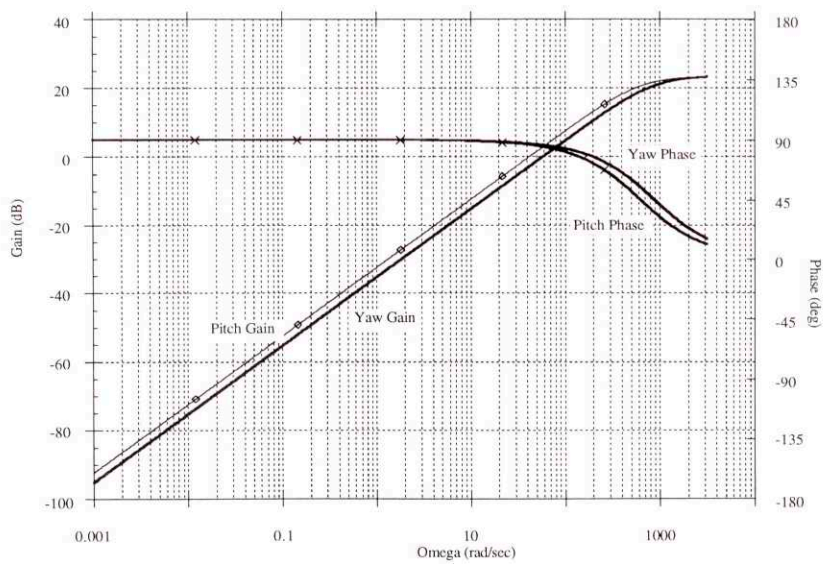

Figure 7-3 H_2 Autopilot Lateral Channel Control Weighting Filter

There are three first order performance filters used in the H_2 design. One each for the roll, yaw and pitch channel. The inputs to these filters are the roll angle θ, and the two lateral accelerations η_y and η_p. The performance weighting filters used are as follows:

$$G(s)_{Roll\ Performance} = \frac{0.5(s + 35)}{s + 1.4} \tag{7.16}$$

$$G(s)_{Yaw\ Performance} = \frac{0.5(s + 3.5)}{s + 0.035} \tag{7.17}$$

$$G(s)_{Pitch\ Performance} = \frac{0.5(s + 3.5)}{s + 0.035} \tag{7.18}$$

Their respective frequency responses can be found in Figures 7-4 and 7-5. It is worth noting that the values needed for these filters are the same as those that were chosen for the H_∞ design.

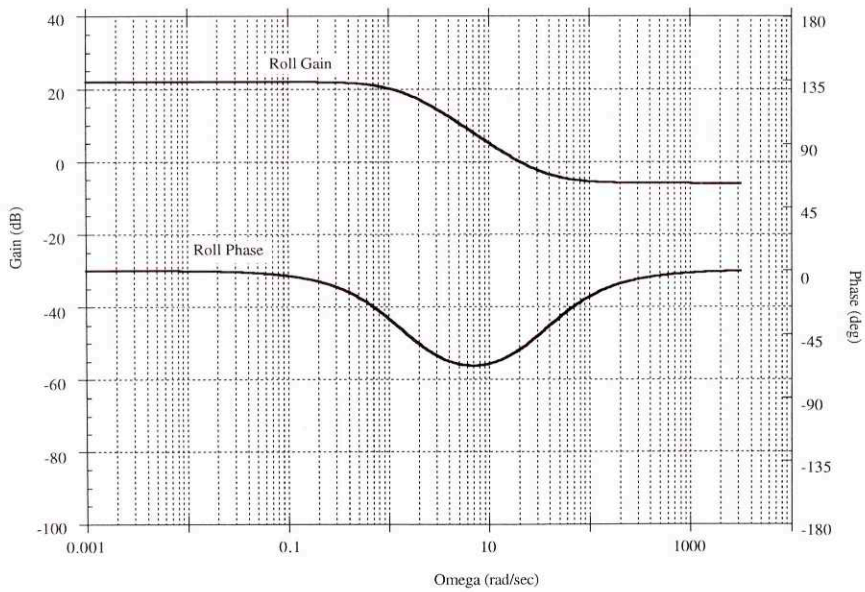

Figure 7-4 H_2 Autopilot Roll Channel Performance Filter

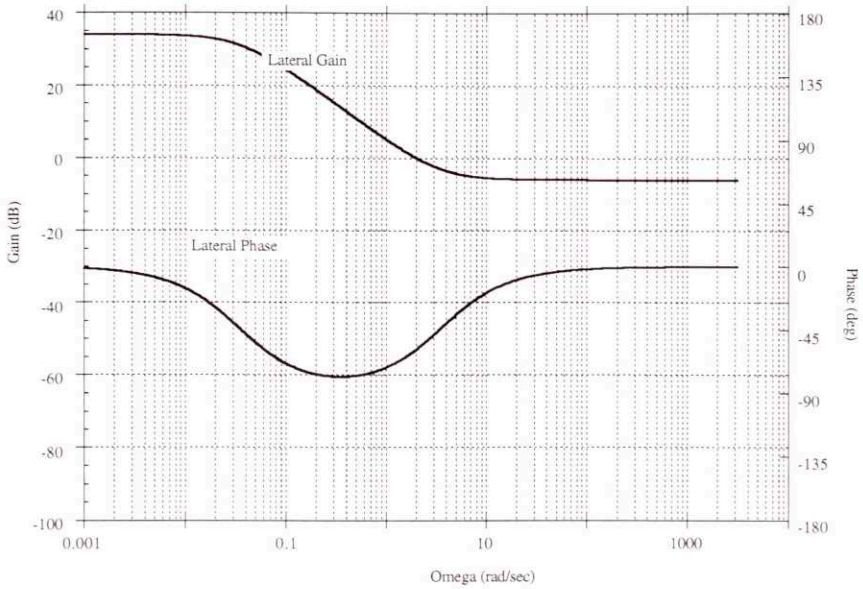

Figure 7-5 H_2 Autopilot Lateral Channel Performance Filter

The values of the A, B, C and D matrices after the augmentation of the filters can be found in Appendix 6.

7.4 Nominal Performance

The final H_2 autopilot has 15 states. The H_2 autopilot poles are shown in Table 7-2. The state space A, B, C, and D matrices of the compensator are shown in Appendix 7.

Real	Imag	Freq.	Damp
-0.035	0.0	0.035	
-0.035	0.0	0.035	
-0.9787	0.0	0.9787	
-1.4	0.0	1.4	
-8.977	0.0	8.977	
-10.62	0.0	10.62	
-51.98	-30.96	60.5	
-51.98	30.96	60.5	0.8591
-70.48	-39.85	80.97	
-70.48	39.85	80.97	0.8705
-133	0.0	133	
-289.8	0.0	289.8	
-302.1	0.0	302.1	
-483.9	-441.6	655.1	
-483.9	441.6	655.1	0.7387

Table 7-2 H_2 Autopilot Poles

The closed loop performance of the system is summarized in Tables 7-3 and 7-4. The risetime requirement is satisfied exactly for the lateral channels, and is slightly too fast in the roll channel. The single loop bode crossover frequencies are within the total allowed error. The roll and pitch channels exhibit a steady state undershoot, while the yaw channel exhibits a slight overshoot. This steady state error is a direct consequence of the design decision not to augment the design plant with integrators. As long as this steady state error is small, it will not affect the missile's performance.

	Yaw	Pitch	Roll
Crossover Frequency (rad/sec)	30.4	30.0	60.2
63% Rise time (sec)	0.20	0.20	0.097
Overshoot (%)	0.89	-0.62	-1.5

Table 7-3 H_2 Autopilot Nominal Performance Results

	Gain Margin (dB)	Phase Margin (deg)
Roll	23.4	34
Yaw	22.4	46
Pitch	-16.5, 28.2	42

Table 7-4 H_2 Autopilot Nominal Bode Stability Margins

The Time domain responses to steps are shown in Figures 7-7 through 7-12. The Bode plots of the individual yaw, pitch and roll channels are shown in Figures 7-13 through 7-15. For these plots, the loop was broken at the plant input and the remaining feedback loops were closed. See Figure 2-2. As defined in Figure 7-6 there are three distinct places where signals can enter the system. They are the normal commands, the perturbations to the plant which are modeled as disturbances at the plant input and disturbances which are reflected at the plant output.

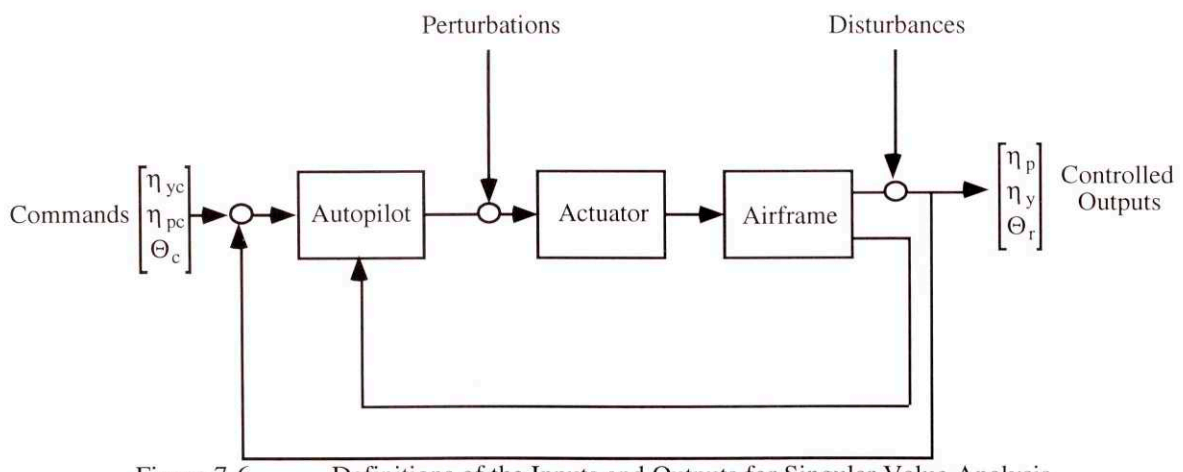

Figure 7-6 Definitions of the Inputs and Outputs for Singular Value Analysis

From these three inputs, four transfer functions may be derived. These are the loop transfer function (Figure 7-16), the sensitivity transfer function (Figure 7-17), the perturbation to the controlled output transfer function (Figure 7-18) and the complementary sensitivity function (Figure 7-19).

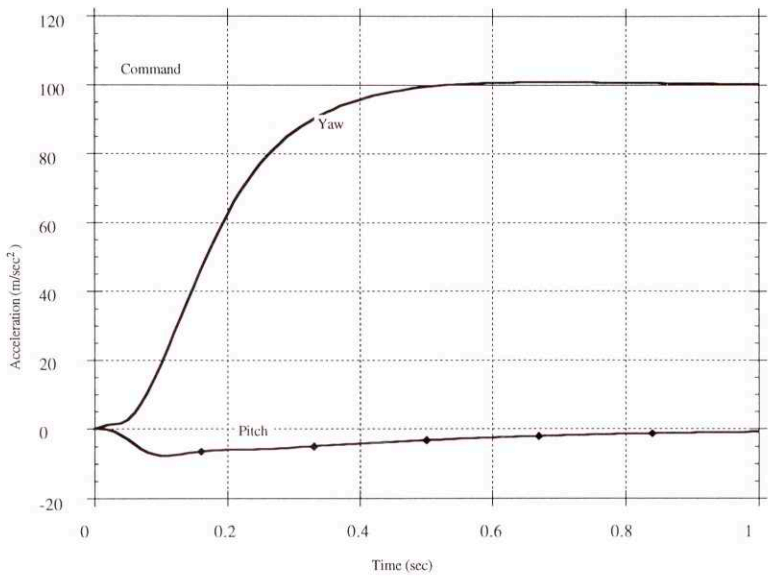

Figure 7-7 H_2 Autopilot Acceleration Responses Due to a Yaw Step Command

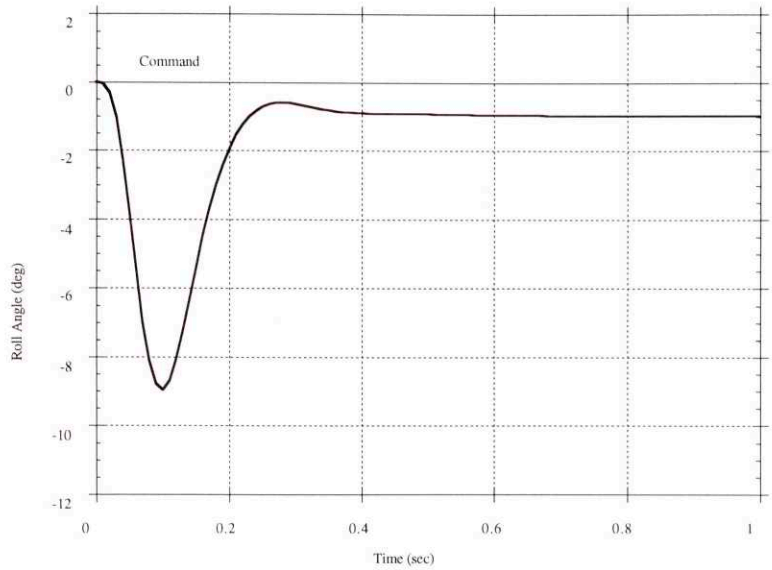

Figure 7-8 H_2 Autopilot Roll Angle Response Due to a Yaw Step Command

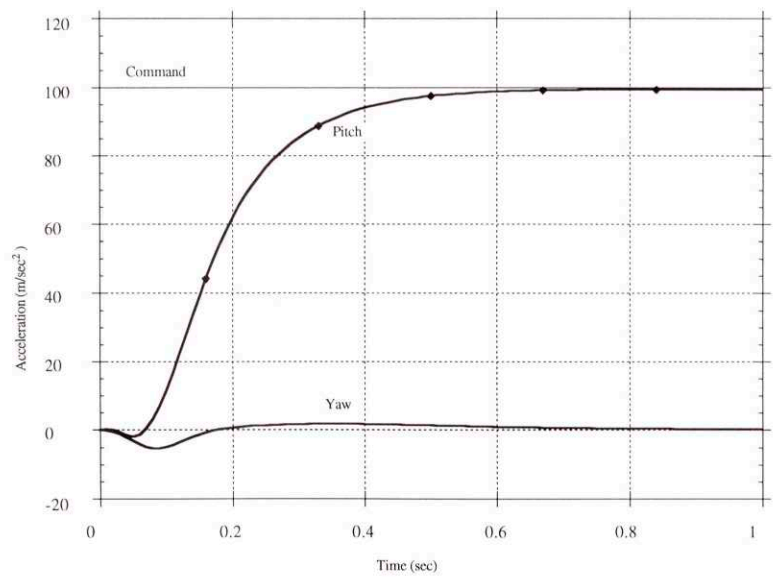

Figure 7-9 H_2 Autopilot Acceleration Responses Due to a Pitch Step Command

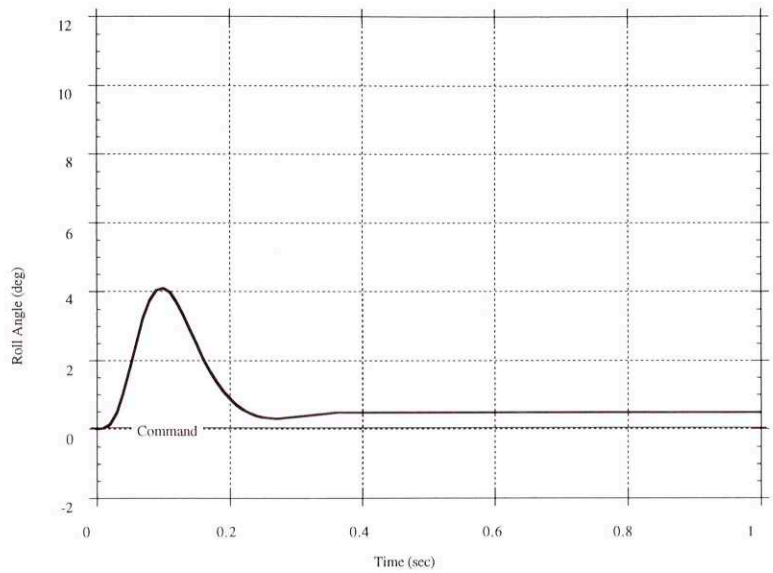

Figure 7-10 H_2 Autopilot Roll Angle Response Due to a Pitch Step Command

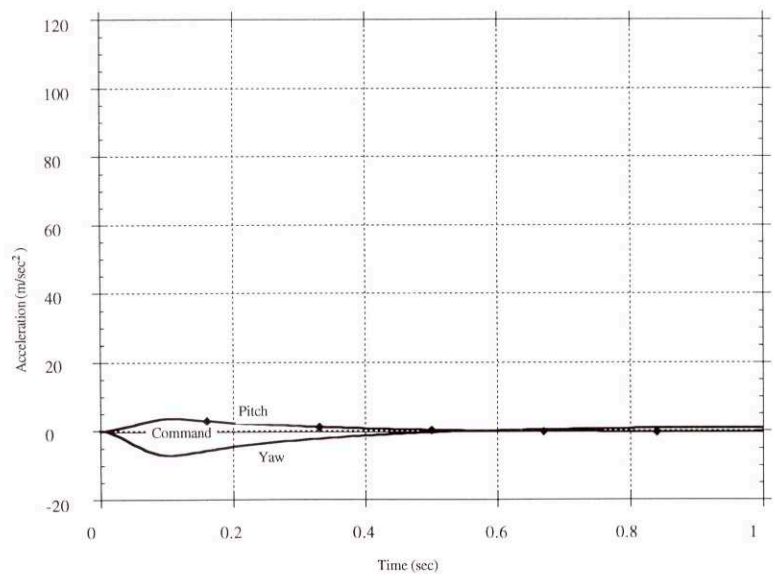

Figure 7-11 H_2 Autopilot Acceleration Responses Due to a Roll Step Command

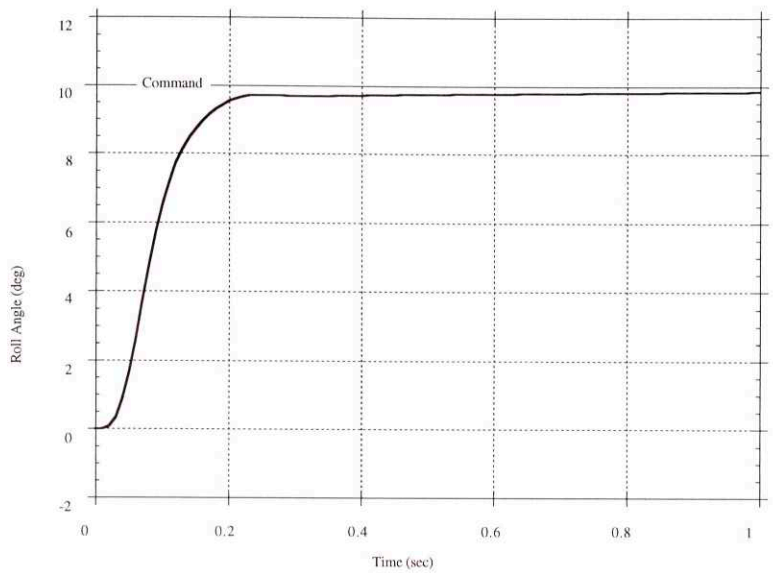

Figure 7-12 H_2 Autopilot Roll Angle Response Due to a Roll Step Command

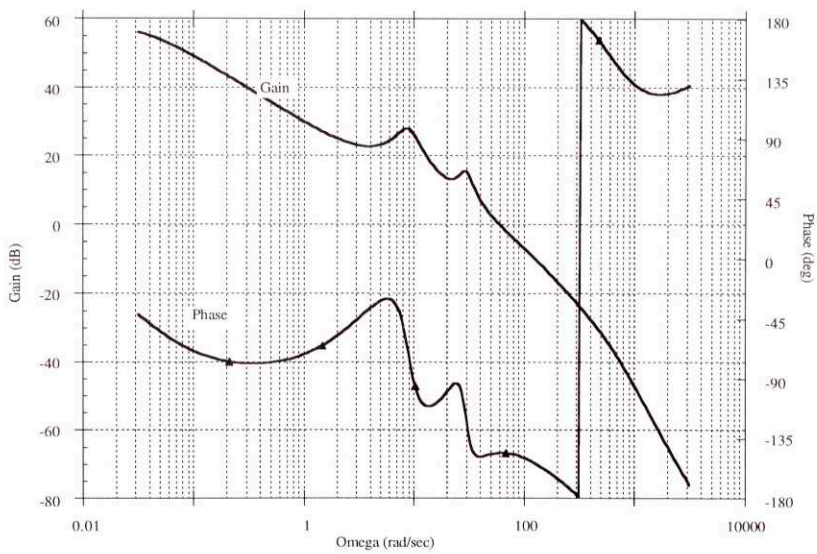

Figure 7-13 H_2 Autopilot Roll Channel Bode Plot

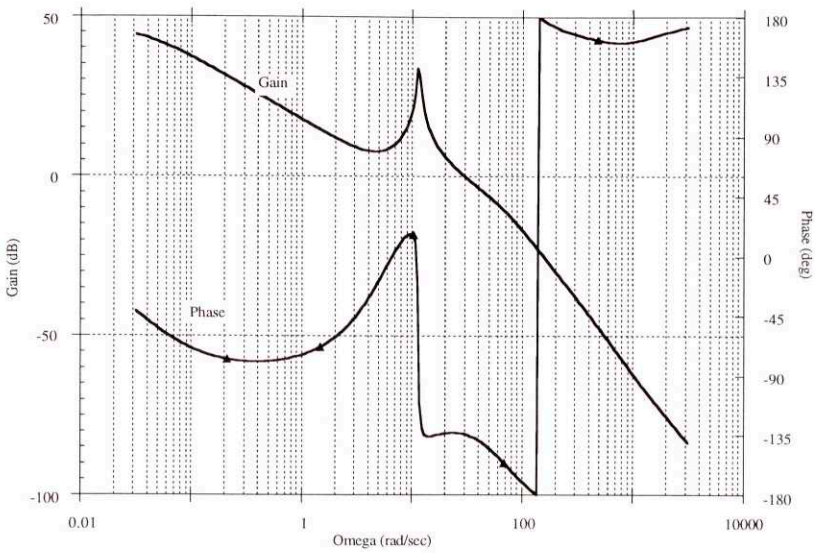

Figure 7-14 H_2 Autopilot Yaw Channel Bode Plot

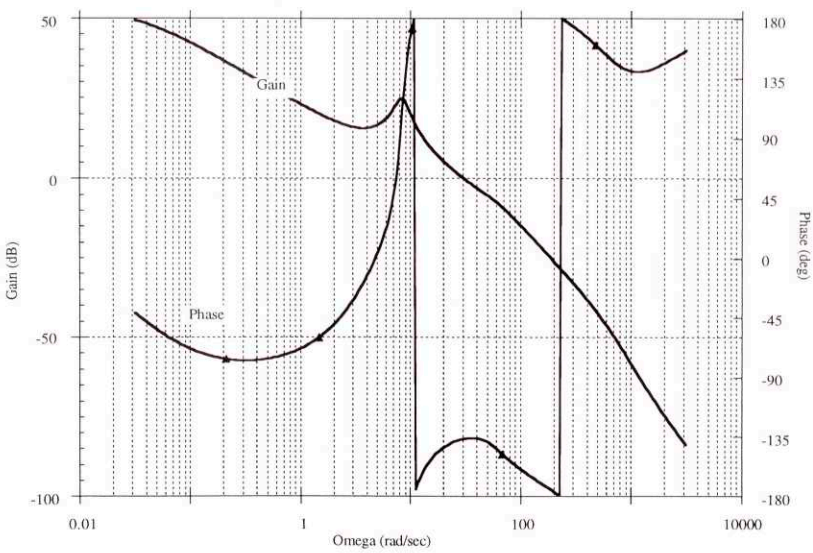

Figure 7-15 H_2 Autopilot Pitch Channel Bode Plot

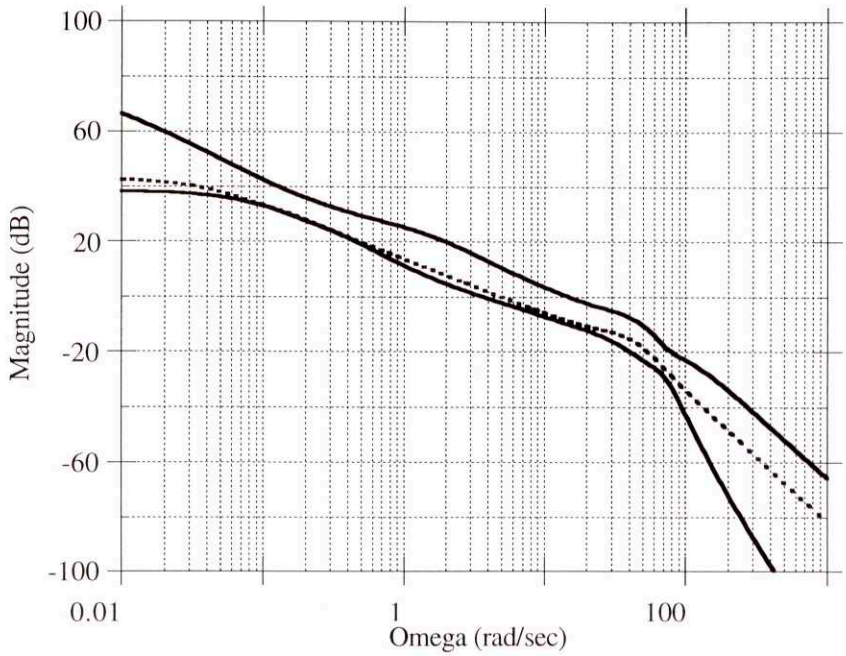

Figure 7-16 H_2 Autopilot Loop Transfer Function

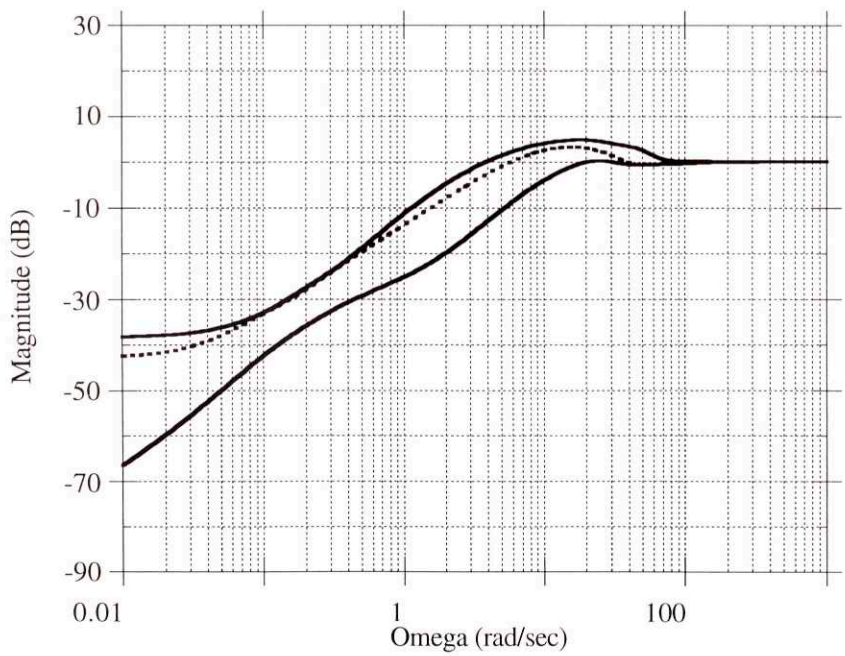

Figure 7-17 H_2 Autopilot Singular Values Disturbances to Achieved

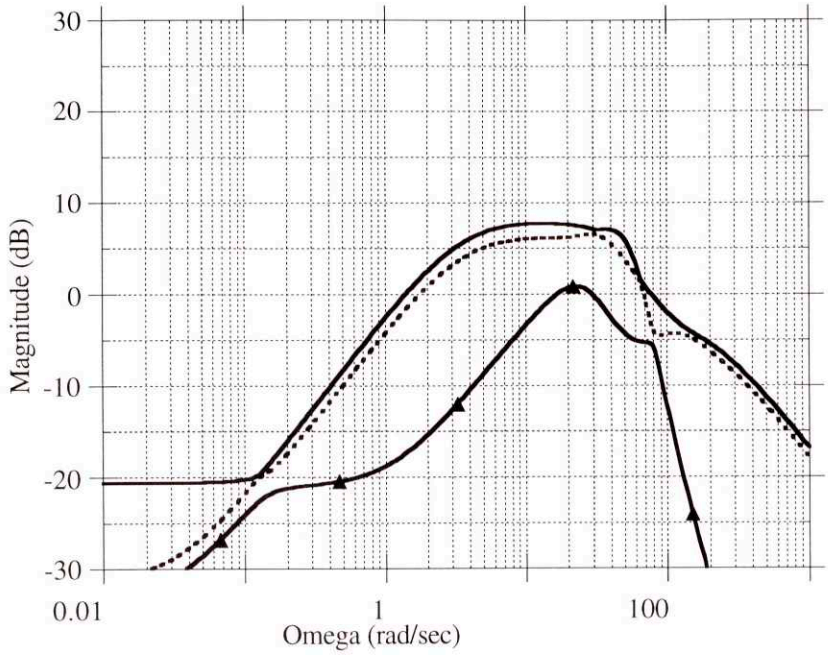

Figure 7-18 H_2 Autopilot Singular Values Perturbations to Achieved

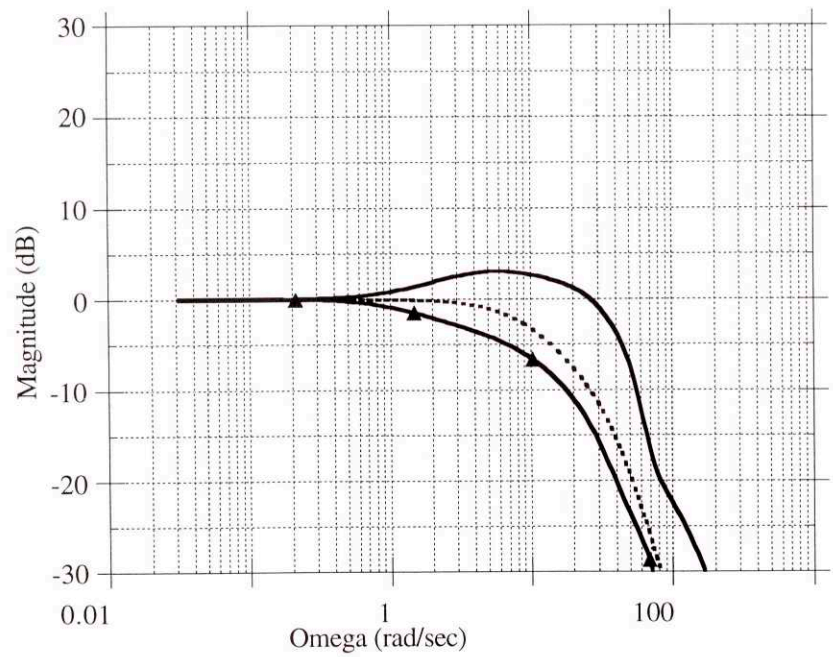

Figure 7-19 H_2 Autopilot Singular Values Commanded to Achieved

Chapter 8 Nominal Comparisons

8.1 Closed Loop Comparisons

The time domain and frequency domain properties of the three autopilots are different as expected. The H_∞ and H_2 controllers performance is almost identical for the nominal design case. Tables 8-1 and 8-2 and Figures 8-1 through 8-3 compare the closed loop performance of the three systems. The LQ design has the largest Bode margins at the nominal design point but also has the most persistent settling time problems in the roll channel. In addition the LQ design has the most cross channel motion resulting from lateral acceleration steps. The H_2 autopilot has the smallest Bode margins for both gain and phase variations.

	LQ			H_∞			H_2		
	Yaw	Pitch	Roll	Yaw	Pitch	Roll	Yaw	Pitch	Roll
Crossover Frequency (rad/sec)	30.7	30.2	59.9	29.6	30.1	60.2	30.4	30.0	60.2
63% Rise time (sec)	0.20	0.20	0.10	0.20	0.20	0.097	0.20	0.20	0.097
Overshoot (%)	2.2	0.0	5.5	0.77	-0.71	-1.4	0.89	-0.62	-1.5

Table 8-1 Autopilot Nominal Performance Results Comparison

	LQ		H_∞		H_2	
	Gain Margin (dB)	Phase Margin (deg)	Gain Margin (dB)	Phase Margin (deg)	Gain Margin (dB)	Phase Margin (deg)
Roll	∞	106	∞	74	23	34
Yaw	∞	73	∞	50	22	46
Pitch	∞	93	-19, ∞	46	-17, 28	42

Table 8-2 Autopilot Nominal Bode Stability Margin Comparison

The poles of the H_∞ and H_2 design are shown in Table 8-3. The two autopilots low frequency poles are approximately the same. It is only after 100 rad/second that the value of the poles substantially disagree.

H_∞				H_2			
Real	Imag	Freq.	Damp	Real	Imag	Freq.	Damp
-0.035	0.0	0.035		-0.035	0.0	0.035	
-0.035	0.0	0.035		-0.035	0.0	0.035	
-0.9805	0.0	0.9805		-0.9787	0.0	0.9787	
-1.4	0.0	1.4		-1.4	0.0	1.4	
-8.999	0.0	8.999		-8.977	0.0	8.977	
-10.56	0.0	10.56		-10.62	0.0	10.62	
-53.59	-29.49	61.17		-51.98	-30.96	60.5	
-53.59	29.49	61.17	0.8761	-51.98	30.96	60.5	0.8591
-76.01	-37.34	84.68		-70.48	-39.85	80.97	
-76.01	37.34	84.68	0.8975	-70.48	39.85	80.97	0.8705
-291.1	0.0	291.1		-133	0.0	133	
-303.9	0.0	303.9		-289.8	0.0	289.8	
-515.9	-386.4	644.6		-302.1	0.0	302.1	
-515.9	386.4	644.6	0.8004	-483.9	-441.6	655.1	
-11290.	0.0	11290		-483.9	441.6	655.1	0.7387

Table 8-3 H_∞ and H_2 Autopilot Poles

Examination of Figure 8-4 shows that at frequencies below one radian per second, the LQ autopilot has a larger loop gain maximum and minimum singular values than do the H_∞ and H_2 designs. This is the result of the integral compensation in the LQ design. In the region between 1 and 10 radians per second the loop gain is approximately the same. At frequencies above 100 radians per second, the minimum singular values of the loop gain for all three designs are indistinguishable, while the maximums are quite different. Figure 8-5 shows how above frequencies of two radians per second the maximum and minimum singular value of the sensitivity transfer functions of the H_2 and H_∞ designs are indistinguishable. The LQ design on the other hand can clearly be distinguished from them. At extremely low frequencies, the LQ design has superior disturbance rejection properties, however at higher frequencies it disturbance rejection properties are inferior to the H_2 and H_∞ designs. As expected, and shown in Figure 8-5 the disturbance properties

of the LQ system and its robustness to plant perturbations are not as good as the H_∞ and H_2 designs (Figure 8-6). The complementary sensitivity plots of the three systems shown in figure 8-7 reveals how similar the maximum singular values of the H_2 and H_∞ designs are.

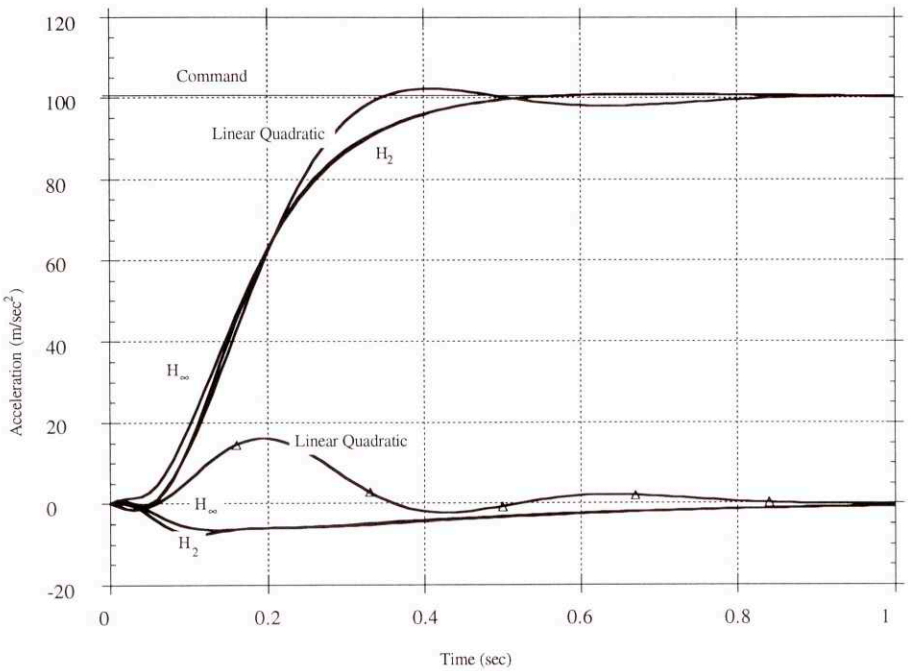

Figure 8-1 Comparison of Acceleration Histories to a Yaw Step Command Nominal

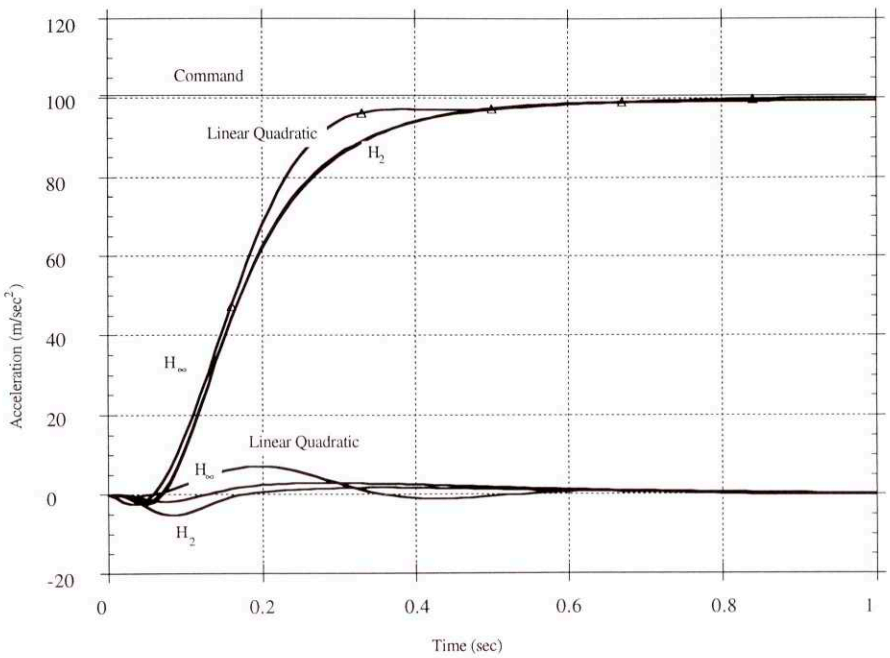

Figure 8-2 Comparison of Acceleration Histories to a Pitch Step Command - Nominal

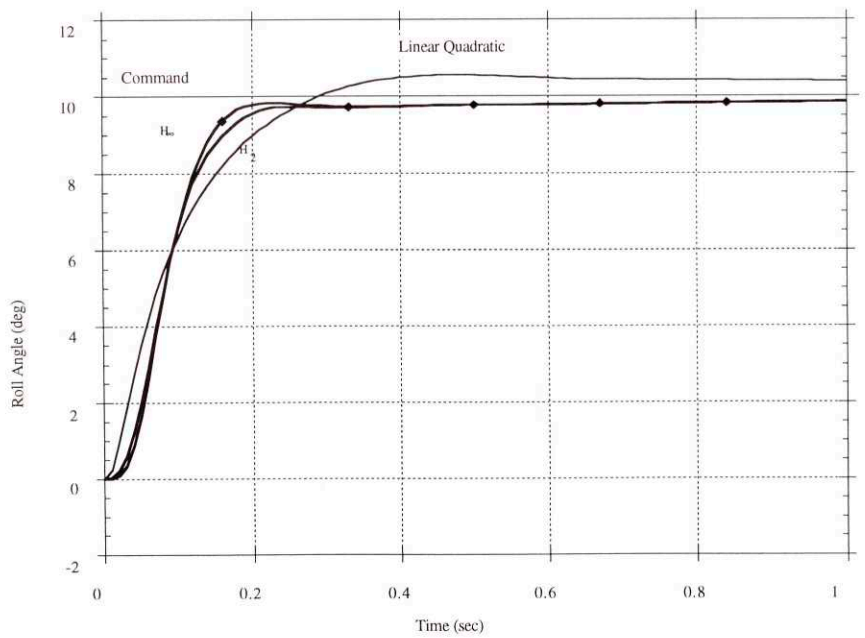

Figure 8-3 Comparison of Roll Angle Histories to a Roll Step Command - Nominal

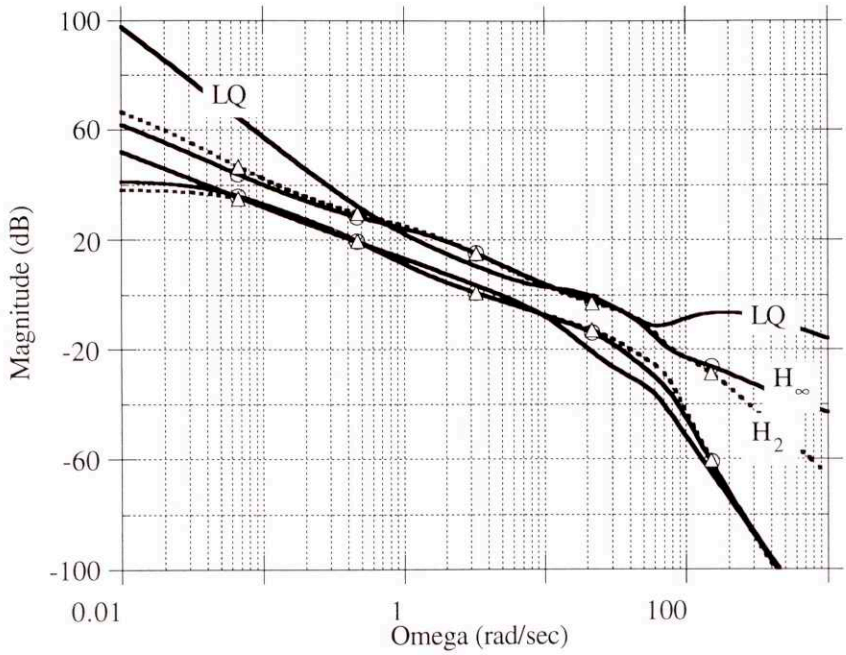

Figure 8-4 Loop Transfer Function - Nominal

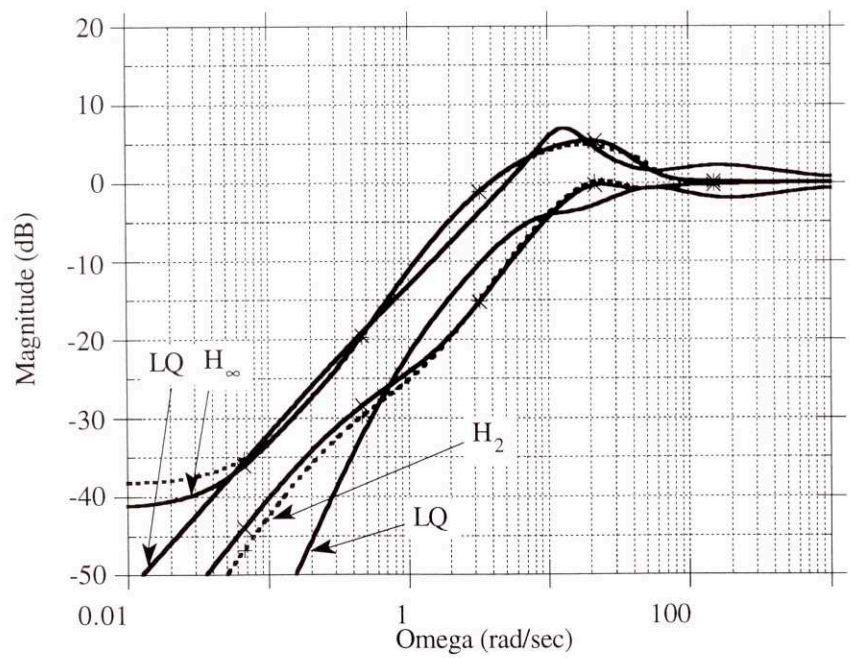

Figure 8-5 Maximum and Minimum Singular Values Disturbances to Controlled Output - Nominal

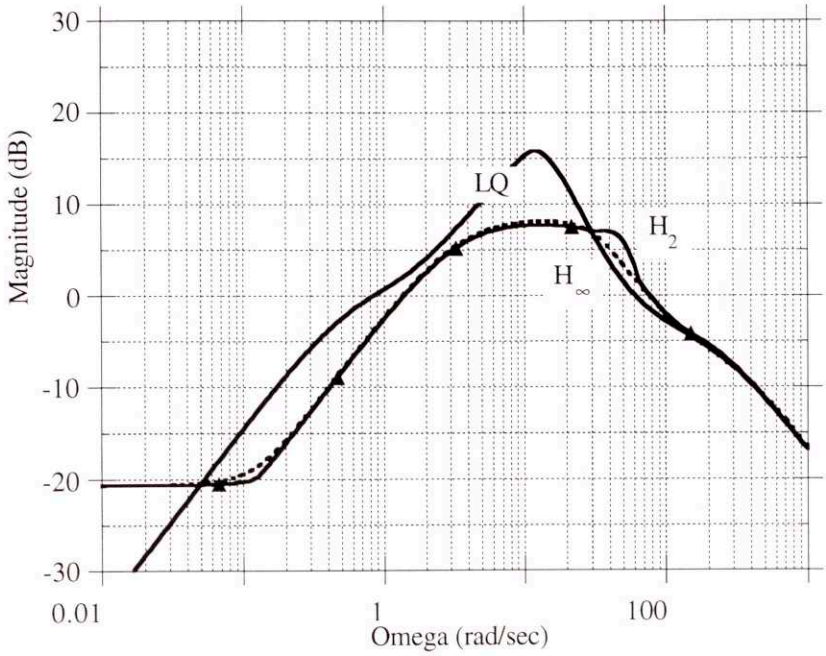

Figure 8-6 Maximum Singular Value Perturbations to Controlled Output - Nominal

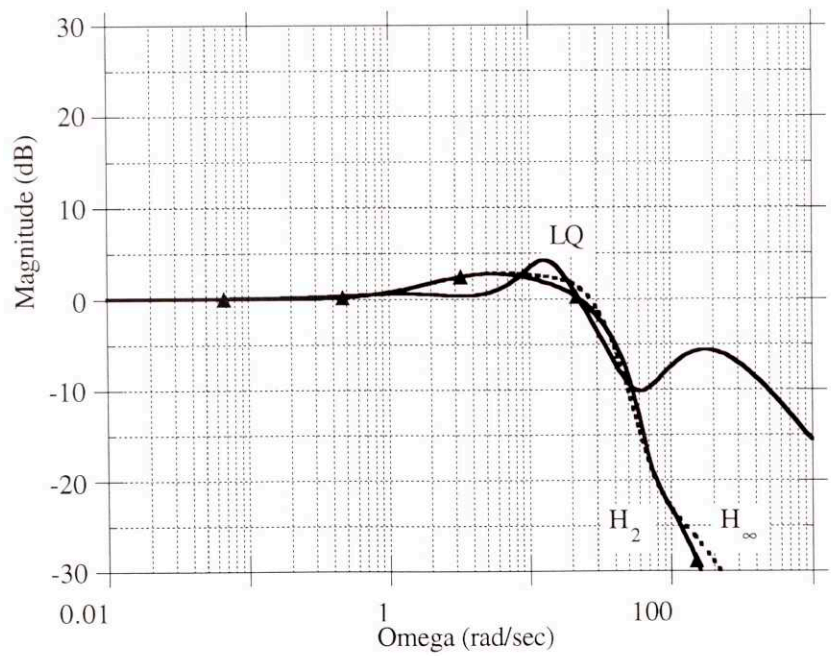

Figure 8-7 Maximum Singular Value Commands to Controlled Output - Nominal

8.2 Computational Requirements

Most onboard processors are implemented in a digital computer. A constraint that is more applicable to missile than most control designs is the complexity of the control system. In general the onboard processors that are in a missile do not have the capacity (in terms of processing speed) of ground based systems. There is a very real premium placed on weight, power and size. Also due to the extremes of temperature and the vibrational levels that an onboard processor experiences, the types of processors carried by missiles have very limited capacities. Because of the premiums placed on weight and size, the amount of storage in a missile is often more limited than that found on the ground.

A digital control law is of the form:

$$\begin{aligned} \dot{x}_k &= Ax_{k-1} + Bu_k \\ x_k &= \dot{x}_k \Delta t + x_{k-1} \\ y_k &= Cx_k + Du_k \\ x &\in R^n,\ u \in R^m,\ y \in R^p \end{aligned} \tag{8.1}$$

This gives the total number of multiplies to be:

$$\#_{multiplies} = \overset{Ax}{n*n} + \overset{Bu}{n*u} + \overset{Cx}{m*n} + \overset{Du}{m*u} + n \tag{8.2}$$

and the total number of adds to be:

$$\#_{adds} = \overset{Ax}{n*(n-1)} + \overset{Bu}{n*u} + \overset{Cx}{m*(n-1)} + \overset{Du}{m*u} + n \tag{8.3}$$

This computational requirement is required for every pass through the code, so if an autopilot is to run at 100 Hertz, the processor must have the resources available to allocate approximately 100 this number of multiplies and adds per second Further requirements are imposed requiring a factor of at most 50% for the processor loading. For sizing purposes this doubles the operation count.

Finally the elements of the A and B matrices are typically stored in double precision (anything to do with accumulations over time such as integrations are usually double precision), and the elements of the C and D matrices are single precision. Each double precision number requires 16 bits and each single precision number is eight bits. This gives a total storage requirement of:

$$Storage_{bits} = \overset{A}{n*n*16} + \overset{B}{n*u*16} + \overset{C}{m*n*8} + \overset{D}{m*u*8} + n \qquad (8.4)$$

An estimate of the processing requirements of the three candidate designs is summarized in Table 8-4. The total number of states for the LQ controller is 3 and there are 15 states for the H_2 and H_∞ controllers. For all designs there are 11 inputs and 3 outputs.

Autopilot	# of multiplies	# of adds	Storage (bits)
LQ	87	81	1008
H_∞	483	465	6864
H_2	483	465	6864

Table 8-4 Approximate Computer Requirements for the Nominal Autopilot Designs

Because of the simpler structure and smaller total size of the LQ compensator, the LQ autopilot requires approximately one fifth of the resources of either the H_2 or H_∞ controllers.

Chapter 9 Perturbation Results (Altitude and Speed)

The three autopilot designs demonstrate excellent performance at the nominal flight condition as expected. However the performance of the three systems degrades when the designs are evaluated at off nominal flight conditions.

The original nominal design condition was Mach 4, medium altitude, a total angle of attack of 15° and a wind angle of 22.5°. The designs' performance have been evaluated at a number of flight conditions found by varying the altitude by ±10% and by varying the speed by ±10%. The missile's angle of attack and wind angle were not changed from the nominal values.

9.1 Variations in Altitude

The autopilot designs were done using a nominal plant linearized around a medium altitude flight condition. However in operation the current missile altitude cannot be exactly known. To evaluate the performance changes of the three designs, linearized airframes were generated for the same missile speed, angle of attack and wind angle, but with the altitudes changed by ±10%. This 10% variation is a conservative number, in an operational situation an Inertial Measurement Unit (IMU) should provide estimates of missile altitude that are better than ±10%.

The autopilots developed in Chapter 5, 6 and 7 were then connected to the perturbed airframes to form a closed loop system and their performances were evaluated.

9.1.1 Decrease Altitude by 10%

When the systems were connected to airframes linearized about an altitude 10% lower than the design point the results changed as shown below in Tables 9-1 and 9-2:

	LQ			H_∞			H_2		
	Yaw	Pitch	Roll	Yaw	Pitch	Roll	Yaw	Pitch	Roll
Crossover Frequency (rad/sec)	37.0	37.2	73.2	34.0	33.0	70.8	34.7	32.9	70.
63% Rise time (sec)	0.18	0.16	0.099	0.17	0.17	0.098	0.16	0.17	0.11
Overshoot (%)	7.0	2.2	5.1	1.4	-0.6	-1.4	1.6	-0.2	-0.9

Table 9-1 Autopilot -10% in Altitude Performance Results Comparison

	LQ		H_∞		H_2	
	Gain Margin (dB)	Phase Margin (deg)	Gain Margin (dB)	Phase Margin (deg)	Gain Margin (dB)	Phase Margin (deg)
Roll	∞	106	∞	82	21	34
Yaw	∞	76	∞	46	18	41
Pitch	∞	95	-19, ∞	40	-17, 27	37

Table 9-2 Autopilot -10% in Altitude Bode Stability Margin Comparison

The closed loop time domain performances are high lighted by Figures 9-1 through 9-6. The maximum singular value of the complimentary sensitivity of the three systems is shown in Figure 9-7

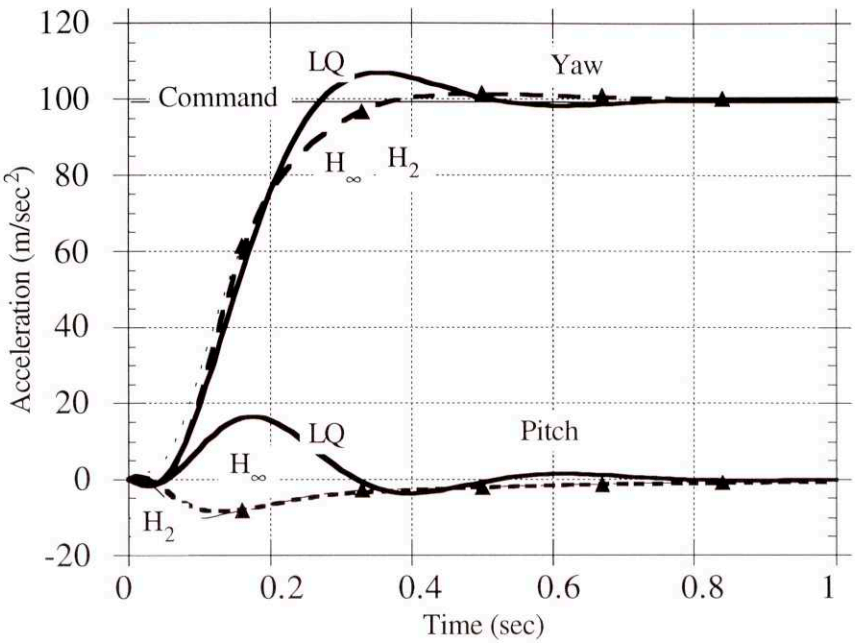

Figure 9-1 The Comparison of Acceleration Histories for a Yaw Step- -10% in Altitude

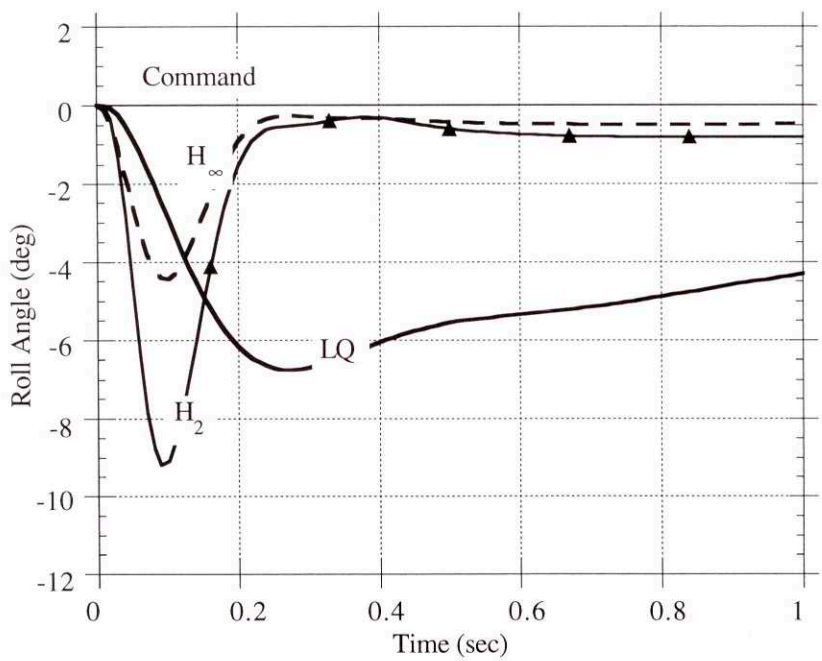

Figure 9-2 The Comparison of Roll Angle Histories for a Yaw Step - -10% in Altitude

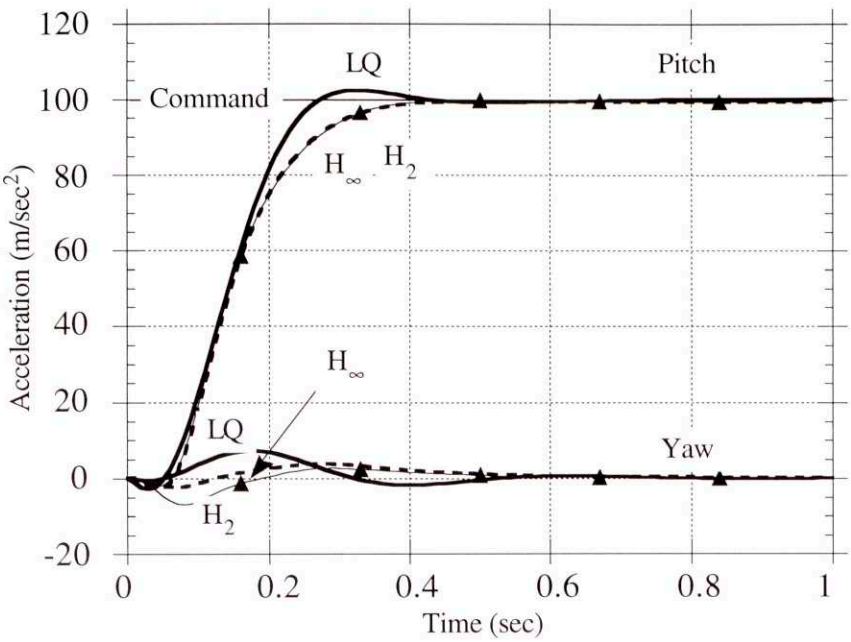

Figure 9-3 The Comparison of Acceleration Histories for a Pitch Step- -10% in Altitude

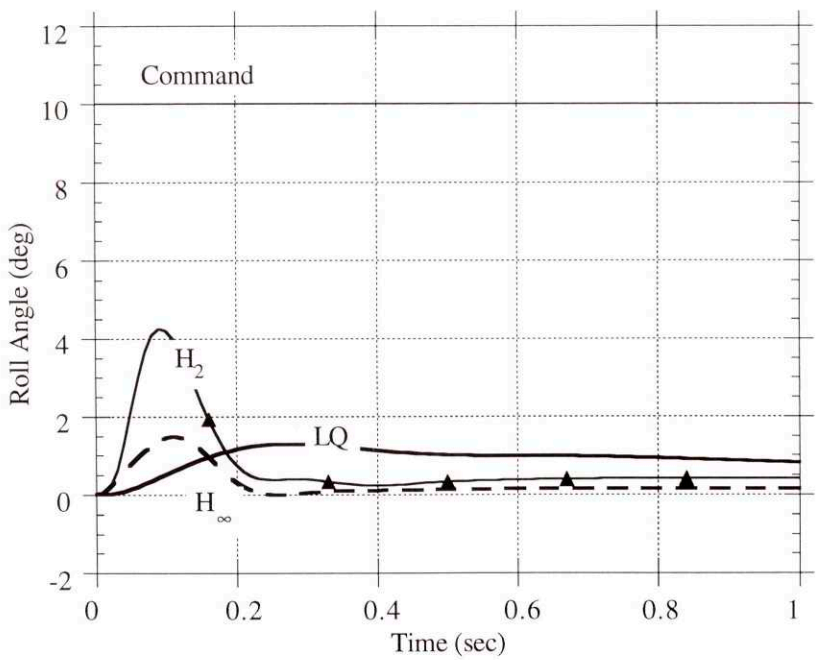

Figure 9-4 The Comparison of Roll Angle Histories for a Pitch Step - -10% in Altitude

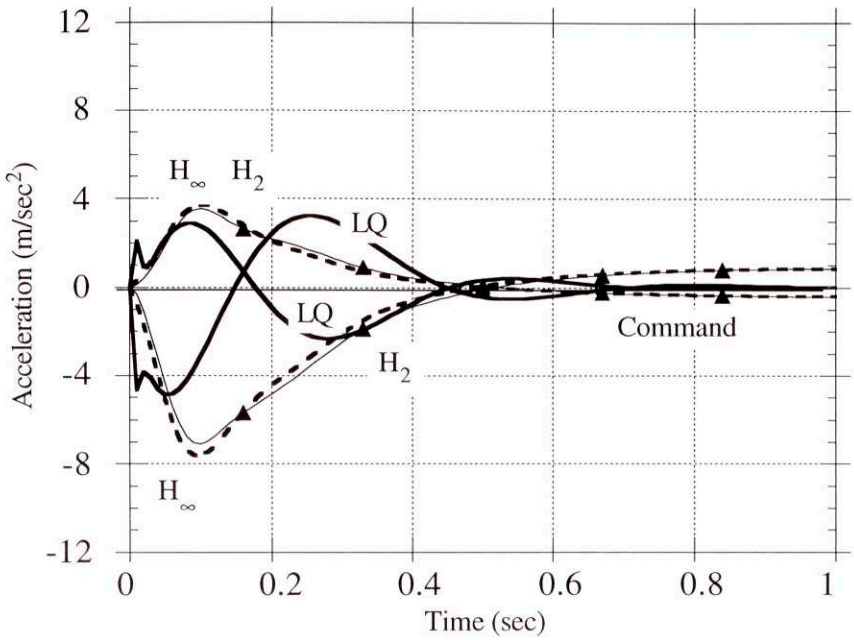

Figure 9-5 The Comparison of Acceleration Histories for a Roll Angle Step- -10% in Altitude

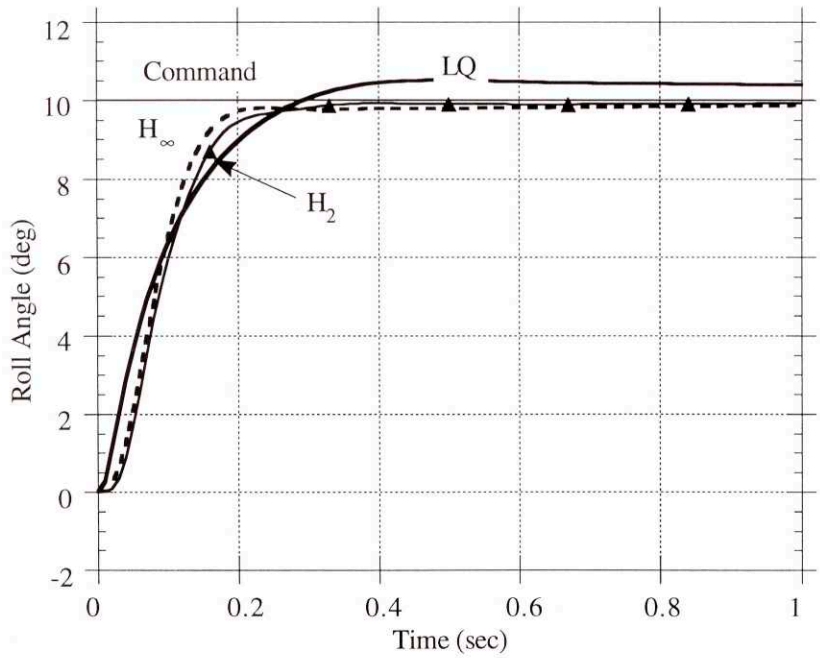

Figure 9-6 The Comparison of Roll Angle Histories for a Roll Angle Step - -10% in Altitude

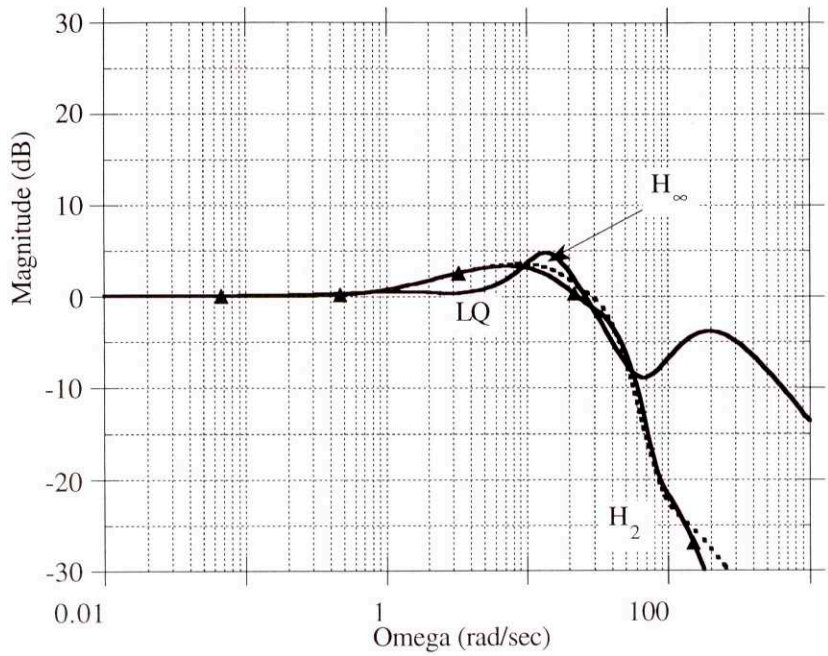

Figure 9-7 Maximum Singular Value Commands to Controlled Output - -10% in Altitude

9.1.2 Increase Altitude by 10%

When the systems were connected to airframes linearized about an altitude 10% higher than the design point the results changed as shown below in Tables 9-3 and 9-4. The time domain performances are highlighted in Figures 9-8 through 9-13. The maximum singular values of the autopilots complimentary sensitivity function are shown in Figure 9-14.

	LQ			H_∞			H_2		
	Yaw	Pitch	Roll	Yaw	Pitch	Roll	Yaw	Pitch	Roll
Crossover Frequency (rad/sec)	25.5	24.5	48.9	25.7	27.6	52.0	26.4	27.6	51.6
63% Rise time (sec)	0.24	0.22	0.10	0.24	0.24	0.097	0.24	0.24	0.10
Overshoot (%)	0	-0.3	6.2	0.4	-1.1	-1.2	0.7	-0.8	-0.4

Table 9-3 Autopilot +10% in Altitude Performance Results Comparison

	LQ		H_∞		H_2	
	Gain Margin (dB)	Phase Margin (deg)	Gain Margin (dB)	Phase Margin (deg)	Gain Margin (dB)	Phase Margin (deg)
Roll	∞	106	∞	67	26	33
Yaw	∞	70	∞	54	27	50
Pitch	∞	91	-20, ∞	50	-17, 30	47

Table 9-4 Autopilot +10% in Altitude Bode Stability Margin Comparison

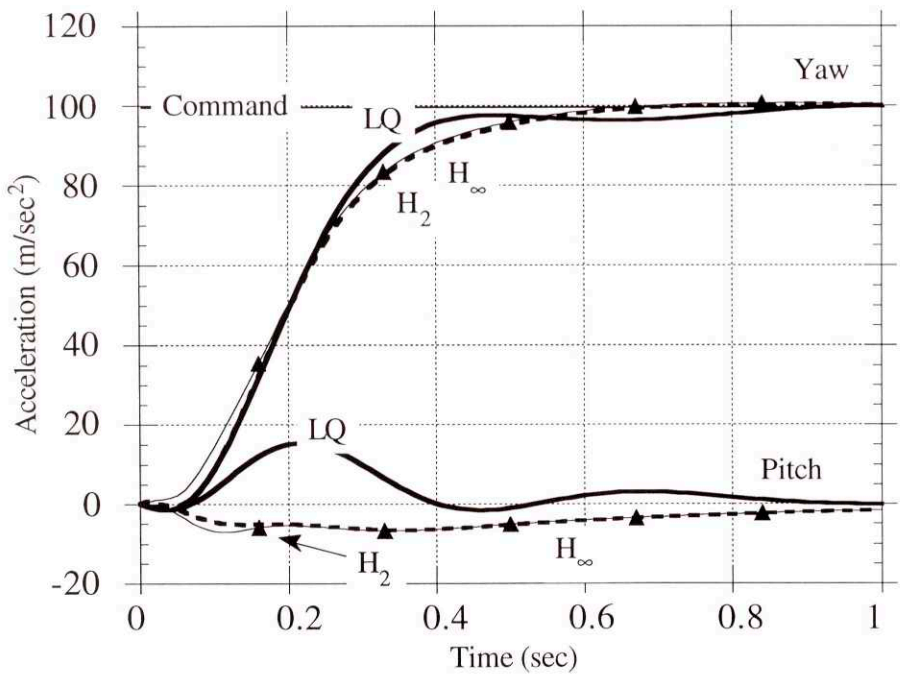

Figure 9-8 The Comparison of Acceleration Histories for a Yaw Step- +10% in Altitude

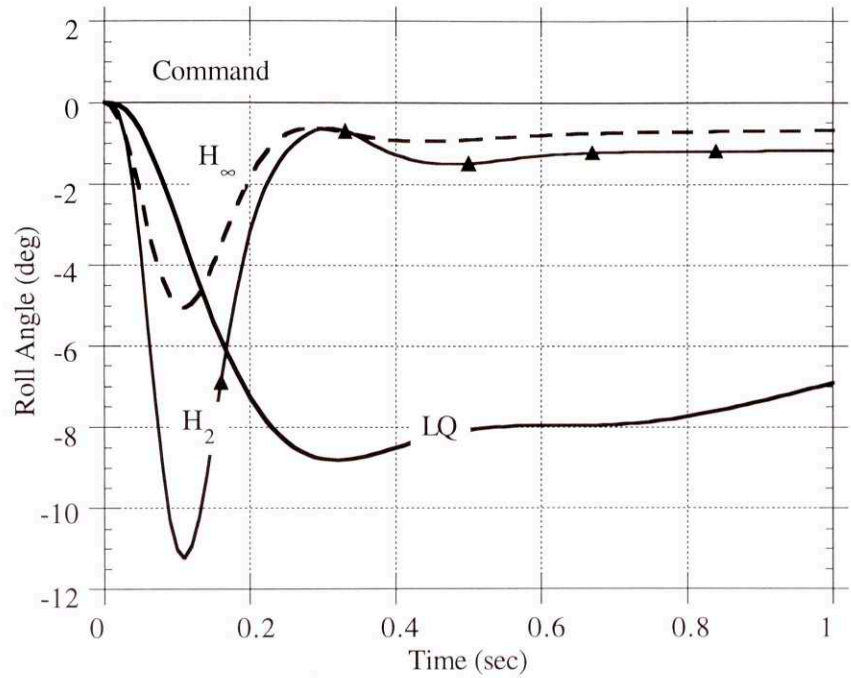

Figure 9-9 The Comparison of Roll Angle Histories for a Yaw Step - +10% in Altitude

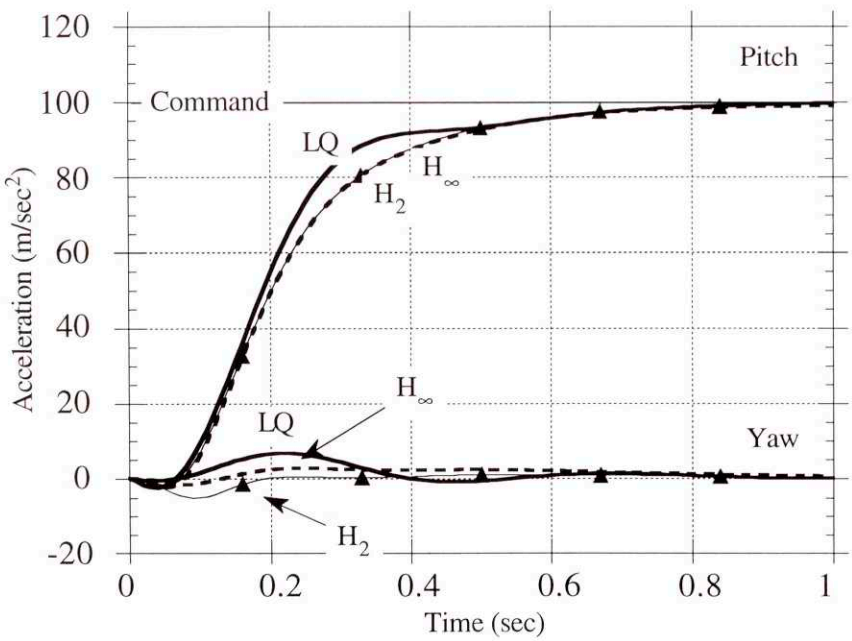

Figure 9-10 The Comparison of Acceleration Histories for a Pitch Step- +10% in Altitude

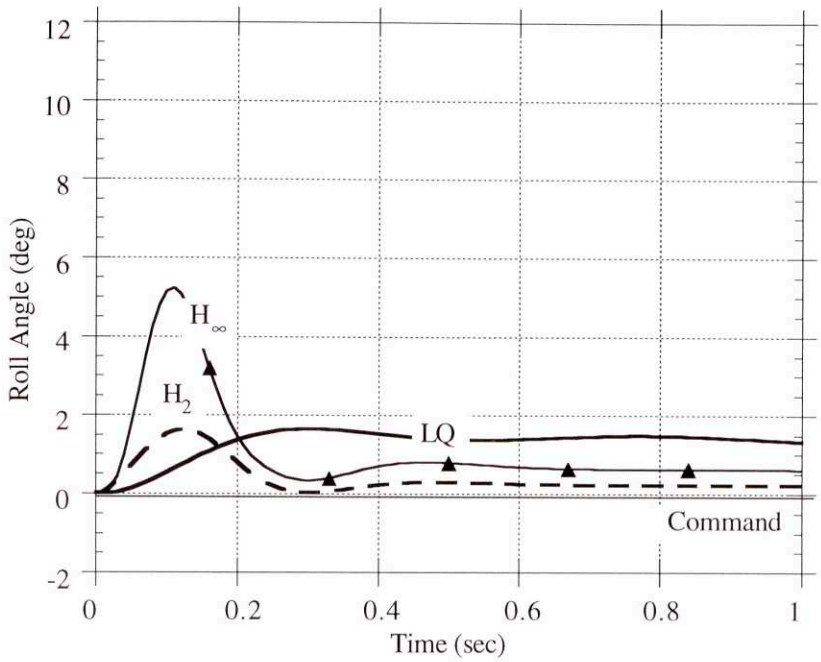

Figure 9-11 The Comparison of Roll Angle Histories for a Pitch Step - +10% in Altitude

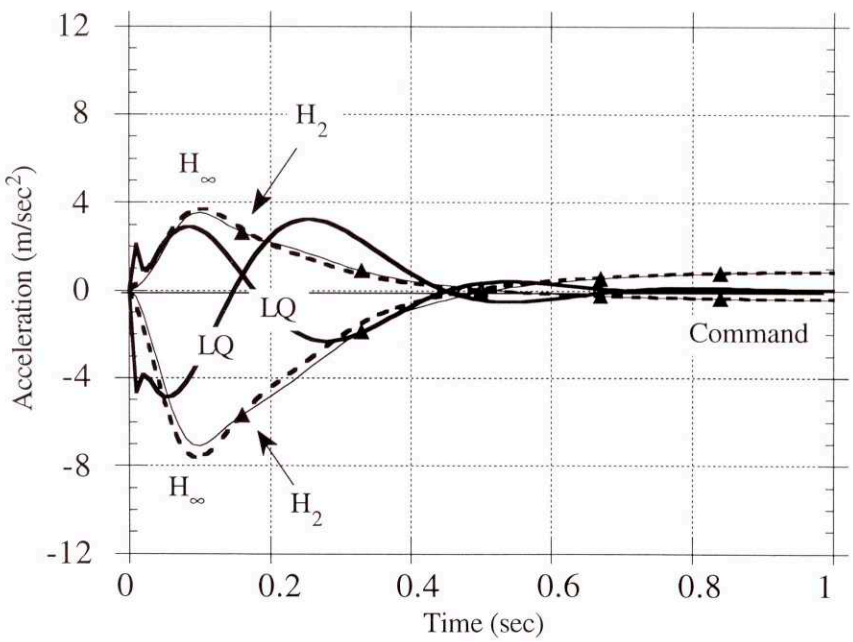

Figure 9-12 The Comparison of Acceleration Histories for a Roll Angle Step- +10% in Altitude

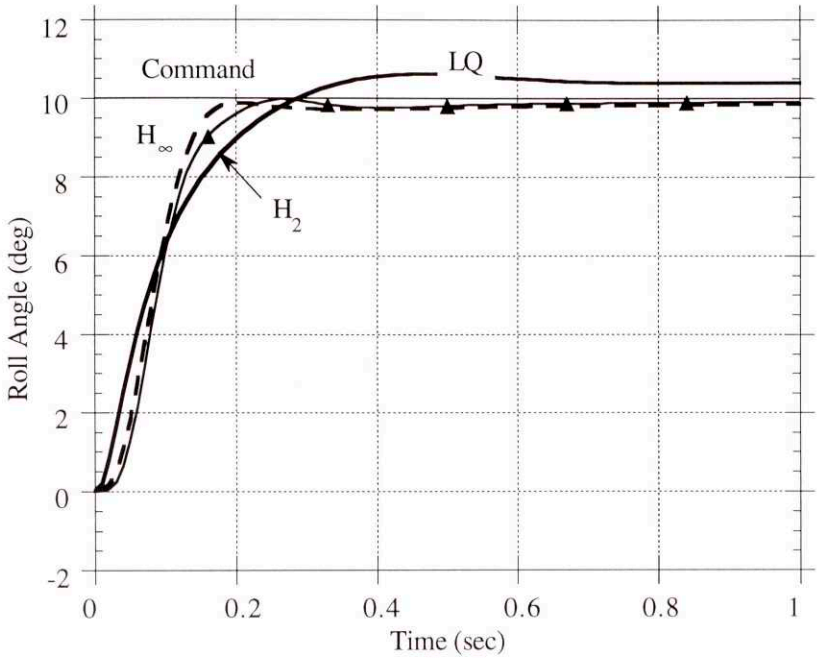

Figure 9-13 The Comparison of Roll Angle Histories for a Roll Angle Step - +10% in Altitude

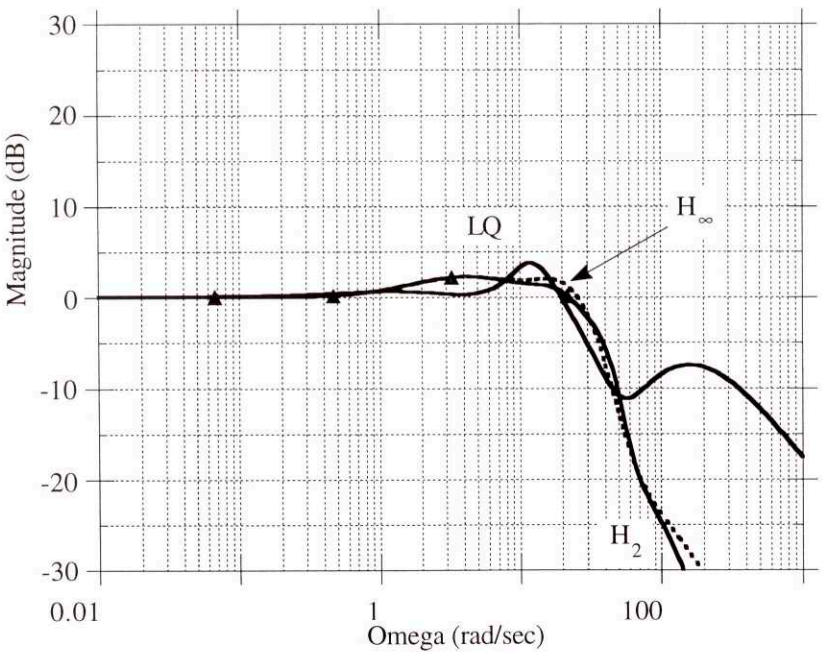

Figure 9-14 Maximum Singular Value Commands to Controlled Output - +10% in Altitude

9.1.3 Conclusions

All three autopilots can handle this 10% variation in altitude. The LQ design shows the greatest change in the Bode crossover frequencies, and its risetime performance changes the most. The single loop stability margins of the LQ design are still the best. The H_2 design still has the smallest single loop gain and phase margins. The H_2 design exhibits a much changed roll channel performance. It now has the greatest roll cross channel motion due to a lateral step.

9.2 Variations in Missile Speed

The autopilot designs of the previous chapters were done using a nominal plant linearized around a flight condition at Mach 4. However in operation the current missile speed cannot be exactly known. To evaluate the performance changes of the three designs, linearized airframes were generated for the same missile altitude, angle of attack and wind angle, but with the missile velocity changed by ±10%. This 10% variation is a conservative number, in an operational situation an IMU should provide estimates of missile speed that are better than the allocated ±10%.

The autopilots developed in the previous chapters were connected to the perturbed airframes to form a closed loop system and their performances were evaluated.

9.2.1 Decrease Missile Velocity by 10%

When the systems were connected to airframes linearized about a missile velocity 10% lower than the design point the results changed as shown below in Tables 9-5 and 9-6.

	LQ			H_∞			H_2		
	Yaw	Pitch	Roll	Yaw	Pitch	Roll	Yaw	Pitch	Roll
Crossover Frequency (rad/sec)	27.2	27.4	54.2	27.0	29.3	54.2	27.8	29.3	54.1
63% Rise time (sec)	0.22	.020	0.10	0.22	0.22	0.097	0.22	0.22	0.10
Overshoot (%)	0.3	-0.06	5.6	3.5	2.2	-1.0	3.7	2.5	-0.89

Table 9-5 Autopilot -10% in Speed Performance Results Comparison

	LQ		H_∞		H_2	
	Gain Margin (dB)	Phase Margin (deg)	Gain Margin (dB)	Phase Margin (deg)	Gain Margin (dB)	Phase Margin (deg)
Roll	∞	102	∞	68	25	33
Yaw	∞	71	∞	52	25	48
Pitch	∞	89	-21, ∞	44	-18, 29	41

Table 9-6 Autopilot -10% in Speed Bode Stability Margin Comparison

The time domain performances are high lighted in Figures 9-15 through 9-20. The maximum singular value of the complementary sensitivity function is shown in Figure 9-21.

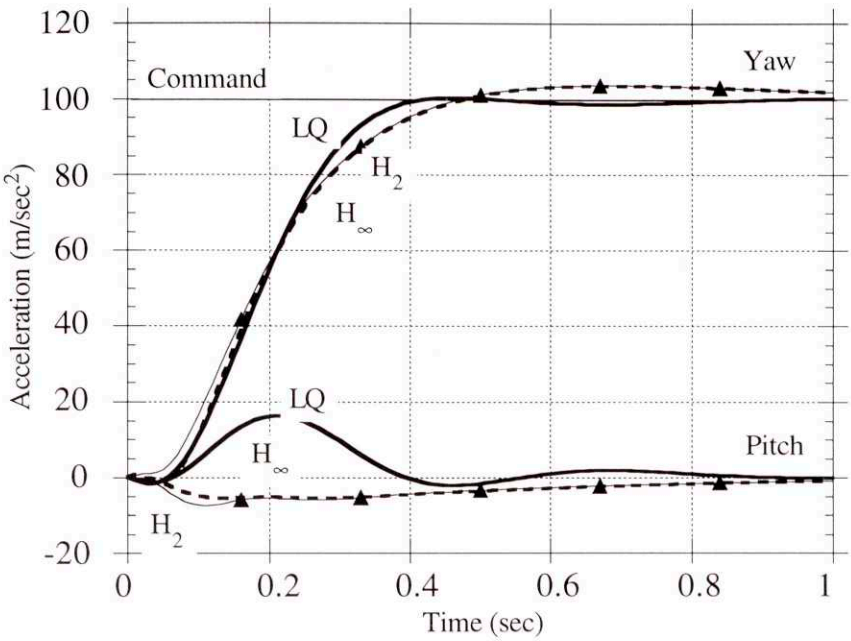

Figure 9-15 The Comparison of Acceleration Histories for a Yaw Step- -10% in Speed

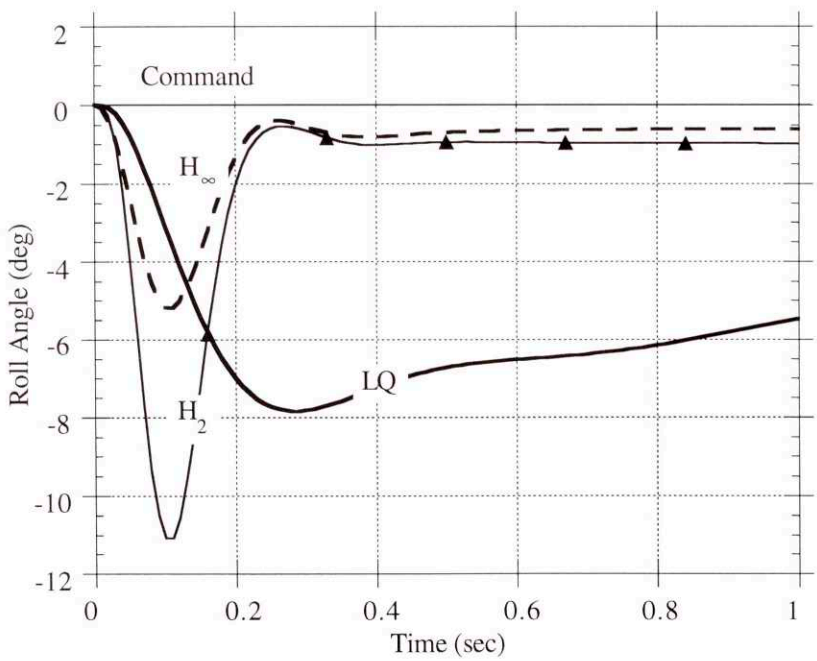

Figure 9-16 The Comparison of Roll Angle Histories for a Yaw Step - -10% in Speed

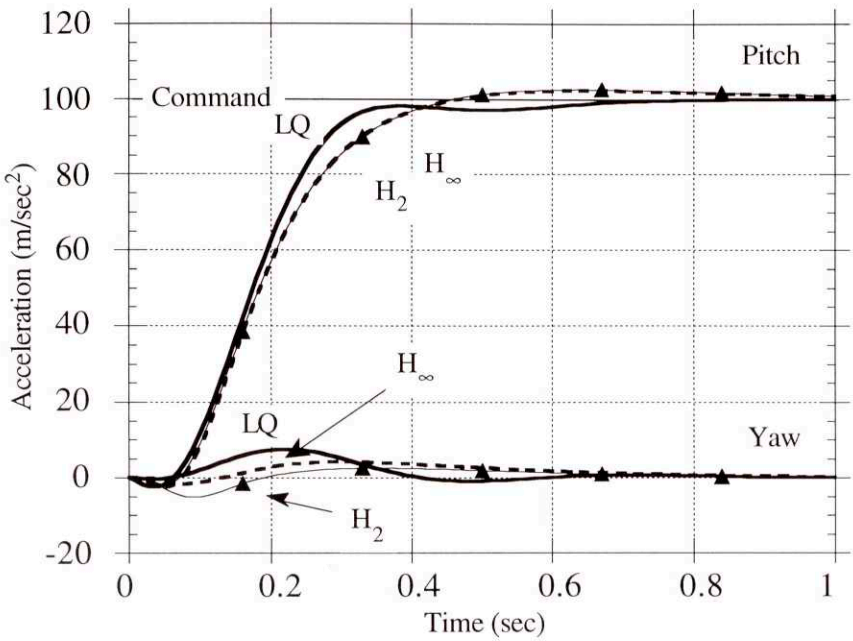

Figure 9-17 The Comparison of Acceleration Histories for a Pitch Step- -10% in Speed

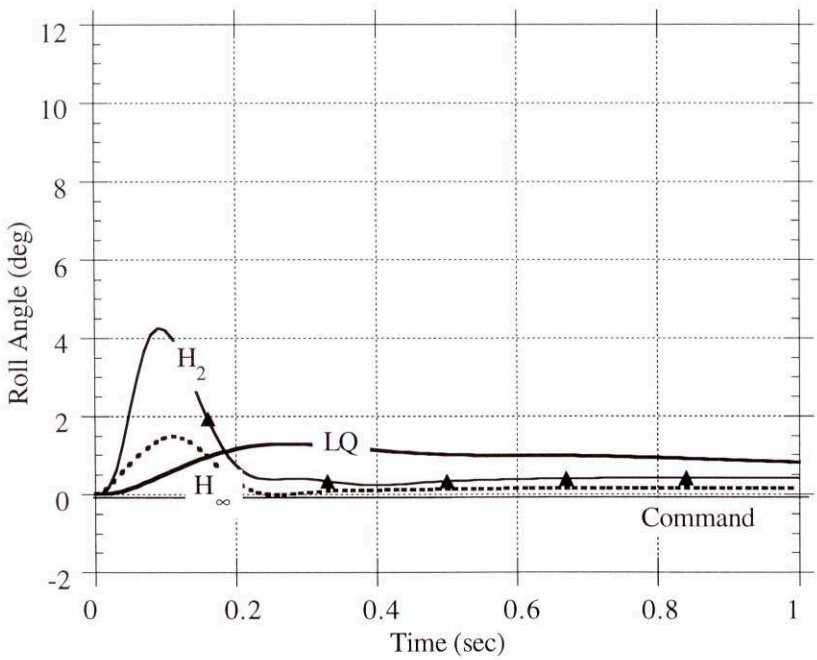

Figure 9-18 The Comparison of Roll Angle Histories for a Pitch Step - -10% in Speed

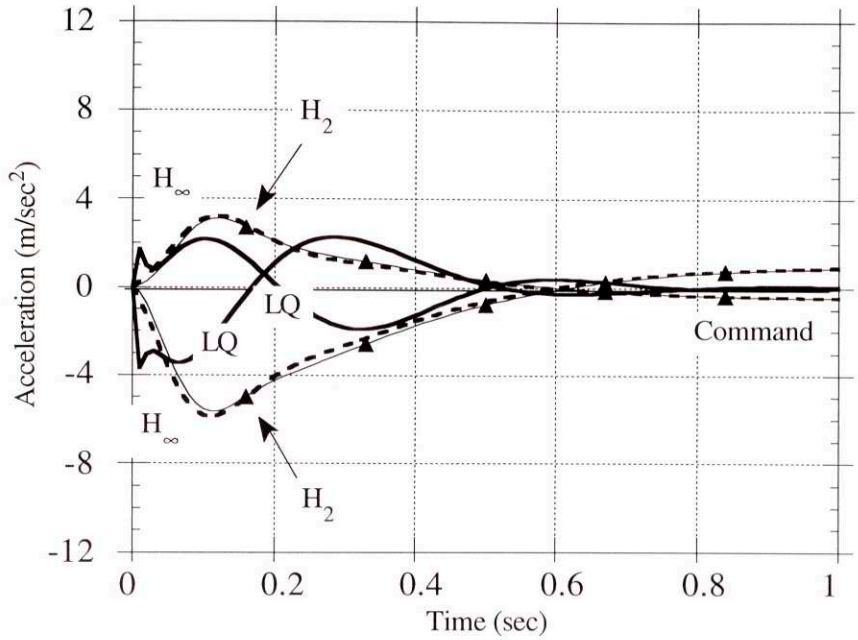

Figure 9-19 The Comparison of Acceleration Histories for a Roll Angle Step- -10% in Speed

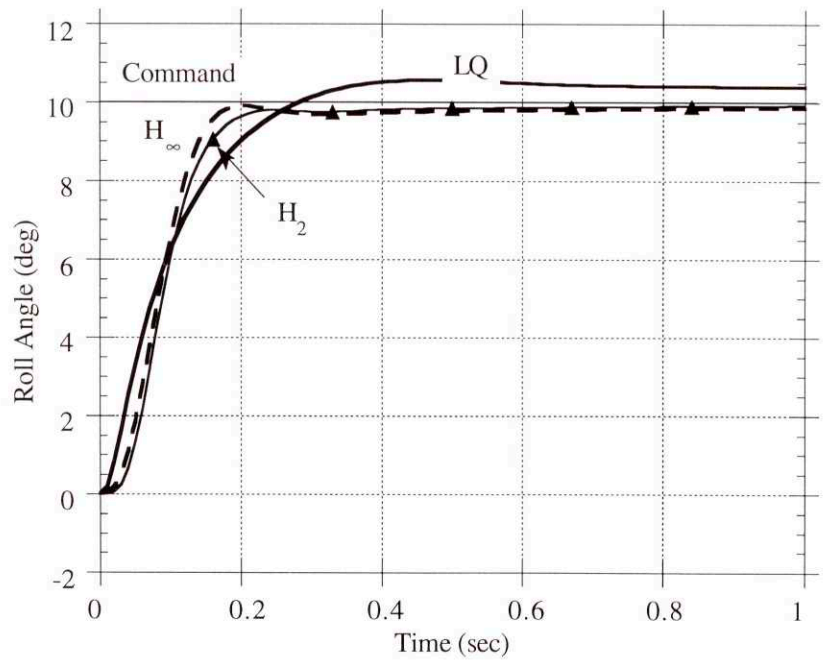

Figure 9-20 The Comparison of Roll Angle Histories for a Roll Angle Step - -10% in Speed

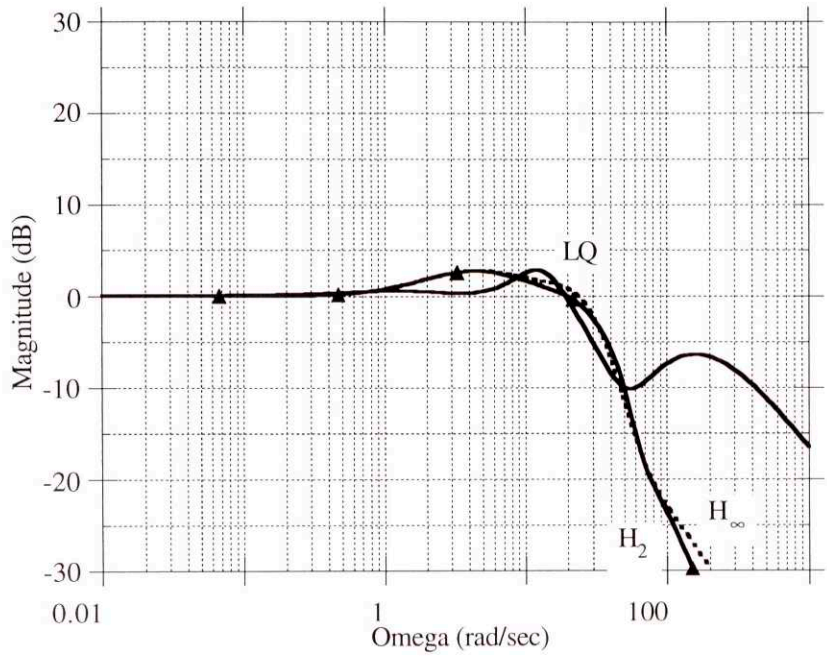

Figure 9-21 Maximum Singular Value Commands to Controlled Output - -10% in Speed

9.2.2 Increase Missile Velocity by 10%

When the systems were connected to airframes linearized about a missile velocity 10% greater than the design point the results changed as shown below in Tables 9-7 and 9-8. The time domain performances are shown in Figures 9-22 through 9-27. The maximum singular value of the complementary sensitivity function is shown in Figure 9-28.

	LQ			H_∞			H_2		
	Yaw	Pitch	Roll	Yaw	Pitch	Roll	Yaw	Pitch	Roll
Crossover Frequency (rad/sec)	34.0	36.3	71.5	31.7	32.8	70.0	32.6	32.8	69.4
63% Rise time (sec)	0.18	0.16	0.099	0.17	0.16	0.097	0.16	0.17	0.11
Overshoot (%)	5.0	11.7	5.1	2.0	8.8	-1.4	1.6	-0.28	-0.86

Table 9-7 Autopilot +10% in Speed Performance Results Comparison

	LQ		H_∞		H_2	
	Gain Margin (dB)	Phase Margin (deg)	Gain Margin (dB)	Phase Margin (deg)	Gain Margin (dB)	Phase Margin (deg)
Roll	∞	107	∞	81	21	34
Yaw	∞	75	∞	47	19	42
Pitch	∞	94	-19, ∞	41	-17, 27	37

Table 9-8 Autopilot +10% in Speed Bode Stability Margin Comparison

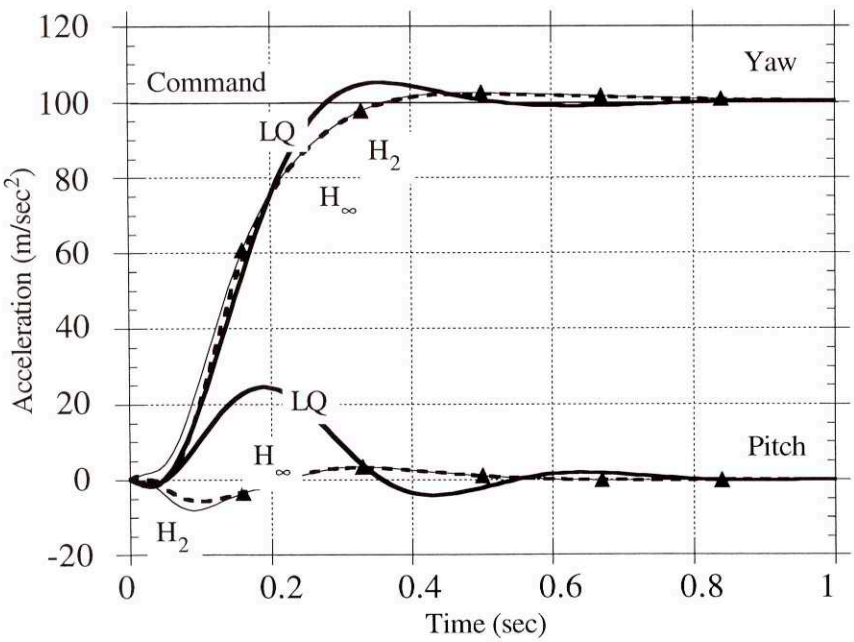

Figure 9-22 The Comparison of Acceleration Histories for a Yaw Step- +10% in Speed

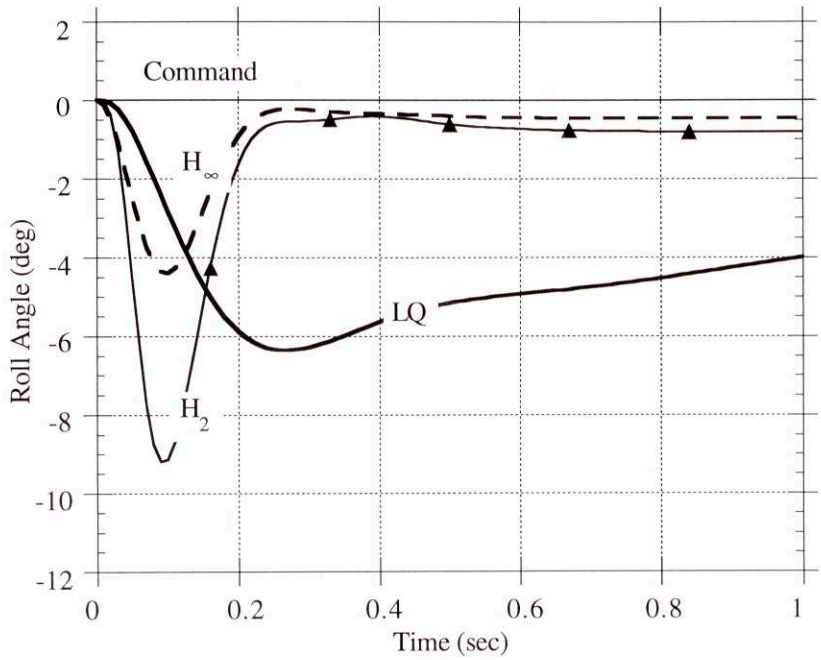

Figure 9-23 The Comparison of Roll Angle Histories for a Yaw Step - +10% in Speed

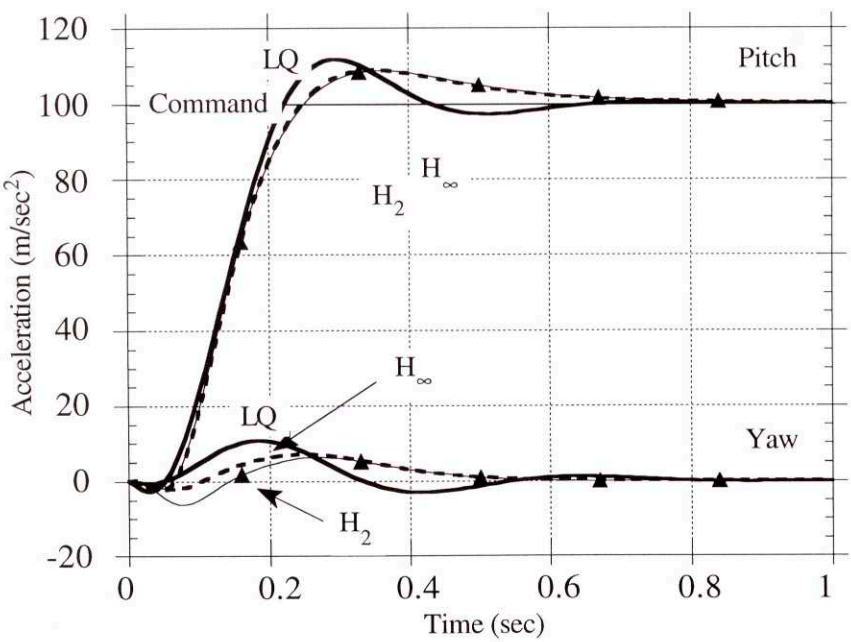

Figure 9-24 The Comparison of Acceleration Histories for a Pitch Step- +10% in Speed

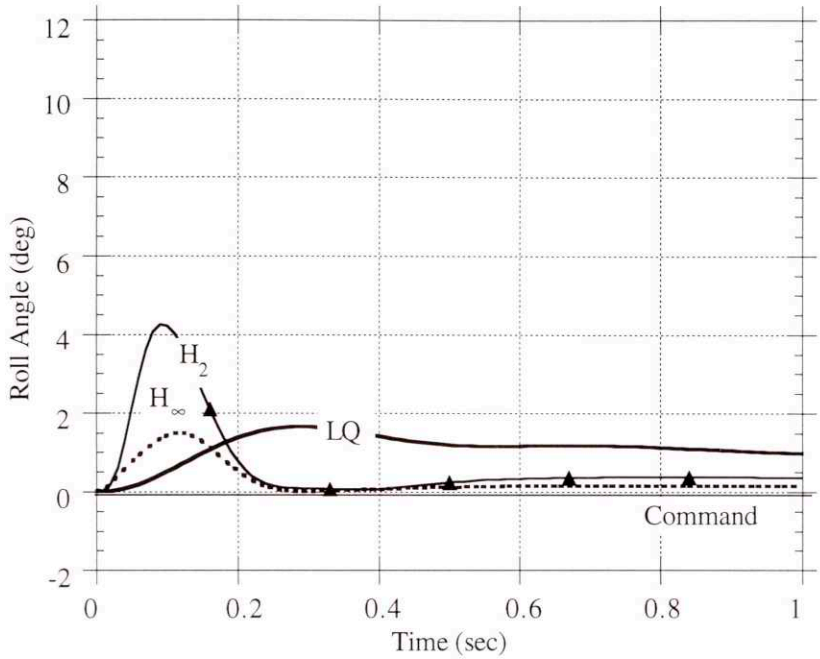

Figure 9-25 The Comparison of Roll Angle Histories for a Pitch Step - +10% in Speed

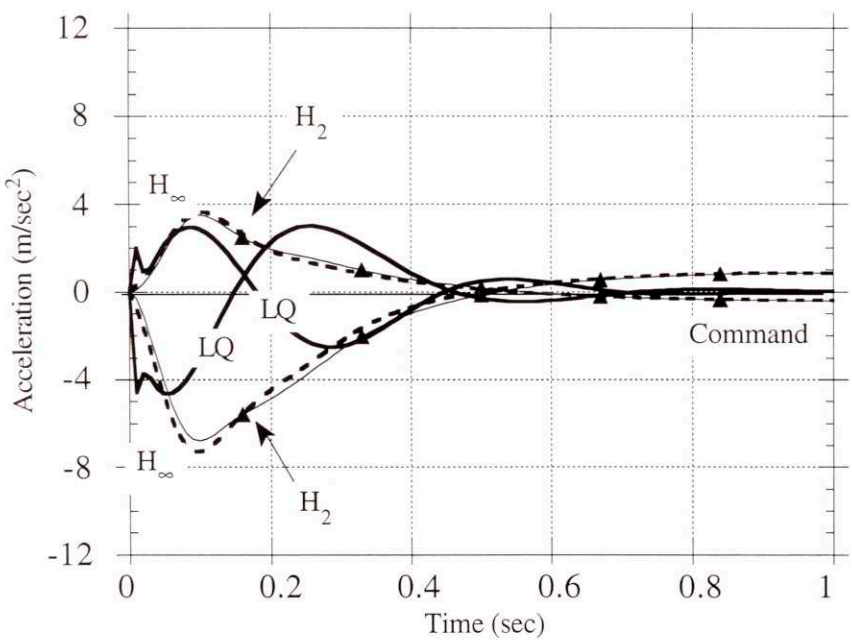

Figure 9-26 The Comparison of Acceleration Histories for a Roll Angle Step- +10% in Speed

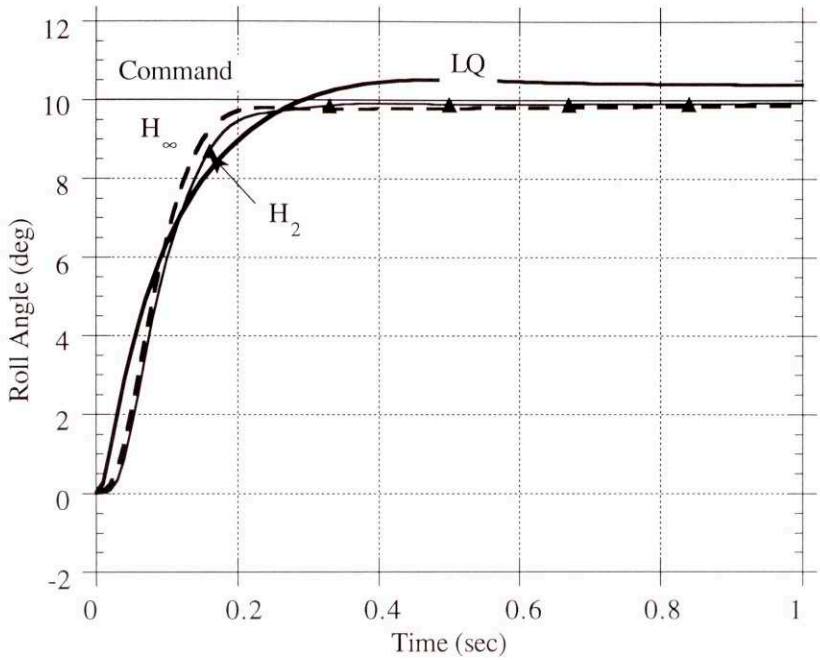

Figure 9-27 The Comparison of Roll Angle Histories for a Roll Angle Step - +10% in Speed

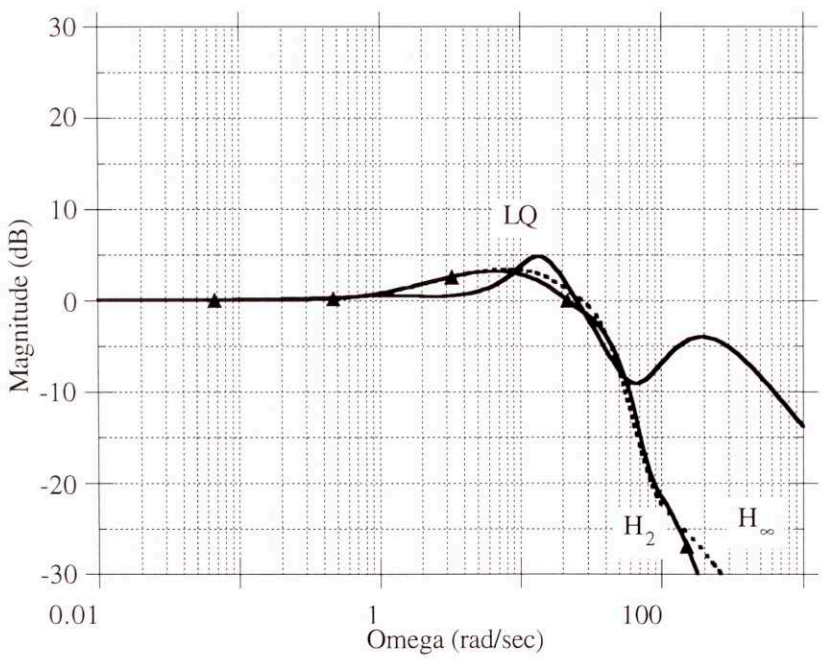

Figure 9-28 Maximum Singular Value Commands to Controlled Output - +10% in Speed

9.2.3 Conclusions

All three autopilots can handle this 10% variation in speed. The LQ design again shows the greatest change in the Bode crossover frequencies, and its risetime performance changes the most. This change in speed results in more of an overshoot than was specified in the design specifications. The single loop stability margins of the LQ design are still the best. The H_2 design still has the smallest single loop gain and phase margins. The H_2 design continues to exhibit the largest cross channel motion in the roll channel.

Chapter 10 Perturbation Results (Angle of Attack and Wind Angle)

The three autopilot designs demonstrate excellent performance at the nominal flight condition as expected. However the performance of the three systems degrades when the designs are evaluated at off nominal flight conditions.

The original nominal design condition was Mach 4, medium altitude, a total angle of attack of 15° and a wind angle of 22.5°. The designs' performance have been evaluated at a number of flight conditions found by varying the angle of attack by ±5° (10° and 20°) and using wind angles of 11.25°, 22.5° and 45°. The altitude and speed remained at the nominal values.

10.1 Variations in Total Angle of Attack

The autopilot designs of the previous chapters were done using a nominal plant linearized around a flight condition 15° degrees total angle of attack. However in operation the current missile angle of attack cannot be exactly known. To evaluate the performance changes of the three designs, linearized airframes were generated for the same altitude, missile speed and wind angle, but with the angle of attack changed by ±5°. This 5 degree variation is a conservative number. In an operational situation an Inertial Measurement Unit (IMU) should provide estimates of missile total angle of attack that are better than ±5°.

The autopilots developed in from the previous chapters were then connected to the perturbed airframes to form a closed loop system and their performances were evaluated.

10.1.1 Decrease Angle of Attack by 5°

When the systems were connected to airframes linearized about an angle of attack of 10° (5° lower than the design point) the results changed to those shown below in Tables 10-1 and 10-2. The time domain performances are high lighted in Figures 10-1 to 10-6. The maximum singular value of the complementary sensitivity function is shown in Figure 10-7.

	LQ			H_∞			H_2		
	Yaw	Pitch	Roll	Yaw	Pitch	Roll	Yaw	Pitch	Roll
Crossover Frequency (rad/sec)	24.7	25.2	64.3	25.6	28.2	54.2	25.8	27.5	54.4
63% Rise time (sec)	0.19	0.18	0.10	0.19	0.20	0.10	0.18	0.20	0.11
Overshoot (%)	9.7	6.1	5.4	11.6	15.4	5.6	11.6	15.2	5.5

Table 10-1 Autopilot Performance Results Comparison 10° α_t

	LQ		H_∞		H_2	
	Gain Margin (dB)	Phase Margin (deg)	Gain Margin (dB)	Phase Margin (deg)	Gain Margin (dB)	Phase Margin (deg)
Roll	∞	88	∞	58	24	31
Yaw	∞	61	∞	47	25	40
Pitch	∞	75	-27, ∞	33	-22, 29	28

Table 10-2 Autopilot Bode Stability Margin Comparison 10° α_t

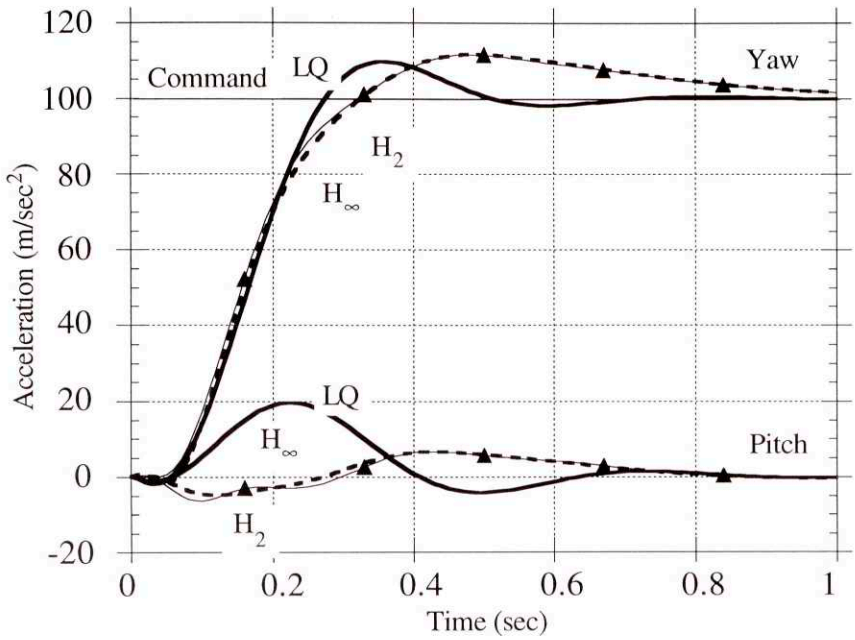

Figure 10-1 The Comparison of Acceleration Histories for a Yaw Step 10° α_t

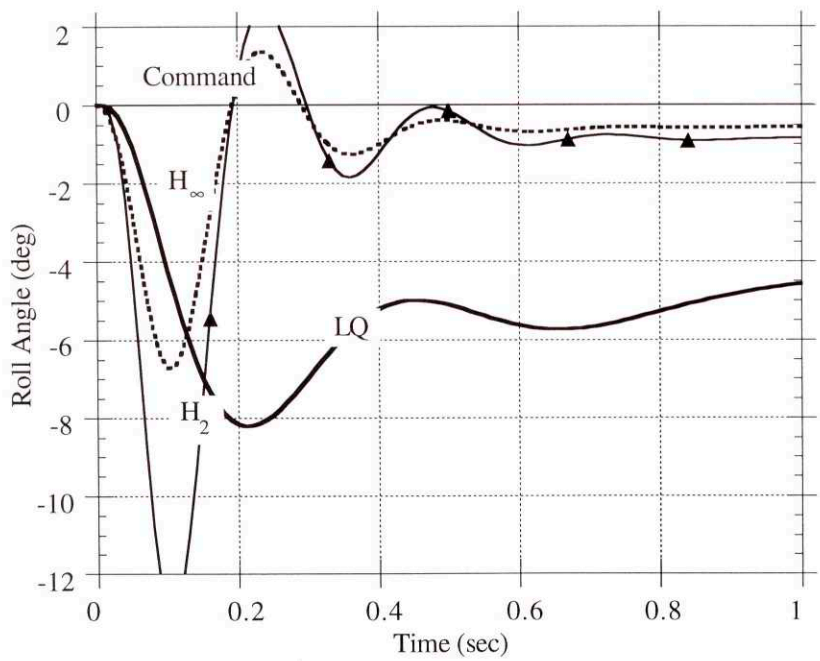

Figure 10-2 The Comparison of Roll Angle Histories for a Yaw Step 10° α_t

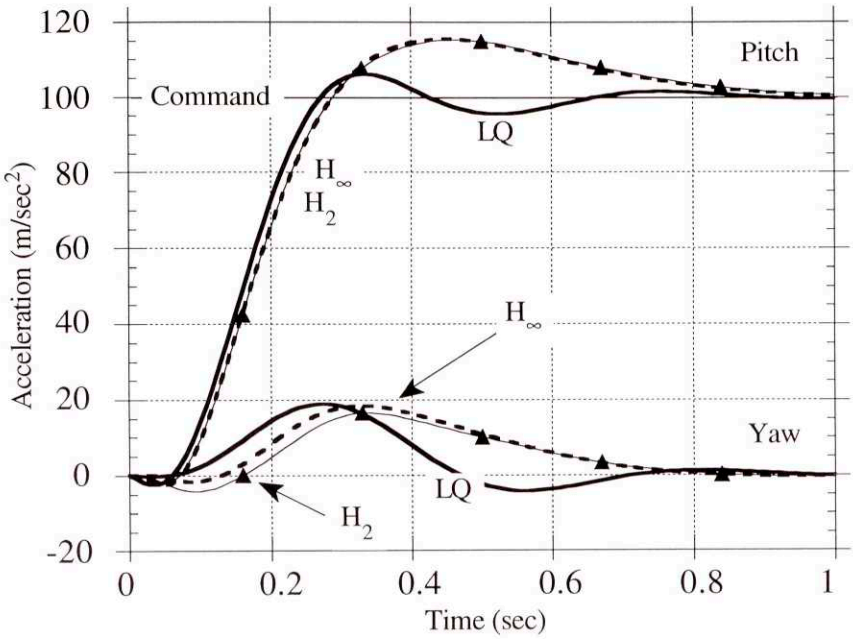

Figure 10-3 The Comparison of Acceleration Histories for a Pitch Step 10° α_t

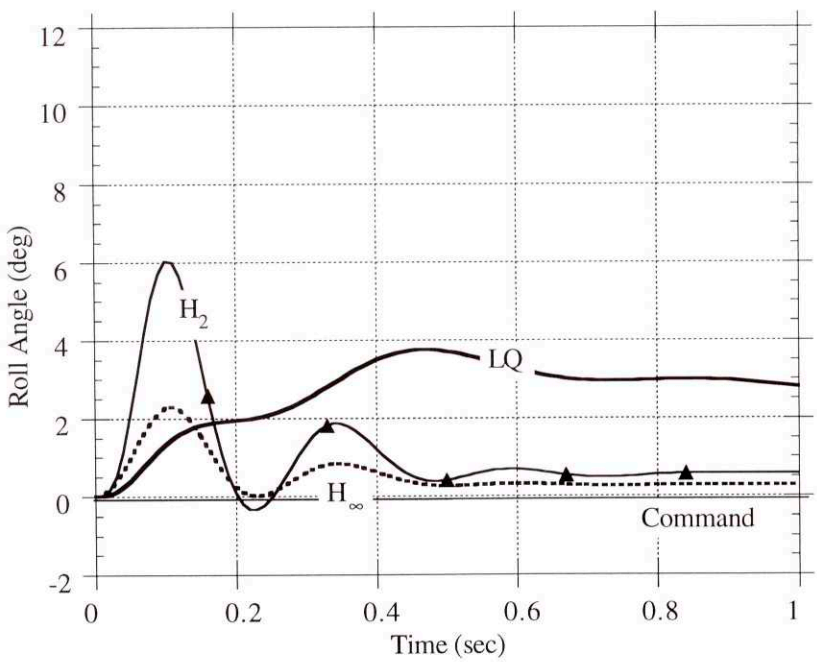

Figure 10-4 The Comparison of Roll Angle Histories for a Pitch Step 10° α_t

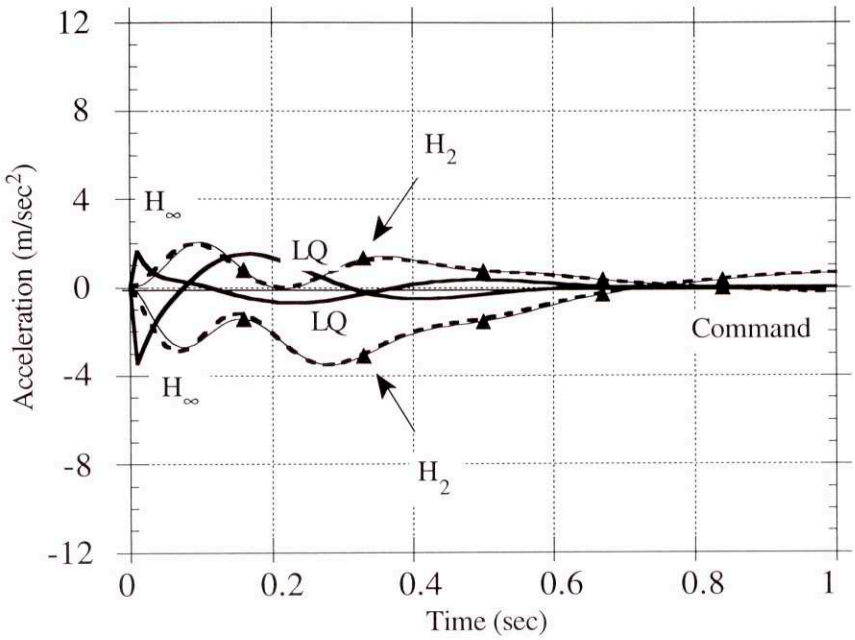

Figure 10-5 The Comparison of Acceleration Histories for a Roll Angle Step 10° α_t

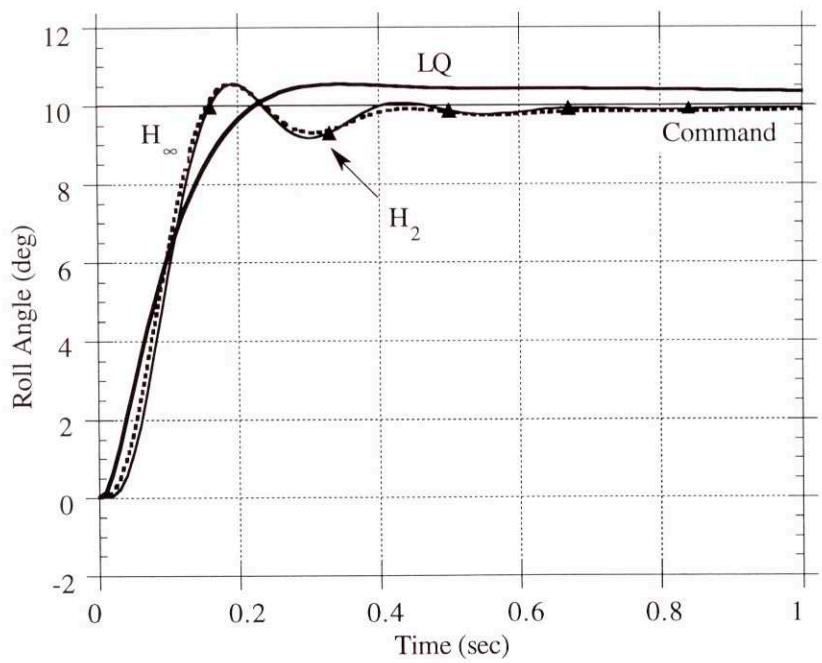

Figure 10-6 The Comparison of Roll Angle Histories for a Roll Angle Step 10° α_t

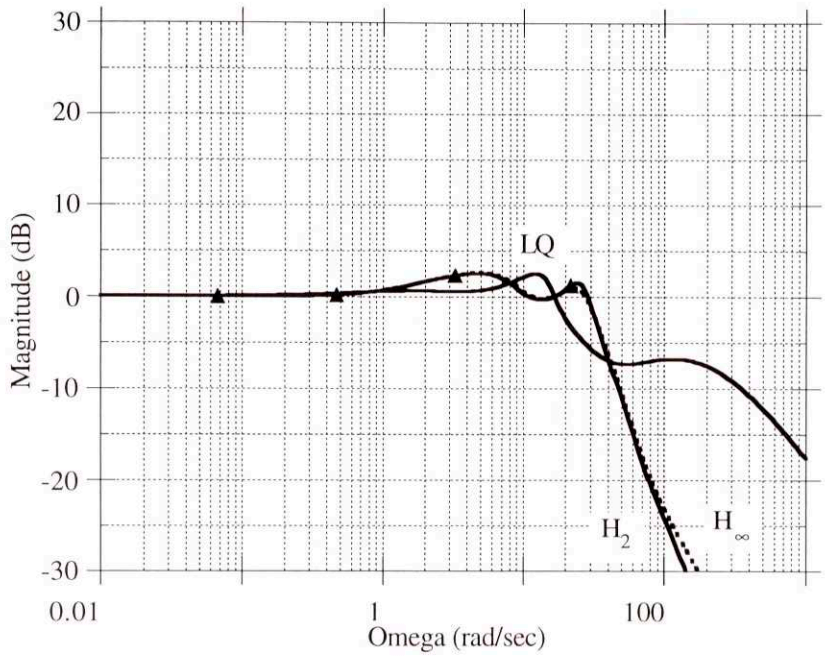

Figure 10-7 Maximum Singular Value Commands to Controlled Output 10° α_t

10.1.2 Increase Total Angle of Attack by 5°

When the systems were connected to airframes linearized about an angle of attack of 20 degrees (5° greater than the design point) the results changed to those shown below in Tables 10-3 and 10-4. The time domain performances are high lighted in Figures 10-8 to 10-13. The maximum singular value of the complementary sensitivity function is shown in Figure 10-14.

	LQ			H_∞			H_2		
	Yaw	Pitch	Roll	Yaw	Pitch	Roll	Yaw	Pitch	Roll
Crossover Frequency (rad/sec)	25.6	36.5	40.4	25.2	33.8	61.1	26.1	37.2	60.3
63% Rise time (sec)	0.19	0.16	0.093	0.19	0.17	0.094	0.19	0.17	0.10
Overshoot (%)	4.7	25	6.4	1.4	21.6	-1.5	2.0	20.5	-0.92

Table 10-3 Autopilot Performance Results Comparison 20° α_t

	LQ		H_∞		H_2	
	Gain Margin (dB)	Phase Margin (deg)	Gain Margin (dB)	Phase Margin (deg)	Gain Margin (dB)	Phase Margin (deg)
Roll	-13, ∞	108	∞	84	24	39
Yaw	∞	68	∞	53	24	50
Pitch	∞	109	-18, ∞	56	-16, 26	54

Table 10-4 Autopilot Bode Stability Margin Comparison 20° α_t

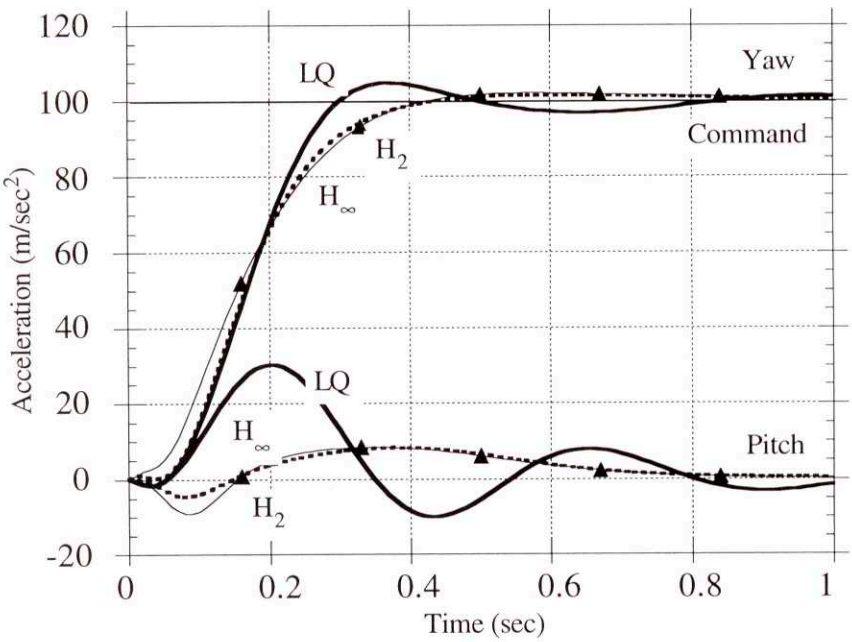

Figure 10-8 The Comparison of Acceleration Histories for a Yaw Step 20° α_t

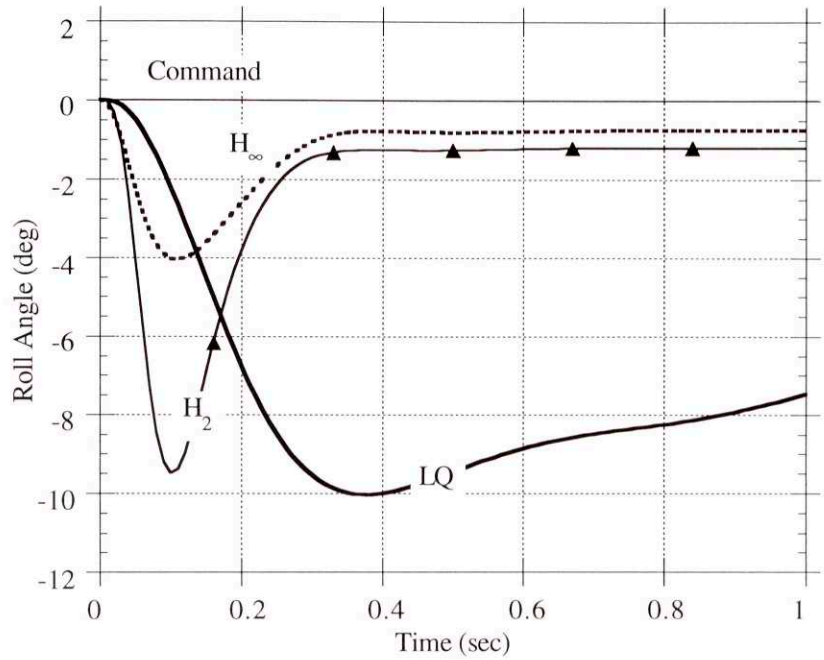

Figure 10-9 The Comparison of Roll Angle Histories for a Yaw Step 20° α_t

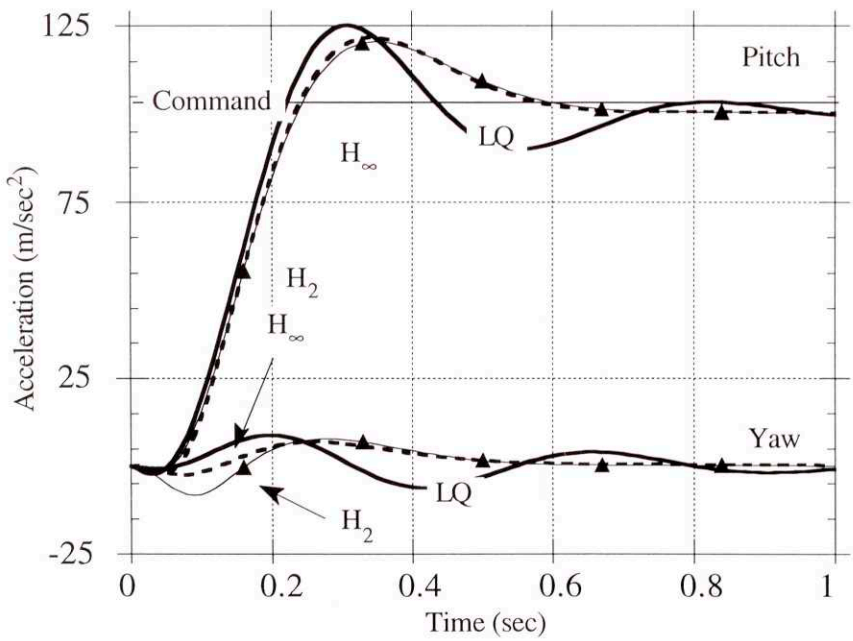

Figure 10-10 The Comparison of Acceleration Histories for a Pitch Step 20° α_t

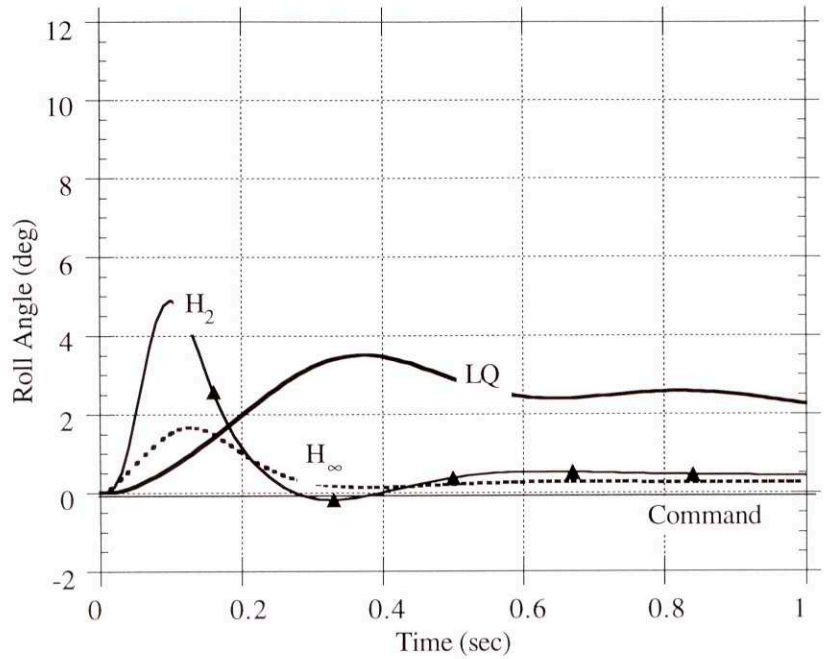

Figure 10-11 The Comparison of Roll Angle Histories for a Pitch Step 20° α_t

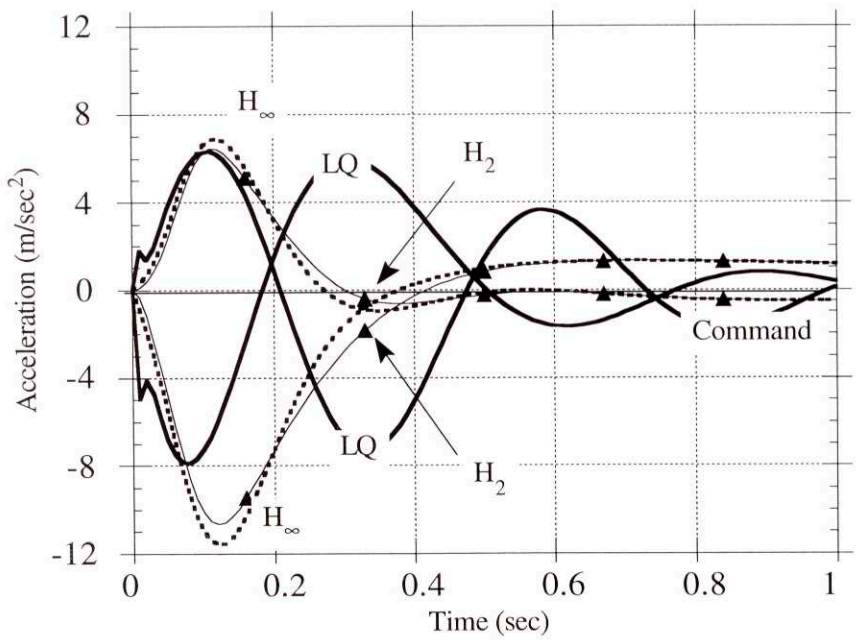

Figure 10-12 The Comparison of Acceleration Histories for a Roll Angle Step 20° α_t

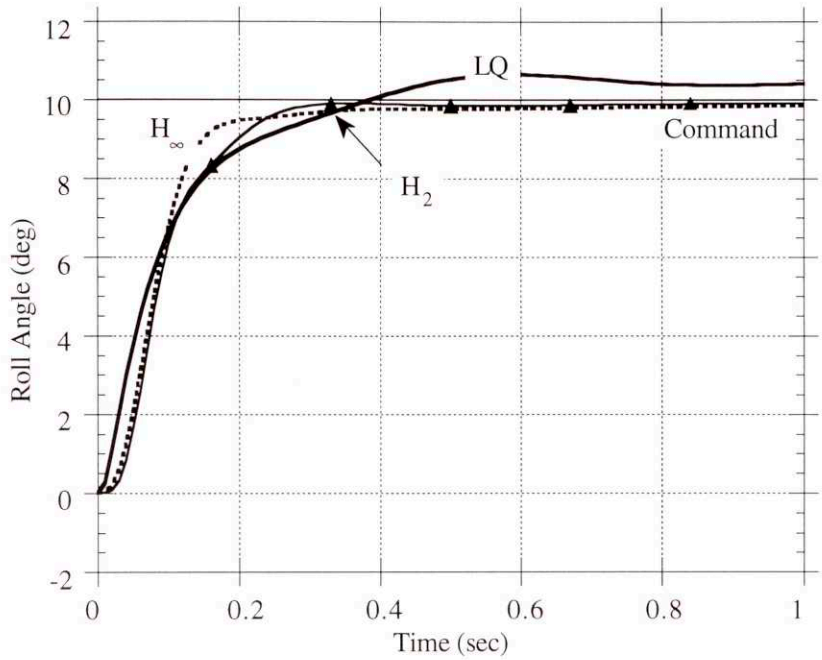

Figure 10-13 The Comparison of Roll Angle Histories for a Roll Angle Step 20° α_t

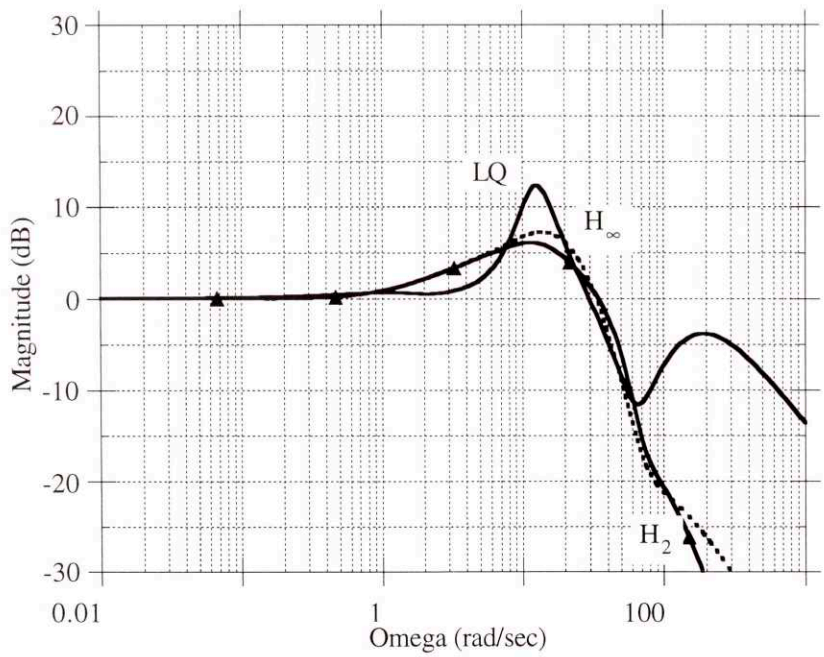

Figure 10-14 Maximum Singular Value Commands to Controlled Output 20° α_t

10.1.3 Conclusions

All three autopilots can handle this 5° variation in angle of attack and still remain stable. The LQ design shows changes comparable to the H_∞ and H_2 designs in the Bode crossover frequencies, and its risetime performance is approximately the same as theirs. On the other hand the LQ design consistently has less over shoot than either of the other two designs. All three designs suffered some single loop stability margin degradation at the 10° flight condition. The single loop stability margins of the LQ design are still the best. The H_2 design still has the smallest single loop gain and phase margins. The H_2 design continues to exhibit the largest cross channel motion in the roll channel.

10.2 Variations in Wind Angle

The autopilot designs of section 4 were done using a nominal plant linearized around a wind angle of 22.5°. However in operation the current missile wind angle cannot be exactly known. To evaluate the performance changes of the three designs, linearized airframes were generated for the same altitude, missile speed, and angle of attack, but with the wind angles changed. The deltas chosen for the analysis are -11.25° and +22.5°. They yield respectively 11.25° and 45° degrees. The 11.25° value gives a more planar airframe design in one channel, however the cross-coupling into the other channel has increased. The 45° angle is the most symmetric flight condition.

The autopilots developed in section 4 were then connected to the perturbed airframes to form a closed loop system and their performances were evaluated.

10.2.1 Wind Angles of 11.25°

When the systems were connected to airframes linearized about a wind angle of 11.25° the responses changed to those shown in Figures 10-15 to 10-20 and summarized in Tables 10-5 and 10-6. Figures 10-21 through 10-24 show the singular values of the four transfer functions. The LQ design exhibits a strong resonance in the vicinity of 10 radians per second.

	LQ			H_∞			H_2		
	Yaw	Pitch	Roll	Yaw	Pitch	Roll	Yaw	Pitch	Roll
Crossover Frequency (rad/sec)	28.8	29.9	54.6	28.8	30.9	56.8	27.9	31.6	56.6
63% Rise time (sec)	0.17	0.18	0.096	0.15	0.20	0.096	0.14	0.20	0.10
Overshoot (%)	67.2	5.2	9.2	53.1	0.03	-1.25	40.8	0.3	1.4

Table 10-5 Autopilot Performance Results Comparison 11.25° Wind Angle

	LQ		H_∞		H_2	
	Gain Margin (dB)	Phase Margin (deg)	Gain Margin (dB)	Phase Margin (deg)	Gain Margin (dB)	Phase Margin (deg)
Roll	-3,∞	102	-11,∞	74	-13, 24	35
Yaw	∞	66	∞	48	29.5	52
Pitch	-9,∞	104	-15,∞	54	-16, 28	52

Table 10-6 Autopilot Bode Stability Margin Comparison 11.25° Wind Angle

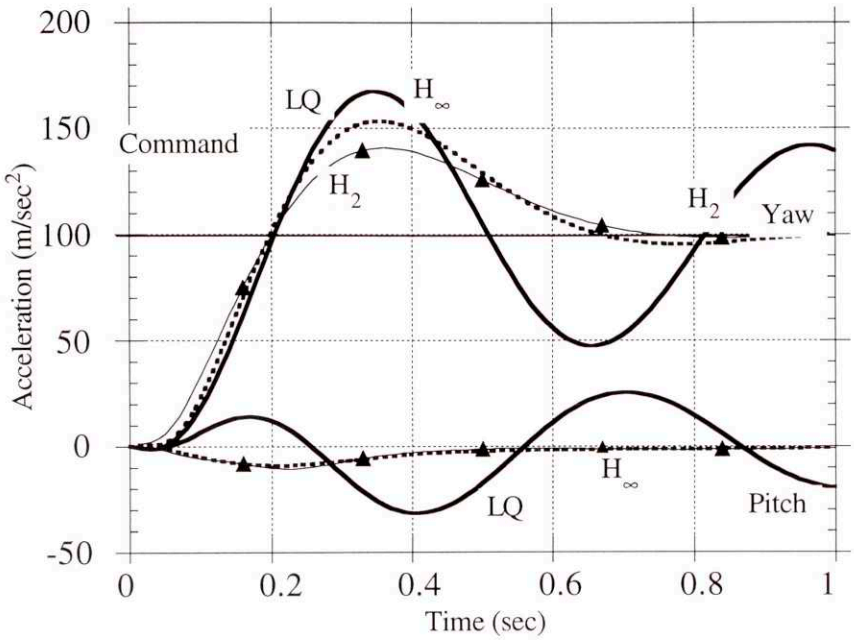

Figure 10-15 The Comparison of Acceleration Histories for a Yaw Step 11.25° Wind Angle

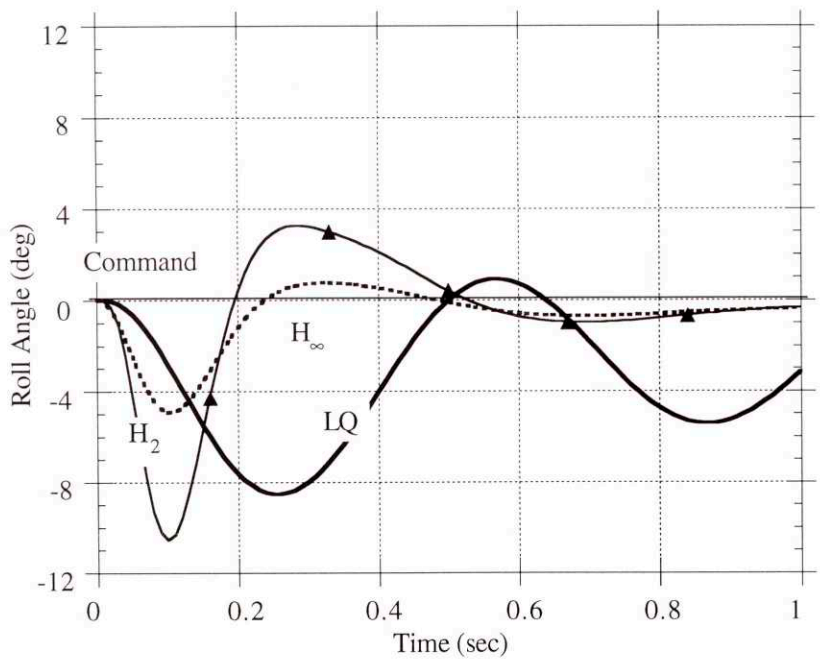

Figure 10-16 The Comparison of Roll Angle Histories for a Yaw Step 11.25° Wind Angle

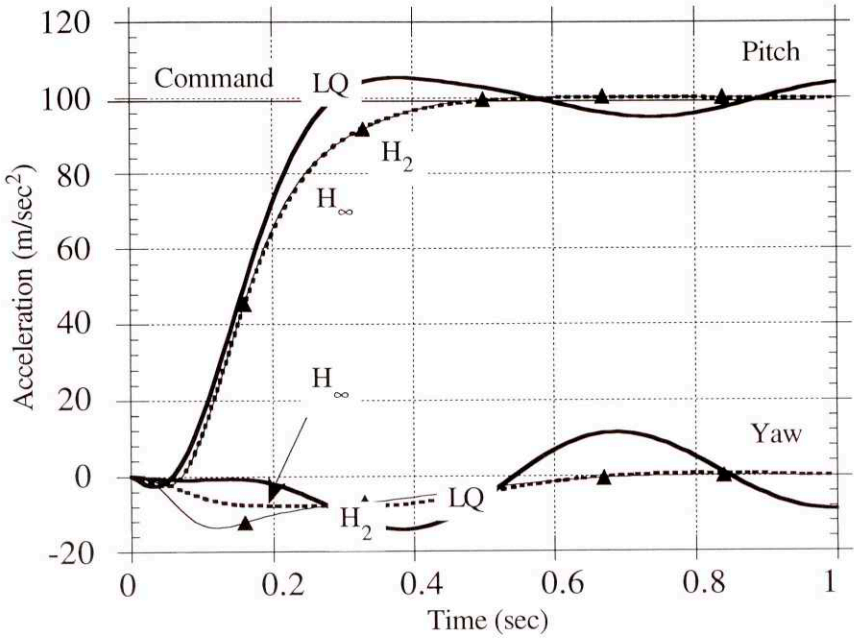

Figure 10-17 The Comparison of Acceleration Histories for a Pitch Step 11.25° Wind Angle

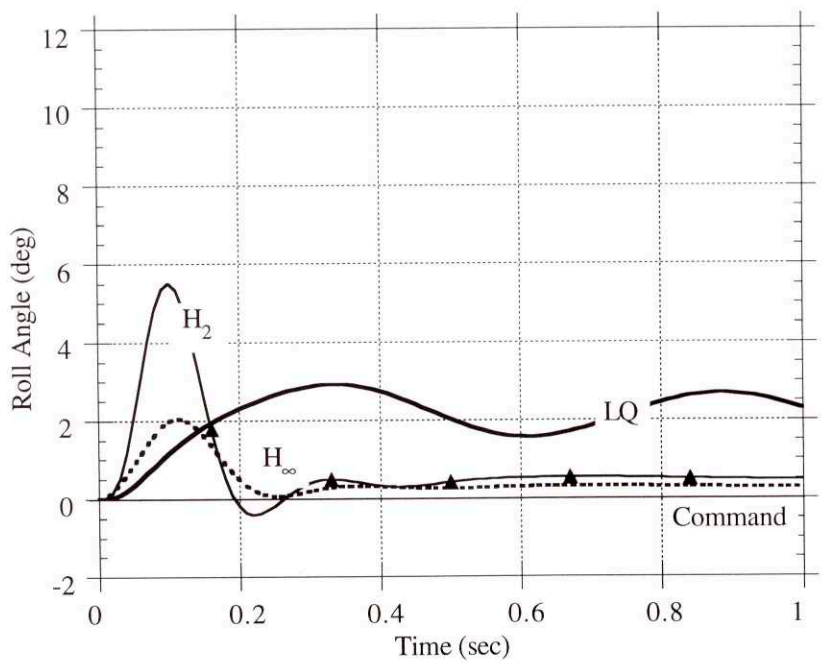

Figure 10-18 The Comparison of Roll Angle Histories for a Pitch Step 11.25° Wind Angle

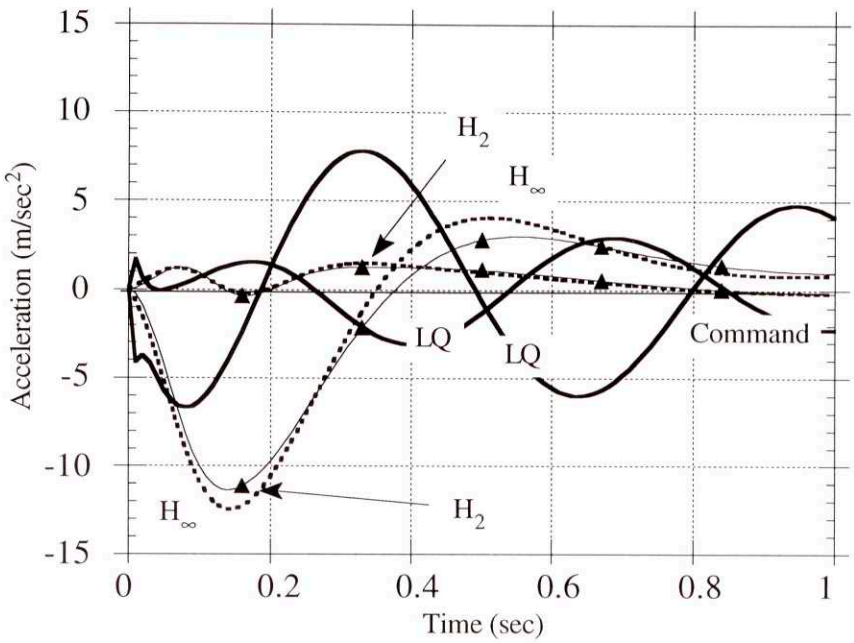

Figure 10-19 The Comparison of Acceleration Histories for a Roll Angle Step 11.25° Wind Angle

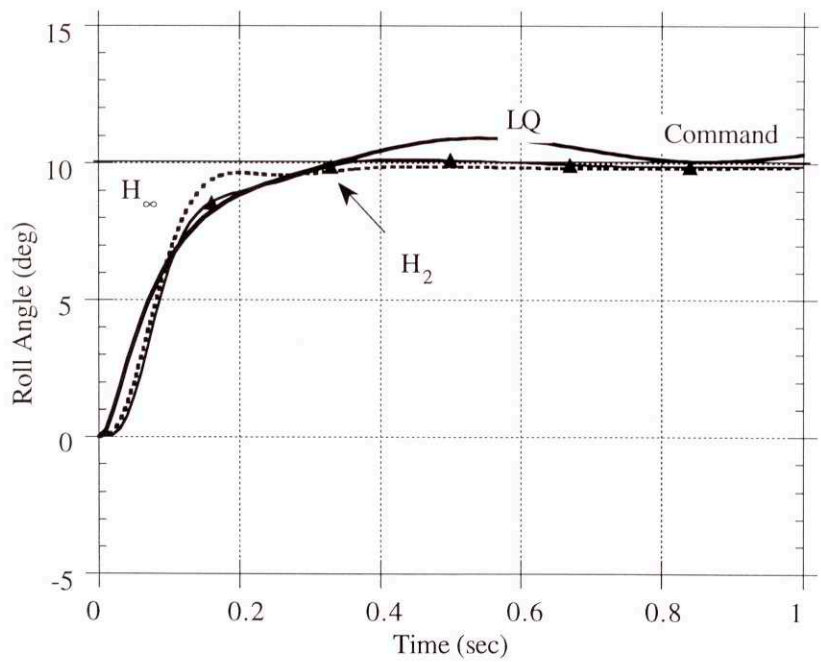

Figure 10-20 The Comparison of Roll Angle Histories for a Roll Angle Step 11.25° Wind Angle

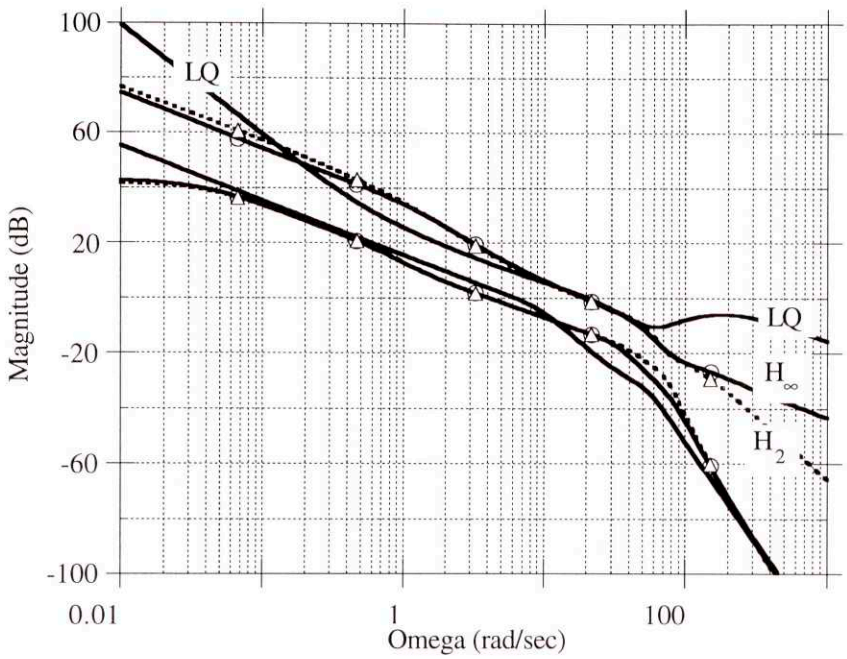

Figure 10-21 Singular Values of the Loop Transfer Function - 11.25° Wind Angle

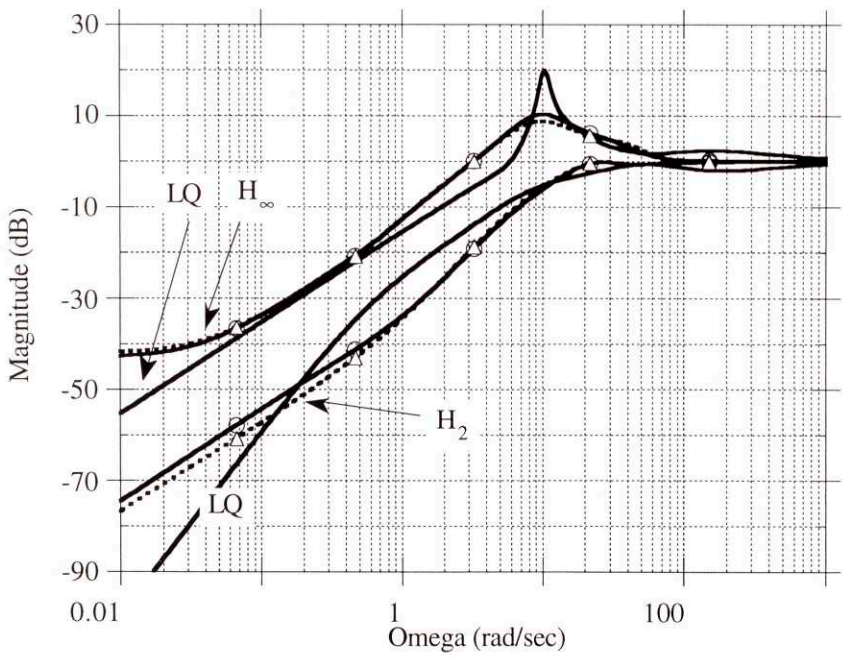

Figure 10-22 Singular Values of the Sensitivity Transfer Function - 11.25° Wind Angle

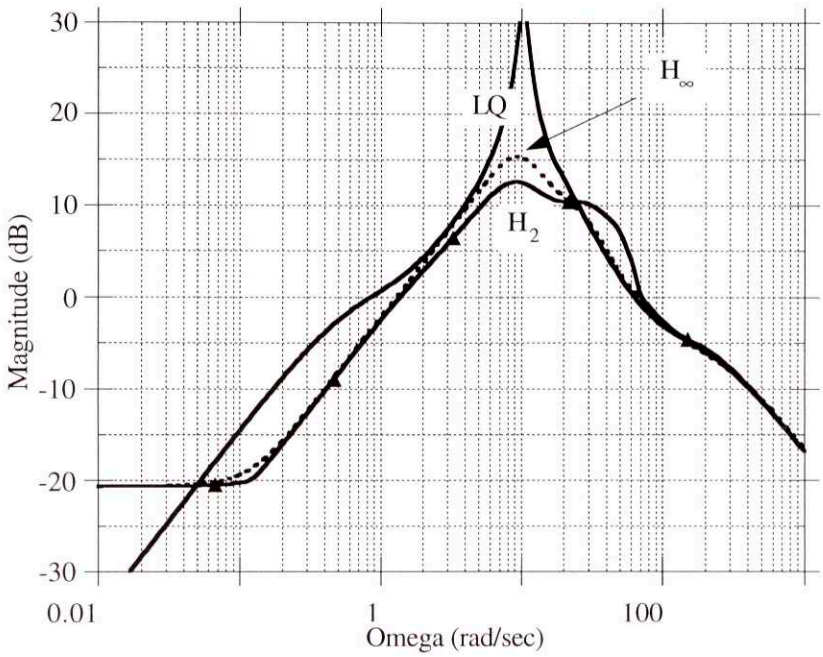

Figure 10-23 Maximum Singular Value Perturbations to Controlled Output 11.25° Wind Angle

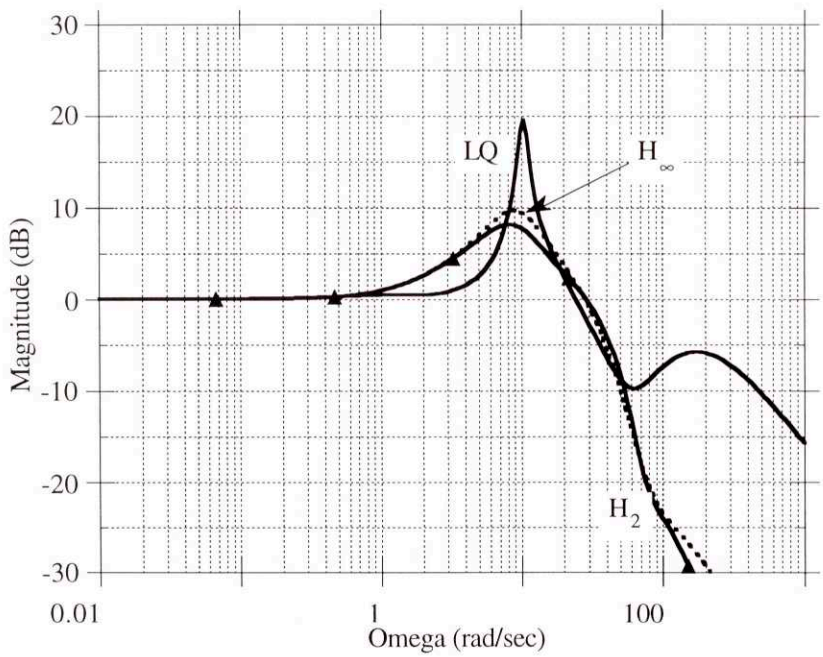

Figure 10-24 Maximum Singular Value Commands to Controlled Output 11.25° Wind Angle

10.2.2 Wind Angles of 45°

When the systems were connected to airframes linearized about a wind angle of 45° the responses changed to those shown in figures and summarized in Tables 10-7 and 10-8. The time domain performances are high lighted in Figures 10-25 to 10-30. The maximum and minimum singular values of the loop transfer function are shown in Figure 10-31. Figure 10-32 shows the sensitivity plot, and 10-33 shows how perturbations may be reflected at the controlled output. The maximum singular value of the complementary sensitivity function is shown in Figure 10-34.

	LQ			H_∞			H_2		
	Yaw	Pitch	Roll	Yaw	Pitch	Roll	Yaw	Pitch	Roll
Crossover Frequency (rad/sec)	30	33	55.5	29.1	32.4	60.9	30.3	32.5	60.2
63% Rise time (sec)	0.19	0.21	0.097	0.18	0.23	0.097	0.18	0.23	0.10
Overshoot (%)	8.3	1.7	6.9	3.8	2.2	-1.4	3.4	2.8	-0.7

Table 10-7 Autopilot Performance Results Comparison 45° Wind Angle

	LQ		H_∞		H_2	
	Gain Margin (dB)	Phase Margin (deg)	Gain Margin (dB)	Phase Margin (deg)	Gain Margin (dB)	Phase Margin (deg)
Roll	∞	86	∞	62	23.3	34
Yaw	∞	83.2	∞	41	23.2	57
Pitch	-37, -33, ∞	112	∞	72	-33, 28	38

Table 10-8 Autopilot Bode Stability Margin Comparison 45° Wind Angle

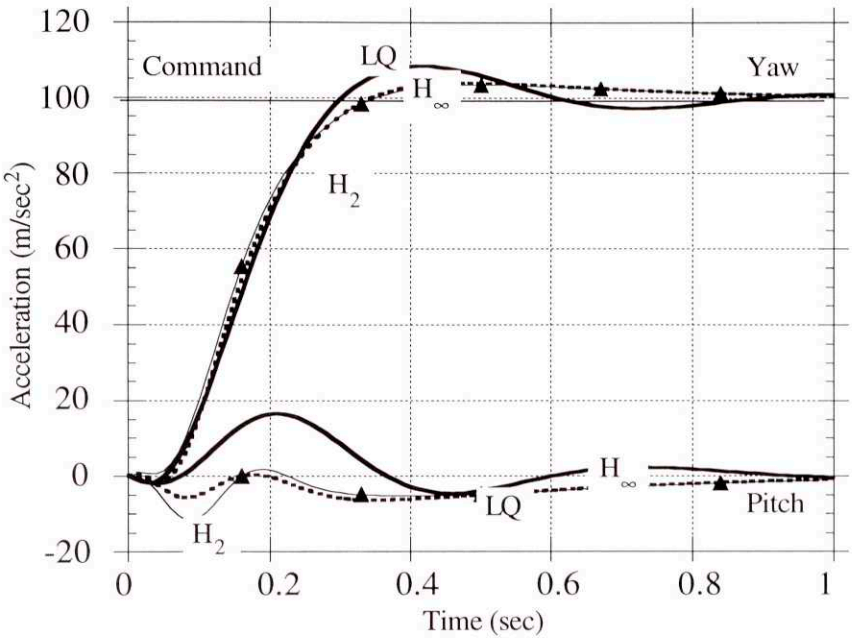

Figure 10-25 The Comparison of Acceleration Histories for a Yaw Step 45° Wind Angle

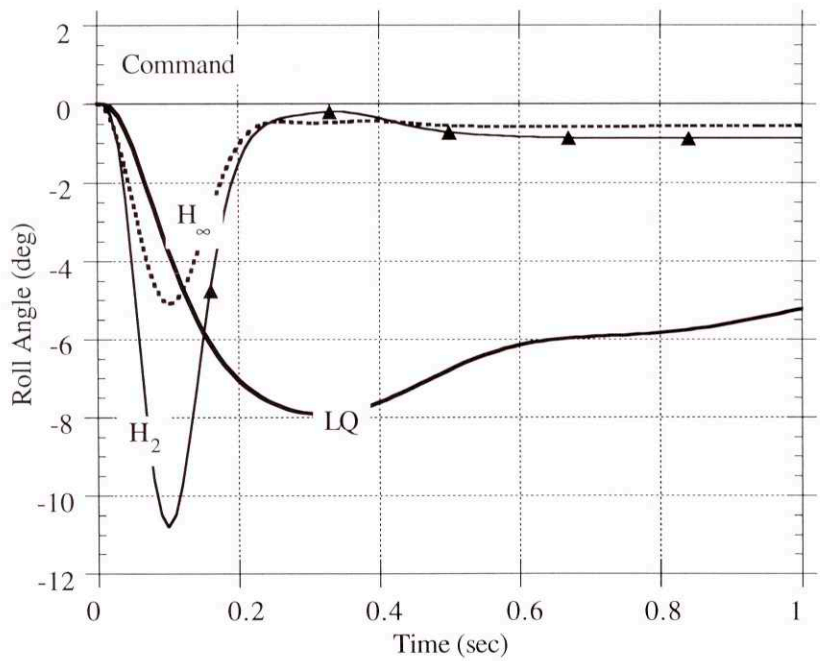

Figure 10-26 The Comparison of Roll Angle Histories for a Yaw Step 45° Wind Angle

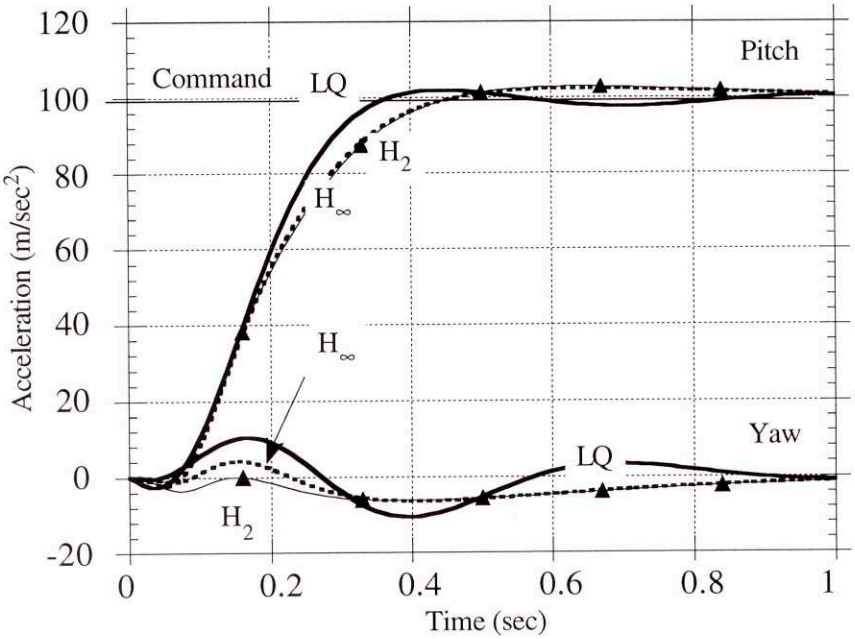

Figure 10-27 The Comparison of Acceleration Histories for a Pitch Step 45° Wind Angle

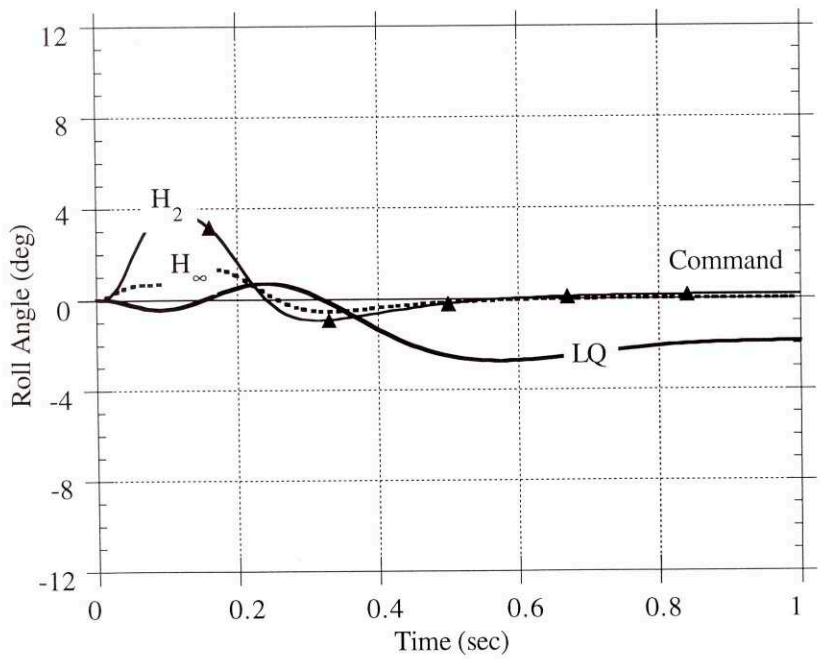

Figure 10-28 The Comparison of Roll Angle Histories for a Pitch Step 45° Wind Angle

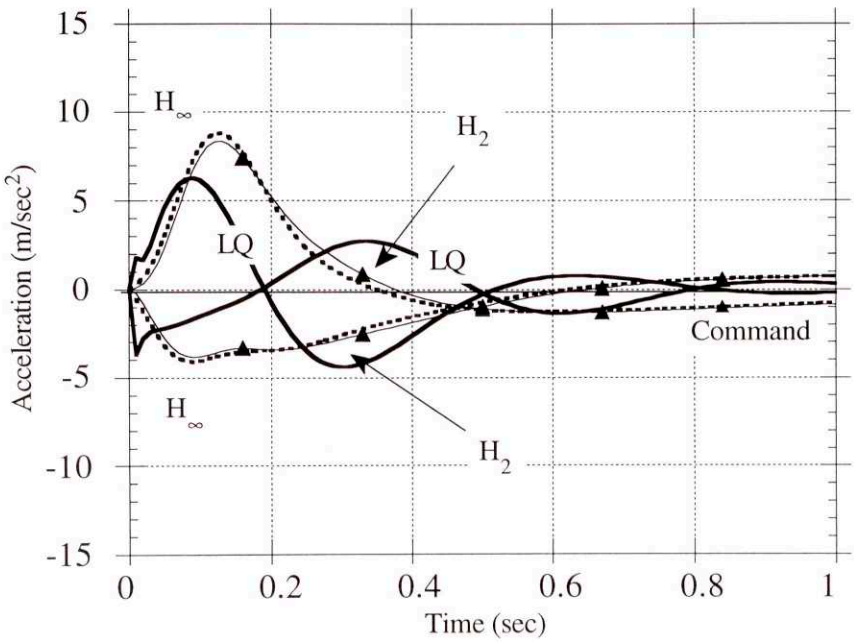

Figure 10-29 The Comparison of Acceleration Histories for a Roll Angle Step 45° Wind Angle

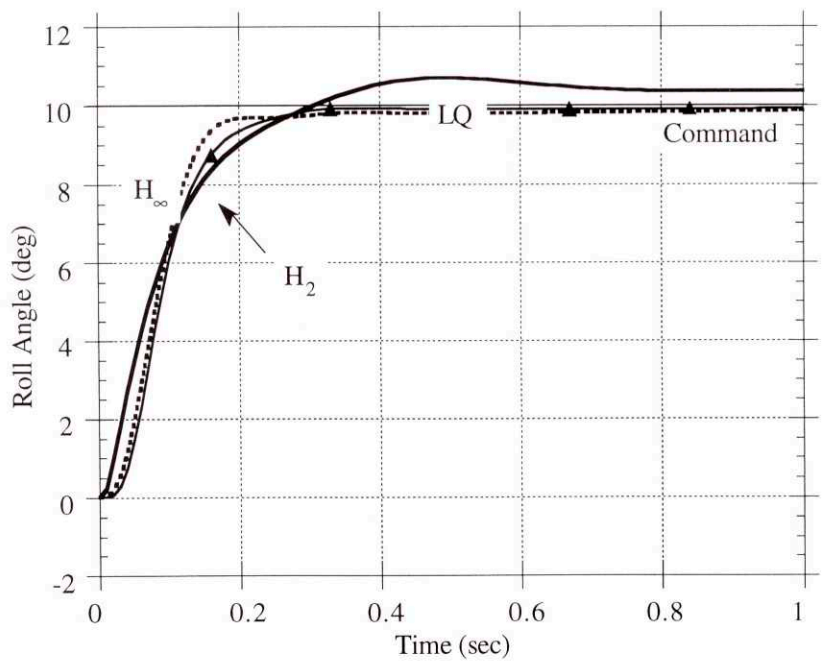

Figure 10-30 The Comparison of Roll Angle Histories for a Roll Angle Step 45° Wind Angle

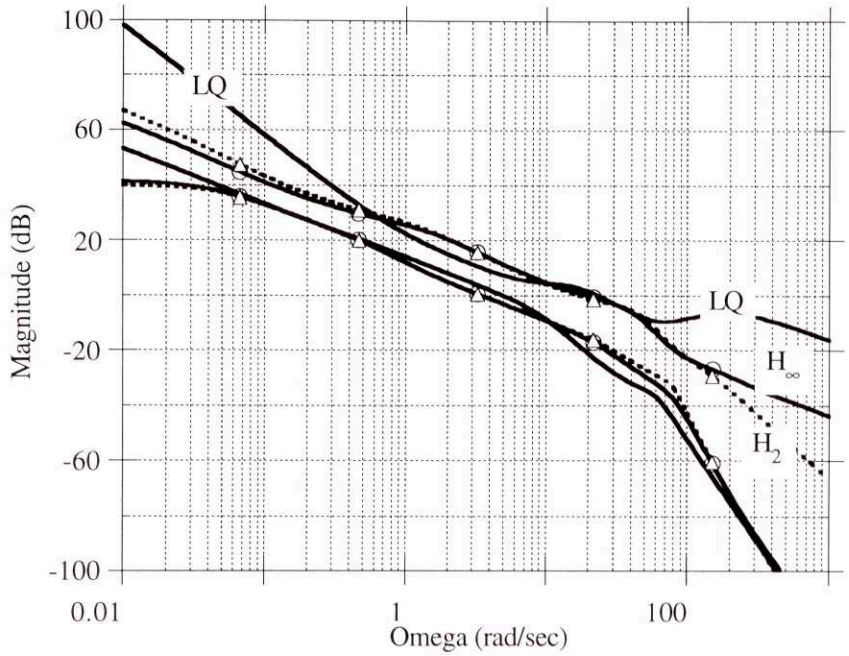

Figure 10-31 Loop Transfer Function Singular Values 45° Wind Angle

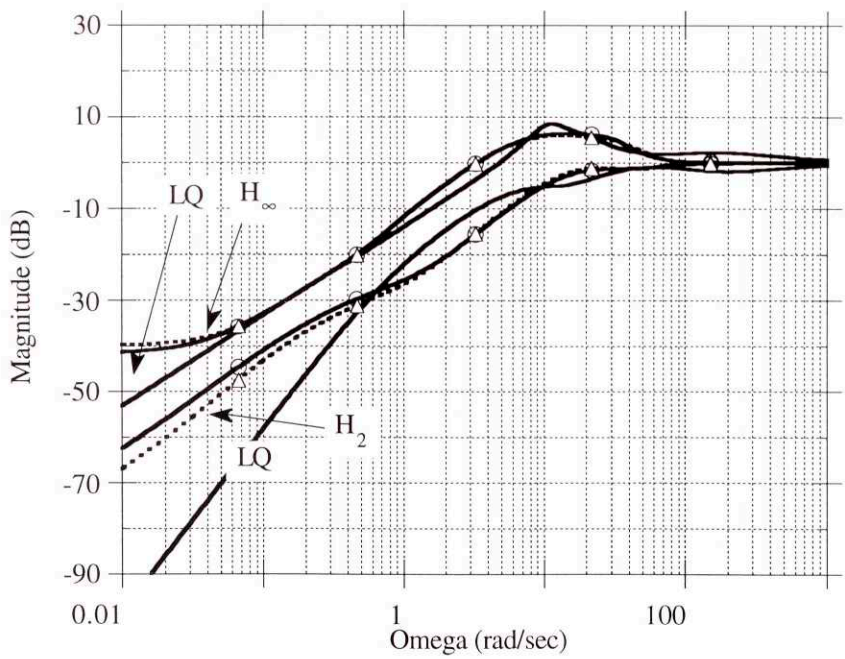

Figure 10-32 Singular Values of the Sensitivity Transfer Function 45° Wind Angle

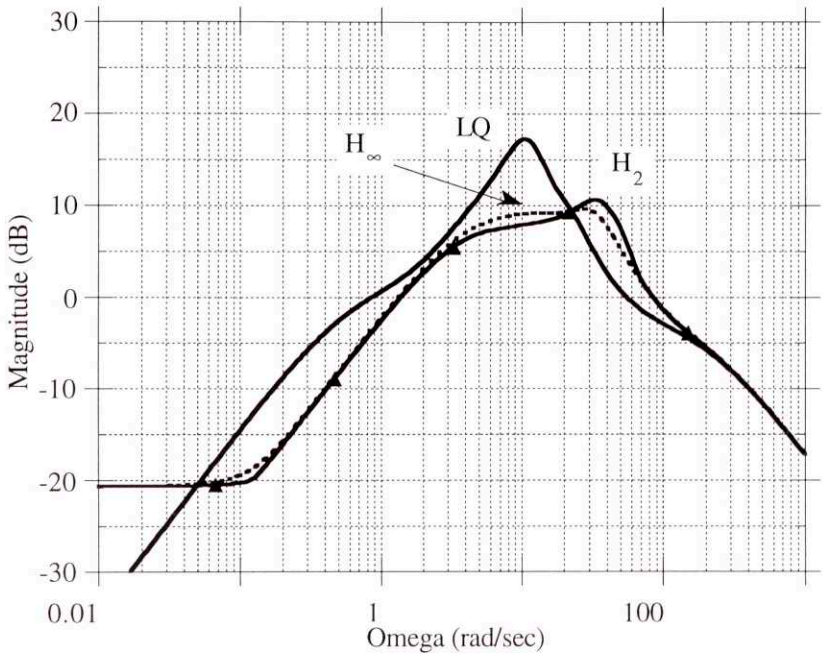

Figure 10-33 Maximum Singular Value Perturbations to Controlled Output 45° Wind Angle

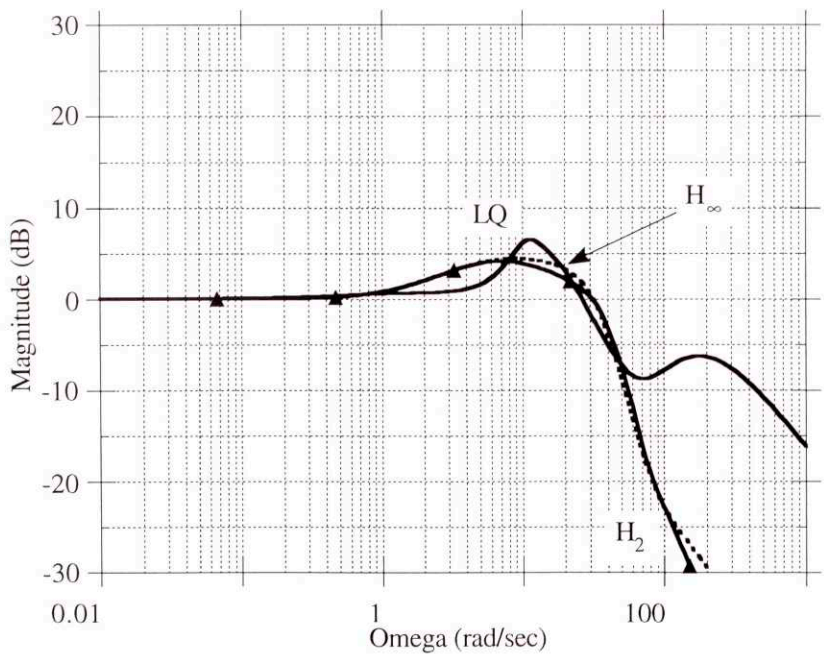

Figure 10-34 Maximum Singular Value Commands to Controlled Output 45° Wind Angle

10.2.3 Conclusions

All three autopilots can handle these changes in wind angle and still remain stable. The LQ design shows changes comparable to the H_∞ and H_2 designs in the Bode crossover frequencies, and its risetime performance is slightly slower than theirs for the 11.25° flight condition for a yaw step. All three designs showed excessive overshoot in the step responses for the 11.25° condition. The overshoot in the LQ design was the worst. All three designs suffered significant single loop stability margin degradation at the 11.25° flight condition, particularly in terms of the low frequency gain reduction. The single loop gain margins of the LQ design are the worst, but its phase margins are the best. The H_2 design's single loop gain and phase margins changed the least. At the 45° condition the LQ design shows the most overshoot and the best single loop stability margins. The roll channel crossover frequency changed the most for the LQ design. The H_2 design continues to exhibit the largest cross channel motion in the roll channel.

Chapter 11 Simultaneous Variations

During a missile engagement it is an unreasonable assumption to assume that only one of the four parameters investigated in sections 6.1 to 6.4 will be in error at a time. In reality all of the estimates of the operational parameters will be in error. However an IMU should provide estimates that are at least as good as ± 10% in altitude, ± 10% in missile speed and ± 5° in missile total angle of attack. To evaluate the performance changes of the three designs, linearized airframes were generated for simultaneous variations in these parameters. Two comparisons are shown, decreasing the altitude by 10%, decreasing the velocity by 10% and reducing the angle of attack to 10°, and increasing the altitude by 10%, increasing the velocity by 10% and increasing the angle of attack to 20°. A wind angle of 22.5° was used for both analyses.

The autopilots developed in section 4 were then connected to the perturbed airframes to form a closed loop system and their performances were evaluated.

11.1 Decreases in Missile Parameters

When the systems were connected to airframes linearized about an altitude decreased by 10%, velocity decreased by 10% and the angle of attack decreased by 5° than the design point the open loop poles and the zeros from the commands to the controlled outputs changed to the values shown in Table 11-1. As can be seen in the table or in Figure 11-1 or Figure 11-2 this point possesses an lightly damped unstable pole pair at approximately 8.5 radians per second.

Airframe Poles

Real	Imag	Freq.	Damp
0	0.0	0	
-0.5667	0.0	0.5667	
0.8514	-8.483	8.526	
0.8514	8.483	8.526	-0.09986
-1.721	-8.453	8.626	
-1.721	8.453	8.626	0.1995
-200	0.0	200	
-200	0.0	200	
-200	0.0	200	

Airframe Zeros

Real	Imag	Freq.	Damp
-36.76	0.0	36.76	
-31.14	0.0	31.14	
30.62	0.0	30.62	
36.47	0.0	36.47	

Table 11-1 Open Loop Perturbed Airframe Poles and Zeros (All Flight Parameters Decreased)

The closed loop performance changed to those shown in Figures 11-3 through 11-8 and summarized in Tables 11-2 and 11-3. The loop transfer function is shown in Figure 11-9, the sensitivity function is shown in Figure 11-10. The perturbations to the plant output is shown in Figure 11-11 and the commands to the controlled outputs transfer function is shown in Figure 11-12.

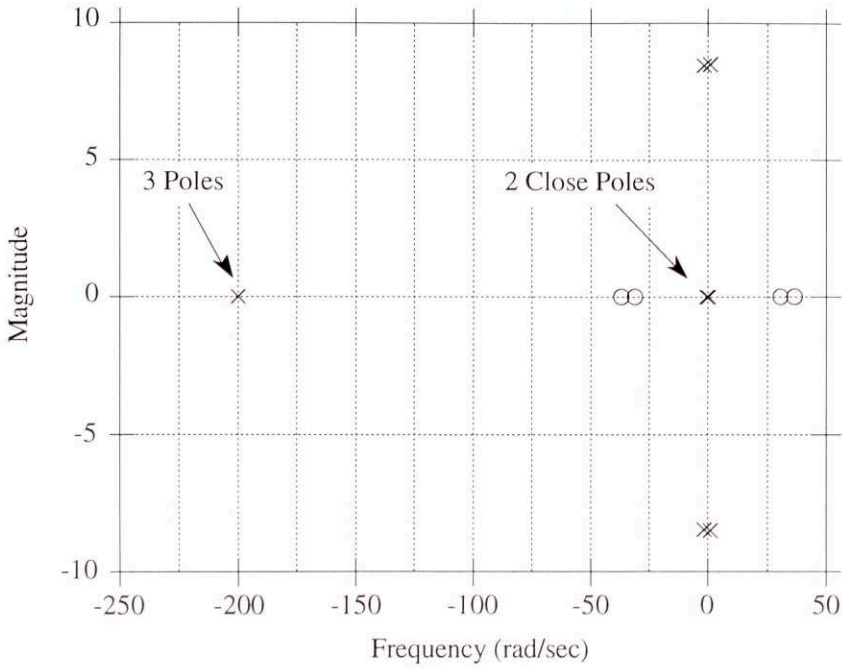

Figure 11-1 Pole Zero Plot of the Perturbed System (All Flight Parameters Decreased)

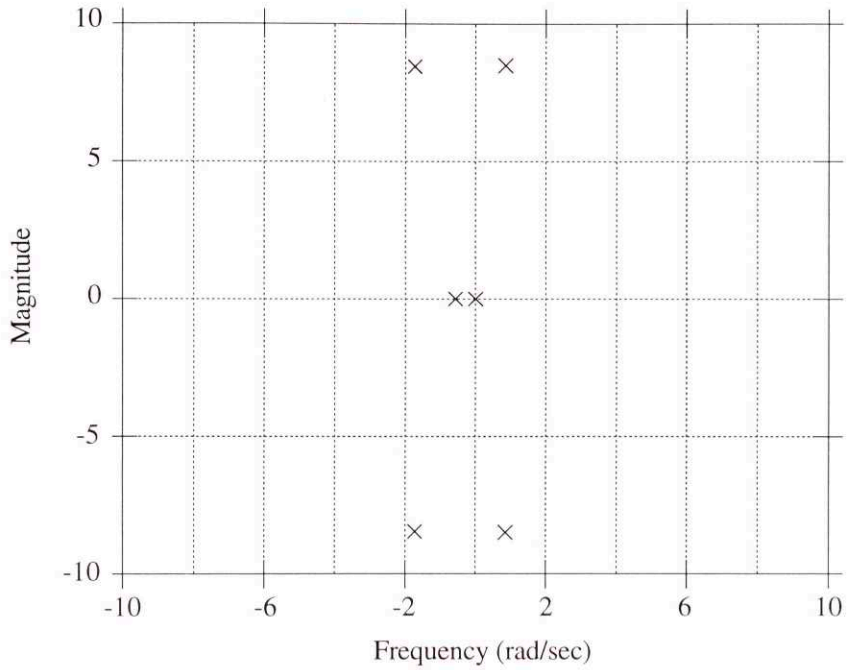

Figure 11-2 Close-up of the Pole Zero Plot of the Perturbed System (All Flight Parameters Decreased)

	LQ			H_∞			H_2		
	Yaw	Pitch	Roll	Yaw	Pitch	Roll	Yaw	Pitch	Roll
Crossover Frequency (rad/sec)	27.6	29.4	69.8	28.3	31.1	57.0	28.6	30.3	57.7
63% Rise time (sec)	0.19	0.18	0.10	0.18	0.19	0.099	0.18	0.18	0.11
Overshoot (%)	7.6	7.5	4.7	11.4	17.6	4.22	11.1	17.5	3.6

Table 11-2 Autopilot Performance Results (All Flight Parameters Decreased)

	LQ		H_∞		H_2	
	Gain Margin (dB)	Phase Margin (deg)	Gain Margin (dB)	Phase Margin (deg)	Gain Margin (dB)	Phase Margin (deg)
Roll	∞	86	∞	61	-46, 23	31
Yaw	∞	65	∞	45	22	37
Pitch	∞	77	-28, ∞	29	-23, 28	24

Table 11-3 Autopilot Bode Stability Margin Comparison (All Flight Parameters Decreased)

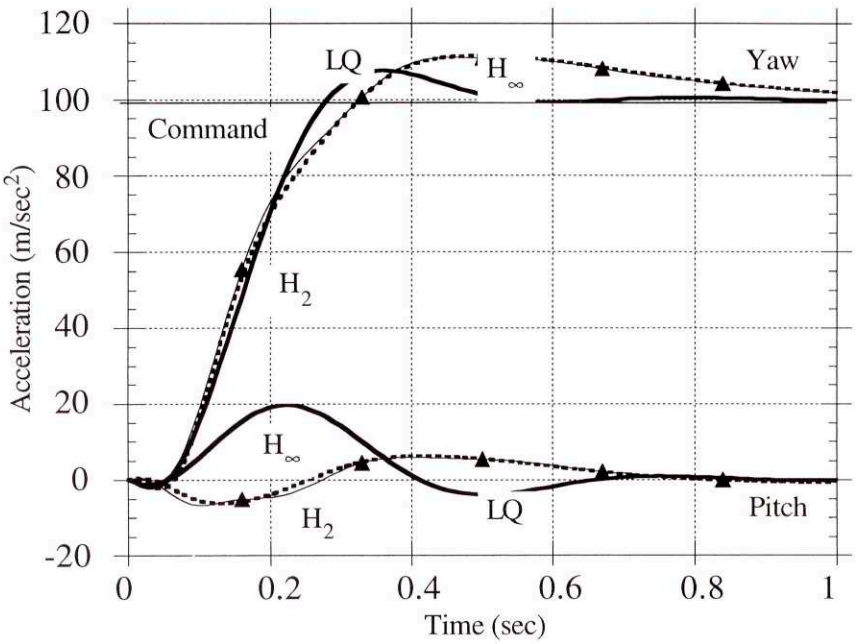

Figure 11-3 The Comparison of Acceleration Histories for a Yaw Step (All Flight Parameters Decreased)

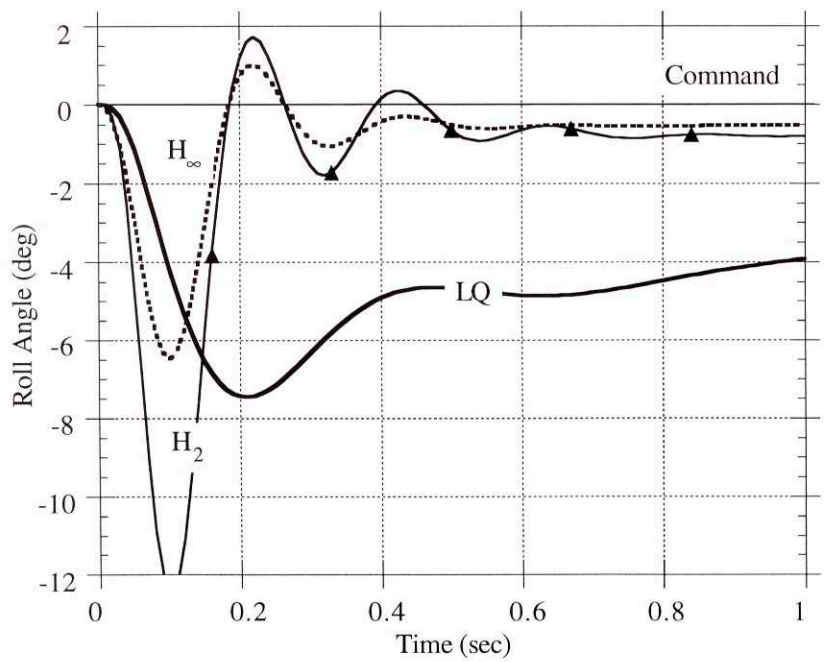

Figure 11-4 The Comparison of Roll Angle Histories for a Yaw Step (All Flight Parameters Decreased)

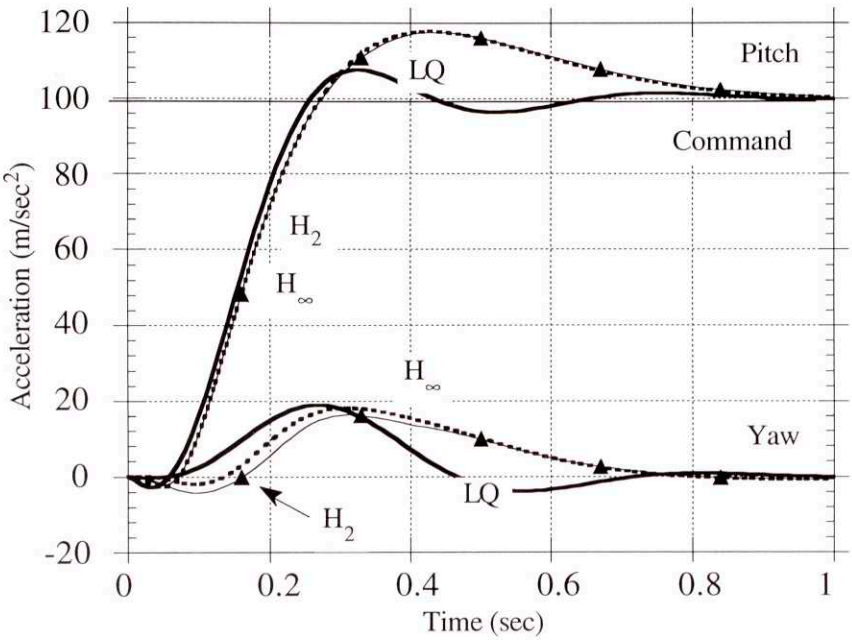

Figure 11-5 The Comparison of Acceleration Histories for a Pitch Step (All Flight Parameters Decreased)

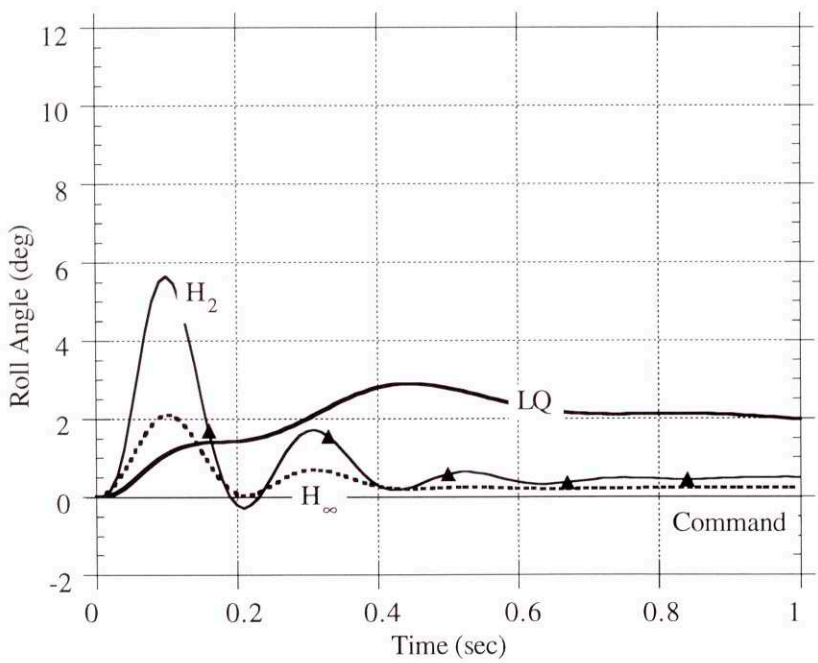

Figure 11-6 The Comparison of Roll Angle Histories for a Pitch Step (All Flight Parameters Decreased)

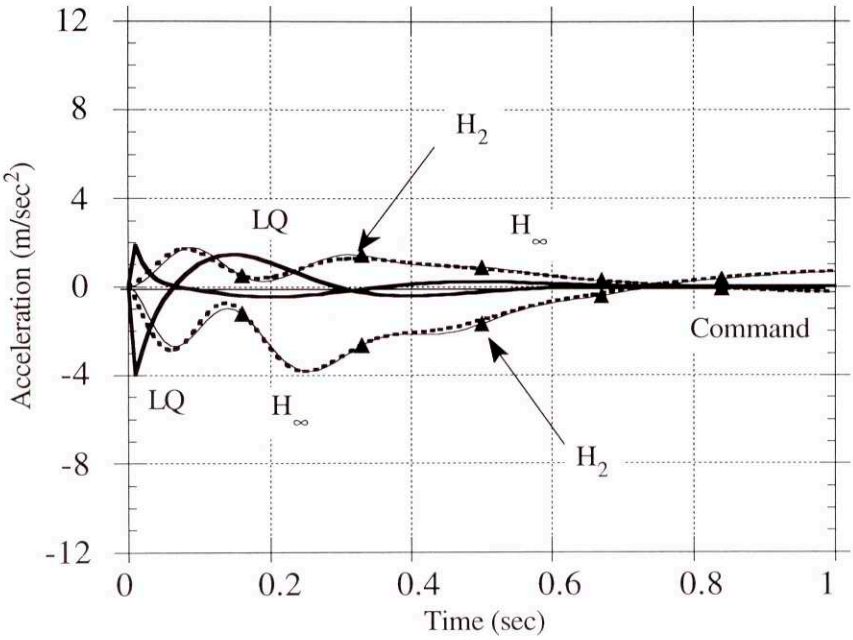

Figure 11-7 The Comparison of Acceleration Histories for a Roll Angle Step (All Flight Parameters Decreased)

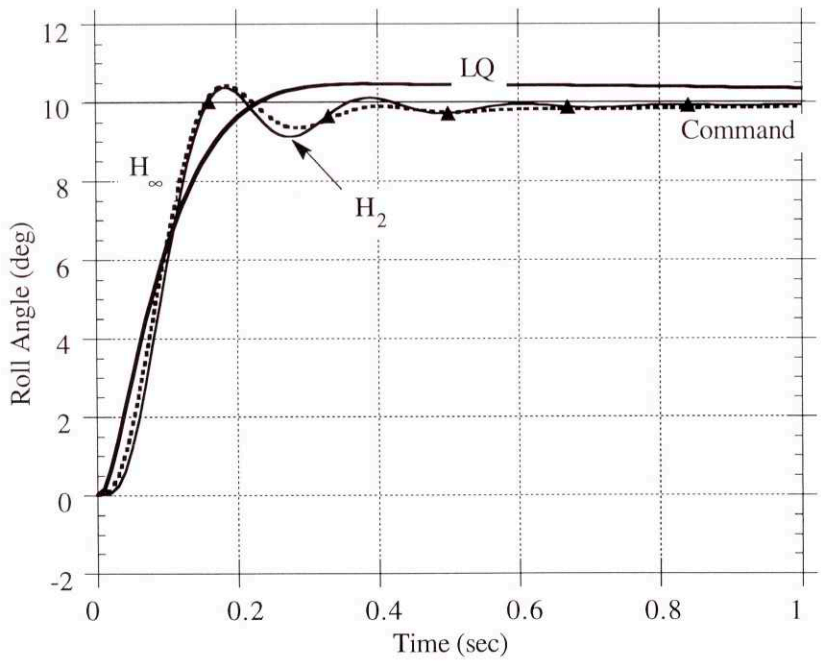

Figure 11-8 The Comparison of Roll Angle Histories for a Roll Angle Step (All Flight Parameters Decreased)

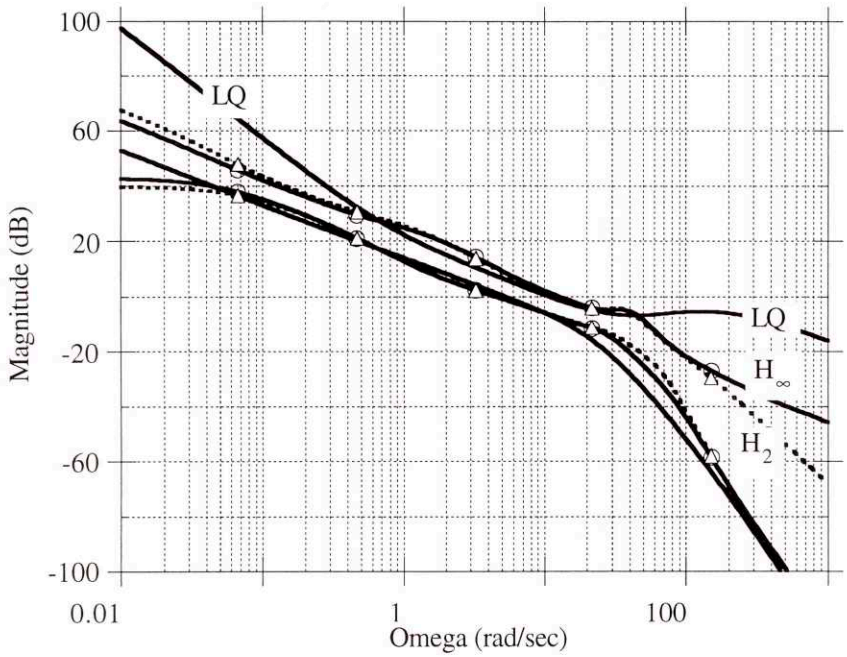

Figure 11-9 Loop Transfer Function (All Flight Parameters Decreased)

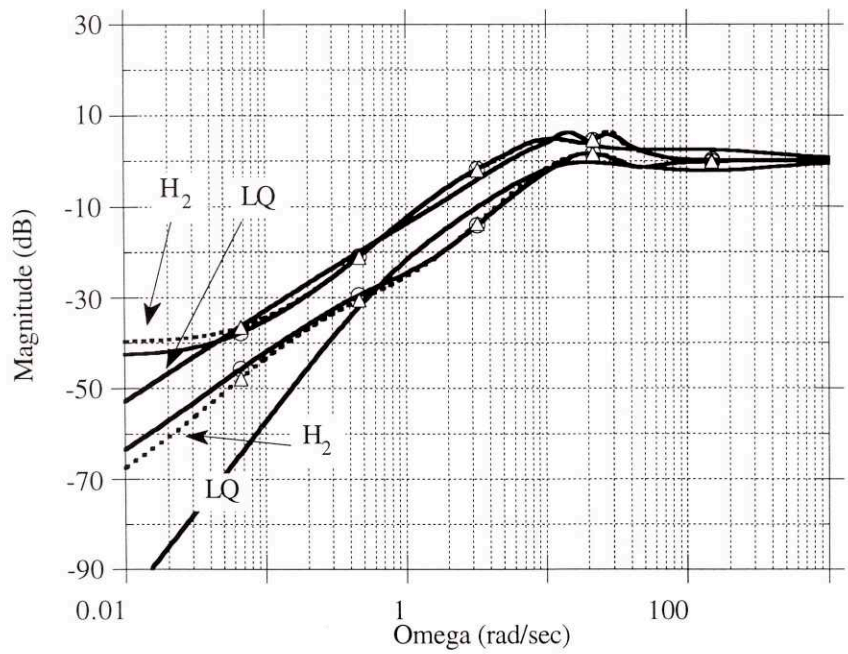

Figure 11-10 Singular Values of the Sensitivity Transfer Function (All Flight Parameters Decreased)

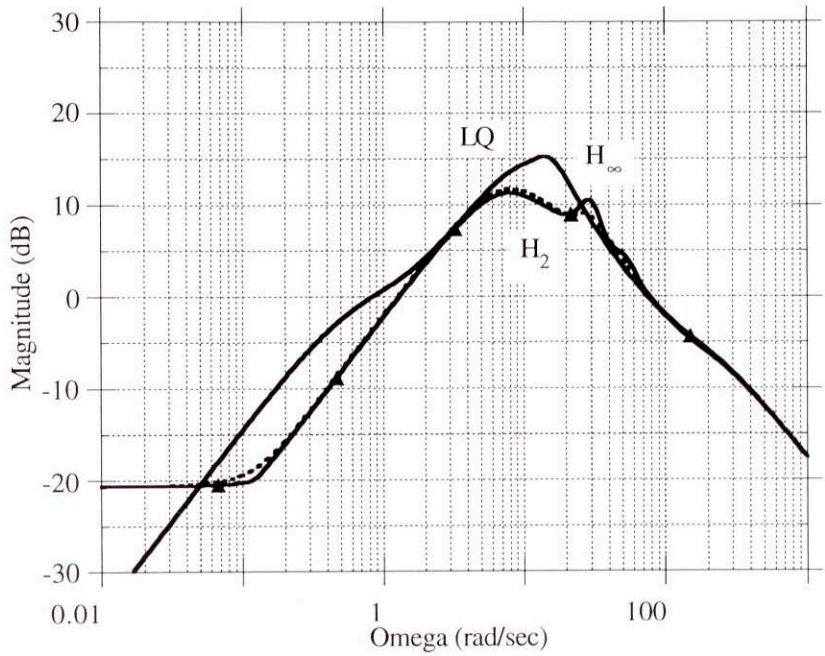

Figure 11-11 Maximum Singular Value Perturbations to Controlled Output Decrease Flight Parameters

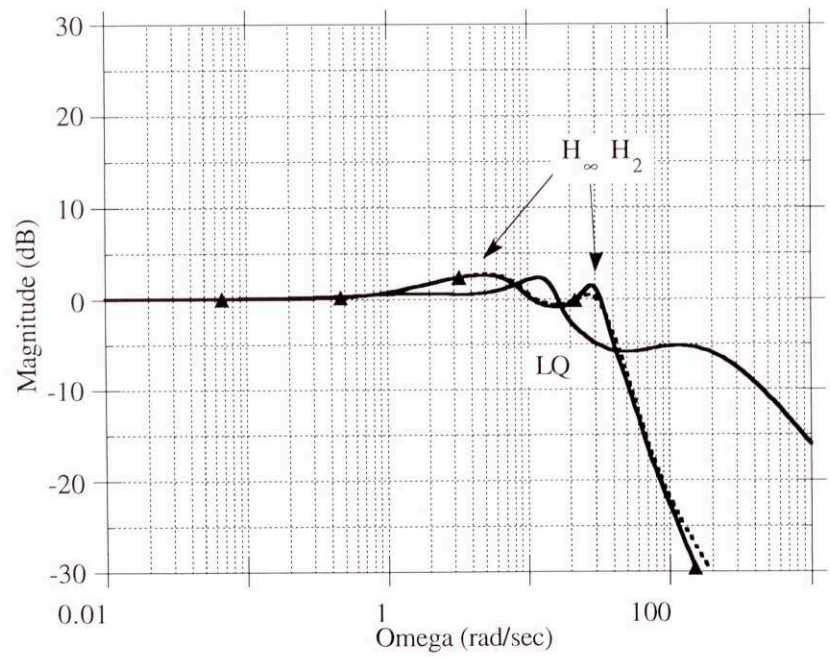

Figure 11-12 Maximum Singular Value Commands to Controlled Output (All Flight Parameters Decreased)

11.1.1 Conclusions

All three autopilots can handle this simultaneous decrease in altitude, speed and angle of attack. This change in the flight condition results in more overshoot in all three controllers and some degradation of the Bode single loop margins. The responses of the LQ design are the best and the LQ does not show as much loss of damping in the roll channel as do the other designs. The LQ continues to have the best Bode margins and the H_2 the worst.

11.2 Increases in Missile Parameters

When the systems were connected to airframes linearized about an altitude increased by 10%, velocity increased by 10% and the angle of attack increased by 5° than the design point the open loop poles and the zeros from the commands to the controlled outputs changed to the values shown in Table 11-4. As can be seen in the table or in Figure 11-13 or Figure 11-14 this point possesses an unstable pole at approximately 10 radians per second.

Airframe Poles

Real	Imag	Freq.	Damp
0	0.0	0	
-0.9846	0.0	0.9846	
-0.3903	-9.634	9.642	
-0.3903	9.634	9.642	0.04048
-10.13	0.0	10.13	
10.14	0.0	10.14	
-200	0.0	200	
-200	0.0	200	
-200	0.0	200	

Airframe Zeros

Real	Imag	Freq.	Damp
-39.44	0.0	39.44	
-32.13	0.0	32.13	
31.94	0.0	31.94	
39.38	0.0	39.38	

Table 11-4 Open Loop Perturbed Airframe Poles and Zeros (Increase All Flight Parameters

The closed loop performance changed to those shown in Figures 11-15 through 11-20 and summarized in Tables 11-5 and 11-6. The loop transfer function is shown in Figure 11-21, the sensitivity function is shown in Figure 11-22. The perturbations to the plant output is shown in Figure 11-23 and the commands to the controlled outputs transfer function is shown in Figure 11-24.

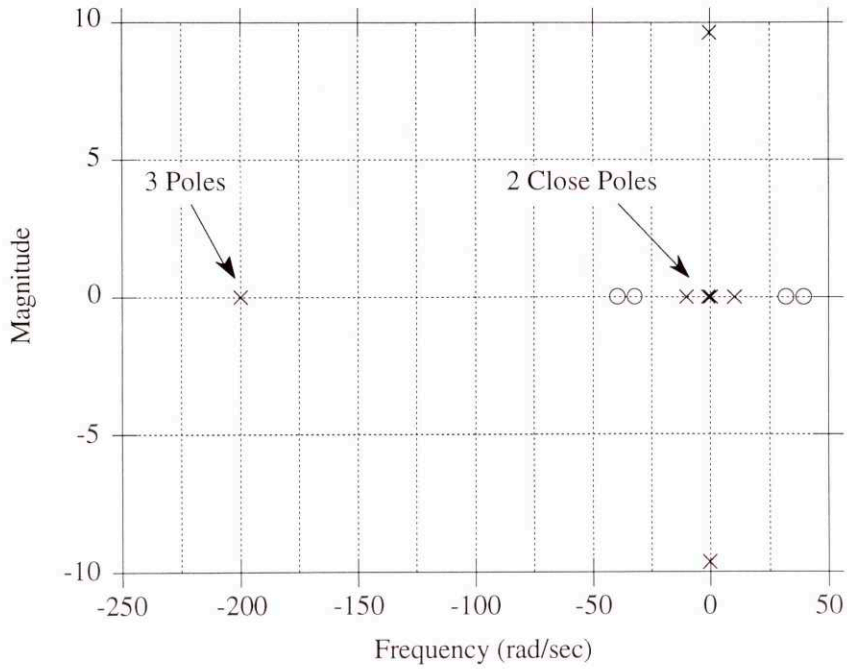

Figure 11-13 Pole Zero Plot of the Perturbed System (All Flight Parameters Increased)

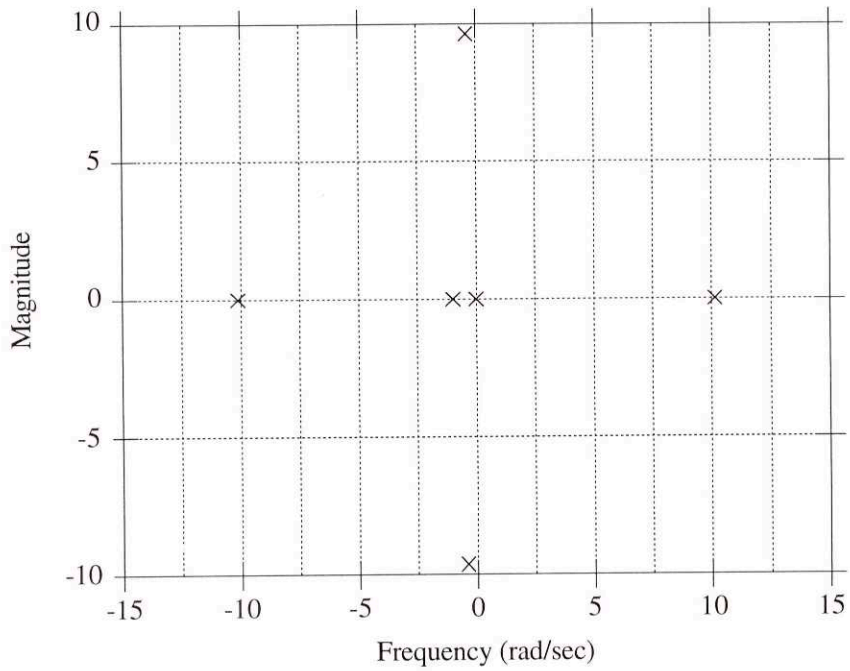

Figure 11-14 Close-up of the Pole Zero Plot of the Perturbed System (All Flight Parameters Increased)

	LQ			H_∞			H_2		
	Yaw	Pitch	Roll	Yaw	Pitch	Roll	Yaw	Pitch	Roll
Crossover Frequency (rad/sec)	29.2	29.6	58.4	30.0	32.7	65.8	30.7	33.0	65.2
63% Rise time (sec)	0.18	0.16	0.098	0.18	0.17	0.096	0.17	0.17	0.10
Overshoot (%)	7.1	17.7	5.5	5.5	15.8	-1.4	5.5	15.2	-0.9

Table 11-5 Autopilot Performance Results Comparison (All Flight Parameters Increased)

	LQ		H_∞		H_2	
	Gain Margin (dB)	Phase Margin (deg)	Gain Margin (dB)	Phase Margin (deg)	Gain Margin (dB)	Phase Margin (deg)
Roll	-15, ∞	100	∞	83	22	37
Yaw	∞	64	∞	44	21	39
Pitch	∞	103	-20, ∞	50	-18, 26	46

Table 11-6 Autopilot Bode Stability Margin Comparison (All Flight Parameters Increased)

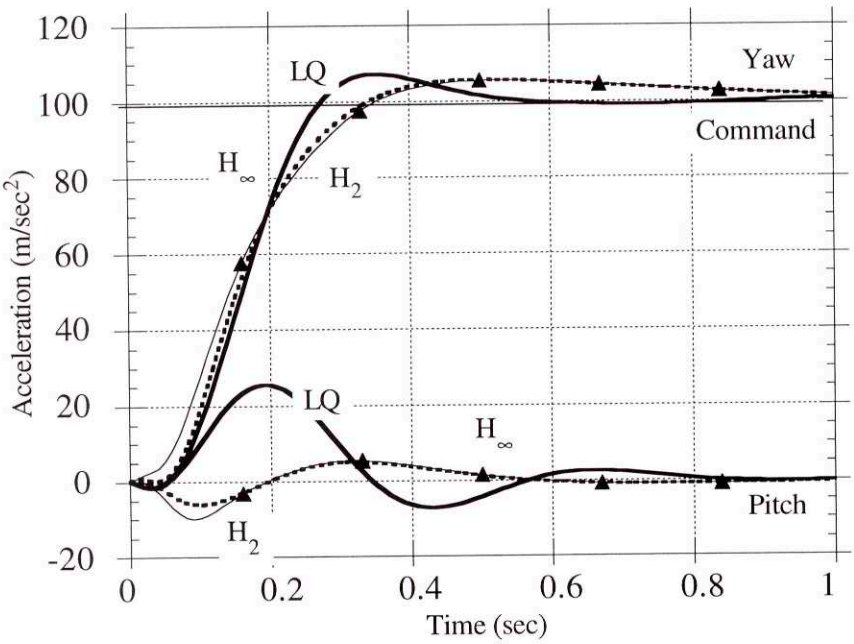

Figure 11-15 The Comparison of Acceleration Histories for a Yaw Step (All Flight Parameters Increased)

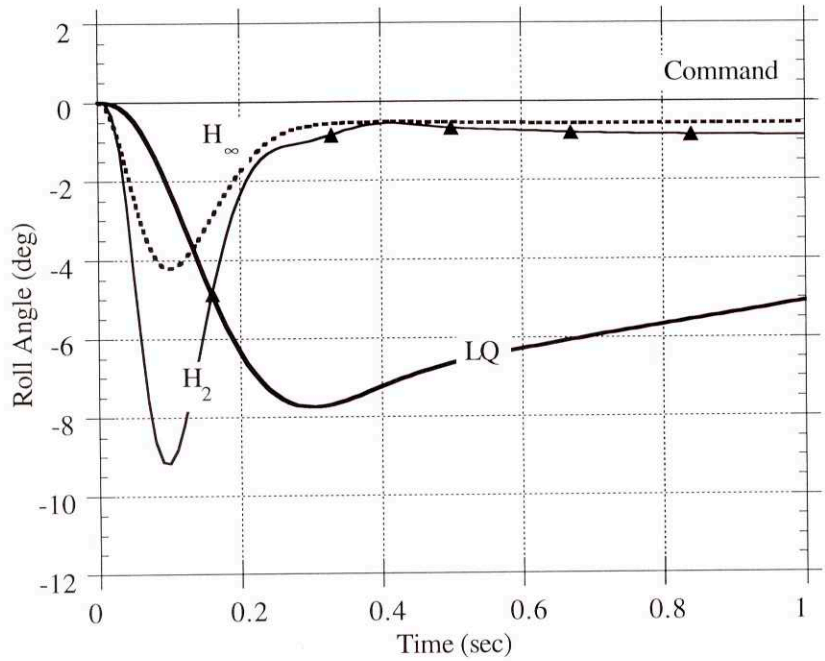

Figure 11-16 The Comparison of Roll Angle Histories for a Yaw Step (All Flight Parameters Increased)

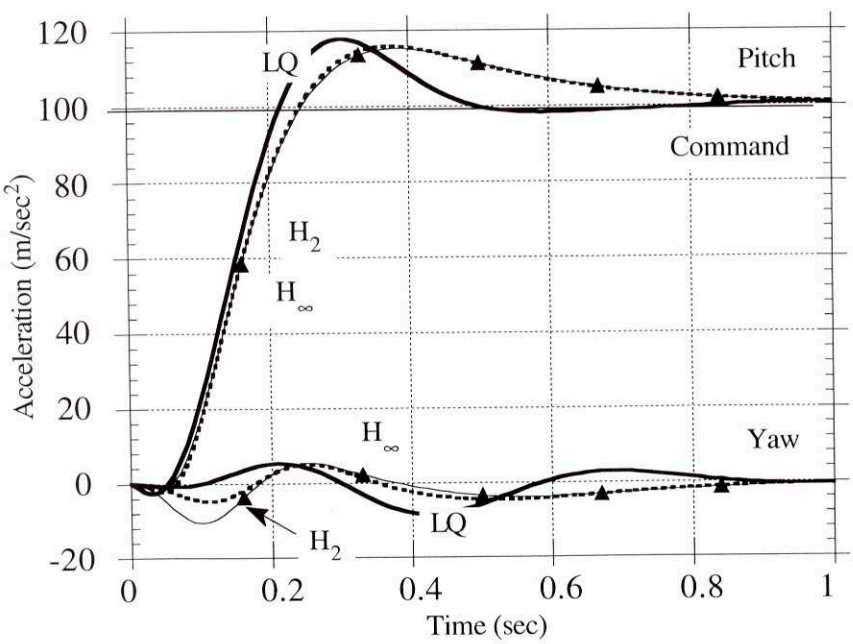

Figure 11-17 The Comparison of Acceleration Histories for a Pitch Step (All Flight Parameters Increased)

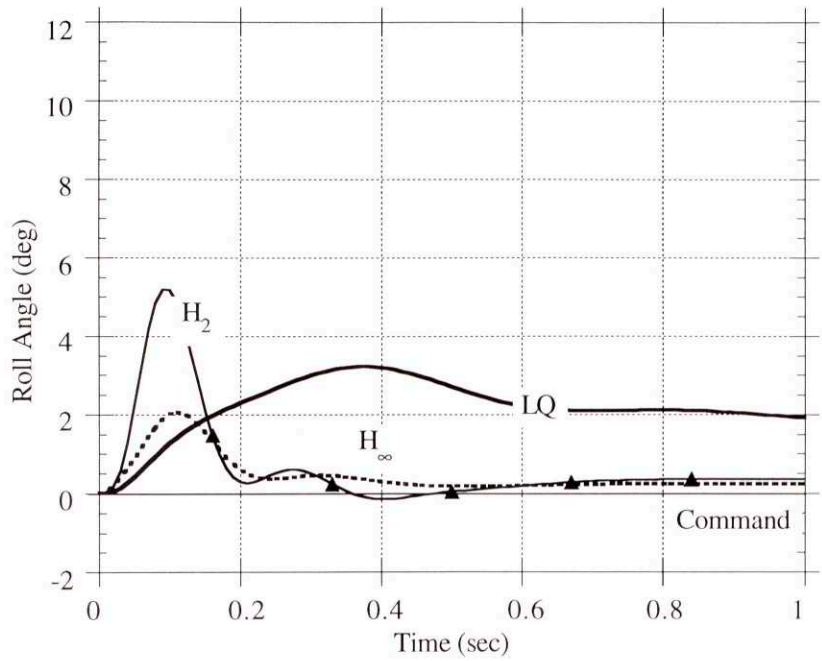

Figure 11-18 The Comparison of Roll Angle Histories for a Pitch Step (All Flight Parameters Increased)

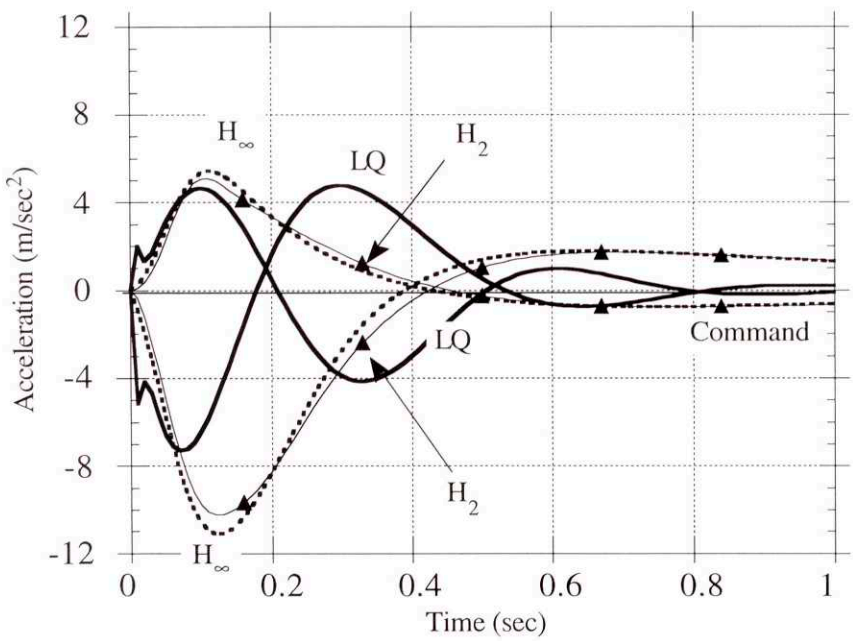

Figure 11-19 The Comparison of Acceleration Histories for a Roll Angle Step (All Flight Parameters Increased)

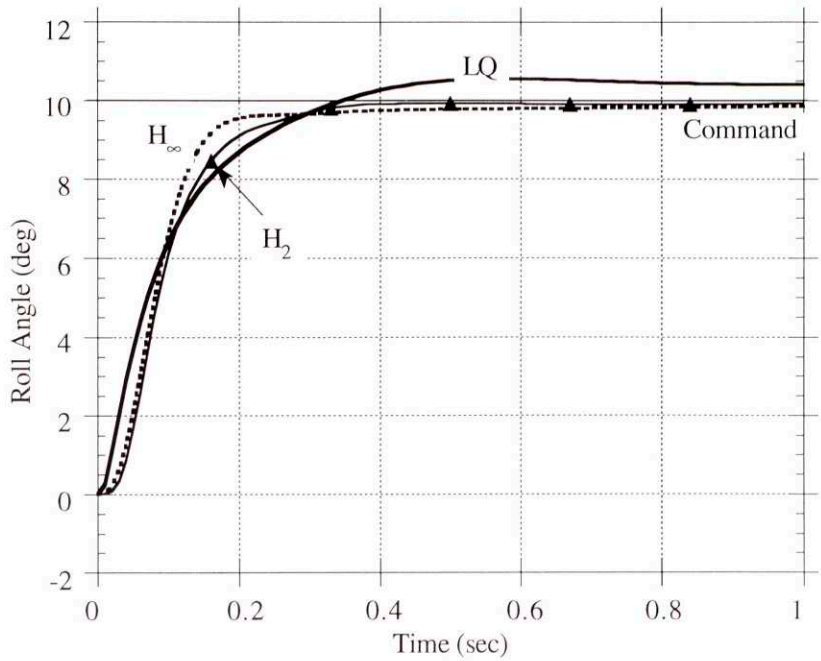

Figure 11-20 The Comparison of Roll Angle Histories for a Roll Angle Step (All Flight Parameters Increased)

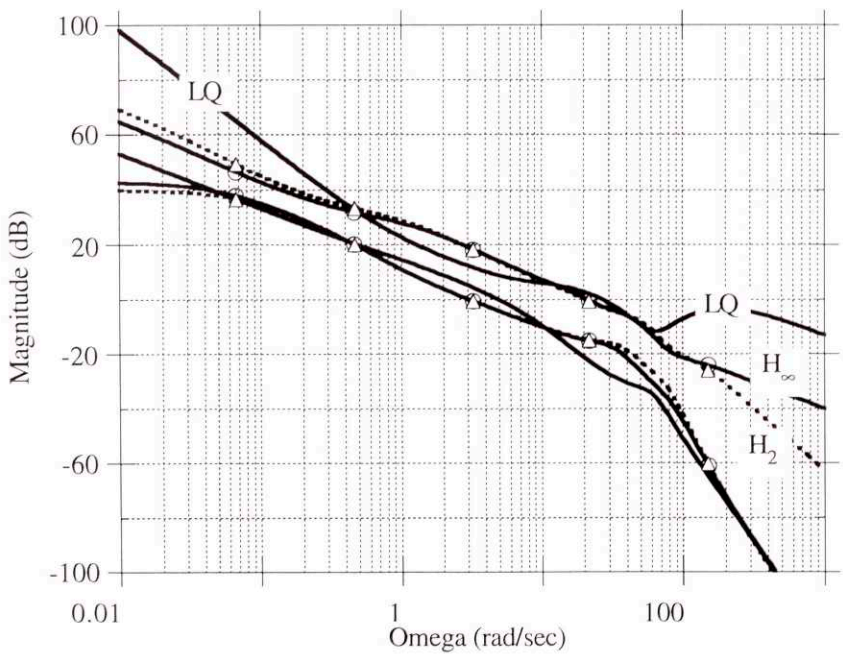

Figure 11-21 Loop Transfer Function Singular Values (All Flight Parameters Increased)

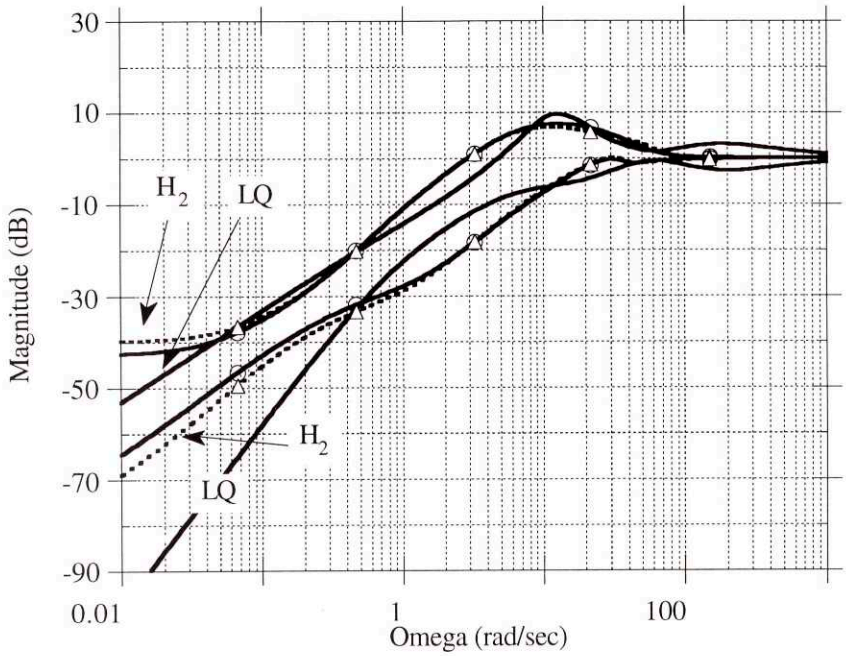

Figure 11-22 Singular Values of the Sensitivity Function (All Flight Parameters Increased)

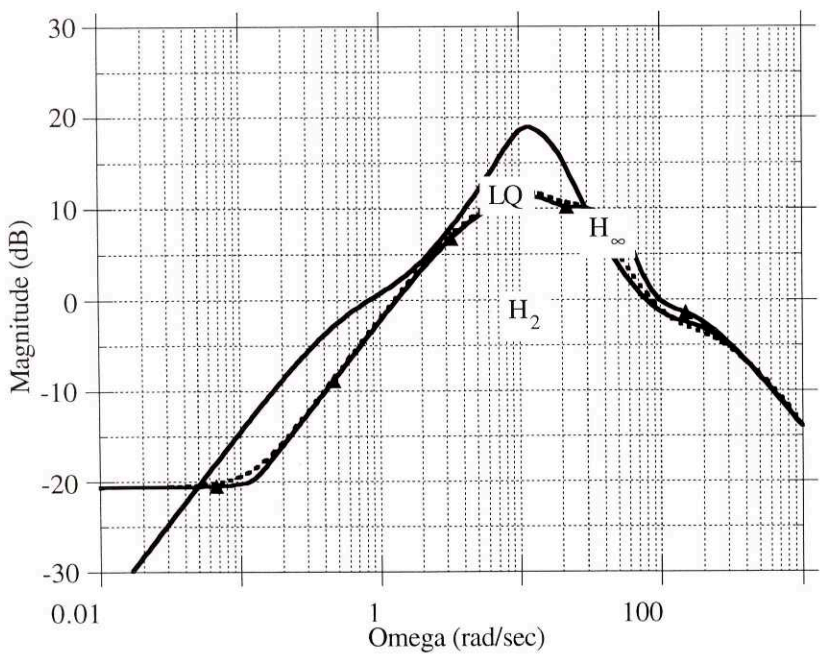

Figure 11-23 Maximum Singular Value Perturbations to Controlled Output (All Flight Parameters Increased)

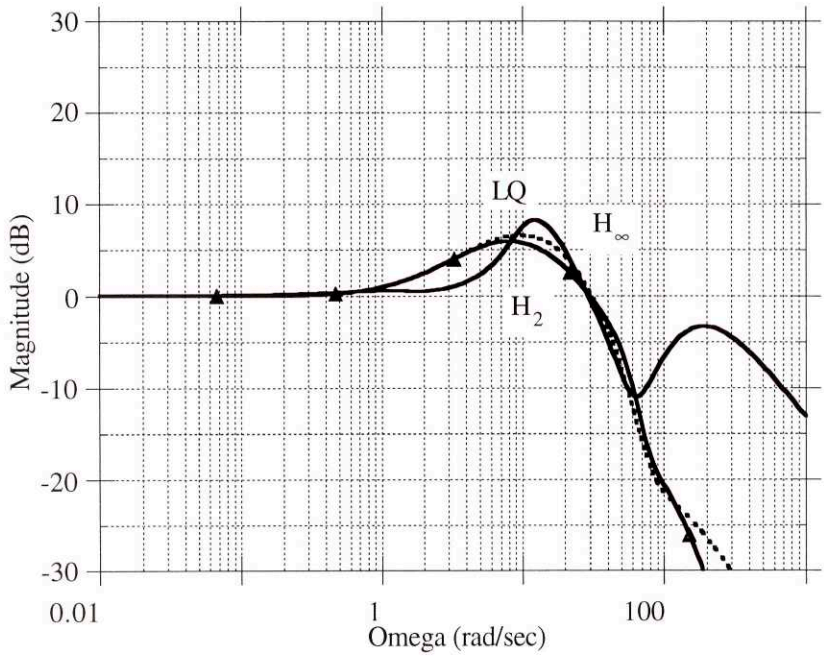

Figure 11-24 Maximum Singular Value Commands to Controlled Output (All Flight Parameters Increased)

11.2.1 Conclusions

All three autopilots can handle this simultaneous increase in altitude, speed and angle of attack. This change in the flight condition results in more overshoot in all three controllers and some degradation of the Bode single loop margins. The LQ continues to have the best Bode margins and the H_2 the worst although the roll channel Bode margin of the LQ design has the smallest gain reduction margin.

11.3 Simultaneous Variations Including Wind Angle

When the systems were connected to airframes linearized about an altitude decreased by 10%, velocity decreased by 10% and the angle of attack decreased by 5° or about an

altitude increased by 10%, velocity increased by 10% and the angle of attack increased by 5° than the design point values and the wind angles were changed to 11.25° and 45° the results changed to those summarized in Tables 11-7 through 11-14.

11.3.1 Decrease Missile Parameters, @ Wind Angles of 11.25° and 45°

	LQ			H_∞			H_2		
	Yaw	Pitch	Roll	Yaw	Pitch	Roll	Yaw	Pitch	Roll
Crossover Frequency (rad/sec)	26.6	28.3	67.2	28	30.9	54.9	28.6	30.6	55.6
63% Rise time (sec)	0.16	0.17	0.099	0.15	0.18	0.98	0.14	0.18	0.10
Overshoot (%)	57.3	13.9	5.3	55.	20.2	3.7	48	20	2.2

Table 11-7 Autopilot Performance Comparison Decrease Flight Parameters ϕ_W = 11.25°

	LQ		H_∞		H_2	
	Gain Margin (dB)	Phase Margin (deg)	Gain Margin (dB)	Phase Margin (deg)	Gain Margin (dB)	Phase Margin (deg)
Roll	-7, ∞	84	-13, ∞	61	-16, 23	33
Yaw	-21, 14	61	∞	44	22	35
Pitch	-8, ∞	81	-14, ∞	30	-15, 28	22

Table 11-8 Autopilot Bode Stability Margin Comparison Decrease Flight Parameters ϕ_W = 11.25°

	LQ			H_∞			H_2		
	Yaw	Pitch	Roll	Yaw	Pitch	Roll	Yaw	Pitch	Roll
Crossover Frequency (rad/sec)	28.4	29.7	71.8	28.5	31	59.1	29.1	30.3	58.9
63% Rise time (sec)	0.18	0.19	0.098	0.17	0.20	0.099	0.16	0.20	0.11
Overshoot (%)	12.7	4.7	4.3	14.3	16.1	4.5	15	16.3	3.6

Table 11-9 Autopilot Performance Comparison Decrease Flight Parameters ϕ_W = 45°

	LQ		H_∞		H_2	
	Gain Margin (dB)	Phase Margin (deg)	Gain Margin (dB)	Phase Margin (deg)	Gain Margin (dB)	Phase Margin (deg)
Roll	∞	89	∞	62	23	32
Yaw	∞	73	-44, -35, ∞	28	21.5	42
Pitch	∞	71	-27, -11, 12	17	-23, 26	22

Table 11-10 Autopilot Bode Stability Margin Comparison Decrease Flight Parameters $\phi_W = 45$

11.3.2 Increase Missile Parameters, @ Wind Angles of 11.25° and 45°

	LQ			H_∞			H_2		
	Yaw	Pitch	Roll	Yaw	Pitch	Roll	Yaw	Pitch	Roll
Crossover Frequency (rad/sec)	28	48.9	51.8	29.8	35.1	65.8	30.8	38.2	64.7
63% Rise time (sec)	0.17	0.15	0.093	0.16	0.16	0.095	0.15	0.16	0.10
Overshoot (%)	41.1	25.7	8.9	30.1	18.9	-1.4	24.2	18.3	0.8

Table 11-11 Autopilot Performance Comparison Increase Flight Parameters ϕ_W = 11.25°

	LQ		H_∞		H_2	
	Gain Margin (dB)	Phase Margin (deg)	Gain Margin (dB)	Phase Margin (deg)	Gain Margin (dB)	Phase Margin (deg)
Roll	-5, ∞	98	-16, ∞	85	-17, 23	39
Yaw	∞	61	∞	44	20	38
Pitch	∞	120	∞	58	26	54

Table 11-12 Autopilot Bode Stability Margin Comparison Increase Flight Parameters $\phi_W = 11.25°$

	LQ			H_∞			H_2		
	Yaw	Pitch	Roll	Yaw	Pitch	Roll	Yaw	Pitch	Roll
Crossover Frequency (rad/sec)	32.1	37.4	57.8	30.5	34.7	68.9	31.9	35.1	66.7
63% Rise time (sec)	0.16	0.17	0.094	0.15	0.18	0.096	0.14	0.18	0.10
Overshoot (%)	15	10	6.4	13	10.7	-1.4	11.9	10.9	-0.5

Table 11-13 Autopilot Performance Comparison Increase Flight Parameters ϕ_W = 45°

	LQ		H_∞		H_2	
	Gain Margin (dB)	Phase Margin (deg)	Gain Margin (dB)	Phase Margin (deg)	Gain Margin (dB)	Phase Margin (deg)
Roll	-14, ∞	109	∞	80	22	35
Yaw	∞	86	∞	57	19	53
Pitch	∞	84	-22, ∞	37	-20, 26	34

Table 11-14 Autopilot Bode Stability Margin Comparison Increase Flight Parameters $\phi_W = 45°$

11.3.1 Conclusions

All three autopilots can handle this simultaneous changes in altitude, speed, angle of attack. and wind angle. These changes in the flight condition results in significant overshoot in all three controllers and degradation of the Bode single loop margins. The LQ controller continues to have the best Bode phase margins and usually the best gain margins. The H_2 usually has the worst Bode margins although the roll channel Bode margin of the LQ design has the smallest gain reduction margin.

Chapter 12 Conclusion and Recommendations

12.1 Conclusions

The design of a flight control system for a modern interceptor missile is a complex task. The designer must concern himself with a whole plethora of issues including: expected operating environment, performance requirements, instrument quality and capability, robustness issues and compensator complexity. There is no one best solution. Three types of control design methods have been investigated. They are: Linear Quadratic control theory, H_2 control theory and H_∞ control theory.

All three design methods work well, and all three provide excellent performance at the nominal design condition. As the actual missile operating point changes from the design point the performance of all three systems degrades. The amount of degradation varies from operating point to operating point and from controller to controller. In general, for the design point analyzed (medium altitude, Mach 4, 15° angle of attack, and a wind angle of 22.5°) all three designs can accommodate changes of ±10% in missile altitude, ±10% in missile speed, and ±5° angle of attack from the design point. In general the LQ design showed the most performance variation due to changes in the altitude, speed or wind angle. On the other hand it was the most robust to variations in the angle of attack. However all three design show sensitivity to wind angle variations. This sensitivity is such that, while the frequency domain performance is still adequate the time domain performances of the three designs has degraded to such an extent that the controller's performance is at best marginal if the wind angle is changed to 11.25°.

Interceptor missile require unique time domain performance characteristics. The final measure of performance for such an interceptor is simple, the target is hit or not. This simple criteria requires that the time performance must not degrade too much. The

guidance algorithms that are used for an engagement are carefully tuned to the flight control system performance. Excessive mismatches render the system useless.

One possible method to avoid the performance degradation is to schedule the autopilot gains on a much smaller grid, and to interpolate between the discrete gain sets. The downside to this gain scheduling and interpolation is an increase in the required storage and through put

As discussed in Chapter 8 there are significant differences between the autopilot designs in terms of their computational requirements. Current military computer design regulations require that the loading of a processor be limited to only 50% to allow for future growth and expansion. The upshot of this is that an H_∞ or H_2 controller should be allocated at least 100K adds and multiplies in the processor sizing phase and 7K bits per operating point of the autopilot design for a 100 Hertz autopilot rate. The LQ design by contrast needs only 20K adds and multiplies and 1K storage per operating point.

Most autopilot processors are concerned with frequencies up to 200 Hertz. The minimum autopilot rate for this frequency is 400 Hertz according to the Nyquist criteria. This in turn changes the requirements to approximately. This data is summarized in Table 12-1.

Autopilot	# of multiplies per sec	# of adds per sec	Storage (bits)
LQ	70K	65K	1008
H_2	400K	375K	6864
H_∞	400K	375K	6864

Table 12-1 More Realistic Computational Requirements for the Autopilot Designs

For many existing MIL-SPEC processors this can easily become prohibitive particularly the H_2 and H_∞ requirements. The use of extensive gain scheduling and interpolation of the

gain sets adds overhead to the existing computation count. A one variable interpolation requires 4 adds and 2 multiplies. A two variable interpolation requires 12 adds and 6 multiplies. The operation counts for these types of interpolations grows geometrically with the number of interpolation variables. Because of the simple structure of the LQ autopilot its design most readily be used with a fin mesh of gain scheduling.

12.2 Recommendations for Future Research

All three of these autopilot design techniques show good performance at their design points. No one technique can be said to be the best technique as all three have their good points and their bad. The μ–synthesis techniques was not evaluated in this thesis. The added performance from such a μ–synthesis autopilot may justify the added complexity induced by its optimal scaling filters. One additional topic for study is the development of a computerized, systematic method for determining the shaping filters of an H_2 or H_∞ autopilot that satisfy time domain requirements for a first iteration of autopilot design. The controller's dependence and sensitivity to wind angle must be further evaluated.

Bibliography

[1] Reichert, R.T., and Yost, D.J., "Modern Robust Control for Missile Autopilot Design."

[2] Reichert, R.T., "Dynamic Scheduling of Modern-Robust-Control Autopilot Designs for Missiles," presented at IEEE CDC 1991.

[3] Lin, C.F., Cloutier, J.R., Evers, J.H., Juang, J.C., and Wang, Q., "High Performance, Adaptive, Robust Bank-to-Turn Missile Autopilot Design," Proceedings of the AIAA Guidance and Control Conference, 1991.

[4] Jackson, P., "Applying μ-Synthesis to Missile Autopilot Design," Proceedings of the 29th Conference on Decision and Control, 1990.

[5] Wise, K.A., "Bank-to-Turn Missile Autopilot Design Using Loop Transfer Recovery," Journal of Guidance and Control, Vol. 13, No. 1, Jan-Feb 1990.

[6] Rogers, W.L., and Collins, D.J., "X-29 $\mathcal{H}_\infty$ Controller Synthesis," Journal of Guidance, Control, and Dynamics, Vol. 15, No. 4, Jul-Aug 1992.

[7] Wise, K.A., Mears, B.C., and Poolla, K., "Missile Autopilot Design Using $\mathcal{H}_\infty$ Optimal Control with μ-Synthesis," Proceedings of 1990 American Control Conference.

[8] Reichert, R.T., "Robust Autopilot Design Using μ-Synthesis," Proceedings of the 1990 American Control Conference.

[9] Benshabat, D.G., and Chait, Y., "Application of Quantitative Feedback Theory to a Class of Missiles," Journal of Guidance, Control, and Dynamics, Vol. 16, No. 1, Jan-Feb 1993.

[10] Bibel, J.E., and Stalford, H.L.,"An Improved Gain-Stabilized μ-Controller for a Flexible Missile," Proceedings of the AIAA Guidance and Control Conference, 1992.

[11] Nesline, F.W., and Zarchan, P., "Robust Instrumentation Configurations for Homing Missile Flight Control," Raytheon Company.

[12] Nesline, F.W., and Nabbefeld, N., "Design of Digital Autopilots for Homing Missiles" Proceedings of Agaard Flight Mechanics Symposium, London England. May 21-24 1979 pp. 29-1 to 29-14

[13] Urban,T.J. , "Synthesis of Missile Autopilots Robust to the Presence of Parametric Variations," SM Degree, MIT, Cambridge MA 1991.

[14] Kwakernaak, H. and Sivan, R., "Linear Optimal Control Systems," Wiley-Interscience, NY.

[15] Doyle, J.C., Francis, B.A. and Tannenbaum, A.R., "Feedback Control Theory," MacMillan, NY, 1992.

[16] Packard, A., and Doyle, J., "The Complex Structured Singular Value," Automatica, Vol. 29, No. 1, pp 71-110, 1993.

[17] Levine, W.S., and Reichert, R.T., "An Introduction to $\mathcal{H}_\infty$ Control System Design," Proceedings of the 29th Conference on Decision and Control, 1990.

[18] Shinners, S.M., "Modern Control System Theory and Design," Wiley-Interscience, New York.

[19] Maciejowski, J.M., "Multivariable Feeback Design," Addison-Wesley Publishing Co., Reading, MA. 1989

[20] Ruth, M.J., "A Classical Perspective on Application of $\mathcal{H}_\infty$ Control Theory to a Flexible Missile Airframe," Applied Physics Laboratory.

[21] Doyle, J.C., Glover, K., Khargonekar, P.P. and Frances, B.A., "State-Space Solutions to Standard $\mathcal{H}_2$ and $\mathcal{H}_\infty$ Control Problems," IEEE Trans. on Automat. Contr., Vol. 34, pp.831-847, Aug. 1989.

[22] Francis, B.A., Helton, J.W. and Zames, G., "$\mathcal{H}_\infty$-Optimal Feedback Controllers for Linear Multivariable Systems," IEEE Trans. on Automat. Contr., AC-29, pp. 888-900, Oct. 1984.

[23] Glover, K. and Doyle, J.C., "State-Space Formulae For All Stabilizing Controllers That Satisfy an $\mathcal{H}_\infty$-norm Bound and Relations To Risk Sensitivity," Systems & Control Letters, 11, pp. 167-172, 1988.

[24] Safonov, M.G., and Wang, W., "Singular Value Properties of LQ Regulators," IEEE Transactions on Automatic Control, Vol. 37, No. 8, Aug. 1992.

[25] Yeh, H-H., Banda, S.S., and Chang, B-C., "Necessary and Sufficient Conditions for Mixed $\mathcal{H}_2$ and $\mathcal{H}_\infty$ Optimal Control," IEEE Transactions on Automatic Control, Vol. 37, No. 3, pp 355-358, Mar. 1992.

[26] Li, X.P., Chang, B.C., Banda, S.S., and Yeh, H.H., "Robust Control Systems Using $\mathcal{H}_\infty$ Optimization Theory," Journal of Guidance, Control, and Dynamics, Vol. 15, No. 4, Jul-Aug 1992.

[27] Zhou, K., "Comparison Between $\mathcal{H}_2$ and $\mathcal{H}_\infty$ Controllers," IEEE Transactions on Automatic Control, Vol. 37, No. 8, Aug. 1992.

[28] Nesline, F.W., and Zarchan, P., "Why Modern Controllers Go Unstable in Practice" AIAA Journal of Guidance and Control. Volume 7 #4 1984 pp 495 - 500

[29] Kleppner, D, and Kolenkow, R. "An Introduction to Mechanics", McGraw-Hill Publishing Co., New York, 1973

Hajek, A., "Lecture Notes on LQG/$\mathcal{H}_\infty$ Central Design," Raytheon Co. 1993.

Doyle, J.C., and Chu, C-C., "Matrix Interpolation and $\mathcal{H}_\infty$ Performance Bounds," Proceedings of the 1990 American Control Conference.

Francis, B.A. and Zames, G. "On $\mathcal{H}_\infty$-Optimal Sensitivity Theory for SISO Feedback Control Systems," IEEE Trans. on Automat. Contr., AC-29, pp. 9-16, Jan. 1984.

Doyle, J.C. and Chu, C.C., "Matrix Interpolation and $\mathcal{H}_\infty$ Performance Bounds," WA4, pp. 129-134.

"μ-Analysis and Synthesis Tool Box", MuSyn Inc. and The MathWorks 1991

"Robust Control Tool Box", The MathWorks 1988

Appendix 1 Nominal Plant State Space Model

θ_r	0	0	0	1.0000e+00	0	0	0	0	0
α_y	0	-4.4530e-01	1.9100e-02	-2.4500e-01	-1.0000e+00	2.5120e-02	4.3710e-02	7.7790e-02	-7.1390e-03
α_p	0	3.3020e-02	-5.1340e-01	-9.6620e-02	2.3920e-02	-1.0000e+00	2.3650e-02	1.2110e-03	7.4590e-02
ω_r	0	-2.0760e+02	1.1490e+02	-3.3760e-01	0	0	1.9920e+03	6.9550e+02	3.0880e+02
ω_y	0	1.0620e+02	-1.4710e+01	9.3470e-02	-3.6060e-01	0	-4.9000e+01	-8.6120e+01	8.2280e+00
ω_p	0	-3.3500e+01	1.2730e+02	4.3710e-02	0	-3.6060e-01	-2.5300e+01	-8.4030e-01	-8.5700e+01
δ_r	0	0	0	0	0	0	-2.0000e+02	0	0
δ_y	0	0	0	0	0	0	0	-2.0000e+02	0
δ_p	0	0	0	0	0	0	0	0	-2.0000e+02

Table A1-1 Nominal Design Plant A Matrix

0	0	0
0	0	0
0	0	0
0	0	0
0	0	0
0	0	0
200	0	0
0	200	0
0	0	200

Table A1-2 LQ Design Plant B Matrix

η_y	0	8.1339e+00	-4.0627e-01	-1.0283e-03	3.9675e-03	0	-3.6111e-01	-6.2826e-01	5.0059e-02
η_p	0	4.8644e-01	-1.0182e+01	4.8085e-04	0	-3.9675e-03	1.6927e-01	-1.1815e-02	6.2507e-01
θ_r	1.0000e+00	0	0	0	0	0	0	0	0
α_y	0	1.0000e+00	0	0	0	0	0	0	0
α_p	0	0	1.0000e+00	0	0	0	0	0	0
ω_r	0	0	0	1.0000e+00	0	0	0	0	0
ω_y	0	0	0	0	1.0000e+00	0	0	0	0
ω_p	0	0	0	0	0	1.0000e+00	0	0	0
δ_r	0	0	0	0	0	0	1.0000e+00	0	0
δ_y	0	0	0	0	0	0	0	1.0000e+00	0
δ_p	0	0	0	0	0	0	0	0	1.0000e+00

Table A1-3 Nominal Design Plant C Matrix

Appendix 2 LQ Design Plant State Space Model

$\int\eta_y$	0.000	0.000	0.000	0.000	8.139	-0.407	-0.001	0.004	0.000	-0.361	-0.628	0.050
$\int\eta_p$	0.000	0.000	0.000	0.000	0.488	-10.187	0.000	0.000	-0.004	0.169	-0.012	0.625
$\int\theta_r$	0.000	0.000	0.000	1.000	0.000	0.000	0.000	0.000	0.000	0.000	0.000	0.000
θ_r	0.000	0.000	0.000	0.000	0.000	0.000	1.000	0.000	0.000	0.000	0.000	0.000
α_y	0.000	0.000	0.000	0.000	-0.445	0.019	-0.245	-1.000	0.025	0.044	0.078	-0.007
α_p	0.000	0.000	0.000	0.000	0.033	-0.514	-0.097	0.024	-1.000	0.024	0.001	0.075
ω_r	0.000	0.000	0.000	0.000	-207.600	114.800	-0.338	0.000	0.000	1993.000	695.800	309.000
ω_y	0.000	0.000	0.000	0.000	106.200	-14.690	0.093	-0.361	0.000	-49.020	-86.170	8.231
ω_p	0.000	0.000	0.000	0.000	-33.480	127.300	0.044	0.000	-0.361	-25.310	-0.841	-85.740
δ_r	0.000	0.000	0.000	0.000	0.000	0.000	0.000	0.000	0.000	-200.000	0.000	0.000
δ_y	0.000	0.000	0.000	0.000	0.000	0.000	0.000	0.000	0.000	0.000	-200.000	0.000
δ_p	0.000	0.000	0.000	0.000	0.000	0.000	0.000	0.000	0.000	0.000	0.000	-200.000

Table A2-1 LQ Design Plant A Matrix

0	0	0
0	0	0
0	0	0
0	0	0
0	0	0
0	0	0
0	0	0
0	0	0
0	0	0
200	0	0
0	200	0
0	0	200

Table A2-2 LQ Design Plant B Matrix

Appendix 3 LQ Compensator

LQ Compensator A Matrix

0.00	0.00	0.00
0.00	0.00	0.00
0.00	0.00	0.00

Table A3-1 LQ Compensator A Matrix

LQ Compensator B Matrix

-1.16	0.52	0.14	0.00	0.00	0.00	0.00	0.00	0.00	0.00	0.00
1.98	0.24	0.59	0.00	0.00	0.00	0.00	0.00	0.00	0.00	0.00
-2.00	-2.97	0.38	0.00	0.00	0.00	0.00	0.00	0.00	0.00	0.00

Table A3-2 LQ Compensator B Matrix

LQ Compensator C Matrix

1.00	0.00	0.00
0.00	1.00	0.00
0.00	0.00	1.00

Table A3-3 LQ Compensator C Matrix

LQ Compensator D Matrix

0.00	0.00	0.23	-1.12	-0.46	0.04	0.11	0.06	0.33	0.08	0.04
0.00	0.00	1.06	1.62	-0.34	0.05	-0.27	-0.01	0.45	0.24	0.06
0.00	0.00	0.67	-1.42	3.12	0.06	0.08	-0.30	0.44	0.12	0.18

Table A3-4 LQ Compensator D Matrix

Appendix 4 H_∞ Design Plant State Space Model

H_∞ Design Plant A Matrix

0.00	0.00	0.00	1.00	0.00	0.00	0.00	0.00	0.00	0.00	0.00	0.00	0.00	0.00	0.00
0.00	-0.45	0.02	-0.25	-1.00	0.03	0.04	0.08	-0.01	0.00	0.00	0.00	0.00	0.00	0.00
0.00	0.03	-0.51	-0.10	0.02	-1.00	0.02	0.00	0.07	0.00	0.00	0.00	0.00	0.00	0.00
0.00	-207.60	114.90	-0.34	0.00	0.00	1992.00	695.50	308.80	0.00	0.00	0.00	0.00	0.00	0.00
0.00	106.20	-14.71	0.09	-0.36	0.00	-49.00	-86.12	8.23	0.00	0.00	0.00	0.00	0.00	0.00
0.00	-33.50	127.30	0.04	0.00	-0.36	-25.30	-0.84	-85.70	0.00	0.00	0.00	0.00	0.00	0.00
0.00	0.00	0.00	0.00	0.00	0.00	-200.00	0.00	0.00	0.00	0.00	0.00	0.00	0.00	0.00
0.00	0.00	0.00	0.00	0.00	0.00	0.00	-200.00	0.00	0.00	0.00	0.00	0.00	0.00	0.00
0.00	0.00	0.00	0.00	0.00	0.00	0.00	0.00	-200.00	0.00	0.00	0.00	0.00	0.00	0.00
0.00	8.13	-0.41	0.00	0.00	0.00	-0.36	-0.63	0.05	-0.04	0.00	0.00	0.00	0.00	0.00
0.00	0.49	-10.18	0.00	0.00	0.00	0.17	-0.01	0.63	0.00	-0.04	0.00	0.00	0.00	0.00
1.00	0.00	0.00	0.00	0.00	0.00	0.00	0.00	0.00	0.00	0.00	-1.40	0.00	0.00	0.00
0.00	0.00	0.00	0.00	0.00	0.00	0.00	0.00	0.00	0.00	0.00	0.00	-350.00	0.00	0.00
0.00	0.00	0.00	0.00	0.00	0.00	0.00	0.00	0.00	0.00	0.00	0.00	0.00	-550.00	0.00
0.00	0.00	0.00	0.00	0.00	0.00	0.00	0.00	0.00	0.00	0.00	0.00	0.00	0.00	-350.00

Table A4-1 H_∞ Design Plant A Matrix

H_∞ Design Plant B Matrix

0.00	0.00	0.00	0.00	0.00	0.00	0.00	0.00	0.00	0.00	0.00	0.00	0.00	0.00	0.00	0.00	0.00
0.00	0.00	0.00	0.00	0.00	0.00	0.00	0.00	0.00	0.00	0.00	0.00	0.00	0.00	0.00	0.00	0.00
0.00	0.00	0.00	0.00	0.00	0.00	0.00	0.00	0.00	0.00	0.00	0.00	0.00	0.00	0.00	0.00	0.00
0.00	0.00	0.00	0.00	0.00	0.00	0.00	0.00	0.00	0.00	0.00	0.00	0.00	0.00	0.00	0.00	0.00
0.00	0.00	0.00	0.00	0.00	0.00	0.00	0.00	0.00	0.00	0.00	0.00	0.00	0.00	0.00	0.00	0.00
0.00	0.00	0.00	0.00	0.00	0.00	0.00	0.00	0.00	0.00	0.00	0.00	0.00	0.00	0.00	0.00	0.00
200.00	0.00	0.00	0.00	0.00	0.00	0.00	0.00	0.00	0.00	0.00	0.00	0.00	0.00	200.00	0.00	0.00
0.00	200.00	0.00	0.00	0.00	0.00	0.00	0.00	0.00	0.00	0.00	0.00	0.00	0.00	0.00	200.00	0.00
0.00	0.00	200.00	0.00	0.00	0.00	0.00	0.00	0.00	0.00	0.00	0.00	0.00	0.00	0.00	0.00	200.00
0.00	0.00	0.00	1.00	0.00	0.00	0.00	0.00	0.00	0.00	0.00	0.00	0.00	0.00	0.00	0.00	0.00
0.00	0.00	0.00	0.00	1.00	0.00	0.00	0.00	0.00	0.00	0.00	0.00	0.00	0.00	0.00	0.00	0.00
0.00	0.00	0.00	0.00	0.00	1.00	0.00	0.00	0.00	0.00	0.00	0.00	0.00	0.00	0.00	0.00	0.00
0.00	0.00	0.00	0.00	0.00	0.00	0.00	0.00	0.00	0.00	0.00	0.00	0.00	0.00	20.00	0.00	0.00
0.00	0.00	0.00	0.00	0.00	0.00	0.00	0.00	0.00	0.00	0.00	0.00	0.00	0.00	0.00	20.00	0.00
0.00	0.00	0.00	0.00	0.00	0.00	0.00	0.00	0.00	0.00	0.00	0.00	0.00	0.00	0.00	0.00	20.00

Table A4-2 H_∞ Design Plant B Matrix

H_∞ Design Plant C Matrix

0.00	0.00	0.00	0.00	0.00	0.00	0.00	0.00	0.00	0.00	0.00	0.00	-350.00	0.00	0.00
0.00	0.00	0.00	0.00	0.00	0.00	0.00	0.00	0.00	0.00	0.00	0.00	0.00	-550.00	0.00
0.00	0.00	0.00	0.00	0.00	0.00	0.00	0.00	0.00	0.00	0.00	0.00	0.00	0.00	-350.00
0.00	8.13	-0.41	0.00	0.00	0.00	-0.36	-0.63	0.05	3.47	0.00	0.00	0.00	0.00	0.00
0.00	0.49	-10.18	0.00	0.00	0.00	0.17	-0.01	0.63	0.00	3.47	0.00	0.00	0.00	0.00
1.00	0.00	0.00	0.00	0.00	0.00	0.00	0.00	0.00	0.00	0.00	33.60	0.00	0.00	0.00
0.00	-8.13	0.41	0.00	0.00	0.00	0.36	0.63	-0.05	0.00	0.00	0.00	0.00	0.00	0.00
0.00	-0.49	10.18	0.00	0.00	0.00	-0.17	0.01	-0.63	0.00	0.00	0.00	0.00	0.00	0.00
-1.00	0.00	0.00	0.00	0.00	0.00	0.00	0.00	0.00	0.00	0.00	0.00	0.00	0.00	0.00
0.00	-1.00	0.00	0.00	0.00	0.00	0.00	0.00	0.00	0.00	0.00	0.00	0.00	0.00	0.00
0.00	0.00	-1.00	0.00	0.00	0.00	0.00	0.00	0.00	0.00	0.00	0.00	0.00	0.00	0.00
0.00	0.00	0.00	-1.00	0.00	0.00	0.00	0.00	0.00	0.00	0.00	0.00	0.00	0.00	0.00
0.00	0.00	0.00	0.00	-1.00	0.00	0.00	0.00	0.00	0.00	0.00	0.00	0.00	0.00	0.00
0.00	0.00	0.00	0.00	0.00	-1.00	0.00	0.00	0.00	0.00	0.00	0.00	0.00	0.00	0.00
0.00	0.00	0.00	0.00	0.00	0.00	-1.00	0.00	0.00	0.00	0.00	0.00	0.00	0.00	0.00
0.00	0.00	0.00	0.00	0.00	0.00	0.00	-1.00	0.00	0.00	0.00	0.00	0.00	0.00	0.00
0.00	0.00	0.00	0.00	0.00	0.00	0.00	0.00	-1.00	0.00	0.00	0.00	0.00	0.00	0.00

Table A4-3 H_∞ Design Plant C Matrix

H_∞ Design Plant D Matrix

0.00	0.00	0.00	0.00	0.00	0.00	0.00	0.00	0.00	0.00	0.00	0.00	0.00	20.00	0.00	0.00
0.00	0.00	0.00	0.00	0.00	0.00	0.00	0.00	0.00	0.00	0.00	0.00	0.00	0.00	20.00	0.00
0.00	0.00	0.00	0.00	0.00	0.00	0.00	0.00	0.00	0.00	0.00	0.00	0.00	0.00	0.00	20.00
0.00	0.00	0.00	1.00	0.00	0.00	0.00	0.00	0.00	0.00	0.00	0.00	0.00	0.00	0.00	0.00
0.00	0.00	0.00	0.00	1.00	0.00	0.00	0.00	0.00	0.00	0.00	0.00	0.00	0.00	0.00	0.00
0.00	0.00	0.00	0.00	0.00	1.00	0.00	0.00	0.00	0.00	0.00	0.00	0.00	0.00	0.00	0.00
0.00	0.00	0.00	-1.00	0.00	0.00	0.00	0.00	0.00	0.00	0.00	0.00	0.00	0.00	0.00	0.00
0.00	0.00	0.00	0.00	-1.00	0.00	0.00	0.00	0.00	0.00	0.00	0.00	0.00	0.00	0.00	0.00
0.00	0.00	0.00	0.00	0.00	-1.00	0.00	0.00	0.00	0.00	0.00	0.00	0.00	0.00	0.00	0.00
0.00	0.00	0.00	0.00	0.00	0.00	-1.00	0.00	0.00	0.00	0.00	0.00	0.00	0.00	0.00	0.00
0.00	0.00	0.00	0.00	0.00	0.00	0.00	-1.00	0.00	0.00	0.00	0.00	0.00	0.00	0.00	0.00
0.00	0.00	0.00	0.00	0.00	0.00	0.00	0.00	-1.00	0.00	0.00	0.00	0.00	0.00	0.00	0.00
0.00	0.00	0.00	0.00	0.00	0.00	0.00	0.00	0.00	-1.00	0.00	0.00	0.00	0.00	0.00	0.00
0.00	0.00	0.00	0.00	0.00	0.00	0.00	0.00	0.00	0.00	-1.00	0.00	0.00	0.00	0.00	0.00
0.00	0.00	0.00	0.00	0.00	0.00	0.00	0.00	0.00	0.00	0.00	-1.00	0.00	0.00	0.00	0.00
0.00	0.00	0.00	0.00	0.00	0.00	0.00	0.00	0.00	0.00	0.00	0.00	-1.00	0.00	0.00	0.00
0.00	0.00	0.00	0.00	0.00	0.00	0.00	0.00	0.00	0.00	0.00	0.00	0.00	-1.00	0.00	0.00

Table A4-4 H_∞ Design Plant D Matrix

Appendix 5 H_∞ Compensator

H_∞ Compensator A Matrix

-0.97	1.65	0.77	0.04	0.03	0.01	-0.09	-0.10	-0.03	0.00	0.00	0.00	0.00	0.00	0.00
0.03	-8.25	0.73	-0.17	-0.10	-0.04	0.39	0.52	-0.04	0.00	0.00	0.00	0.00	0.00	0.00
0.01	0.60	-10.12	-0.09	-0.10	-0.03	0.19	0.00	0.49	0.00	0.00	0.00	0.00	0.00	0.00
-0.96	293.18	384.35	-699.50	22.30	11.61	1851.10	621.32	278.03	0.00	0.00	0.00	0.00	0.00	0.00
0.03	82.79	-6.85	22.14	-42.08	7.27	-48.93	-67.80	4.50	0.00	0.00	0.00	0.00	0.00	0.00
0.01	-24.50	106.31	11.54	7.27	-49.39	-25.65	-2.72	-65.26	0.00	0.00	0.00	0.00	0.00	0.00
-5190.70	3693.90	-1666.90	-287.76	-74.35	237.60	-1765.50	-513.11	-334.84	1348.60	612.89	-61560.00	-64683.00	-39401.00	-19477.00
-2850.50	2118.60	-975.11	-128.51	-7.43	127.62	-814.64	-584.88	-175.37	648.41	332.36	-33566.00	-36440.00	-16440.00	-10430.00
-1467.10	888.51	-235.65	-63.73	-21.94	106.39	-416.01	-136.73	-407.57	365.09	265.48	-17236.00	-18685.00	-10815.00	-2696.30
0.00	0.00	0.00	0.00	0.00	0.00	0.00	0.00	0.00	-0.04	0.00	0.00	0.00	0.00	0.00
0.00	0.00	0.00	0.00	0.00	0.00	0.00	0.00	0.00	0.00	-0.04	0.00	0.00	0.00	0.00
0.00	0.00	0.00	0.00	0.00	0.00	0.00	0.00	0.00	0.00	0.00	-1.40	0.00	0.00	0.00
-519.07	356.72	-173.91	-17.46	-7.35	23.79	-150.00	-51.17	-33.47	134.86	61.29	-6156.00	-6818.30	-3940.10	-1947.70
-285.06	176.07	-93.39	-9.37	-2.41	12.89	-80.78	-28.07	-17.93	64.84	33.24	-3356.60	-3644.00	-2194.00	-1043.00
-146.71	95.28	-70.93	-4.79	-1.87	8.71	-41.39	-14.08	-10.05	36.51	26.55	-1723.60	-1868.50	-1081.50	-619.63

Table A5-1 H_∞ Compensator A Matrix

H_∞ Compensator B Matrix

0.33	-0.13	-1.57	0.04	0.02	-1.55	0.05	0.02	0.00	0.05	0.01
-1.52	-0.05	0.04	-0.21	0.00	0.12	1.47	-0.10	0.01	-0.25	0.05
0.02	1.51	0.02	0.00	-0.17	0.00	-0.20	1.58	0.01	0.03	-0.28
102.43	-46.91	-1.55	0.12	0.00	-1131.40	35.68	18.61	-183.11	-56.25	-25.59
-4.77	-1.08	0.05	1.47	-0.20	35.68	-67.49	11.77	-1.43	26.63	-5.13
1.60	3.43	0.02	-0.10	1.58	18.61	11.77	-79.33	-0.57	-2.00	30.86
25.97	-12.51	0.00	0.01	0.01	-183.11	-1.43	-0.57	-94.58	13.93	6.23
71.03	3.73	0.05	-0.25	0.03	-56.25	26.63	-2.00	13.93	-123.98	0.51
-8.31	-74.97	0.01	0.05	-0.28	-25.59	-5.13	30.86	6.23	0.51	-125.95
-1.62	0.00	0.00	0.00	0.00	0.00	0.00	0.00	0.00	0.00	0.00
0.00	-1.62	0.00	0.00	0.00	0.00	0.00	0.00	0.00	0.00	0.00
0.00	0.00	-1.62	0.00	0.00	0.00	0.00	0.00	0.00	0.00	0.00
0.00	0.00	0.00	0.00	0.00	0.00	0.00	0.00	0.00	0.00	0.00
0.00	0.00	0.00	0.00	0.00	0.00	0.00	0.00	0.00	0.00	0.00
0.00	0.00	0.00	0.00	0.00	0.00	0.00	0.00	0.00	0.00	0.00

Table A5-2 H_∞ Compensator B Matrix

H_∞ Compensator C Matrix

-16.04	11.02	-5.37	-0.54	-0.23	0.74	-4.63	-1.58	-1.03	4.17	1.89	-190.20	-199.84	-121.73	-60.18
-8.81	5.44	-2.89	-0.29	-0.07	0.40	-2.50	-0.87	-0.55	2.00	1.03	-103.70	-112.59	-50.79	-32.23
-4.53	2.94	-2.19	-0.15	-0.06	0.27	-1.28	-0.44	-0.31	1.13	0.82	-53.25	-57.73	-33.42	-8.33

Table A5-3 H_∞ Compensator C Matrix

Appendix 6 H_2 Design Plant State Space Model

H_2 Design Plant A Matrix

0.00	0.00	0.00	0.00	0.00	0.00	0.00	0.00	0.00	0.00	0.00	0.00	0.00	0.00	0.00
0.00	0.00	0.00	0.00	0.00	0.00	0.00	0.00	0.00	0.00	0.00	0.00	0.00	0.00	0.00
0.00	0.00	0.00	0.00	0.00	0.00	0.00	0.00	0.00	0.00	0.00	0.00	0.00	0.00	0.00
0.00	-0.21	0.11	0.00	0.00	0.00	1.99	0.70	0.31	0.00	0.00	0.00	0.00	0.00	0.00
0.00	0.11	-0.01	0.00	0.00	0.00	-0.05	-0.09	0.01	0.00	0.00	0.00	0.00	0.00	0.00
0.00	-0.03	0.13	0.00	0.00	0.00	-0.03	0.00	-0.09	0.00	0.00	0.00	0.00	0.00	0.00
0.00	0.00	0.00	0.00	0.00	0.00	-0.20	0.00	0.00	0.00	0.00	0.00	0.00	0.00	0.00
0.00	0.00	0.00	0.00	0.00	0.00	0.00	-0.20	0.00	0.00	0.00	0.00	0.00	0.00	0.00
0.00	0.00	0.00	0.00	0.00	0.00	0.00	0.00	-0.20	0.00	0.00	0.00	0.00	0.00	0.00
0.00	0.01	0.00	0.00	0.00	0.00	0.00	0.00	0.00	0.00	0.00	0.00	0.00	0.00	0.00
0.00	0.00	-0.01	0.00	0.00	0.00	0.00	0.00	0.00	0.00	0.00	0.00	0.00	0.00	0.00
0.00	0.00	0.00	0.00	0.00	0.00	0.00	0.00	0.00	0.00	0.00	0.00	0.00	0.00	0.00
0.00	0.00	0.00	0.00	0.00	0.00	0.00	0.00	0.00	0.00	0.00	0.00	-0.73	0.00	0.00
0.00	0.00	0.00	0.00	0.00	0.00	0.00	0.00	0.00	0.00	0.00	0.00	0.00	-0.88	0.00
0.00	0.00	0.00	0.00	0.00	0.00	0.00	0.00	0.00	0.00	0.00	0.00	0.00	0.00	-0.63

Table A6-1 H_2 Design Plant A Matrix

H_2 Design Plant B Matrix

0.00	0.00	0.00	0.00	0.00	0.00	0.00	0.00	0.00	0.00	0.00	0.00	0.00	0.00	0.00	0.00	0.00
0.00	0.00	0.00	0.00	0.00	0.00	0.00	0.00	0.00	0.00	0.00	0.00	0.00	0.00	0.00	0.00	0.00
0.00	0.00	0.00	0.00	0.00	0.00	0.00	0.00	0.00	0.00	0.00	0.00	0.00	0.00	0.00	0.00	0.00
0.00	0.00	0.00	0.00	0.00	0.00	0.00	0.00	0.00	0.00	0.00	0.00	0.00	0.00	0.00	0.00	0.00
0.00	0.00	0.00	0.00	0.00	0.00	0.00	0.00	0.00	0.00	0.00	0.00	0.00	0.00	0.00	0.00	0.00
0.00	0.00	0.00	0.00	0.00	0.00	0.00	0.00	0.00	0.00	0.00	0.00	0.00	0.00	0.00	0.00	0.00
200.00	0.00	0.00	0.00	0.00	0.00	0.00	0.00	0.00	0.00	0.00	0.00	0.00	0.00	200.00	0.00	0.00
0.00	200.00	0.00	0.00	0.00	0.00	0.00	0.00	0.00	0.00	0.00	0.00	0.00	0.00	0.00	200.00	0.00
0.00	0.00	200.00	0.00	0.00	0.00	0.00	0.00	0.00	0.00	0.00	0.00	0.00	0.00	0.00	0.00	200.00
0.00	0.00	0.00	1.00	0.00	0.00	0.00	0.00	0.00	0.00	0.00	0.00	0.00	0.00	0.00	0.00	0.00
0.00	0.00	0.00	0.00	1.00	0.00	0.00	0.00	0.00	0.00	0.00	0.00	0.00	0.00	0.00	0.00	0.00
0.00	0.00	0.00	0.00	0.00	1.00	0.00	0.00	0.00	0.00	0.00	0.00	0.00	0.00	0.00	0.00	0.00
0.00	0.00	0.00	0.00	0.00	0.00	0.00	0.00	0.00	0.00	0.00	0.00	0.00	0.00	15.00	0.00	0.00
0.00	0.00	0.00	0.00	0.00	0.00	0.00	0.00	0.00	0.00	0.00	0.00	0.00	0.00	0.00	15.00	0.00
0.00	0.00	0.00	0.00	0.00	0.00	0.00	0.00	0.00	0.00	0.00	0.00	0.00	0.00	0.00	0.00	15.00

Table A6-2 H_2 Design Plant B Matrix

H_2 Design Plant C Matrix

0.00	0.00	0.00	0.00	0.00	0.00	0.00	0.00	0.00	0.00	0.00	0.00	-725.00	0.00	0.00
0.00	0.00	0.00	0.00	0.00	0.00	0.00	0.00	0.00	0.00	0.00	0.00	0.00	-875.00	0.00
0.00	0.00	0.00	0.00	0.00	0.00	0.00	0.00	0.00	0.00	0.00	0.00	0.00	0.00	-625.00
0.00	8.13	-0.41	0.00	0.00	0.00	-0.36	-0.63	0.05	3.47	0.00	0.00	0.00	0.00	0.00
0.00	0.49	-10.18	0.00	0.00	0.00	0.17	-0.01	0.63	0.00	3.47	0.00	0.00	0.00	0.00
1.00	0.00	0.00	0.00	0.00	0.00	0.00	0.00	0.00	0.00	0.00	33.60	0.00	0.00	0.00
0.00	-8.13	0.41	0.00	0.00	0.00	0.36	0.63	-0.05	0.00	0.00	0.00	0.00	0.00	0.00
0.00	-0.49	10.18	0.00	0.00	0.00	-0.17	0.01	-0.63	0.00	0.00	0.00	0.00	0.00	0.00
-1.00	0.00	0.00	0.00	0.00	0.00	0.00	0.00	0.00	0.00	0.00	0.00	0.00	0.00	0.00
0.00	-1.00	0.00	0.00	0.00	0.00	0.00	0.00	0.00	0.00	0.00	0.00	0.00	0.00	0.00
0.00	0.00	-1.00	0.00	0.00	0.00	0.00	0.00	0.00	0.00	0.00	0.00	0.00	0.00	0.00
0.00	0.00	0.00	-1.00	0.00	0.00	0.00	0.00	0.00	0.00	0.00	0.00	0.00	0.00	0.00
0.00	0.00	0.00	0.00	-1.00	0.00	0.00	0.00	0.00	0.00	0.00	0.00	0.00	0.00	0.00
0.00	0.00	0.00	0.00	0.00	-1.00	0.00	0.00	0.00	0.00	0.00	0.00	0.00	0.00	0.00
0.00	0.00	0.00	0.00	0.00	0.00	-1.00	0.00	0.00	0.00	0.00	0.00	0.00	0.00	0.00
0.00	0.00	0.00	0.00	0.00	0.00	0.00	-1.00	0.00	0.00	0.00	0.00	0.00	0.00	0.00
0.00	0.00	0.00	0.00	0.00	0.00	0.00	0.00	-1.00	0.00	0.00	0.00	0.00	0.00	0.00

Table A6-3 H_2 Design Plant C Matrix

H_2 Design Plant D Matrix

0.00	0.00	0.00	0.00	0.00	0.00	0.00	0.00	0.00	0.00	0.00	0.00	0.00	0.00	15.00	0.00	0.00
0.00	0.00	0.00	0.00	0.00	0.00	0.00	0.00	0.00	0.00	0.00	0.00	0.00	0.00	0.00	15.00	0.00
0.00	0.00	0.00	0.00	0.00	0.00	0.00	0.00	0.00	0.00	0.00	0.00	0.00	0.00	0.00	0.00	15.00
0.00	0.00	0.00	1.00	0.00	0.00	0.00	0.00	0.00	0.00	0.00	0.00	0.00	0.00	0.00	0.00	0.00
0.00	0.00	0.00	0.00	1.00	0.00	0.00	0.00	0.00	0.00	0.00	0.00	0.00	0.00	0.00	0.00	0.00
0.00	0.00	0.00	0.00	0.00	1.00	0.00	0.00	0.00	0.00	0.00	0.00	0.00	0.00	0.00	0.00	0.00
0.00	0.00	0.00	-1.00	0.00	0.00	0.00	0.00	0.00	0.00	0.00	0.00	0.00	0.00	0.00	0.00	0.00
0.00	0.00	0.00	0.00	-1.00	0.00	0.00	0.00	0.00	0.00	0.00	0.00	0.00	0.00	0.00	0.00	0.00
0.00	0.00	0.00	0.00	0.00	-1.00	0.00	0.00	0.00	0.00	0.00	0.00	0.00	0.00	0.00	0.00	0.00
0.00	0.00	0.00	0.00	0.00	0.00	-1.00	0.00	0.00	0.00	0.00	0.00	0.00	0.00	0.00	0.00	0.00
0.00	0.00	0.00	0.00	0.00	0.00	0.00	-1.00	0.00	0.00	0.00	0.00	0.00	0.00	0.00	0.00	0.00
0.00	0.00	0.00	0.00	0.00	0.00	0.00	0.00	-1.00	0.00	0.00	0.00	0.00	0.00	0.00	0.00	0.00
0.00	0.00	0.00	0.00	0.00	0.00	0.00	0.00	0.00	-1.00	0.00	0.00	0.00	0.00	0.00	0.00	0.00
0.00	0.00	0.00	0.00	0.00	0.00	0.00	0.00	0.00	0.00	-1.00	0.00	0.00	0.00	0.00	0.00	0.00
0.00	0.00	0.00	0.00	0.00	0.00	0.00	0.00	0.00	0.00	0.00	-1.00	0.00	0.00	0.00	0.00	0.00
0.00	0.00	0.00	0.00	0.00	0.00	0.00	0.00	0.00	0.00	0.00	0.00	-1.00	0.00	0.00	0.00	0.00

Table A6-1 H_2 Design Plant D Matrix

Appendix 7 H_2 Compensator

H_2 Compensator A Matrix

-0.97	1.65	0.77	0.04	0.03	0.01	-0.09	-0.10	-0.03	0.00	0.00	0.00	0.00	0.00	0.00
0.03	-8.25	0.73	-0.17	-0.10	-0.04	0.39	0.52	-0.04	0.00	0.00	0.00	0.00	0.00	0.00
0.01	0.60	-10.12	-0.09	-0.10	-0.03	0.19	0.00	0.49	0.00	0.00	0.00	0.00	0.00	0.00
-0.96	293.18	384.35	-699.50	22.30	11.61	1851.10	621.32	278.03	0.00	0.00	0.00	0.00	0.00	0.00
0.03	82.79	-6.85	22.14	-42.08	7.27	-48.93	-67.80	4.50	0.00	0.00	0.00	0.00	0.00	0.00
0.01	-24.50	106.31	11.54	7.27	-49.39	-25.65	-2.72	-65.26	0.00	0.00	0.00	0.00	0.00	0.00
-10.71	209.42	108.65	-114.29	-5.17	-2.21	-274.21	-3.38	-1.24	35.30	-15.07	-208.85	8906.00	-272.23	-110.08
-33.18	302.63	-19.86	-35.00	23.94	-1.99	-9.95	-308.18	4.36	-28.59	-6.99	-267.67	-257.45	10968.00	52.88
-14.35	-53.72	369.19	-15.87	-4.03	29.35	-3.34	4.37	-311.57	7.72	42.97	-110.37	-108.22	54.66	7714.70
0.00	0.00	0.00	0.00	0.00	0.00	0.00	0.00	0.00	-0.04	0.00	0.00	0.00	0.00	0.00
0.00	0.00	0.00	0.00	0.00	0.00	0.00	0.00	0.00	0.00	-0.04	0.00	0.00	0.00	0.00
0.00	0.00	0.00	0.00	0.00	0.00	0.00	0.00	0.00	0.00	0.00	-1.20	0.00	0.00	0.00
-0.80	6.20	2.74	-0.08	-0.33	-0.14	-0.65	-0.15	-0.08	2.65	-1.13	-15.66	-107.05	-20.42	-8.26
-2.49	-4.15	1.60	-0.02	0.55	-0.06	-0.23	-0.30	0.03	-2.14	-0.52	-20.08	-19.31	-77.38	3.97
-1.08	0.79	-7.83	0.00	-0.06	0.76	-0.09	0.02	-0.34	0.58	3.22	-8.28	-8.12	4.10	-71.39

Table A7-1 H_2 Compensator A Matrix

H_2 Compensator B Matrix

0.42	-0.17	-2.00	0.06	0.02	-1.97	0.06	0.02	0.00	0.06	0.02
-1.93	-0.07	0.06	-0.26	0.00	0.15	1.86	-0.12	0.01	-0.31	0.07
0.03	1.92	0.02	0.00	-0.21	0.00	-0.25	2.00	0.02	0.03	-0.35
130.00	-59.54	-1.97	0.15	0.00	-1435.90	45.28	23.62	-232.40	-71.39	-32.48
-6.06	-1.37	0.06	1.86	-0.25	45.28	-85.66	14.93	-1.82	33.80	-6.51
2.03	4.35	0.02	-0.12	2.00	23.62	14.93	-100.68	-0.72	-2.54	39.16
32.97	-15.87	0.00	0.01	0.02	-232.40	-1.82	-0.72	-120.03	17.68	7.90
90.15	4.73	0.06	-0.31	0.03	-71.39	33.80	-2.54	17.68	-157.36	0.65
-10.55	-95.15	0.02	0.07	-0.35	-32.48	-6.51	39.16	7.90	0.65	-159.86
-2.05	0.00	0.00	0.00	0.00	0.00	0.00	0.00	0.00	0.00	0.00
0.00	-2.05	0.00	0.00	0.00	0.00	0.00	0.00	0.00	0.00	0.00
0.00	0.00	-2.05	0.00	0.00	0.00	0.00	0.00	0.00	0.00	0.00
0.00	0.00	0.00	0.00	0.00	0.00	0.00	0.00	0.00	0.00	0.00
0.00	0.00	0.00	0.00	0.00	0.00	0.00	0.00	0.00	0.00	0.00
0.00	0.00	0.00	0.00	0.00	0.00	0.00	0.00	0.00	0.00	0.00

Table A7-2 H_2 Compensator **A** Matrix

H_2 Compensator C Matrix

-0.03	0.20	0.09	0.00	-0.01	0.00	-0.02	0.00	0.00	0.09	-0.04	-0.51	21.68	-0.66	-0.27
-0.08	-0.13	0.05	0.00	0.02	0.00	-0.01	-0.01	0.00	-0.07	-0.02	-0.65	-0.63	26.70	0.13
-0.03	0.03	-0.25	0.00	0.00	0.02	0.00	0.00	-0.01	0.02	0.10	-0.27	-0.26	0.13	18.78

Table A7-3 H_2 Compensator C Matrix

Appendix 8 Transfer Function Derivations

Four types of transfer functions will be used to evaluate the autopilots' properties. They are the:

Loop Transfer
Sensitivity
Complementary Sensitivity
Perturbation to Output

Loop Transfer

The loop transfer function shows how the various inputs to the autopilot result in values at the output of the plant. There are 3 inputs to the compensator and 3 controlled outputs from the plant. The remaining internal loops are closed. As seen in Figure A8-1 there is no feedback for this transfer function.

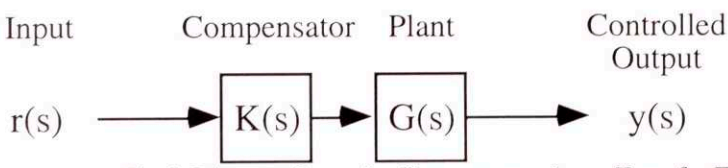

Figure A8-1 Block Diagram Setup for Compensator Loop Transfer Function

Denoting the compensator as K and the plant as G the transfer function is derived as:

$$y(s) = G(s)K(s)r(s)$$

where r is the input vector to the compensator and y is the controlled output vector of the plant.

Sensitivity

The sensitivity function shows how disturbances (such as instrument noise, wind gusts, etc.) are reflected in the plants controlled outputs. There are 3 disturbance inputs and 3 controlled outputs from the plant. As seen in Figure A8-2 the disturbances are injected at the plant output and fed back to the compensator. The remaining internal feedback loops are closed.

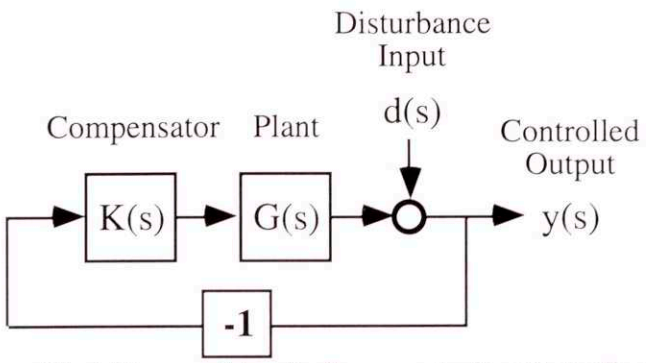

Figure A8-2 Block Diagram Setup for Compensator Sensitivity Transfer Function

The transfer function may be derived as follows:

$$y(s) = d(s) - G(s)K(s)y(s)$$

$$y(s) + G(s)K(s)y(s) = d(s)$$

$$y(s) = \left(I + G(s)K(s)\right)^{-1} d(s)$$

Complimentary Sensitivity

The complementary sensitivity function shows how commands are reflected in the plants controlled outputs. There are 3 commands and 3 controlled outputs from the plant. As seen in Figure A8-3 The commands are injected at the plant input.

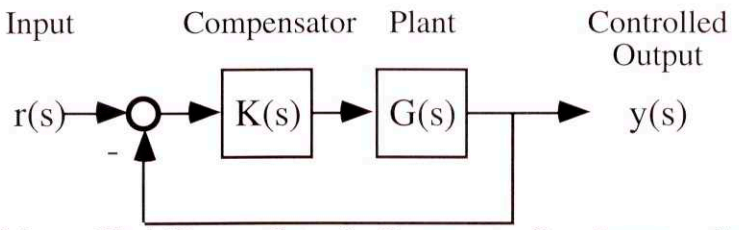

Figure A8-3 Block Diagram Setup for Compensator Complementary Sensitivity Transfer Function

The transfer function may be derived as follows:

$$y(s) = G(s)K(s)\big(r(s) - y(s)\big)$$

$$y(s) = G(s)K(s)r(s) - G(s)K(s)y(s)$$

$$y(s) + G(s)K(s)y(s) = G(s)K(s)r(s)$$

$$y(s) = \big(I + G(s)K(s)\big)^{-1}G(s)K(s)r(s)$$

Perturbation Sensitivity

The final transfer function shows how perturbations at the plant input are reflected in the controlled outputs. There are 3 perturbation inputs and 3 controlled outputs. As shown in Figure A8-4 the inputs are injected at the input to the plant.

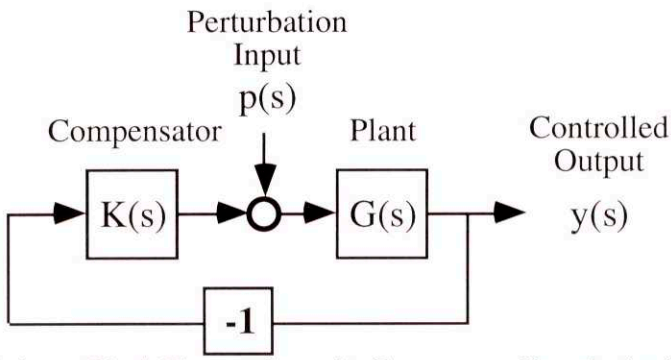

Figure A8-4 Block Diagram Setup for Compensator Perturbation Sensitivity

The transfer function may be derived as:

$$y(s) = G(s)\big(p(s) - K(s)y(s)\big)$$

$$y(s) = G(s)p(s) - G(s)K(s)y(s)$$

$$y(s) + G(s)K(s)y(s) = G(s)p(s)$$

$$y(s) = \big(I+G(s)K(s)\big)^{-1}G(s)p(s)$$